FLOW INJECTION INSTRUMENTATION FOR THE

IN SITU MONITORING OF NUTRIENTS IN SEA WATER

By

Anthony R. J. David, B.Sc., C.Chem., M.R.S.C.

A thesis submitted to the University of Plymouth in partial fulfilment for the

degree of

DOCTOR OF PHILOSOPHY

Department of Environmental Sciences

Faculty of Science

In collaboration with

The Plymouth Marine Laboratory

December 1996

ABSTRACT

FLOW INJECTION INSTRUMENTATION FOR THE

IN SITU MONITORING OF NUTRIENTS IN SEA WATER

Anthony R. J. David

In order to investigate the biogeochemistry of aquatic ecosystems, a quantitative understanding of primary production and the temporal and spatial distribution of nutrients is necessary. This thesis describes the development of a submersible FI based nutrient sensor for the *in situ* determination of nitrate in estuarine and coastal waters. Chapter One describes the role of nitrogen in the global and marine nitrogen cycles and provides an overview of laboratory and *in situ* methods for its determination. Chapter Two describes the key parameters for a field instrument and culminates with the overall design specification for the system. Chapter Three describes in detail the design, build and optimisation of the key individual components of the system, e.g. sample delivery system, injection valve, reduction column, reaction column, flowcell, on-board control system and the housing of the complete integrated system. Chapter Four describes the optimisation and analytical performance of the FI instrument prior to field trials. The key operational parameters such as flowcell path length, injection volume and detector response were investigated. LOD, reproducibility and linear range were determined and the control programme for the on-board computer is reported. For example, a LOD of 0.01 µM Nitrate-N, a linear range of 0 - 140 µM Nitrate-N and a reproducibility of ± 5 % were achieved. Chapter Five describes the field experiments where the FI system was initially used as a bench instrument and compared to a laboratory FI method which had been validated by participation in two inter-laboratory exercises and for nitrate in river and sea water. The first submersed deployments

involved the optimisation of the system operational characteristics and developing the field techniques. The final part of this chapter describes the weekly field studies of Barn Pool in Plymouth Sound using the submersed nutrient sensor for a period of two months. The operation and performance of the submersed sensor was assessed against an air segmented continuous flow analyser during a Land Ocean Interaction Study (LOIS) North Sea cruise aboard the *RVS Challenger*. The results from this exercise and the relevant salinity and turbidity measurements are presented in Chapter Six.

ACKNOWLEDGEMENTS

AUTHORS DECLARATION

At no time during the registration for the degree of Doctor of Philosophy has the author

been registered for any other university award. The work was financed with the aid of a

studentship from the Natural Environment Research Council, and with CASE support

contributed by the Plymouth Marine Laboratory. The work described in this thesis has

entirely been carried out by the author. Relevant scientific seminars and conferences were

regularly attended at which work was often presented; external institutions were visited for

consultation purposes, and papers were prepared for publication.

Publications:

1.   T. McCormack, A.R.J. David, P.J. Worsfold and R. Howland, (1994), *Anal. Proc.*,

31, 81.

2.   T. McCormack, A.R.J. David, P.J. Worsfold, *Frontiers in Analytical Spectroscopy*,

D.L. Andrews and A.M.C. Davies, (eds), RSC, Cambridge, (1995), pp129 - 135.

Conferences Attended:

1.   Perstorp Analytical Environmental Analysis Seminar, The Wildlife and Wetlands

Trust, Slimbridge, March 18th 1993.

2.   Oceanology International 94, Brighton, March 8 - 11th 1994.

3.   R & D Topics Meeting, University of Hertfordshire, July 18 - 19th 1994.

4.   Second MAST Days and EUROMAR Market, Sorrento, 7 -10th November 1995.

External Contacts:

Dr. Alan Morris, PML

Mr. Robin Howland, PML

Signed......................

Date.........11.5.97........

Contents

CONTENTS

CHAPTER FIVE   FIELD EXPERIMENTS

List of Figures

List of Figures

List of Tables

List of Tables

Chapter One
Introduction

1. INTRODUCTION

1.1. THE GLOBAL NITROGEN CYCLE

The circulation of nitrogen between inorganic compounds within the environment and proteins in living organisms is called the nitrogen cycle and a schematic diagram of the global nitrogen cycle is shown in Fig.1.1. Nitrogen is an essential constituent of all living organisms, both plant and animal, and it is present in their tissues in the form of proteins. It is present in relatively large concentrations in natural waters, rocks, sediments and the atmosphere although its availability as compounds that can be utilised by most forms of life is restricted. This deficiency in biologically available nitrogen in terrestrial and aquatic systems makes it one of the most important growth limiting nutrients. Herbivorous animals acquire the necessary nitrogen by consuming the proteins of plants; carnivorous animals by consuming the proteins in other animals. Nitrogen, in the form of dinitrogen (N_2) contributes to 78% by volume of the earth's atmosphere. Compared to oxygen, nitrogen has very low chemical reactivity and is therefore not directly available to the majority of living organisms. Dinitrogen has 3 covalent bonds linking the 2 nitrogen atoms ($N \equiv N$) and these have to be broken before compounds can be formed. This process requires 950 kJ mol^{-1} of energy to break all three bonds. Despite this, some plants acquire nitrogen directly by fixing it in their root systems, e.g. leguminous plants such as peas. Other plants are able to fix nitrogen by symbiotic association with certain nitrogen-fixing bacteria such as *Clostridium pastorianum* or *Azotobacter*. For most plants however, nitrogen is acquired in the form of nitrate or in a form which is readily converted to nitrate. A supply of fixed nitrogen to soil is essential for the life of plants and ultimately animals. Nitrates are naturally replenished in the cycle by :
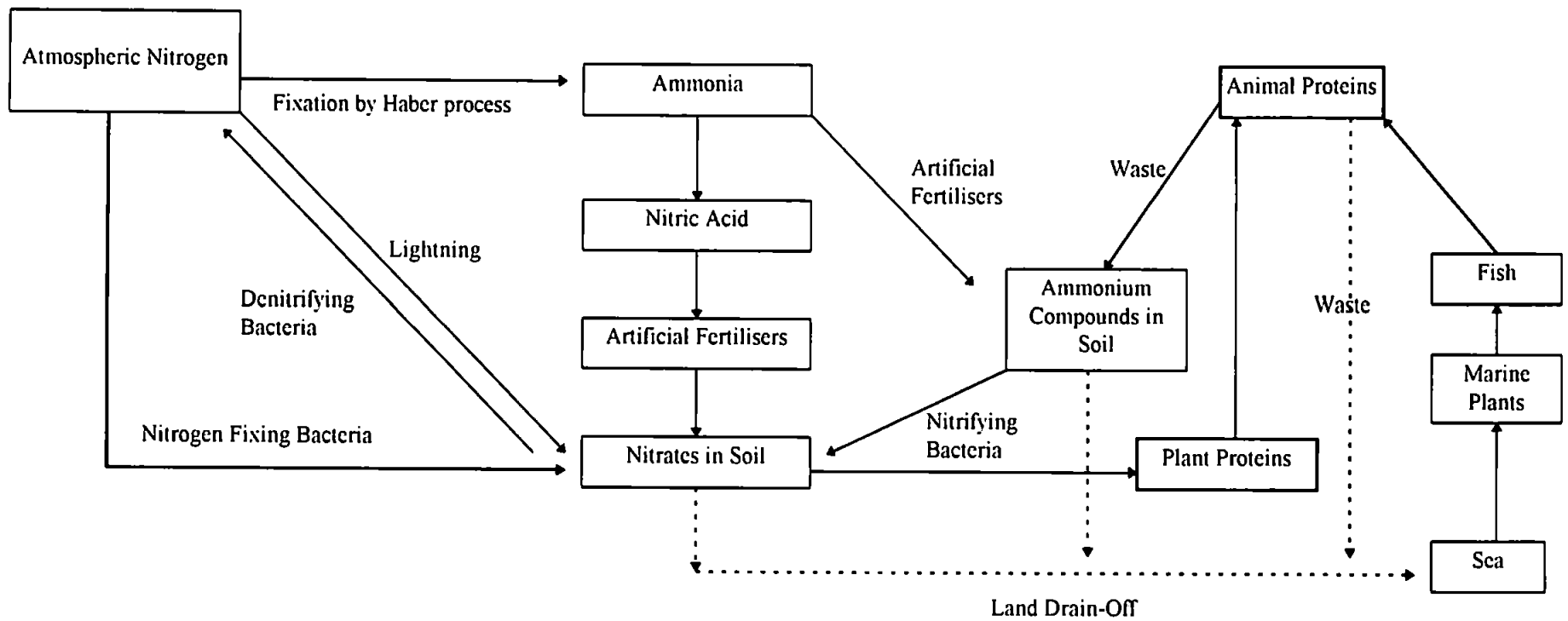
Figure 1.1.   Schematic diagram of the global nitrogen cycle.

1. Fixation of nitrogen in the atmosphere by electrical discharges during thunderstorms and washed down by rain as nitric acid.

2. The oxidation of ammonia produced by the decay of dead bodies of plants and animals - this oxidation is carried out by bacteria in the soil. Nitrosifying bacteria convert ammonia to nitrite and nitrifying bacteria convert nitrite to nitrate. The process is reversed by denitrifying bacteria in the soil which convert nitrates into free nitrogen.

The growth of plants in cultivated ground is stimulated by increasing the natural nitrate content in the soil. This can be achieved by the addition of either farmyard manure containing nitrogenous animal products or sodium nitrate or ammonium nitrate artificial fertilisers.

Anthropogenic activities are increasingly affecting the global biogeochemical nitrogen cycle. Estimates suggest that by the end of the century the production of nitrogen fertilisers will equal levels of biologically fixed nitrogen in the global terrestrial ecosystem [1]. Increased combustion temperatures increase the amount of NO_x which increases the amount of acidified rain and consequently adds to the global cycle.

1.2. THE MARINE NITROGEN CYCLE

The marine nitrogen cycle as shown in Fig.1.2, is a complex and integral part of the global nitrogen cycle. Within the marine nitrogen cycle, there are numerous interactive processes occurring as a result of physical, chemical, biological and anthropogenic activity. Sea water, in addition to dissolved dinitrogen, contains inorganic and organic nitrogen compounds. The principal inorganic forms being nitrate, nitrite and ammonia. Organic nitrogen is derived from the decay and metabolism of marine organisms. The overall concentrations of both inorganic and organic nitrogen are predominately controlled by biological factors although physical effects within the water column results in a redistribution of these species.

3

Atmospheric N
N₂

air-sea interface

denitrification   Dissolved N₂   fixation

Inorganic N

NO₃⁻   assimilation   Organic N
(living tissue)

NO₂⁻   nitrification

NH₄⁻

sediment-water interface

Ammonification

Organic N
(sediments)
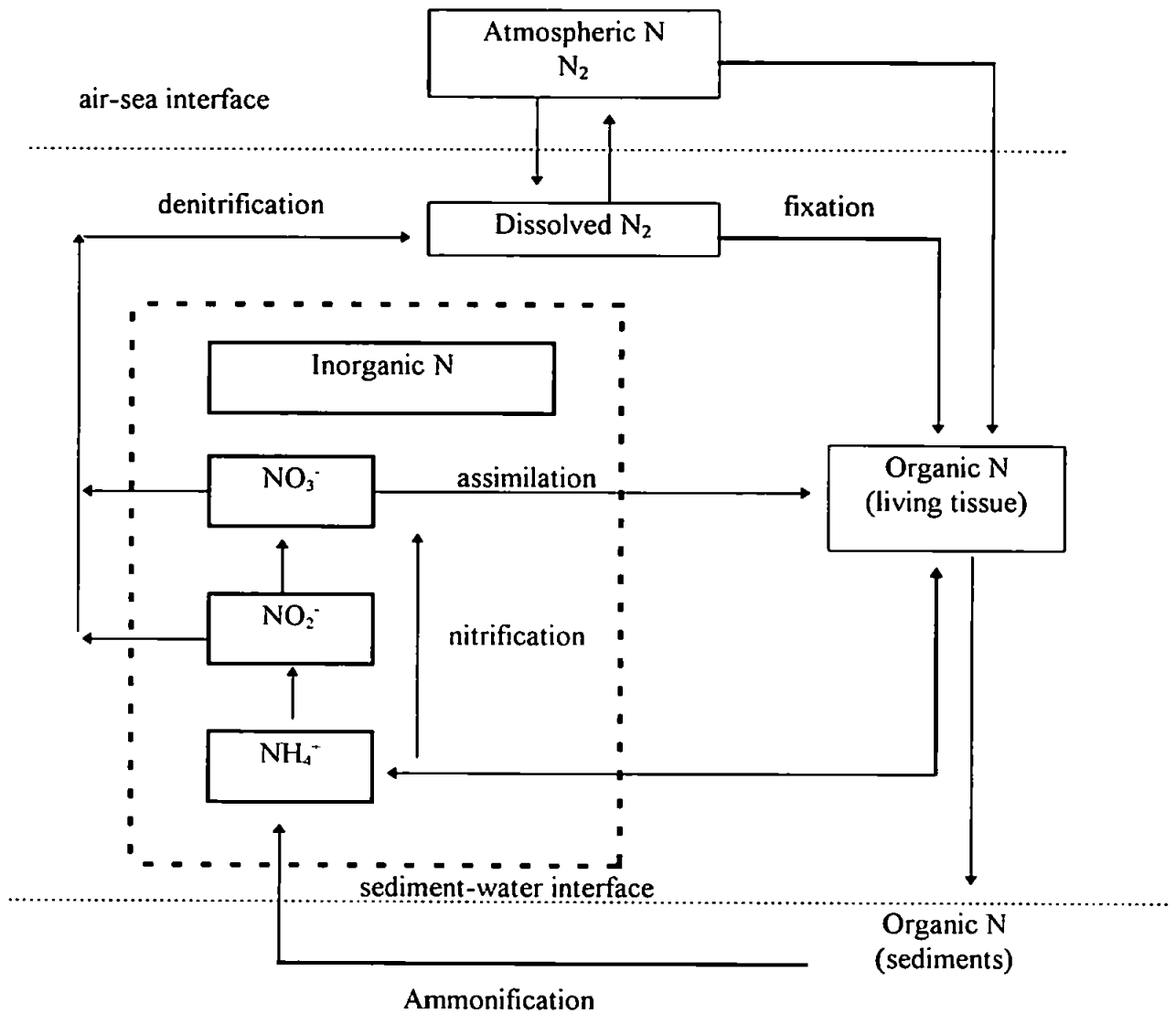
Figure 1.2. Schematic diagram of the marine nitrogen cycle

The major reservoirs of nitrogen contained within the world's oceans are shown in Table 1.1. Upwelling and sinking of dead organisms coupled with biological activity essentially produces a dynamic equilibrium within the system. Animals, plants and bacteria all have complementary functions in the depletion and regeneration of the various forms of nitrogen within the marine nitrogen cycle. Marine animals contribute to the cycle by the excretion of ammonia into the system. This is by no means a totally closed system as the deposition of organic nitrogen by sedimentation processes accounts for the removal of in the region of 9 x 10⁶ tonnes annually [1]. Fixed nitrogen from rivers and rainwater enters the system at a

much higher rate, ca 8×10^7 tonnes annually, and an unknown amount of atmospheric nitrogen is fixed by the blue-green algae *vide infra*.

Table 1.1. **Reservoirs of nitrogen in the world's oceans.**

Species	Tonnes	Reference
Di-nitrogen	2.2×10^{13}	[2]
Nitrate	5.7×10^{11}	[3]
Nitrite	5.0×10^8	[1]
Ammonium	7.0×10^9	[1]
Nitrous Oxide	2.0×10^8	[1]
Dead organic matter (dissolved)	5.3×10^{11}	[1]
Dead organic matter (particulate)	$3.0 \times 10^8 - 2.4 \times 10^{11}$	[1]
Total Biomass	4.9×10^8	[4]

Nitrite is found in sea water as an intermediary in the microbial reduction of nitrate or in the oxidation of ammonia. It can also be excreted by certain phytoplankton during luxury feeding when excess nitrates and phosphates are present. Natural levels are generally low, $< 0.1 \mu g\ l^{-1}$ NO_2-N, although this can increase to $> 2\ \mu g\ l^{-1}$ where oxic conditions become anoxic. The tolerance of fish towards nitrite varies as to type, becoming lower towards acid-pH values. High nitrite levels, $> 2\ \mu g\ l^{-1}$, reduce the oxygen content of water and are highly poisonous to fish[5, 6].

1.2.1. Nitrogen fixation in the marine environment

Marine counterparts of terrestrial and freshwater organisms capable of fixing nitrogen have been found in seawater and marine sediments, e.g. azotobacter, clostridium. The process is endothermic and requires significant amounts of organic material as an energy source so it is unlikely that these organisms fix significant amounts of atmospheric nitrogen [7]. In contrast, the blue-green algae *trichodesmium thiebautii*, has been shown to fix nitrogen on

a large scale in tropical and sub-tropical waters despite low levels of inorganic nutrients due to phytoplankton proliferation [8, 9, 10]. It has been suggested that these organisms obtain the energy required for nitrogen fixation from solar radiation [11] where the molecular nitrogen instead of carbon acts as an acceptor for the hydrogen liberated photochemically from the water. As a consequence, nitrogen fixation does not occur in darkness [12]. Fixation is inhibited if an alternative source of inorganic nitrogen such as nitrate or ammonia is available which the organisms will use in preference to molecular nitrogen [13,10]. Nitrogen fixing phytoplankton in the sea was found to be capable of supporting the growth of *trichodesmium sp.* at rates which are similar to those of species which rely totally on nitrate [9]. Nitrogen fixation may indirectly benefit other organisms, since some species of blue-green algae, e.g. *calothrix scopulorum*, liberate extracellular nitrogen as they grow. This has been shown to be utilised by a variety of algae, fungi and bacteria [14, 15].

1.2.2. Assimilation of fixed nitrogen

Marine phytoplankton synthesise their protein from nitrate, ammonia and nitrite whereas bacteria only assimilate these forms when organic nitrogen is not available. Uptake of nutrients is usually confined to the euphotic layer of the ocean as it is consequential with photosynthesis [16,17]. There is a hyperbolic relationship between the concentration of nitrate and ammonia and the rate of uptake. When levels fall below 10 μg l^{-1}, nitrogen deficient organisms are produced before cell division finally ceases. In the absence of light, these deficient cells are able to utilise ammonia and nitrate, but not nitrite, converting them to organic compounds such as chlorophyll. Prior to conversion to amino acids, the assimilated nitrate must first be converted to ammonia. To facilitate this endothermic reaction, a donor hydrogen and a source of high energy phosphate such as adenosine

triphosphate is required. These may be produced by respiration but are more likely to be produced as a result of photosynthesis.

Reduction of nitrate to ammonia takes place in four stages:

1. production of nitrite: $NO_3^- + 2H^+ + 2e^- \longrightarrow NO_2^- + H_2O$

2. production of hyponitrite: $2NO_2^- + 4H^+ + 4e^- \longrightarrow N_2O_2^{2-} + 2H_2O$

3. production of hydroxylamine: $N_2O_2^{2-} + 4H^+ + 4e^- \longrightarrow 2NH_2OH$

4. production of ammonia: $NH_2OH + 2H^+ + 2e^- \longrightarrow NH_3 + H_2O$

In the first stage, the nitrate is reduced by a molybdenum containing nitrate reductase and is catalysed by the reduced coenzyme II which is produced by the chloroplasts. Ammonia is then converted into glutamic acid by its reaction with α-ketoglutaric acid in the presence of reduced adenine nicotinamide dinuleotide phosphate (NADPH).

$HOOC.CO.(CH_2)_2.COOH + NH_3 + 2NADPH \longrightarrow$

$HOOC.CH(NH_2)CH_2CH_2.COOH + 2NADPH + H_2O$
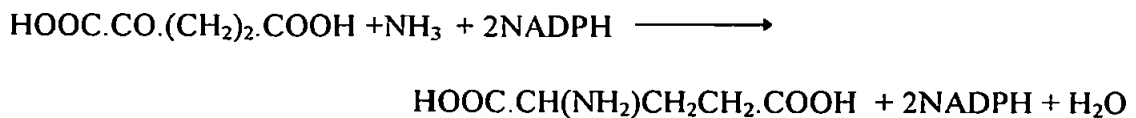
The amino acids required as building blocks for algal proteins are formed from the glutamic acid by transamination with pyruvic acid which gives rise to alanine and the reformation of α-ketoglutaric acid.

$CH_3COCOOH + HOOC.CH(NH_2)CH_2CH_2.COOH \longrightarrow$

$CH_3CH(NH_2)COOH + HOOC.CO(CH_2)_2COOH$
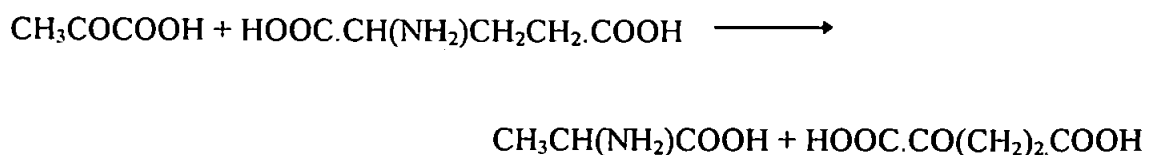
Proteins are then sequenced by the combination of the various amino acids with RNA and DNA with the energy provided by the adenosine triphosphate.

1.2.3. Regeneration of nitrate

The regeneration process by which organic nitrogen compounds are re-converted to nitrate via ammonia is by bacterial action, either as free-floating or attached to organic and inorganic suspended matter [18]. Aerobic bacteria use dissolved and suspended organic material as food and their energy requirements are satisfied by the oxidation of organic material to carbon dioxide using dissolved oxygen. Some bacteria are able to utilise other sources of oxygen such as nitrate and sulphate when conditions are anoxic. In the absence of nitrogen and phosphorus from the organic material, some species of bacteria can utilise dissolved inorganic nitrogen and phosphorus. The bacteria will die when the food supply is exhausted or conditions become unsuitable at which point autolysis of the dead cells liberates ammonia and phosphorus.

The next stage of the regeneration process is nitrification This is a two stage oxidation process where the ammonia is first oxidised to nitrite, mediated by species such as *nitrosomonas*.

1. $NH_4^+ + OH^- + 1\frac{1}{2}O_2 \longrightarrow H^+ + NO_2^- + 2H_2O$
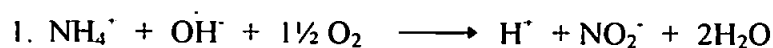
   The next stage is the oxidation of nitrite to nitrate which is mediated by species such as nitrobacter.

2. $NO_2^- + \frac{1}{2}O_2 \longrightarrow NO_3^-$

   The net reaction is:

   $NH_4^+ + 2O_2 \longrightarrow NO_3^- + H_2O + 2H^+$
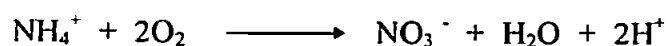
The first stage is usually rate limiting. At the second stage, the nitrate is highly oxidised, soluble and biologically available.

The overall process is oxygen demanding, which can create anoxic conditions in some aquatic systems. This is because *nitrosomonos* and *nitrobacter* are strict aerobes that require oxygen concentrations > 2 mg l^{-1} to function correctly. They are also pH and

8

temperature sensitive, requiring an optimum pH range of 8.4 to 8.6 and a temperature of > 15 °C.

1.2.4.   Denitrification

Denitrification can be considered as the biological reduction of nitrate to nitrogen or nitrous oxide [19]. Micro-organisms such as pseudomonas are able to reduce nitrate to molecular nitrogen. When these bacteria grow in oxygen depleted or completely anoxic water, they utilise nitrate as alternative electron acceptors to oxygen in the oxidation of organic matter. The extent of the denitrification process is controlled by the oxygen supply and the available energy produced by the organic material.

1.3.   NUTRIENTS IN THE AQUATIC ENVIRONMENT

1.3.1.   Marine food web

Seawater contains a complex, delicately balanced mix of organisms which all interact and play an important role in the marine life-cycle; this interaction can be illustrated using the *Food Chain* or *Web* concept shown in Fig. 1.3. This concept is not entirely precise as the pelagic food web is not fully understood and is dependent on many variables such as light, nutrients and temperature. Additionally, many species in the chain switch diets during various stages of their development and others feed at different trophic levels. Despite these difficulties however, the food web concept does give an overall picture of how the different trophic levels are dependent on each other. At the start of the 'classical' chain are the photosynthetic plant organisms known as phytoplankton. The larger phytoplankton, i.e. those which are normally caught in nets, consist mainly of two groups of microscopic algae such as diatoms (bacillariophyta - unicellular marine or freshwater algae) and diflagellates. Phytoplankton growth, or *Primary Production*, is the photosynthetic conversion of

9

inorganic micronutrient elements into energy-rich organic compounds such as proteins, fats and carbohydrates.

Production Levels

Size Range

Size Range		Production Levels

Piscavores
salmon, dogfish

Planktivores
*herring, mackerel,
squid, lantern fish*

| Megaplankton
(20 - 200cm) | Megazooplankton
*chaetognaths,
euphausiids* |

| Macroplankton
(2 - 20cm) | Macrozooplankton
carnivorous crustacea |

| Mesoplankton
(0.2- 20mm) | Mesozooplankton |

Microbial Loop

| Microplankton
20 - 200μm | Large ciliates | Diatoms and
dinoflagellates |

| Nanoplankton
2 - 20μm | Heterotrophic
Nanoflagellates | Nanophytoplankton |

| Picoplankton
0.2 - 2μm | Heterotrophic
Bacteria | Cyanobacteria |

Dissolved organic   &   Particulate organic
material   material

Figure 1.3. General diagrammatic representation of the marine food chain or web showing the microbial loop and its relationship to the 'classical' food web.

Primary productivity is generally considered to be synonymous with photosynthesis but this is not strictly correct as a very small proportion of the primary productivity can result from

10

chemosynthetic bacteria. The total amount of material fixed in the primary production process is the *Gross Primary Production*. A small proportion of this is used by phytoplankton to maintain their life process, which is *Respiration*, leaving a lesser amount called the *Net production* for transfer and support of other trophic levels. The *Standing crop* is the total mass of plant material present in a given amount of water at any one time. At each level organic matter is lost through excretion or natural mortality and bacteria play an important role by breaking this matter down for re-use by plants. The surface layers of seawater contain millions of these pelagic organisms per cubic metre.

Herbivorous zooplankton graze on the phytoplankton, converting it to animal tissue which is the *Secondary Production* stage. The herbivore zooplankton are in turn grazed upon by carnivorous zooplankton and fish predators and this is the *Tertiary Production* stage. All major animal phyla are represented in zooplankton as adults, larvae and eggs. Some are visible to the naked eye but most are only visible with magnification.

1.3.2.   Primary production

Photosynthesis is the ability of green plants to use energy from sunlight to convert inorganic materials to energy-rich organic molecules. Marine plants behave in a similar way to terrestrial plants in this respect. In the past 20 years however, changes have been made to the 'classical' model of the food web where [20] it has been suggested that a great deal of the phyto-photosynthesis is probably carried out by organisms of < 30 μm. Prior to this period, activity from these smaller organisms was generally ignored because they passed through collection nets or were destroyed on filters. Sophisticated methods of study and equipment such as satellite oceanography, transmission electron microscopy (TEM) and Nucleopore® filters, have revealed their importance to the overall system and consequently the classical model has been modified. The smaller phytoplankton in the nanoplankton size

range, 2.0 to 20.0μm, are now thought to account for up to 80% of the primary production and 75% of the standing crop [21].

In common with terrestrial plants, marine phytoplankton require nutrients and trace concentrations of elements such as manganese, iron, molybdenum, copper, vanadium and zinc for healthy growth. The roles of many of these elements in the metabolism of algae are well established. Iron, as the non-haem protein complex ferredoxin, plays an essential part in the light reaction of photosynthesis. Manganese in known to be present in the enzyme co-factors involved in photosynthesis and in the reduction of nitrate in which co-factors containing molybdenum are important. Copper-complexes serve as co-factors in oxidation-reduction cycles [6]. The most important of the micronutrient elements are nitrogen and phosphorus which are considered to be growth limiting [6]. Organisms such as diatoms with siliceous frustiles also require a source of silicon.

1.3.3.   Phosphorus

Phosphorus occurs in seawater as a variety of dissolved or particulate forms that are controlled by similar biological and physical processes to those which control the marine chemistry of nitrogen [22]. It has been shown that in the winter months dissolved phosphorus occurs almost entirely as orthophosphate [23]. By direct assimilation of the ortho-phosphate, phytoplankton normally satisfies their requirements for the element which rapidly decreases the ortho-phosphate from March onwards when phytoplankton proliferate. During May and June, the predominant form is organic phosphorus due to the excretions of zooplankton and fish. After the algal blooms have subsided, the regeneration of inorganic phosphorus is rapid. Phosphorus compounds such as adenosine triphosphate and nucleotide co-enzymes are essential to photosynthesis and other processes within phytoplankton. At phosphate concentrations above 10 μg l^{-1} the growth rate of many

species of phytoplankton is not dependent on the overall phosphate concentration. Below this critical level however, cell division becomes progressively inhibited until photosynthesis ceases. It is unlikely that phosphorus is growth limiting in marine systems as nitrate is usually exhausted before the phosphate falls to this critical level. Bacteria in marine systems satisfy their requirements for the element from the detritus on which they feed. If this food source is low in phosphorus they can assimilate dissolved inorganic phosphate from the water. The phosphorus contained in the tissue of dead organisms is rapidly converted to phosphate by the phosphatase enzymes in their cells. Zooplankton satisfy their phosphorus requirements by grazing on phytoplankton. Excess phosphorus is expelled in the form of faecal pellets which contain organic phosphates and ortho-phosphate. The organic phosphates in the faecal pellets are hydrolysed by the action of phosphorylase enzymes which are present. The inorganic phosphate is leached from the pellets, together with any remaining organic phosphorus compounds which are subsequently converted to ortho-phosphate by the action of bacteria and enzymes.

1.3.4.   N:P Ratio

The concept of growth limiting nutrients in an aquatic environment relies on the fact that absolute and relative quantities of the essential nutrients regulate primary production. It is therefore assumed that the ratio by which these nutrients are assimilated by the algae are relative to the composition of their cell material. Nitrogen and phosphorus are assimilated from seawater in an approximately constant ratio of 15:1 (N:P). This ratio holds true for many water bodies but variations do occur in some regions such as the Mediterranean, where the ratio is higher than average and the South Atlantic where ratios have been found to be below average. Ratios of 5:1 and 8:1 are common for inshore waters and for surface waters the ratio may approach zero after prolific phytoplankton growth has removed most of the nitrate.

1.4. NITRATE

1.4.1. Occurrence

Compared to the lithosphere, the world's oceans are the second largest planetary nitrogen reservoir, Table 1.2. The levels of nitrate dissolved in seawater are relatively low and thus it is a limiting factor in phytoplankton production in the euphotic surface layers of sea water. Despite this, nitrate in marine systems represents a significant part of the marine, and hence global, nitrogen cycle.

Table 1.2.   Major planetary nitrogen reservoirs

Nitrate Reservoir	Tonnes	Reference
Lithosphere	1.94×10^{16}	[24, 25]
Oceans	2.33×10^{14}	[1, 2, 3, 26]
Pedosphere	4.89×10^{11}	[1, 2, 27]

When compared to terrestrial systems, the world's oceans can be considered nutrient-poor deserts. For example, fairly rich agricultural land contains approximately 0.5 % N in the upper metre which is sufficient to support 50 kg of dry organic matter. Under ideal conditions, terrestrial plants can produce several kilograms of dry organic matter in excess of their own needs per year per square metre. Thus, the reservoir of nitrogen in that square metre of soil is sufficient to allow a plant to grow for many years. As a result, it is possible for terrestrial systems to have long-lived plants that continue to grow for many years. Growth will only be limited if the nutrients are not replenished. In comparison, the richest ocean water only contains approximately 0.00005 %, or 1/10 000 of that found in soil. This means that a metre of such water would only permit production of 5 g of dry organic matter. However, terrestrial plants may have root systems which may only penetrate a depth of 1 metre so the reservoir of nitrogen available is finite. Marine phytoplankton should have access to the nutrients in a water column that extends as deep as the organisms

14

can exist. Assuming ideal light conditions, plant production could extend down to 100 - 120 metres. This is known as the 'Compensation Depth' which is the point at which there is no net production and marks the lower limit of the photic zone. This would result in a potential production of 500 g of dry organic matter. Production levels of this magnitude do not occur in reality due to other limiting factors which rarely permits production in excess of 25 g of dry organic matter. Nitrate concentration is not constant in the water column and light penetration is affected by the quality of the water and phytoplankton growth, i.e. as production increases so the light penetration decreases. The result of this is that less of the nitrate in original 100 metre water column is available to the phytoplankton, thus reducing overall productivity. Nitrate uptake by the phytoplankton also reduces the concentration. The result of all these factors acting together reduces theoretical production to the extent where estimates suggest that when production reaches a density of 2 g m^{-3} the original 100 metre compensation depth has in fact been reduced to as little as 3.5 metres [28]. In general, the rate of production between terrestrial and marine plants may not be significantly different but the differences in nutrient concentration preclude that rate from continuing for long periods in the sea. However, below the photic zone there exists a vast reservoir of nitrate which remains largely unavailable to phytoplankton due to physical factors such as density and climatic conditions. If this reservoir was freely available then large standing crops would be sustainable for long periods of time.

The concentration of nitrate in coastal waters is regulated by advective movement of nitrate to the surface layers which is then subject to microbial oxidation and uptake by organisms. Assimilation of nitrate by organisms such as phytoplankton for subsequent production of protein by photosynthesis generally confines such activity to the upper euphotic layers where light penetration is sufficient for the process to proceed. This invariably causes seasonal trends in the nitrate concentrations in coastal waters where winter cooling within

the water column causes vertical mixing, allowing the upwelling of nutrients to enrich the surface layers. If light penetration is sufficiently high then uptake will deplete nutrient concentrations at a faster rate than the enriching transportation processes. Therefore, nitrate concentrations tend to follow a regular seasonal cycle of high values in autumn, winter and early spring to low values in late spring and summer [5]. Long-term studies have found this seasonal trend to be correct. For example, the 1983 Royal Society "The Nitrogen Cycle of the United Kingdom - A Study Group Report" [29], found nitrate levels in the English Channel ranged from 98 μg l $^{-1}$ in winter to 7 μg l $^{-1}$ in summer as shown in Fig. 1.4.
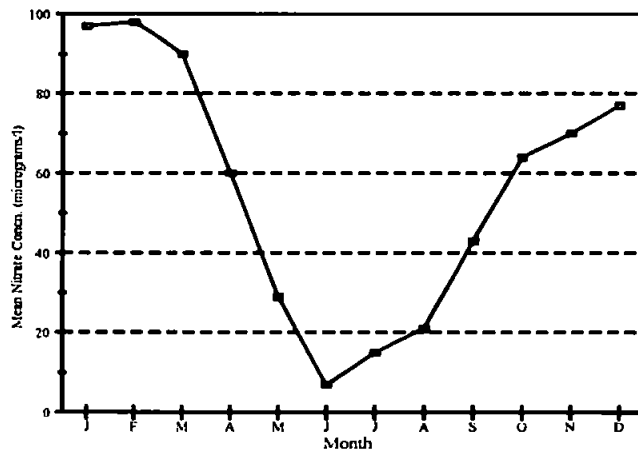
Figure 1.4.   Mean monthly nitrate concentrations in the English Channel for

the period 1969-77

1.4.2.   Nitrate in freshwater systems

Nitrate levels in freshwater systems have increased significantly in the past 50 years which has been mainly attributed to more intensive agricultural practices that have promoted the use of nitrogenous fertilisers. In 1950 the global use of nitrogen fertilisers was reported as 14 million tonnes. By 1985 this figure had increased to 125 million tonnes [30].

Nitrate fertilisers are not totally bound in the soil and therefore leach into the various inland watercourses if not taken up by plants. However, this is not always an immediate effect and

16

will depend on the agricultural activity and geology of a particular area [31]. Other factors such as sewage outfalls and animal effluents have contributed to the overall increase in nitrogenous matter found in freshwater systems. Table 1.3. shows the global levels of nitrates entering the marine nitrogen cycle from river systems. River nitrate levels tend to follow a definite seasonal pattern that is related to the flow of the river [38, 39].

During the growing season, nitrate levels in a river system tend to be lower despite the application of nitrate fertilisers to the adjacent land which is partly due to plant uptake of nitrates.

Table 1.3.   Global riverine nitrate inputs to the marine nitrogen cycle

Annual Input of NO_3-N from all sources	Year	Remarks	Reference
Tonnes			
7.1×10^6	1963	Human impact minimised	[32]
3.7×10^6	1982	Pristine rivers	[33]
3.5×10^6	1981	Thinly populated areas	[34]
3.0×10^6	1983	Pristine	[35]
24.0×10^6	1983	Includes anthropogenic contributions and ammonium	[35]
6.0×10^6	1991	Includes ammonium	[36]
15.2×10^6	1993	Includes anthropogenic sources, nitrate only	[37]

Maximum transpiration and evaporation also occurs at this time which tends to reduce the available water in the soil which is capable of leaching out nitrates. Towards the end of the growing season, nitrate levels in the river system increase as shown in Fig.1.5.
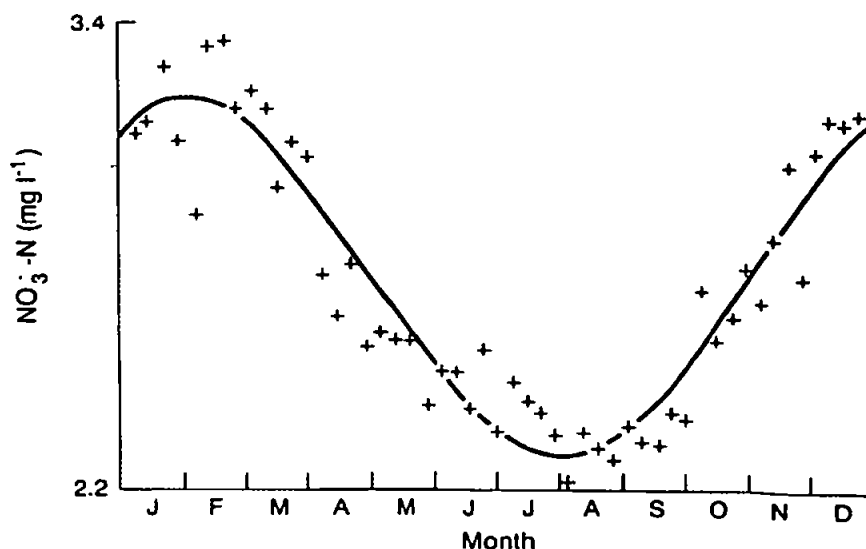
Figure 1.5. Weekly nitrate concentrations for the River Frome showing seasonal variation of nitrate concentration, from |39|

The 1992 Royal Commission on Environmental Pollution [40] reported the following nitrate levels in selected U.K. rivers, Table 1.4. Nitrate levels are low in the Upper Teith, which drains upland moor in the Central Region of Scotland.

Table 1.4.   1992 Royal Commission nitrate data for selected UK rivers

River	Sample Location	Nitrate-N mg l⁻¹		
		Min	Mean	Max
Teith	Upper	0.1	0.2	0.3
(Central region Scotland)	Lower	0.2	0.3	1.0
Tyne	Upper	2.7	3.5	4.6
(East Lothian)	Lower	2.8	4.5	6.7
Tay at Perth		0.09	0.65	1.02
Cuckmere (Sussex)	Upper	0.8	2.0	3.0
	Lower	2.2	3.4	5.4
Stour (Kent) at Wye		4.0	6.0	9.0
Great Eau (Lincs.)		5.4	8.5	12.6

Further downstream the nitrate levels are also low which is due to a low population and low agricultural activity in the lower reaches. Intensive agriculture, both improved grassland and arable, is practised over the entire range of the East Lothian Tyne catchment area which is reflected by the high nitrate levels to be found. The impact of a sewage works in the lower reach of the Tyne can be seen in the higher nitrate levels downstream.

1.4.3.   Estuaries

Nitrate enters the sea from land drain-off via estuaries, which despite being small in area by comparison, should not be considered as just pathways between freshwater and seawater. Estuaries have complex chemical and biological processes which can have an overall effect on the marine nitrogen cycle. They are the most perturbed regions of the marine environment, mainly due to anthropogenic activities such as sewage, transportation, urbanisation and waste discharges. Nutrients are recycled within an estuary between the overlying water and the biologically active sediments. Inorganic and organic nitrate inputs can be quite large and some of the dissolved material can precipitate out as the salinity changes towards the mouth of the estuary to form rich intertidal mud banks. Nutrient input can be continuous or episodic, e.g. after storm conditions, and can lead to transient algal blooms within the estuary. Nutrients can also enter estuaries in bottom water which is a return flow into an estuary which compensates for low-salinity surface out-flow. The intertidal and subtidal sediments are usually muddy and contain many micro-organisms and burrowing invertebrates. The surface area of the water/sediment interface is increased by the burrows and the micro-organisms at the interface actively mineralise the organic material that settles out. Microbial action can break down the complex organic material down to form carbon dioxide and water and releases nutrients such as nitrate and phosphate. The transfer of materials within an estuarine system is influenced by the morphological and hydrodynamical properties of the estuary which controls water

19

circulation, residence time and sedimentation. Estuaries can be classified into the following

three hydrodynamical categories which are based on the balance of freshwater and tidal

flows [37]:

1. Highly stratified/salt wedge.

2. Partially stratified.

3. Well mixed.

The classification of a particular estuary may change over a period of time in response to

seasonal changes to river flow, river spates and neap tides.

Where the residence time of water in the estuary is short compared to biological activity and

there is only one source of nitrate, e.g. a single riverine input, a simple nitrate-salinity

dilution results, as shown in Fig. 1.6. This is described as 'Conservative-behaviour' where

there is no net loss or gain of nitrate. 'Non-Conservative' behaviour occurs when there is a

net gain or loss in nitrate. Deviations above the idealised salinity-nitrate line are indicative of

point-source additions of nitrate such as industrial wastes.
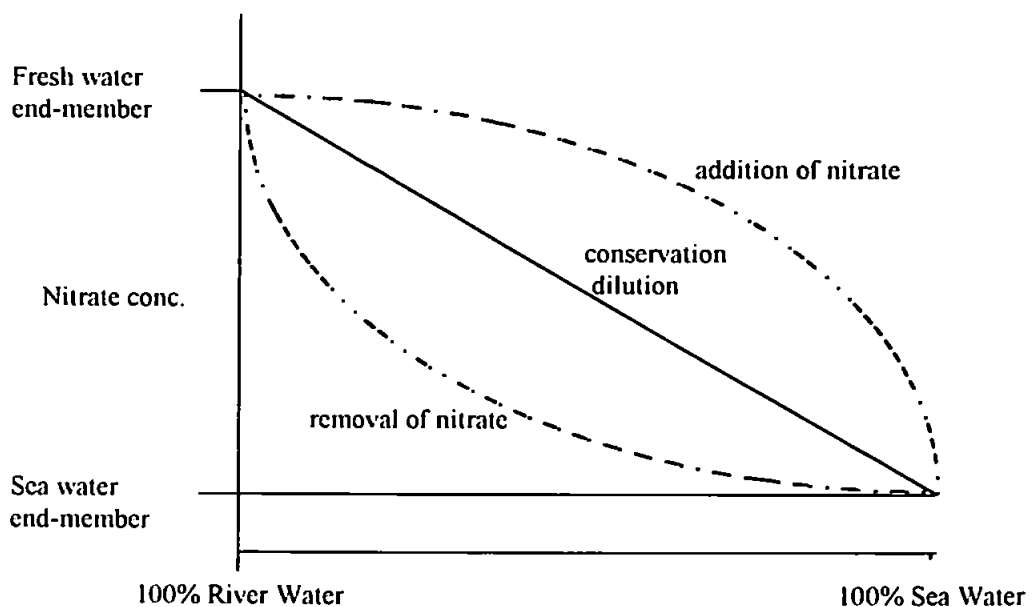
Figure 1.6.   Conservative and non-conservative behaviour of nitrate in
estuaries.

Deviation below the conservative dilution line is indicative that nitrate removal, e.g. biological activity, has occurred. Such deviations from the idealised salinity-nitrate dilution are not always unequivocal if there are nitrate fluctuations in the end members, i.e. freshwater and seawater. For example, if the nitrate concentration in river water is increased (in spate conditions) over a shorter timescale than the residence time in the estuary, the nitrate-salinity relationship could be mistaken for a point-input into the estuary [37].

1.5. MONITORING NITRATE

1.5.1. Introduction

As greater pressure is placed upon the environment through anthropogenic activities and climatic changes, effective monitoring and control of nitrate pollution is vital to ensure the protection of what is becoming a very delicately balanced environment.

The increased use of nitrogen based fertilisers, nitrates in particular, has caused the pollution of many inland watercourses by land drain-off due to the high solubility of this ion, e.g. the solubility of ammonium nitrate is 118.3 g in 100 g water at 0 °C.

Globally, it has been suggested [33] that the average nitrate concentration for pristine rivers is 0.1mg l^{-1} Nitrate-N. The UNEP/WHO concluded that less than 10% of the worlds rivers could be classified as pristine [41]. In 1987 it was reported that European rivers averaged 0.45 mg l^{-1} Nitrate-N compared to the remaining worlds rivers which averaged 0.25 mg l^{-1} Nitrate-N. It was also shown that 10% of European rivers contained levels in the region of 4.5 to 25 mg l^{-1} Nitrate-N, thus exceeding the EC drinking water directive 80/788 [42] Maximum Allowable Concentration (MAC) of 11.3 mg l^{-1} Nitrate-N [43]. When sampled in 1983/84, 125 UK ground water supplies feeding some 1.8 million people were also found to exceed the 11.3 mg l^{-1} Nitrate-N limit [44] compared to 90 supplies in 1980 and 60 supplies in 1960 [38]. Furthermore, it has been suggested that the level by which the EC

limit is being increased by is 1 - 2 mg l^{-1} Nitrate-N annually, particularly in agricultural regions [30]. It can be seen that nitrate levels have increased and that nitrate pollution is in fact a serious problem for health and the environment. Consequently, legislation has been introduced in an attempt to reverse the effects of increased nutrient enrichment of natural waters, and minimise the health risks thought to be associated with high nitrate levels in drinking water supplies. The EC Nitrate Directive 91/676 [45] was put in place to protect waters against pollution caused by nitrates from agricultural sources and recognises that the excessive use of fertilisers constitutes an environmental risk. This directive accepts that there is risk from both inorganic and organic fertilisers and has the necessary statutory tools to control nitrate pollution. The two objectives of the directive are:

1.   To avoid a high concentration of nitrate in ground and surface waters.

2.   To avoid eutrophication of surface, estuaral, coastal and marine waters.

Previous control measures were primarily concerned with health issues but this is the first directive which includes controls to safeguard the environment. The 91/676 nitrate directive compels member states to designate all areas which are at risk from nitrate pollution. The vulnerable zones are defined in annex 1 of the directive as:

1. Surface freshwaters, especially those intended for abstraction for drinking water, which either contain or could contain if protective action is not taken, more than the concentration laid down in Directive 75/440 (50 mg l^{-1}) [46].

2. Freshwaters, estuaries and coastal waters which are eutrophic, or may become eutrophic in the near future if protective action is not taken.

3. Groundwaters which contain more than 50 mg l^{-1} nitrate , or could contain than that amount if protective action is not taken.

The influx of nitrates from freshwater systems contributes to the overall marine nitrogen cycle and this effect will be at a maximum where estuarine and coastal waters merge. There is a fine balance between sufficient nutrients to promote healthy but controlled growth of

22

micro-organisms and an excess, which is likely to cause excessive algal blooms. This in turn will have a deleterious effect on the higher organisms by stripping the oxygen from the immediate environment.

1.5.2.   Health issues

The risk to human health from nitrate polluted water is not totally proven but there is sufficient evidence to cause concern. Methaemoglobinaemia ('Blue-Baby' syndrome) and stomach cancer are the two areas of concern.

Methaemoglobinaemia or 'Blue-Baby Syndrome' is a well recognised medical condition that mostly affects babies less than six months old and is caused by the ingestion of nitrate which is converted to nitrite in the gut. The nitrite then restricts the uptake of oxygen by a complexing link with the haemoglobin. This normally only accounts for 2% of the total haemoglobin but when the level rises to 10% the characteristic blue-tinge of an oxygen starved baby is observed. Adults are less likely to be affected because of the better developed enzyme-reduction system in the gut which is able to reverse the effect on the haemoglobin. Death can result from this condition but only when 45 - 65% of the total haemoglobin has been converted. It should be noted that the last recorded death in the U.K. from this condition was in 1950 and the last reported case was in 1974 [47]. However, methaemoglobinaemia is not a notifiable disease so these claims are difficult to substantiate and it is unlikely that there is a serious risk in the UK providing the levels are not allowed to rise to the 1970 WHO level of 50 mg l $^{-1}$ nitrate.

Stomach cancer has been linked to nitrate pollution of drinking water by the action of bacteria in the intestinal tract which is capable of converting nitrate to nitrite. This can then react with digestion products to produce N-nitroso compounds [48]. Work has identified these compounds as potential carcinogens in humans [49]. Although some work has proposed a positive connection between high nitrates in drinking water and stomach cancer [50] it is reasonable to expect that due to the enormous variations in diet, environment and

lifestyle it is not easy to positively establish a direct link in the UK. Despite this there is a definite need to monitor the situation given that the disease takes a long time to develop and that nitrate levels in drinking water have been steadily rising over the years.

1.5.3.   Eutrophication

Nutrient enrichment of natural waters affects both the freshwater and marine ecosystems [51]. Ultimately, this results in a simplification of the aquatic ecosystem where the higher-order plants decline and the lower organisms such as algae proliferate. Some such organisms are just unsightly, some are toxic to shellfish and fish and some may be harmful to mammals, e.g. *aphanizomenon flos-aquae* Blue-Green Alga. Toxicity assessments of over 200 blue-green algal blooms from European countries prior to 1989 revealed that 44 to 75% had produced toxins as shown in Table 1.5. In the case of the small number of blue-green blooms assessed in Hungary, Greece and Italy; all had produced toxins. In 1989, 60 to 70% of the blooms tested in the UK had produced toxins [52].

Table 1.5.   Incidence of toxicity of blue-green algae in European freshwaters prior to 1989

Origin	Number of sites with blooms tested	Number of sites with toxic blooms	% Incidence of bloom toxicity
United Kingdom	24	18	75
Finland	103	45	44
Sweden	27	15	56
Hungary	3	3	100
Greece	4	4	100
Italy	2	2	100

Nutrient enrichment of freshwater abstracted for drinking water is a major concern due to the presence of toxic algal growth. In 1990, the UK's National Rivers Authority (NRA)

24

detected blue-green algae in 90% of their regions water supplies, of which 70% of the algal strains isolated were toxic to humans [53].

Coastal Eutrophication: Coastal waters which have become enriched with nutrients and have poor mixing and tidal flow can suffer from eutrophication and this was identified by the Joint Group of Experts on the Scientific Aspects of Marine Pollution (GESAMP) (1990) [54] as being the second most serious threat to the coastal marine environment (after coastal development). Species with high growth and reproduction rates become dominant and this reduces the diversity of the species present in a particular area. Oxygen is also less readily available to the benthic community due to bacterial oxidation of the excess organic matter. In areas of poor tidal mixing and stratified waters animals inhabiting the sea bed will die as the oxygen level diminishes and in extreme cases organisms inhabiting the overlying water may also be killed [55].

Eutrophication is more easily induced in warmer coastal waters because oxygen is less soluble in warm water and the bacteria have a higher metabolic rate. If anoxic conditions persist, sulphur bacteria begin to flourish. These obtain their energy by converting sulphate in organic material to sulphide ions. The dissolved sulphide forms hydrogen sulphide in the water which may be toxic to animals.

Highly productive conditions can also lead to the over production of organisms such as *chrysochromulina polylepis* which secrete toxins. These toxic blooms (Red Tides) can kill everything in their path. In 1988 such a bloom occurred in the Skaggerak and was carried by currents along the Norwegian coast. It killed almost every pelagic and benthic organism in its path and threatened to kill the fish stocks of the many fish farms in the area. Fish production exceeds land-based production in Norway so it was a major threat to the country's economy. Human life can also be affected if shell fish such as clams, mussels, oysters, etc. ingest and accumulate the toxins in their body tissue. The shell fish are not

generally affected by the toxins but a single clam can accumulate enough toxin to kill a human being [56].

1.6. DETERMINATION OF NITRATE

Determinations of nitrate in natural waters as the single ion and combined with nitrite as Total Oxidised Nitrogen (TON) have been carried out by a variety of methods as shown in Table 1.6.

1.6.1. Chemiluminescence

Chemiluminescence (CL) techniques have been used to determine trace amounts of nitrate and nitrite in seawater [76]. This method depends on selective reduction of the species to nitric oxide which is swept from the sample by a helium carrier gas. The nitric oxide is then reacted with ozone to form nitrogen dioxide. The return of the nitrogen dioxide to the ground state is accompanied by the release of a photon which is subsequently detected by a photomultiplier tube.

The sequence of reactions involved in the CL determination of nitrate are as follows:

1. $NO_3^+ + H^+ \leftrightarrow NO_2^-$

2. $NO_2^- + H^+ \leftrightarrow HONO \longrightarrow NO$

3. $NO + O_3 \longrightarrow NO_2^* \longrightarrow NO_2 + h\nu$

1.6.2. Ion selective electrodes

The nitrate ion selective electrode develops a potential across a thin, inert porous membrane behind which a water immiscible liquid ion-exchanger is held. The electrode responds to nitrate ion activity between 0.14 and 1400 mg l^{-1} Nitrate-N which is currently not sensitive enough for levels found in seawater [80]. A further drawback is that chloride and bicarbonate interfere when their weight ratios to nitrate are > 10:1 and > 5:1 respectively.

26

The electrodes behave satisfactorily in buffered solutions over the pH range of 3 to 9 but can be erratic when pH is not stable. The electrode responds to NO_3^- activity rather than concentration. Therefore, solution ionic strength must remain constant in all samples and standards. This can be achieved by using a buffer solution of silver sulphate to eliminate Cl^- Br^-, I^-, S^{2-} and CN^-, sulfamic acid to remove NO_2^- and pH 3 buffer to eliminate HCO_3^- and to maintain a constant ionic strength.

1.6.3.   Voltammetry

Recent developments in electrode membrane technology have overcome interference and improved sensitivity such as the $[Os\ (bipy)_2(pvp)_{10}Cl]Cl$ modified glassy electrode [79]. This device has been used as a detector for nitrate after first reducing it to nitrite in a FI based system.

1.6.4.   Chromatographic techniques

Various chromatographic techniques have been proposed for the determination of nitrate and nitrite, including ion chromatography [77], ion exclusion chromatography [81] and ion-interaction chromatography [82]. The major advantage of chromatographic techniques is the ability to determine a range of different ions simultaneously, e.g. nitrate, chloride and sulphate. A comparison of ion chromatography, segmented flow analysis and flow injection for the determination of nitrate found ion chromatography and segmented flow analysis to have better detection limits. However, the sampling rate of 30 - 60 samples per hour for FI is significantly better than that of ion chromatography at 10 samples per hour [83].

27

Table 1.6.   Examples of methods for the determination of nitrate in natural waters

Technique	Sample	Method	Linear Range	Reference
CFA	Seawater	Indirect spectrophotometric	$0 - 400\ \mu g\ l^{-1}$	[57]
Manual	Seawater	Indirect spectrophotometric	$0 - 60\ \mu g\ l^{-1}$	[58]
FIA	Seawater, potable, waste	Indirect spectrophotometric	$1 - 25\ \mu M$	[59]
CFA	Natural waters	Indirect spectrophotometric	N/A	[60]
FIA	Natural waters	Indirect spectrophotometric	$0 - 5\ mg\ l^{-1}$	[61]
rFIA	seawater	Indirect spectrophotometric	N/A	[62]
Manual	natural waters	Indirect spectrophotometric	$2 - 100\ \mu l^{-1}$	[63]
FIA	Surface, ground waters	Indirect spectrophotometric	$0 - 2\ mg\ l^{-1}$	[64]
FIA	natural	Indirect spectrophotometric	$0 - 12\ mg\ l^{-1}$	[65]
CFA	seawater	Indirect spectrophotometric	$0 - 5000\ nM\ \&\ 0 - 35\ \mu M$	[66]
FIA	natural	Indirect spectrophotometric	N/A	[67]
FIA	natural	Indirect spectrophotometric	$0.05 - 1.0\ mg\ l^{-1}$ $0.5 - 10\ mg\ l^{-1}$	[68]
CFA	seawater	Indirect spectrophotometric	$0 - 100\ nM$	[69]
FIA	seawater	Indirect spectrophotometric	$1 - 20\ \mu M$	[70]
Potentiometry	Water	Nitrate selective electrode	$1 - 1000\ mg\ l^{-1}$	[71]
Fluorimetry	Natural waters	-	$10^{-4} - 3\ mg\ l^{-1}$	[72]
Polarography	Potable and river waters	Reaction between nitrate and uranyl ion	$10^{-2} - 0.1\ mg\ l^{-1}$	[73]
Polarography	Hydroponic waters	Nitration of organics	$10^{-1} - 70\ mg\ l^{-1}$	[74]
Direct UV	Natural waters	-	-	[75]
Chemiluminescence	Seawater	-	-	[76]
Chromatographic	Seawater	-	-	[77]
Amperometric				[78]
Amperometric				[79]

28

1.6.5. Direct spectrophotometric methods

There have been several methods proposed for direct UV absorption of the nitrate ion at 210 nm for use in natural waters. The sample is first filtered and then acidified with sulphuric acid to remove hydrogen carbonate. Nitrite is then removed by the addition of sulphamic acid. Reliable results have been obtained for natural waters low in organic matter such as humic acid. For waters containing higher levels of organic matter and/or iron, corrections have to be made for the resultant positive bias. The correction factor is usually determined by measuring the solution at absorbance at 275 nm where the nitrate ion has negligible absorbance. The absorbance of the solution at 275 nm is then multiplied by an empirical correction factor. Nitrate concentration is relative to the difference of the two absorbencies but the main problem is that the correction factor is dependent on the nature of the water. Different manual correction methods have been proposed to overcome interference from organic substances such as coagulation with aluminium hydroxide followed by filtration [84] and a zinc-copper reduction of nitrate to assess non-nitrate absorption contribution [75]. Measurement at several different wavelengths followed by empirical correction has also been reported [85]. The problem of interference was also overcome by selective removal of the interfering species by the addition of sodium hydroxide solution to give a sample pH of 12.6. The sample was then passed through an activated charcoal filter [86]. The main drawback with all these manual correction techniques is that they are not easily automated.

1.6.6. Indirect spectrophotometric methods

Methods for nitrate determinations have been based on indirect spectrophotometry after first reacting the sample with reagents such as 2,6 xylenol [87] or brucine [88]. Other

indirect methods require an initial reduction stage of nitrate to nitrite either by homogeneous or heterogeneous reduction methods.

Homogeneous reduction: has been effected by the use of hydrazine [89, 90], where the time to reach equilibrium can be in the region of 20 hours. More recent work on the hydrazine reduction methods has reduced reaction times to around 1½ - 2 hours [91, 92].

Heterogeneous reduction: methods have utilised reduction columns of various dimensions containing a variety of powdered or granular metals such as zinc [93, 94], amalgamated zinc [95], cadmium [96], amalgamated cadmium [97, 63] and copperised-cadmium [58, 66, 98]. Reduction methods utilising cadmium powder and granules have been investigated and optimised by Nydahl. The nitrite yield from the reduction of nitrate using various types of reductors was compared, and the effect of pH, temperature, chloride concentration and contact time (flow rate) through a packed reduction column was investigated. Maximum yield approaches 100% at pH 9.5 and temperature was reported to have little effect between 20 - 30 °C, but at 10 °C the reduction was significantly slower [99]. Copperised-cadmium wire [100,101] and copperised cadmium-silver wire (95% Cd) [60,102] have also been used successfully in the reduction stage. Hydes and Hill [103] described the use of a copperised granulated 50:50 cadmium-copper alloy reduction column and van Staden [104] reported the successful use of a copper tube pre-column followed by a copperised-cadmium tube reduction column. The use of copperised-cadmium is now well established for the nitrate reduction stage for the determination of TON. The reduction conditions are adjusted so that the nitrate is quantitatively reduced to nitrite and no further. The principle reaction is:

$$NO_3^- + Me_{(s)} + 2H^+ \longrightarrow NO_2^- + Me^{2+} + H_2O$$
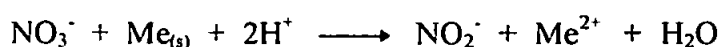
The reduction yield is dependent on the metal used in the reductor, the solution pH, and the activity of the metal surface. The use of a reaction solution which is too alkaline or a metal reductor with an inactive surface will result in partial reduction of the nitrate. Conversely, if the reaction solution is too acidic or the metal reductor is too electronegative or highly active, the reduction process will proceed further than the nitrite step. In both situations low nitrate values will be obtained.

Copperised-cadmium filings or granules are very effective in the heterogeneous reduction stage. However, in weak alkaline or neutral conditions the cadmium ions formed during the nitrate reduction stage react with the hydroxyl ions to form a precipitate. Furthermore, the reduction potential required for the reduction of nitrate to nitrite is dependent on the hydrogen ion activity within the solution. This suggests that the pH is changed if the solution is not buffered especially in the vicinity of the metal reductor surfaces. The pH of seawater rarely falls outside the limits of 7.7 - 8.2 [105] and therefore ammonium chloride is added to act as a buffer and as a complexant:

$$2NH_4^+ \longrightarrow 2NH_3 + 2H^+$$

$$Cd^{2+} + 2NH_3 \longrightarrow [Cd(NH_3)_2]^{2+}$$
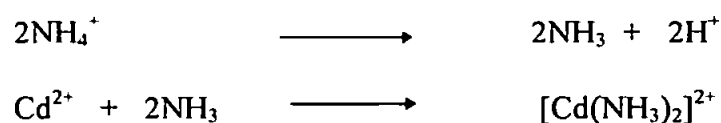
The ammonia is bound in the diamine complex. Under controlled conditions, nitrite that is present in the seawater passes through the reduction stage without further reduction. This will therefore contribute to the total value as Total Oxidised Nitrogen (TON) at the subsequent diazotisation and coupling stage.

The most commonly used chemistry involves the diazotisation of the reduced nitrate and subsequent coupling with sulphanilamide and N-(1-naphthyl)ethylenediamine [106] as

shown in Fig. 1.7, which has been optimised for field use for a period of 30 days in a remotely deployed FI based TON monitor [107].

$$H_2N - O_2S \underbrace{\qquad}_{\text{Sulphanilamide}} NH_2 + NO_2^- + 2H^+ \longrightarrow$$

$$\left[H_2N - O_2S \underbrace{\qquad}_{\text{Diazonium ion}} N=N \right]^+ + 2H_2O$$

$$\underbrace{\qquad}_{\text{N-(1-naphthyl) ethylenediamine}} \begin{array}{c} NH \\ | \\ CH_2 \\ | \\ CH_2 \\ | \\ NH_2 \end{array} \quad +$$

$$H_2N - O_2S \underbrace{\qquad}_{\text{Azo dye}} N=N \underbrace{\qquad} \begin{array}{c} NH \\ | \\ CH_2 \\ | \\ CH_2 \\ | \\ NH_2 \end{array} + H^+$$
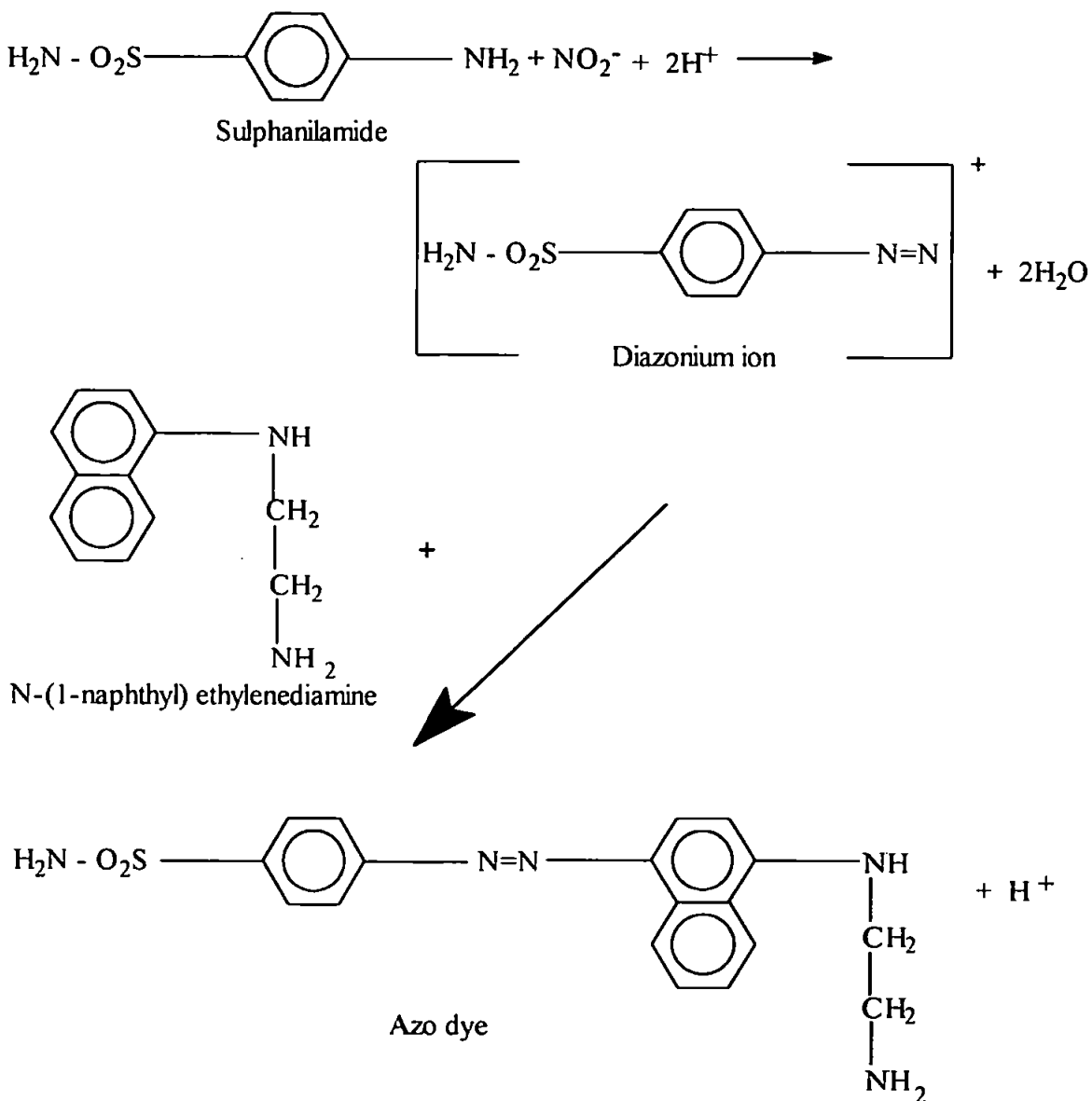
Figure 1.7.   Diagram showing the various stages of the diazotisation and coupling reaction

1.6.7.   Automated methods

Since the early 1960's there has been a requirement for water laboratories to carry out increasing numbers of routine analyses. Method automation has enabled these increasing numbers of samples to be analysed with improved efficiency. Discrete analysers, air

segmented continuous flow analysers and flow injection analysers have handled the bulk of this automation and improvements in both hardware and software have improved reliability and reduced the risk of human error.

Discrete analysers: are computer controlled systems which analyse the samples sequentially for the chosen determinands. A typical instrument of this type essentially consists of a computer module and a chemistry module.

The computer module controls the operation and data processing functions of the system. The chemistry system typically comprises of the following:

1. a sample carousel.

2. a temperature controlled reaction carousel to provide reproducible reaction and final colour development.

3. a sample probe to facilitate transfer of sample from sample carousel to reaction tube.

4. reagent reservoirs and delivery system.

5. mixers.

6. a suitable spectrophotometer for the particular determination.

For each method the following parameters are pre-programmed: Sample/diluent volumes, reagent dispense volumes, reaction temperatures, mixing requirements, reaction time, detection conditions and mathematical computations performed.

Discrete analysers are versatile, simple to operate and can deal with large sample numbers. Many are highly sophisticated and consequently require minimal operator intervention and can usually operate unattended. This removes the risk of operator error and improves analytical precision..

Air segmented continuous flow analysers: are in widespread use in the water industry and nitrate determination in natural waters is one of the most frequent methods for which the technique is applied [108]. It is based on the fundamental principles of Skeggs

33

[109] and converts a series of discrete samples into a continuous flowing stream by a pumping system. Reagents are added by continuous pumping and merging of the sample and reagent streams. This stream is segmented with air before reagent addition which typically allows between 20 and 80 samples to be processed in an hour. The insertion of standards in the sample steam provides regular datum points during a particular analysis. There is usually no problem with distinguishing between the samples at the detection stage as the regular timing between stages is controlled. However, unless precautions are taken to prevent carryover, interaction can occur in a continuous system causing loss in discrimination between successive samples at the detection stage.

Following the work on nitrate determinations in sea water by Morris and Riley [97] in 1963, Brewer and Riley [57] eliminated some of the problems associated with air segmented continuous flow techniques by using EDTA to segment the stream. Oudot and Montel [66] devised a high sensitivity method for the determination of nanomolar concentrations of nitrate and nitrite in sea water using a air-segmented CFA. The technique has also been applied to the analysis of silicate [110, 111], phosphate [110] and ammonia [112].

Air-segmented continuous flow analysis has been widely used at sea for the analysis of all major nutrient species and until the mid 1980's was the only technique that was available at a reasonable cost for the automated analysis.

Flow injection analysis: (FI) techniques were developed by Ruzicka and Hansen [113, 114] to overcome some of the practical problems associated with air segmented continuous flow analysis that were perceived by some workers [108]. FI differs from air-segmented continuous flow analysers in that the sample is injected directly into a moving stream without the addition of air. The main distinction between air-segmented CFA and FI is that the continuous mixing of sample and reagents in a turbulent stream segmented by bubbles is replaced by periodic mixing in an unsegmented laminar stream. Periodic mixing is achieved

by injecting the sample, or reagent in the case of Reverse Flow Injection, into a carrier stream flowing to the detector, where the analyte species forms in the reaction zone which contains both sample and reagent. The reaction does not have to go to completion, and due to the flow being incompressible, the extent of the reaction will be similar in all samples. This gives significant advantages over air-segmented CFA, including faster analysis rates and less complicated equipment which has resulted in FI being readily adapted to the analysis of sea water nutrients. In 1979, Anderson [59] described a method for the simultaneous determination of nitrite and nitrate using flow injection analysis. It allowed up to 30 samples per hour to be analysed with a relative precision of 1 % in the range 0 - 0.05μ M for Nitrite-N and 0 - 0.1μM for Nitrate-N. Similar work was carried out later that year by Gine *et al.* [61] where up to 90 samples were analysed with a relative precision of 0.5 and 1.5 % for nitrite and nitrate respectively; in the range of 0.1 - 0.5 mg l^{-1} for NO_2 and 1 - 5 mg l^{-1} for NO_3. Van Staden *et al.* [64] reported a development of this method that utilised copperised cadmium wire in a pre-valve in-valve reduction technique, to allow synchronous determinations of nitrite and (nitrite + nitrate) using one manifold and detector. In 1983 Johnson and Petty [62] described a modification to previous methods by using reverse flow injection analysis whereby the sample was the carrier stream and reagents injected into it. Using a flowcell of Betteridge *et al.* [115] design, this method gave a LOD of 0.1μM and allowed up to 70 samples per hour to be analysed with a relative precision of 1 %. FI is finding increased use in the water industry where laboratories which had previously used air-segmented CFA have introduced FI to complement their working practices. FI is the preferred technique for small batch sizes and low level concentrations where speed of analysis is essential to eliminate the risk of airborne contamination. FI techniques are also readily adaptable to on-line monitoring of a water course.

Over the past 20 years, FI has been established as a reliable technique with the level of sensitivity for monitoring micronutrient species in the environment and has been accepted as a standard method for the examination of waters and associated materials [116] for which laboratory instrumentation is readily available [68]. It is for these reasons that FI has been selected as the technique for incorporation in a submersible nutrient sensor; the basic principles of which are described in greater detail in the section 1.7.

1.7.   FLOW INJECTION ANALYSIS

1.7.1.   Basic principles

Flow Injection (FI) is based on the injection of a liquid sample into a moving, unsegmented carrier stream of a suitable liquid. The injected sample forms a zone which is transported towards a detector that continuously records the absorbance, electrode potential or other parameter as the sample passes through the flow cell [117, 113, 114]. FI is finding increasing applications in research, routine analysis, teaching of analytical chemistry, monitoring of chemical processes, sensor testing and development, and enhancing the performance of various instruments as well as measurement of diffusion coefficients, reaction rates, stability constants, composition of complexes and extraction constants and solubility products [118, 119, 120, 121, 122, 123]. The versatility of FI has allowed the method to be adapted to different detection systems such as electrochemistry, molecular spectroscopy and atomic spectroscopy, using numerous manifold configurations. FI systems may be designed to dilute or to preconcentrate the analyte; to perform separations based on solvent extraction [124], ion exchange [125], gas diffusion or dialysis [126]; and to prepare unstable reagents *in situ*. Examples of FI manifolds are shown in Figure 1.8.
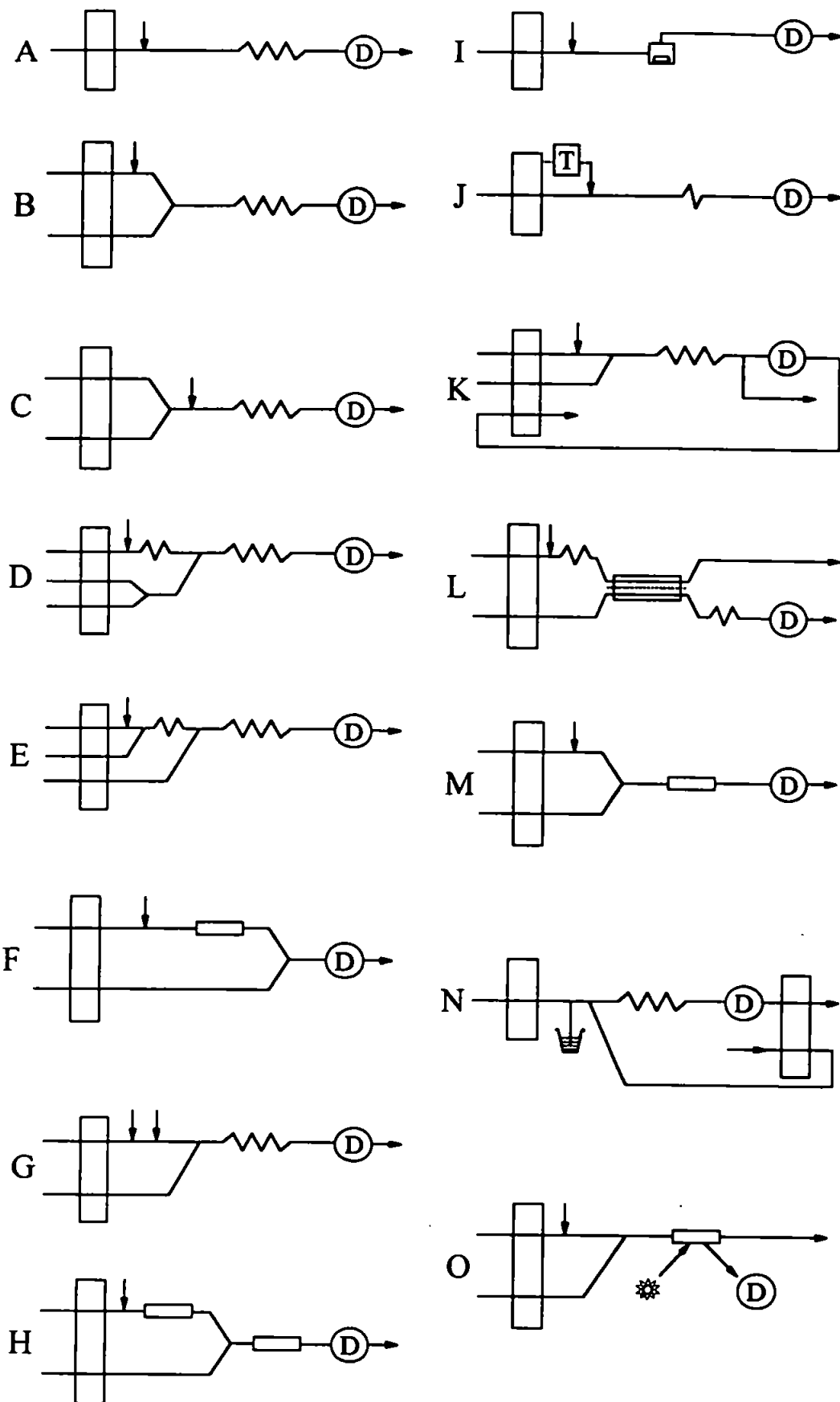
Figure 1.8.   Examples of FI manifolds:

A. single line; B. twin line with single confluence point; C. reagent pre-mix into single line; D. twin line with reagent pre-mix and single confluence point; E. three line with two confluence points; F. packed in-line reaction column; G. double injection and single confluence; H. sequential reactors (with immobilised enzymes); I. single line with mixing chamber; J. single line stopped flow; K. solvent extraction; L. dialysis, ultrafiltration or gas diffusion; M. twin line, single confluence with packed reactor; N. hydrodynamic injection; O. twin line single confluence optosensing on solid surface.

37

Optimisation and design of the flow channels to achieve maximum sampling frequency, best reagent and sample economies, and proper exploitation of the chemistries is possible through understanding of the physical and chemical processes taking place during the movement of the fluids through the FI channel.

The simplest FI analyser, shown schematically in Fig. 1.9., consists of a pump, which is used to propel the carrier stream through a narrow tube; an injection port, by means of which a well-defined volume of a sample solution is injected into the carrier stream in a reproducible manner; and a microreactor in which the sample zone reacts with the components of the sample stream, forming a species which is sensed by a flow through detector and recorded.
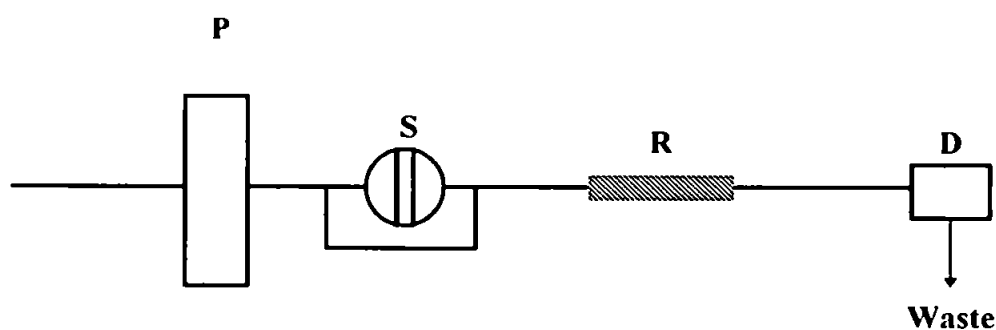
Figure 1.9. Schematic diagram of a simple FI system. where P is the pump, S is the injection valve, R is the reaction column and D is the detection system.

A typical recorder output from a simple FI system has the form of a peak as shown in Figure 1.10. The height (H), width (W) or area (A) are all related to the concentration of the analyte. The time span between the sample injection (S) and the peak height (H), is the residence time (T), during which the chemical reaction takes place. With rapid response times, typically in the range of 5 - 20 seconds, a sampling frequency of two samples per minute can be achieved. The injected sample volumes may be between 1 and 200 µl which in turn requires no more than 0.5 ml of reagent per sampling cycle. This makes FI a simple,

automated microchemical technique, which is capable of a high sampling rate and a low sample and reagent consumption.
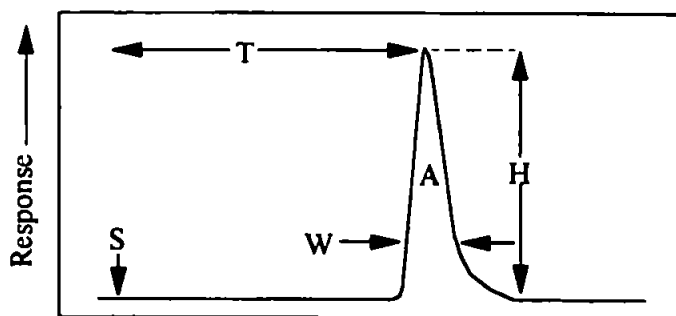
Figure 1.10. Typical output from a chart recorder connected to a simple FI system. Recording commences at S, H is the peak height, W is the peak width, A is t he peak area and T is the residence time.

FI is based on the combination of three principles: Sample injection, controlled dispersion of the injected sample zone, and reproducible timing of its movement from the injection point to the detector. The chemical reactions take place whilst the sample material is dispersing within the reagent, the concentration gradient of the sample zone being formed by the physical dispersion processes where the sample zone broadens as it moves downstream and changes from the original asymmetrical shape to a more symmetrical and eventually Gaussian form [114]. For standard conditions, the procedure is totally reproducible in that one injected sample behaves the same way to all other subsequently injected samples.

1.7.2. Dispersion coefficient (D)

A sample contained in the sample loop of the injection valve is homogeneous and has an original concentration C^o that, if it could be scanned by a detector, would give a square

signal the height of which would be proportional to the sample concentration. When the sample zone is injected, it follows the movement of the carrier stream, forming a dispersed zone, the form of which depends on the geometry of the channel and the flow velocity [127]. Therefore, the response curve has the shape of a peak reflecting a continuum of concentrations (concentration gradient). This continuum of concentrations can be viewed as being composed of individual elements of fluids, each having a certain concentration, C. The dispersion coefficient, D is defined as the ratio of concentrations of sample material before and after the dispersion process.

$$D = C^\circ/C$$

If D = 2, the sample solution has been diluted 1:1 with the carrier stream. For convenience, sample dispersion has been defined as limited (D - 1 - 3), medium (D - 3-10), and large (D > 10). The FI peak is a result of two kinetic processes that occur simultaneously: the physical process of zone dispersion and the chemical process resulting from reactions between sample and reagent species. The underlying physical process is well reproduced for each individual injection cycle; yet it is not a homogeneous mixing, but a dispersion, the result of which is a concentration gradient of sample within the carrier stream. The dispersion coefficient is a theoretical concept, which does not correspond to any actual concentration within the dispersed sample zone. A dispersed sample zone is not composed of discrete elements of fluid, but only imagined by the detector at any time as an apparent discrete section of the concentration gradient. The D value is always related to a certain time, which is the period elapsed from the sample injection, to the moment the dispersed element of sample material passes through the observation field of the detector.

1.7.3.   Effect of sample volume on peak height

By injecting increasing volumes of solution, a series of curves will be recorded, all starting from the same point of injection S. The height of the individual peaks will increase until an upper limit steady state has been reached. At this final level the recorded absorbance will correspond to the concentration of undiluted sample $C^°$, and D = 1. The rising edge of all curves coincides and has the same shape regardless of the injected volumes. Where n = Sv / $S_{1/2}$, Sv is the sample volume, and $S_{1/2}$ is the volume of the sample solution necessary to reach 50 % of the steady state value, corresponding to D = 2. By injecting two $S_{1/2}$ volumes, 75 % of $C^°$ is reached, corresponding to D = 1.33; and so on. Injection of five $S_{1/2}$ volumes results in D = 1.03 and injection of seven $S_{1/2}$ volumes results in D = 1.008, corresponding to 99.2% of $C^°$. An increase in peak height and in sensitivity of measurement is achieved by increasing the volume of the injected sample solution. Dilution of overly concentrated samples is best achieved by reducing the injected volumes.

1.7.4.   Effect of channel length and flow rate on peak height

The microreactor between the injection port and the detector may have different lengths, diameters, and geometry. The influence of coil length (L) and inner diameter of the tubing (d) on the dispersion has been studied in detail [117]. The use of small diameter tubing will result in lower $S_{1/2}$ values, because the same sample volume will occupy a longer length of tube (θ) since Sv = $\pi(5d)^2\theta$ and will, owing to the restricted contact with the carrier stream, be less easily mixed and dispersed. If the tube diameter (d) is halved, the sample will occupy a fourfold longer portion of the tube (θ), and, hence, the $S_{1/2}$ value will be four times smaller. There are practical considerations that prevent the use of channels with too narrow a bore or too tightly packed reactors because; the flow resistance will increase; the

system might easily become blocked by solid particles, and the flow cell used in spectrophotometic detector must have an optical path with an inner diameter of 0.5 - 1 mm, to allow sufficient light to pass through. The optimum internal diameter of tubes (usually PTFE) connecting the injection port and the detector is 0.5 mm although 0.75 mm internal diameter is useful for the construction of systems with large dispersion, and 0.3 mm for systems with limited dispersion. The mean residence time (T) will depend, for a reaction system made of tubing of uniform internal diameter, on the tube length (L), the tube diameter (d), and the pumping rate (Q). For systems of medium dispersion, where the sample has to be mixed and made to react with the components of the carrier stream, an increase in the tube length (L) in order to increase (T) would be required. However, dispersion of the sample zone increases with the distance travelled, and this band broadening eventually results in loss of sensitivity and lower sampling rate. This effect can be eliminated by decreasing the pumping rate (Q) and keeping (L) as short as is practically possible.

1.7.5.   Effect of channel geometry on peak height

The effectiveness of various mixing geometry's is shown in Fig. 1.11. A coiled tube is the most frequently used geometric form of the FI reaction column. There are however different channel geometry's, these are: straight tube, coiled tube, mixing chamber, single bead string reactor, and 3D or knitted reaction column. The function of these all reaction columns is to increase the intensity of radial mixing. Thus, the reagent becomes more readily mixed with the sample, and the axial dispersion of the sample zone is reduced. In a straight tube of uniform diameter, the parabolic profile formed by laminar flow remains undisturbed up to a flow velocity not normally reached in a typical FI system, and since the radial diffusion occurring in the time frame of an FI experiment is not sufficient to offset the axial dispersion

initially formed during sample injection, an asymmetrical peak is recorded. A coiled tube is

the most frequently used reactor geometry since it can conveniently accommodate any

length of tubing in an experimental set-up and also because secondary flow within the coiled

tubing promotes mixing in the radial direction.
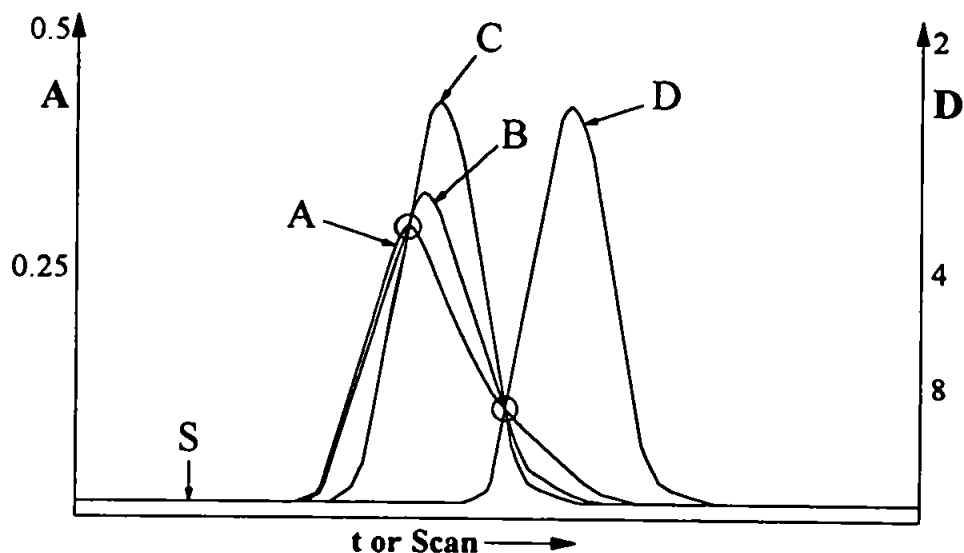
Figure 1.11. **Dispersion of a dye injected as a sample zone into reaction columns of**

identical lengths with different configurations. A, straight tube; **B,** coiled
tube; **C,** 'knitted tube'; **D,** SBSR reactor [117]

The result is a more symmetrical, higher and narrower peak than if an identical straight tube

length had been used. The tighter the coiling of the tube is, the more pronounced this effect.

Also, the longer the tube is, the longer the time for mixing and therefore a more symmetrical

peak is obtained.

The mixing chamber was first used in the early FI titration systems [117] where a magnetic

stirrer was used to promote reproducible homogeneous mixing of sample and reagents. But

the use of this type of geometry has many drawbacks, such as large dispersion giving

reduced sensitivity, low sample throughput and large sample and reagent volumes, which is

undesirable for systems which need to moderate their consumption. A single bead string

reactor (SBSR) [128] is the most effective device to promote radial mixing in a tubular reactor. The SBSR allows symmetrical peaks to be obtained within the time domain and channel length of a typical FI manifold. However, small air bubbles and solid particles tend to be trapped in SBSR which may increase carry-over and flow resistance. A three dimensional disorientated (3-D reactor) or 'knitted' reactor can be made by tightly and irregularly knotting a suitable length of tubing. The chaotic movement of the carrier stream through a spatially disorientated path promotes very effective radial mixing without the drawbacks of a single bead string reactor.

1.8.   *IN-SITU* MONITORING

Pollution of the world's water poses a major threat to the health and well-being of millions of people and global eco-systems. Loss of biodiversity through the extinction of certain species caused by anthropogenic activities has given rise to governmental and regulatory bodies taking action against polluters. To achieve this, there is a need for a greater understanding of the various background environmental processes for which the means of conducting continuous studies is essential.   Long-term studies and continuous measurements using research vessels is logistically and cost prohibitive. Therefore, reliable low cost in-situ techniques offer a solution to this problem.

The current problems associated with compiling long-term or continuous data can be summarised as follows:

• High cost and logistics of using research vessels for long-term routine surveys.

• Samples collected for analysis at a later time relies on good sample preservation techniques. This can lead to erroneous results with no means of replacing samples.

- Trace metal analysis requires elaborate cleanroom conditions to avoid contamination from the laboratory environment.

- Existing methods require some degree of human input to perform tasks which can introduce experimental error.

- Weather conditions during research cruises may not permit complete data sets to be compiled.

- Processing of data can take several months.

Quantitative knowledge of nutrients and primary production is essential for investigating the ecology and biogeochemistry of aquatic ecosystems.

Nitrate levels are currently measured by collecting discrete samples from a particular study area which can either be analysed at the collection site if convenient or transported to a central laboratory to be analysed later. This monitoring scheme may not detect short-term changes such as storms events or point discharges between sampling events. There is considerable evidence to suggest many of the sample preservation techniques introduce some level of variance into nitrate determinations. For example, freezing of coastal and estuarine water at -10 °C for nitrate determination was found to give variance on samples tested [129] whereas freezing at -20 °C was found to be acceptable by Clementson *et al.* [130]. The US EPA [131] methodology for analysis for anions in water states that unpreserved samples must be analysed within 48 hours otherwise they can be preserved with sulphuric acid at pH < 2 for 28 days. However, this has been shown to have an effect on environmental samples where nitrite is converted to nitrate by further microbial activity, whereas pH 12 is thought to eliminate the conversion causing bacteria [132]. Consequently, significant errors may be introduced into preserved samples and in both cases

the cost and logistics of continuously monitoring a particular environment would generally be prohibitive.

Advances in analytical chemistry have made it feasible to perform a wide range of chemical determinations *in-situ*. The development of flow injection techniques and light-emitting diode/photodiode detectors have been particularly important in this respect. The application of *in-situ* automated FI techniques can produce low-cost, rapid analysis with high sampling frequency analytical systems that are simple and easily maintained [133]. Clinch *et al.* [65, 134] developed an automatic field nitrate monitor based on FI that successfully completed a 9 month field trial on the River Frome in Dorset [135]. FI techniques have also been developed for environmental monitoring of phosphate [136] ammonia [137] aluminium [138], all using solid state LED/photodiode detectors. These early systems were based on mains powered microcomputers which are unsuitable for use in portable battery powered systems. Advances in microchip technology have resulted in the availability of specialised microcontroller devices for control and automation of a variety of everyday uses. This technology has been exploited in the development of *in-situ* FI monitoring systems for the analysis of nitrate and phosphate in freshwater [139, 140]. The microcontroller system used in these instruments automated all functions required for a field-based operation, i.e. control of peristaltic pumps, injection and switching valves, data acquisition, processing and logging. The systems are powered by 12 volt sealed lead-acid batteries which are capable of 2 - 3 weeks operation depending on the mode of operation.

There are additional constraints for the *in-situ* monitoring of seawater, i.e. systems must be submersible to facilitate measurements at a particular point in the water column. In 1986 and 1989 Johnson *et al.* [141, 142] reported the use of a submersible FI system to monitor silicate, sulphide and nitrate concentrations in sea water that gave good correlation with laboratory techniques to depths of 2500 m and pressures of 1000 Bar. The effects these

extremes of temperature, pressure and salinity on flow analysis and chemistries used in these systems have all been studied [143].

1.9. RESEARCH OBJECTIVES

The overall objective of the study was to develop a submersible FI based sensor for the *in-situ* determination of nitrate in estuarine and coastal waters.

Specific objectives were:

1. To design and construct a solid-state FI manifold for the determination of nitrate in estuarine and coastal waters, with a limit of detection of 0.001mg l^{-1} and a linear range of 0 to 1.0 mg l^{-1} Nitrate-N.

2. To compare the analytical performance of the FI manifold based system with a validated laboratory technique in terms of detection limit, precision, accuracy and linear range.

3. To design and construct rugged submersible instrumentation to enable *in situ* nitrate determinations to be carried out at depths of up to 30 metres.

4. To compare the analytical performance of the integrated submersed system with a validated laboratory technique for Tamar estuary samples.

5. To compare the submersible FI instrumentation for nitrate determination with the traditional continuous flow methodology (Autoanalyzer®) during a North Sea cruise.

Chapter Two
Design Specification

2. DESIGN REQUIREMENTS

This chapter describes the requirements for each of the key parameters for a submersible field instrument, i.e., construction, operation and performance and the justification for their selection. The key specifications are given in the conclusions section.

2.1. SYSTEM REQUIREMENTS

The following criteria were established for the sensor at the start of the research in order to meet the scientific objective of providing useful and validated environmental analytical data for total oxidised nitrogen (TON) in coastal and estuarine waters.

- **Autonomous** - capable of automatic control of pumps, sample injection valve, switching valve, etc. with on-board computer control.

- **Submersible** - operate at depths of up to 30 metres in coastal and estuarine waters.

- **Compact** - capable of deployments from small research vessels that do not have heavy lifting gear.

- **Modular system** - different specification components to be selectable depending on the type of deployment.

- **Continuous monitoring** - Able to operate for one full tidal cycle, i.e. up to 13 hours operation, at 30 minute intervals without the need for human intervention.

- **Rugged construction** - able to withstand harsh environmental conditions and rough handling during deployment and retrieval.

- **Low running costs** - low reagent consumption to permit extended deployments.

- **Simple field maintenance** - service and consumable items able to be replaced quickly.

- **Accuracy and Precision** - must be comparable to a laboratory FI system with an overall target of ± 5 %, see section 2.4.

- The initial design concept for the integrated system is shown in Fig. 2.1. and illustrates how the modular approach was perceived.

Reagent module containing reagent bags

Sample inlet

Filtration module

Instrument module

Battery pack
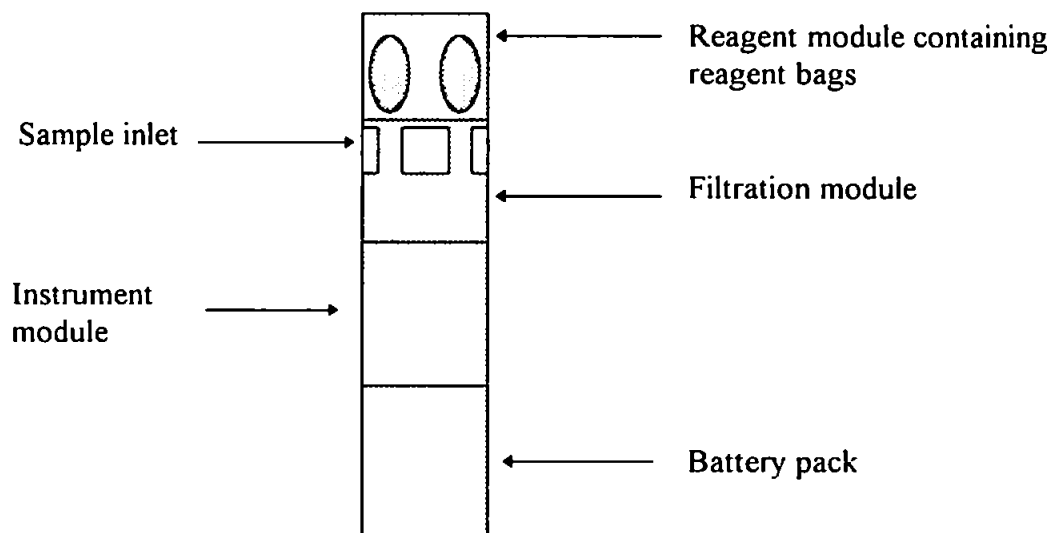
Figure 2.1.   Schematic diagram of the initial modular design concept for the integrated system

It is recognised that in the longer-term a multi-chemistry system, e.g. nitrate and phosphate, would offer distinct scientific advantages but it is important to emphasise that the primary aim of this research was to produce a reliable single chemistry system. Nitrate was selected as the rate limiting nutrient in most coastal waters [6] and because of its importance in maintaining drinking and freshwater quality [42,46]. During the project, two commercial *in situ* nitrate sensors based on syringe pumps [144,145] and a direct reading UV system [146] were introduced onto the market but have not yet been shown to be totally reliable. It was felt that the FI approach would not only produce a reliable system for the determination of nitrate *in situ* but that the established benefits of on-line sample treatments and flexible chemistries [113,114] would provide greater versatility than the syringe based approach.

49

2.2. SAMPLE TREATMENT

The different deployment locations for which the sensor is designed will invariably require some form of sample treatment due the levels of suspended material such as plankton and organic and inorganic particulate matter found in these waters. For example, daylight falls to approximately 1 % of its surface value at approximately 100 m in clean oceanic waters. In coastal waters this value is reached at approximately 10 - 30 m. In turbid estuarine waters the same value is reached at less than 3 m [147]. In surface waters the total suspended matter concentrations are higher and more variable in coastal and estuarine waters than they are in the open ocean [148]. This is caused by the combined inputs of particulates from river run-off and atmospheric transport and the internal generation of particulates from primary production. On a global scale, approximately 90% of riverine particulate material is retained in estuarine systems. The material that does escape has a higher concentration in coastal waters than in open ocean waters and in some situations plumes of suspended material can be transported for considerable distances. For example, in periods of high discharge the Amazon can form a plume with concentrations of total suspended material exceeding 5000 μg l^{-1} and extending seawards for approximately 100 km [149]. Concentrations of total suspended matter exhibit large temporal and spatial variations. For example, < 100 to > 3000 μg l^{-1} have been reported in a variety of coastal regions but concentrations of total suspended matter can fall as low as < 10 μg l^{-1} in open ocean waters [150]. Failure to incorporate the appropriate level of filtration in the nutrient sensor would result in poor peak resolution caused by scatter within the flowcell and premature degradation and/or blockage of the reduction column. Larger material would quickly cause complete blockage of the switching and injection valves. For the coastal and estuarine water deployments intended during the development and field testing of the

sensor, membrane filters were considered to be the most suitable method of providing simple but effective sample filtration. Membrane filters are generally blocked by particles close in size to that of pore size of the filter. Filter life may also be prematurely curtailed by loading with larger particles so the use of a pre-filter is a successful method of prolonging filter life. By employing one or more pre-filters to remove contaminants of decreasing size the final filter can be protected, thus optimising performance and filter life [151]. Any filtration system utilised will introduce some level of flow restriction to the instrument and therefore it is important to select the correct level and type of filter medium for the application. If the filter media is too restrictive causing poor flow rate, the pumping system will be unable to initiate and maintain adequate flow rates throughout the system. The flow rate through the sample line will be approximately 15 ml min $^{-1}$, therefore the flow rate for the filter must be greater than this. Typical flow rates for syringe type membrane filters [152, 153] are shown in Table 2.1.

Table 2.1.   Typical flow rates for syringe type membrane filters

Diameter/Pore size	Flow rate for water (ml min $^{-1}$ @ 2 bar)					
	5.0 μm	3.0 μm	0.8 μm	0.45 μm	0.2 μm	0.1 μm
25 mm ∅	19.6	14.7	8.1	2.2	1.3	0.9
47 mm ∅	69.4	52.1	28.6	7.8	4.7	3.1

A 25 mm diameter syringe filter, as shown in Fig. 2.2., was selected to minimise the filter dead volume (typically ≤ 50 μl for a 25 mm diameter filter) so that the flush through time of the sample line would be kept to a minimum. This would allow a higher sampling rate if required, i.e. sample line is completely flushed through thus avoiding memory effects from the previous sample.
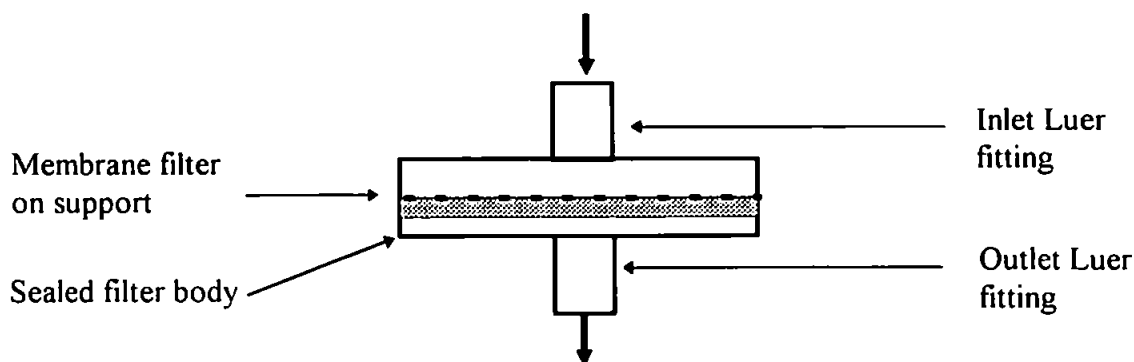
Figure 2.2.   Schematic diagram of syringe membrane filter

For sample treatment purposes for the prototype sensor, sterile non-pyrogenic 25 mm diameter 5.0 µm pore syringe filters were selected. 'Gelman' Sciences syringe filters, type 'Versapore' acrylic copolymer on non-woven support were initially selected for the Plymouth coastal and estuarine water deployments. This type of filter medium is particularly suited to the filtration of reagents, pharmaceuticals and biological solutions and unlike some filter media it does not affect the reliability of nutrient determinations [154]. It is a non-migrating medium, i.e. no shedding of particulates into the filtered stream, which ensures a cleaner downstream effluent which will not cause blockage to valves and the flowcell. Other membrane materials such as PTFE and polypropylene would have also been suitable. For longer deployments in very heavily loaded waters an additional filtration module would be required which would need an additional power and control system.

2.3.   ANALYTICAL PERFORMANCE

Limit of detection: For the examination of waters and associated materials, laboratory FI instruments are required to have a limit of detection of 0.12 mg l^{-1} NO$_3$-N [116] or better. The levels of nitrate in estuarine, coastal and open ocean waters vary considerably as shown in Table 2.2., which makes the selection of an appropriate limit of detection (LOD) and

linear range dependent on the location of the deployment. From the levels reported, it was decided to set a LOD of 0.01 mg l^{-1} Nitrate-N for the prototype nutrient sensor in order to accommodate any deployment scenarios.

Table 2.2.   Typical Nitrate-N concentrations found in natural waters.

Location	Mean nitrate concentration		Reference
	mg l^{-1} NO_3-N	μM NO_3-N	
Estuaries	0.01 - 10	0.7 - 714	[155]
Coastal waters	0.01 - 0.06	0.7 - 4.2	[155]
Deep Ocean	0.025 - 0.5	1.7 - 35.7	[97]

To date, comprehensive information on the analytical performance of commercial field instruments is not available. For one commercial syringe-based wet chemistry system, ranges from 0 - 120 μM are quoted [144]. This is reported to be selectable over 3 separate steps, i.e. varying cell path lengths of 5, 10 and 20 mm. This suggests ranges of 0 - 40, 40 - 80 and 80 - 120 μM [144, 156]. Another syringe-based wet-chemistry system is quoted as having an accuracy of $\pm$ 2 % of calibration values during the maintenance-free time [145]. First results from the 'Valeport' direct-reading UV nitrate sensor suggests a range of 4 - 12 μM (0.05 - 0.17 mg l^{-1}) Nitrate-N[146].

Dynamic Range: The prototype sensor was required to determine TON levels in estuarine and coastal waters. Therefore the instrument should be capable of measuring TON levels found in both of these situations. Nitrate levels vary considerably in these locations, so it was essential for the system to have the capability of the linear range being user-set prior to deployment. Another option would have been to have a system that was range selectable *in situ* during deployment. For the purposes of this investigation however, a pre-selected

range was considered to be the most appropriate approach rather than incorporating more complicated switching routines which could lead to more downtime. Given that the majority of the field testing would be carried out in Plymouth coastal waters and the Tamar estuary, it was decided to set a range of 0 - 1 mg l^{-1} (0 - 73 μM). This range was encountered during the work carried out to optimise the coupling and diazotisation chemistry for *in-situ* deployments [107].

Precision: The precision of a flow injection (FI) system depends on the detector stability, the reproducibility of the sample injection, the physical dispersion of the sample slug within the system and the chemical reaction which is being used. During the sample residence time within the FI system, the extent to which sample and carrier mix is controlled by the fluid flow patterns in the reaction zone. Most FI analyses are based on the measurement of a species resulting from the mixing and reaction of the sample with the appropriate reagent so adequate mixing is required. However, as the extent of mixing increases, sensitivity and sampling frequency will decrease, i.e. very broad shallow peaks with long residence time in the system. Therefore, correct design of the FI manifold and the use of precision components are essential if good analytical performance is to be achieved. The construction of the FI manifold is also important as the flow properties within such a system can change significantly if the tubing is not in a fixed position. For example, if the length of tubing used as the reaction column is simply coiled loosely and allowed to move freely the extent of axial mixing within the tube will be reduced and change as the tube moves, thus affecting sensitivity and precision. It is therefore essential to be able to maintain the standard instrument configuration even when tubing is replaced during maintenance.

Precision is defined as the agreement between a set of replicate results of the same parameter and this can only be shown by extensive bench testing with known standards, i.e.

in this situation by looking at the raw output from the detector. It is a measure of the random error in an analytical method and is usually expressed as a standard deviation, or more usefully as a relative standard deviation (rsd) A target precision of ± 5 % for within batch and ± 5 % day to day variance was set.

Accuracy: The accuracy of the system is the closeness of the result to the true value. This was also set at ± 5 % and was assessed by comparing results for estuarine with those obtained using a laboratory FI procedure, which was benchmarked by participation in an ICES Intercomparison Exercise for Nutrients in Sea Water (NUTS I/C 5) [157].

2.4. SALINITY

Spectrophotometry depends on the production of a chromophore with a linear concentration-absorbance relationship. However, this relationship is sometimes difficult to obtain in FI due to a refractive index effect known as the Schlieren Effect. This effect can contribute to the observed signal and is more evident in a single channel system if the sample reaches the detector without proper mixing with the carrier stream [107, 115, 143, 158, 159]. The sensor is designed to operate in estuarine and coastal waters and therefore should be optimised for TON determinations in the complete salinity range of 0 to 35 ‰. Therefore, the appropriate precautions should be taken to overcome the effects of the refractive index (RI) difference between the carrier and sample streams. Inadequate mixing of sample and carrier streams produces a number of liquid interfaces, all with a different RI, which consequently affects the amount of light falling on the detector. The resultant sample signal in this situation can be noisy with a decrease in sensitivity and reproducibility. The effect is more pronounced at the front and tail of portion of a sample peak where the

concentration and RI gradients are highest. Good mixing conditions produce a continuous concentration gradient along the injected sample. Therefore, the manifold design should produce sufficient mixing prior to the detector and the detector should also be designed to help reduce this effect [115]. If a well mixed peak reaches the detector in a pulsed fashion, i.e. through poor sample delivery, the Schlieren Effect can manifest itself as a undulating signal sample peak, where the oscillations are determined by the frequency of the pulsations. There have been numerous reported methods for minimising the Schlieren effect, e.g. by injecting the sample into a chemically inert carrier stream, e.g. water, and adding the reagent downstream at a confluence point [158, 160] and dual wavelength detection [143]. For a field instrument to perform reliably it has be to be relatively uncomplicated. Therefore in this research, the focus was on optimising fundamental instrumental parameters such as injection volume, reduction column design, diazotisation reactor length, mixing geometry and flowcell design, all of which have a marked effect on the Schlieren signal in a FI system.

2.5.   POWER REQUIREMENTS

The selection of a suitable power supply must be made early in the design process so that the housing can be tailored to accommodate all of the major components and therefore the power pack dimensions must be included in the overall design. The important considerations [161] which influence the selection of a particular battery include:

Type of battery: primary, secondary or reserve.

Electrochemical system: matching the advantages/disadvantages and battery characteristics with the system requirements.

56

Voltage: nominal or operating voltage, maximum and minimum permissible voltage, discharge profile, start-up time, voltage delay.

Load current and profile: Constant current, constant resistance or constant power; value of load current, single-valued or variable load, pulse load.

Duty cycle: Continuous or intermittent.

Temperature requirements: Temperature range over which operation is required.

Service life: Length of time operation required.

Physical requirements: Size, shape, weight and type of connections.

Shelf-life: Active/reserve battery system; charged/discharged state; storage time, temperature and other conditions.

Charge-discharge cycle (if rechargeable): Float or cycling service; life or cycle requirement; availability and characteristics of charging source; charging efficiency.

Environmental conditions: Vibration, shock, spin, acceleration, atmospheric conditions, (pressure, humidity, temperature)

Safety and reliability: Permissible variability; failure rates; freedom from outgassing or leakage, use of potentially hazardous or toxic components, type of effluent or significant gases.

Unusual or stringent operating conditions: Very long term or extreme temperature storage, standby or operation, high reliability for special applications, rapid activation for standby batteries, no voltage delay, special packaging for batteries, unusual mechanical requirements.

Maintenance and resupply: Ease of battery acquisition, accessible distribution, ease of battery replacement, available charging facilities, special charging facilities, recovery or disposal.

Cost: Initial cost and life cycle cost

Selection of the power source for the prototype sensor is discussed further in Chapter 3.

2.6. COMPUTING HARDWARE AND SOFTWARE

The hardware should be constructed to withstand the environmental conditions likely to be encountered in a field instrument which is primarily to be used in a marine environment. Salt water can have a catastrophic effect on electronic equipment if the adequate protection is not incorporated in the design of such a system. The system should also be capable of withstanding extreme physical conditions which are likely to be encountered during deployment. The software should be capable of automatic control of all mechanical functions within the sensor during bench testing and field deployments. The system should be capable of direct serial communication with a PC to permit the downloading and capture of the raw data produced by the detection system. The system should therefore be compatible with PC communications software and the data output capable of being imported into a PC spread sheet software package. This method was chosen so that the sensor performance could be monitored during each sample without the potential problems associated with on-board data processing.

2.7. SYSTEM CONSTRUCTION

Physical size and weight are important, particularly when operating from small research vessels and with small numbers of personnel to hand. Therefore, the overall size of the integrated sensor system should be kept to the minimum that is practicably possible. If possible, the weight of each module should to be kept in the range of 15 - 25 kg which is the Health and Safety Executive (HSE) regulation maximum for single handed lifting to

waist height [162]. The target operational depth for the prototype system for operating in estuarine and coastal waters was 30 metres. To allow for a reasonable safety margin a maximum operational depth of 45 metres was therefore specified for the pressure vessel of the prototype system. A modular construction, i.e. separate instrument and reagent packs was considered to be beneficial as this would enable different specification components to be selected depending on the nature of the deployment. For example, an estuarine deployment may require additional filtration to cope with the high suspended solids to be found in these systems, see section 2.2. Alternatively, the nutrient sensor could be deployed alongside other devices on a test platform with power supplied by the host system negating the requirement for a separate power pack. To withstand the corrosive conditions found in estuarine and coastal waters and for such an instrument to survive the rough treatment during deployment, it should be ruggedly constructed from materials that are not susceptible to corrosion.

2.8. DEPLOYMENT SCENARIOS

For a semi-continuous monitoring system to offer significant advantages over existing sampling methods it should have the ability to operate independently for a set period of time, which in this case was targeted at 13 hours, i.e. one complete tidal cycle. Therefore, power supply and reagents had to be sufficient for that period of time. The following basic operational specification was identified as essential for the nutrient sensor TON determinations prototype, e.g. sample every 30 minutes, semi-continuous sampling, i.e. every 90 seconds. The system should be capable of numerous deployment scenarios; from a simple drop deployment from a research vessel to a tethered buoy deployment as shown in Fig. 2.3.

Surface Buoy to hold sensor at required depth. Could also provide additional power, communications interface.

Submersed sensor at required depth; anchored in position.

Anchoring device and cable
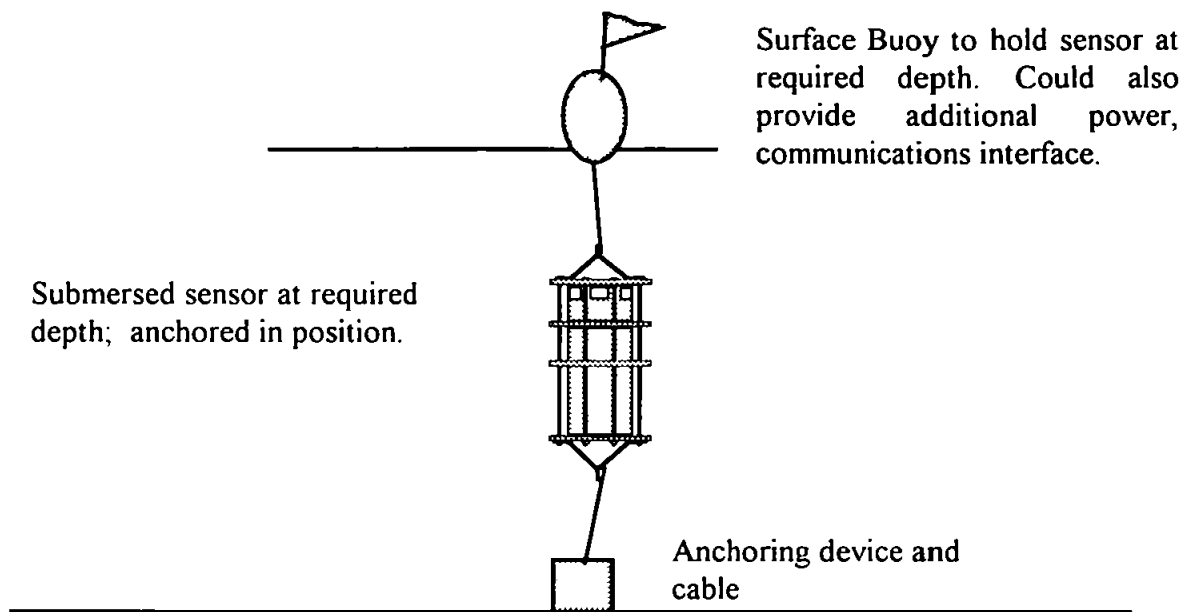
Figure. 2.3. **Typical configuration for a submersible buoy mounted deployment**

The surface buoy could easily be replaced with a sub surface buoy with an acoustic release on the anchor cable if there was a problem with security of the system.

2.9. COMMUNICATIONS

If required, data communication methods suitable for a field instrument should enable remote interrogation or facilitate automatic transfer of data to a base station. The three most likely options are UHF/VHF radio, satellite and the cellular telephone network. Line of site UHF/VHF radio telemetry systems have been a traditional means of communication with remote equipment. This particular method requires a shore base facility and consequently incurs additional cost of maintenance. Satellite communications are becoming more common place and the platforms are becoming smaller and costs are reducing. The actual satellite link still tends to be costly for a single system but there are methods of spreading the cost over several units by using the same signature for each unit. By programming each unit to download data at different times during a 24 hour period, up to

23 units can use the same platform signature and thus only incur a single daily satellite charge [163]. Although the cellular telephone network does not offer the same potential for global cover as satellite communications, (subject to weather conditions and orbit), it does have distinct advantages for coastal applications. Firstly there are no support charges associated with traditional UHF/VHF telemetry and the coverage extends over most of the UK coastal waters [164]. Secondly, the deployed system can be in immediate contact with a base station via the normal land line telephone network for data transmission or to warn of a pollution incident. Therefore, the cellphone network should be fully investigated to determine the actual coverage provided.

2.10.   CONCLUSIONS

The target specification for the prototype nutrient sensor is shown in Table 2.3.

Table 2.3.   Target specification for the prototype nutrient sensor

Property	Specification
Construction	Modular, rugged corrosion resistant
Operational depth	30 metres
Operational duration	1 tidal cycle (13 hours)
Weight	Each module < 15 kg
Computing	PC compatible with facility for direct serial communication
Accuracy	± 5 %
LOD	0.1 μM / 0.001 mg l^{-1} Nitrate-N
Range(s)	0 - 70 μM / 0 - 1 mg l^{-1} Nitrate-N
Precision	± 5 %
Sampling frequency	< 3 minutes

Chapter Three
Prototype Nutrient Sensor

3. PROTOYPE NUTRIENT SENSOR

This chapter describes the design, development and laboratory testing of a submersible , FI based TON sensor. The key individual components, i.e. the reagent and sample delivery system, injection valve, reduction column, reaction coil, flowcell, computer system and integrated system are considered in detail. It is essential for field deployment that each of the component parts and the integrated sensor are able to withstand the physical effects of remote and continuous operation with minimal servicing and replacement of parts. In order to achieve this detailed and meticulous laboratory investigation is an essential prerequisite.

3.1. EXPERIMENTAL

3.1.1. Reagent and sample delivery

Propulsion system: The original pumps used were identical to those used in a terrestrial nutrient monitor developed at UOP [139], i.e. 12 volt DC 8 roller, single tensioner 4 channel pumps (Ismatec type: Mini-S/8/12VDC/60:1). Extended use of these pumps found that the lateral force required to initiate flow in the smaller diameter tube caused premature bearing failure. They were subsequently replaced with 12 volt DC, 8 roller, 2 channel with separate tensioners for each channel, (Type 'Ismatec' CA1-E/8/12VDC/100:1) [165].

Pump tubing selection: In order to assess the long term reliability, e.g. 30 days, of a flow injection based system, reliability trials on the component subjected to the most wear and therefore the weakest link, i.e. the pump tubing, were carried out under various conditions. The selection of pump tubing for testing was based on manufacturers published performance figures [165] which states life expectancy in hours under certain conditions. A test rig and testing regime were devised to investigate the selected tubing material under controlled conditions. Prior to testing, a sample of each tube type was sectioned using a

specially constructed cutter to examine the bore profile and measure tube dimensions using a shadowgraph. The tubes were subjected to hardness tests to compare grades of material supplied. The pump tube test rig consisted of a 4 channel peristaltic pump (Ismatec-Mini-S-820) controlled by a time switch set to continuously run the pump through a 10 minutes on, 10 minutes off cycle. At the start of the test, the pump rollers were cleaned and lightly lubricated with the recommended silicone oil spray. The samples of tubing selected for testing were connected to a manifold which allowed the continuous pumping of water from a reservoir in the test rig. At regular intervals during the test period, the flow rate from each tube was determined by measuring the length of time taken to fill a 25 ml volumetric flask to the mark. The test was run for 40 days and on completion of the test each pump/tube contact area was visually inspected to assess wear. Further tests were then carried out to determine effects of temperature on flow rate. New tubes were selected and the test rig was set up as before in a temperature controlled chamber, allowing sufficient time for the chamber to stabilise at the set temperatures. The test lasted a total of 17 days after which the tube/pump contact areas were inspected.

Tube connections: The normal practice for joining the flexible pump tubing to the PTFE manifold is to use push-fit connection as shown in Fig. 3.1. In normal circumstances this method is quite acceptable but where there is likely to be increased pressure a more secure joint is required. A major adhesive manufacturer (Loctite UK Ltd) was approached regarding the problem of bonding the PTFE tubing to the flexible pump tubing. A special-purpose adhesive and primer was supplied for evaluation and used in conjunction with a push-fit connection.
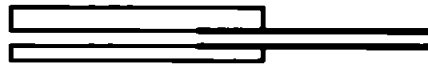
Figure 3.1. Normal push-fit tubing connection Flexible PVC tubing to PTFE tubing

The use of adhesive lined heatshrink tubing, (RS Stock No. 381-567), over a normal push-fit joint was also investigated. This was achieved by first abrading the outer surface of the PTFE tubing and then thoroughly degreasing all contact surfaces with clean alcohol. A normal push-fit connection was made and a length of the heat-shrink was placed over the joint as shown in Fig.3.2. The original size of the heat-shrink tubing used was 4 mm which on heating to 100 ° C with a heat gun would shrink down to 1 mm diameter. The hot-melt adhesive lining would then provide additional sealing, Fig. 3.3.
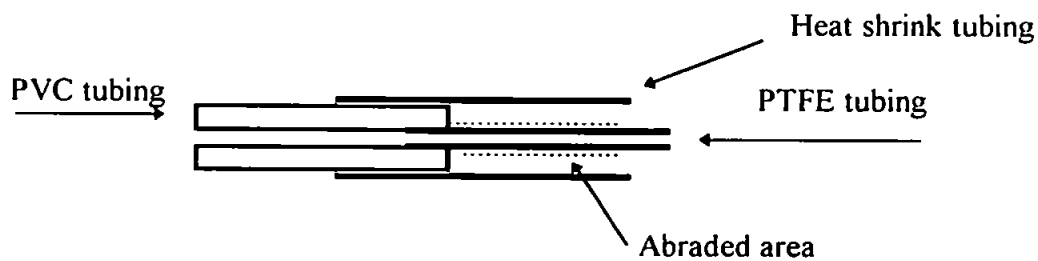
Figure 3.2. Heat-shrink tubing connection before heating
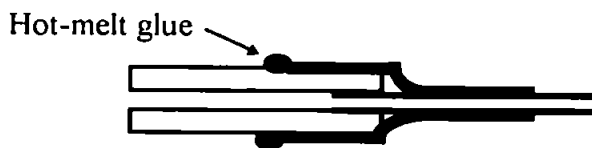
Figure 3.3. Heat-shrink tubing connection after heating

The hot melt adhesive does not bond directly to the PTFE, but provides additional joint strength by gripping the abraded surface. Pull-off tests were carried out to determine the strength of the joints.

Flange-connector for flexible pump tubing: A piece of 2 mm OD / 1 mm ID ABS rigid plastic tubing was cut to a length of 15 mm. A flange was then formed using a heated flanging tool (Ismatec Cat. No. IC0043). When cool, the face of the flange was polished flat using a piece of 1200 grit wet and dry abrasive paper. The bore of the standard ¼" flange connectors and washers then had to be drilled out to 2 mm to accept the slightly oversize ABS tubing. The connector was then assembled as shown in Fig. 3.4. The end of the PVC pump tubing was softened using a heat gun and the end stretched over a tapered metal rod and allowed to cool. When cool, the PVC tubing had retained the shape of the tapered rod which allowed it to be pushed over the 2 mm OD ABS tubing. The ends of the tubing were then trimmed and cleaned. When satisfied with the assembly, the free end of the ABS tubing was coated with 'Loctite' 406 adhesive, an instant cyanoacrylate adhesive designed for bonding rubbers and plastics.
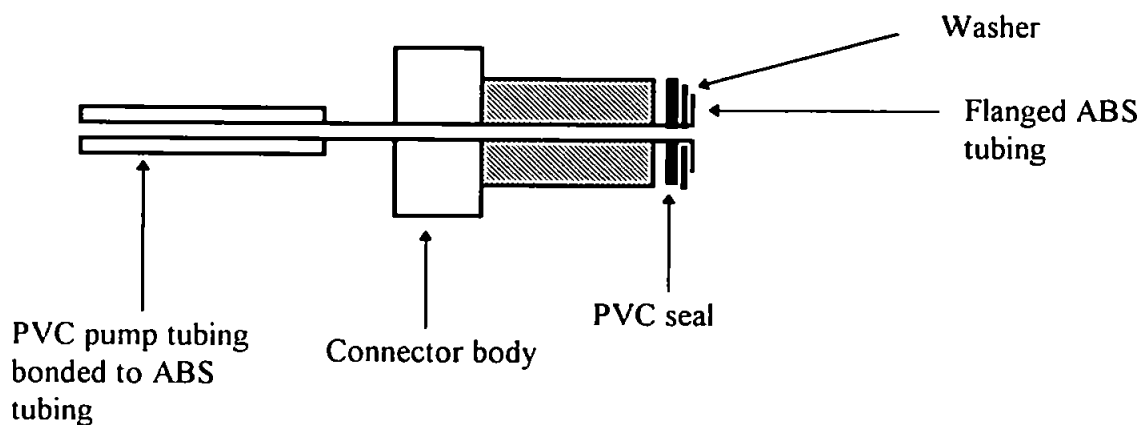
Figure 3.4. **Custom built ABS flange connector**

The stretched end of the pump tubing was then pushed over the adhesive coated ABS tubing and the bond was allowed to fully cure. After curing, the bond was subjected to pull-off tests using the same procedure as before.

3.1.2. Injection valve

Experience using a mechanical injection valve found reliability and operating deficiencies. The size and original configuration of the valve also required attention so that it could be incorporated in a compact field instrument. This section describes how a standard 'Burkhard' motorised multi-port 4-way injection valve was modified to improve performance and reliability. The standard valve was disassembled and re-configured to fit the instrument module to allow better field maintenance and adjustment. The standard configuration of the valve as supplied is shown in Fig. 3.5.
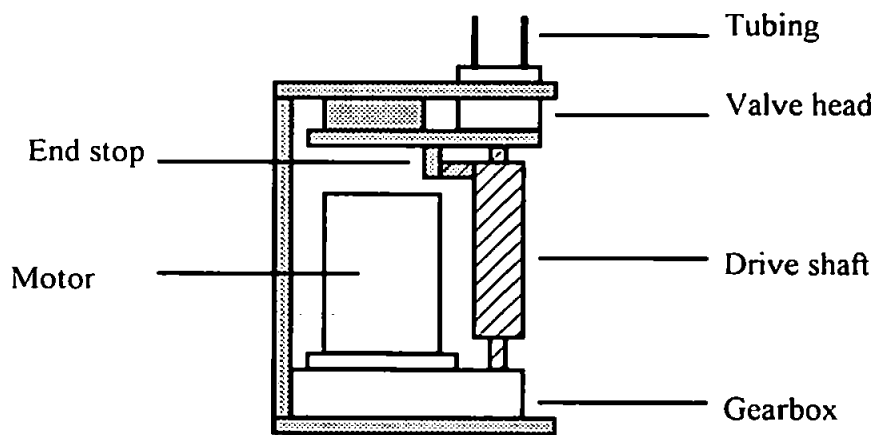
Figure 3.5. Schematic diagram of the standard unmodified injection valve configuration

The injection valve head was positioned so that all maintenance and adjustment of pumps and injection valve could be effected from the top of the instrument as shown in Fig. 3.6. To achieve this, the valve motor and gearbox were split so that the gearbox could be modified to allow the drive shaft to exit from the opposite side to the original. The injection valve head was then mounted on instrument baseplate using specially made spacers. The drive shaft was also modified to suit.

During the modification work, the valve gearbox was dismantled and thoroughly cleaned to remove the original lubricating grease. When clean, the gearbox was re-assembled and re-

lubricated. A problem which occurred frequently during bench testing was the shearing of the roll pin used to connect the motor drive shaft to the valve head shaft.
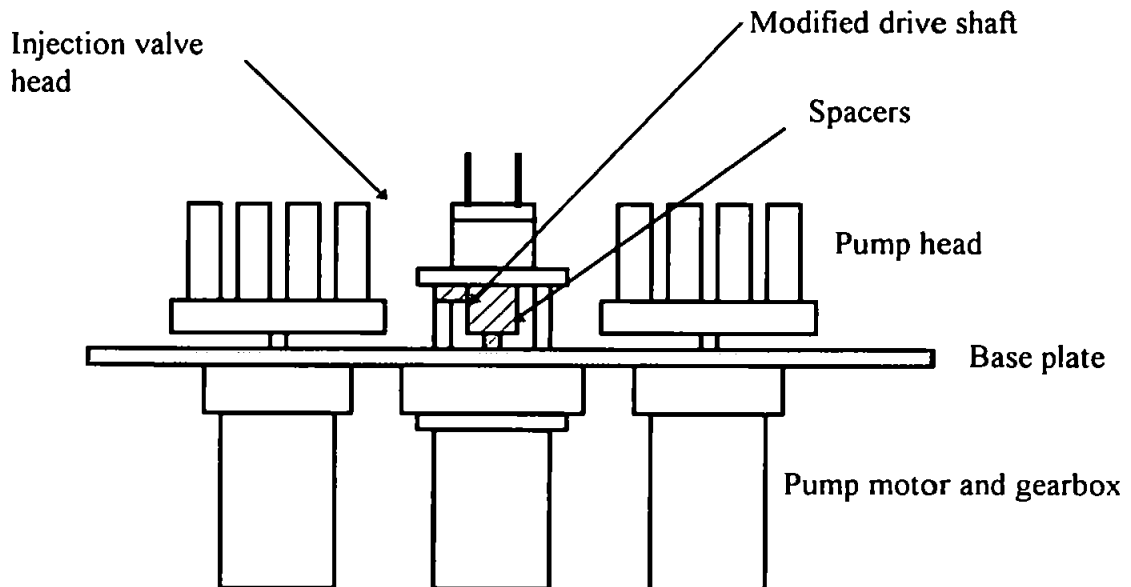
Figure 3.6. Schematic diagram showing the layout of the modified injection valve on the instrument base plate to allow all adjustments to be carried out from the top of the instrument

This was rectified by increasing the size of the cross bore from 1.5 mm to 2.0 mm and replacing the spring steel roll pin with a high-tensile steel dowel pin. No drive shaft problems were encountered after this modification. When examined closely, the construction of the valve head was found to be very poor. A large gap between the PTFE end plate and the valve body was found as shown in Fig. 3.7. which explained why the performance of the valve was dependant on the tightness of the retaining screws. This was eliminated by making circular packing shims to fit under the body of the valve head as shown in Fig. 3.8. Sufficient packing was added to raise the height of the valve body and eliminate the gap which allowed leakage. The retaining screws could then be tightened sufficiently to prevent loosening during operation without stalling the valve head.
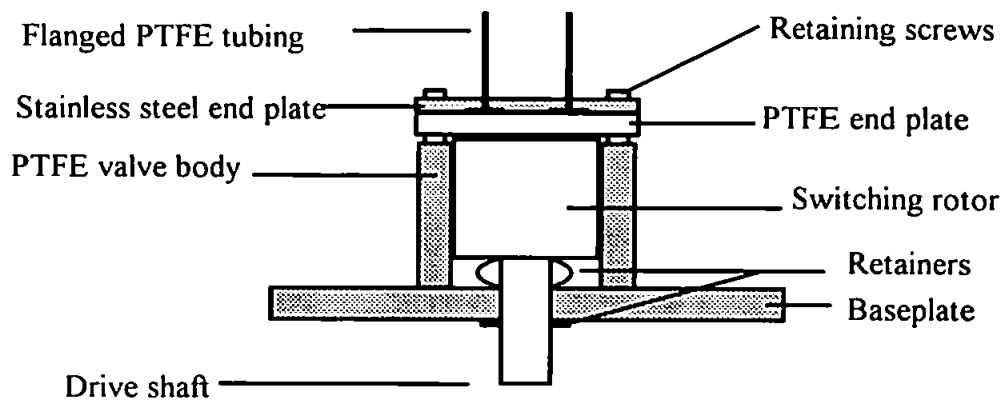
Figure 3.7. Diagram of valve head showing gap between PTFE end plate and body
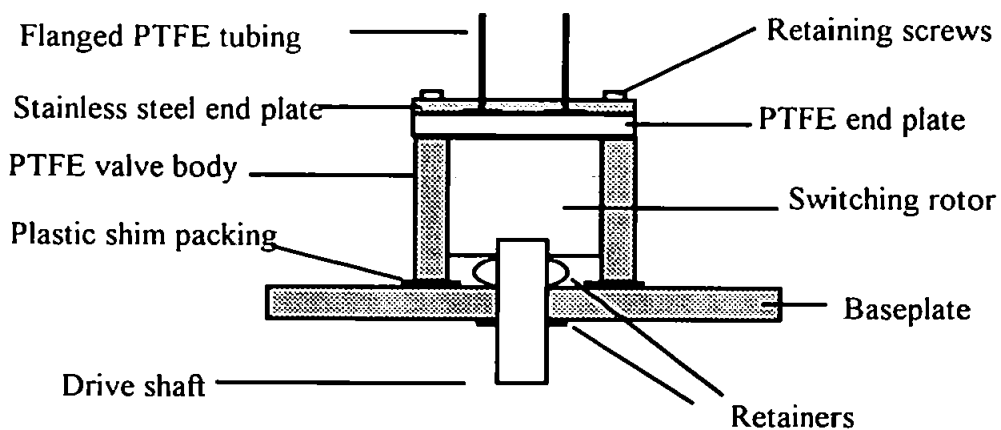
Figure 3.8. Diagram of modified valve head showing plastic shim packing in place

Standard manifold connections to the injection valve used in the nutrient sensor FI manifold are shown in Figs.3.9 (fill position) and 3.10 (inject position).
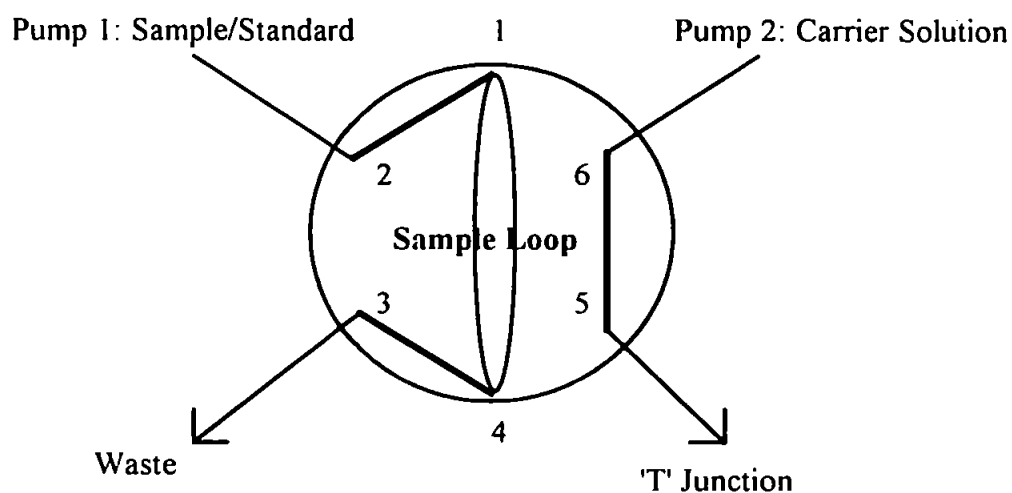
Figure 3.9. Flow diagram of injection valve in fill position
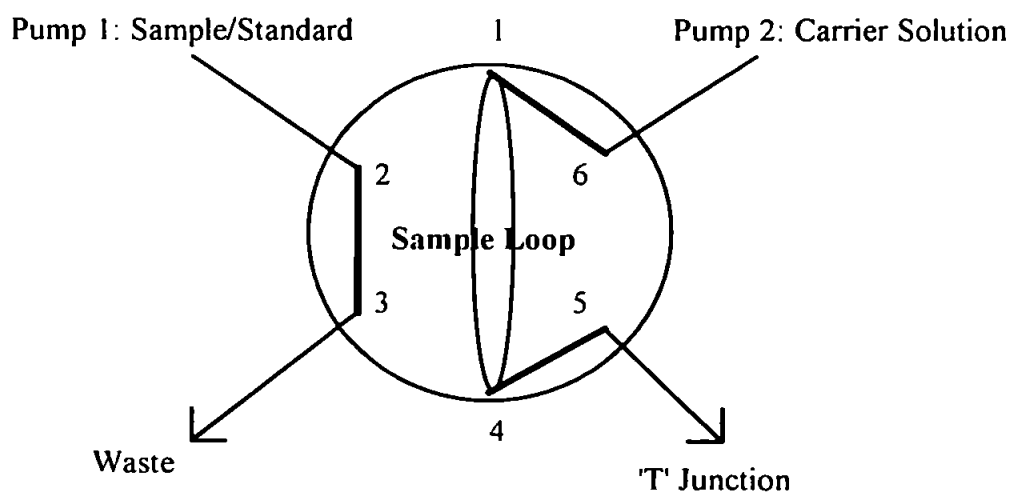
Figure 3.10. Flow diagram of injection valve in inject position

3.1.3. Reduction column

As stated in chapter 1, copperised-cadmium is widely used for the heterogeneous reduction of nitrate to nitrite prior to the diazotisation and coupling reaction. This section describes the work carried out to optimise the technique and produce a ruggedised reduction column suitable for use in a field instrument.

Packed reduction column: For most of the bench testing and early non-submersed field trials, the FI instrument utilised a copperised-cadmium packed reduction column [107]. This was prepared by adding 50 ml of 10 g l⁻¹ copper sulphate solution to 5 g of 100 mesh (0.15 mm ø) cadmium powder and stirring for 2 minutes. The copperised-cadmium slurry was then filtered off and washed with 2 M hydrochloric acid followed by ammonium chloride solution (10 g l⁻¹). Finally, the washed copperised-cadmium was packed into a 40 mm x 2 mm ID glass tube, plugged at one end with glass wool, by drawing up the slurry in a Pasteur pipette and injecting it into the tube.
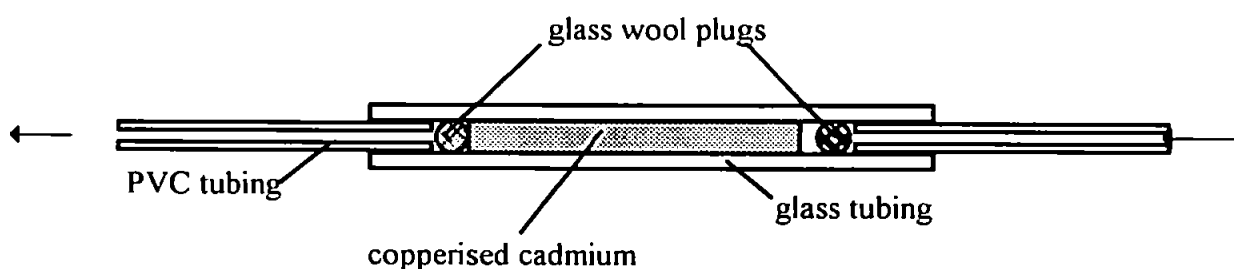
Figure 3.11.   **Diagram of a packed reduction column with simple push-fit tube connections**

The tube was gently tapped to help settle out and pack down the copperised-cadmium particles. This process was repeated until the tube was filled to within 10 mm of the unplugged end. The open end was then plugged with clean glass wool and the inlet and outlet connections were push fits using PVC tubing as shown in Fig. 3.11.

Copperised-cadmium wire columns: Copperised-cadmium and copperised cadmium-silver wire columns have been successfully used for the reduction of nitrate to nitrite [57,97,98,99]. Therefore, to assess the properties of this method a wire reduction column was constructed using a modified version of the method described in PML's Nutrient Analysis Techniques [166]. Wearing disposable gloves for personal safety reasons and to

prevent re-contamination of the wire, a 1 m length of 1.0 mm diameter cadmium wire (99.99%) was degreased using IPA and clean absorbent paper. The wire was carefully inserted into a 1.05 m length of 1.3 mm ID clear flexible PVC tubing. The wire was positioned centrally in the tubing and the tube ends cut to give approximately 10 mm at each end for the connections. The column was then clamped vertically in a retort stand and 10% HCl was flushed through from the lower end using a syringe. Flushing from the bottom upwards gave a more efficient wash than pouring the solutions in from the top of the column. The column was flushed through with 'Milli-Q' water. Copperisation of the cadmium wire was achieved by flushing through 2% (w/v) copper sulphate solution from the bottom of the column and holding this in the column for a few minutes, this was flushed out using Milli-Q water. The column was finally filled with 10 g l^{-1} ammonium chloride solution and the ends plugged to seal the solution in to prevent oxidation. The wire reduction column was fitted to the FI manifold and a series of nitrate standards were analysed.

Ruggedisation of the packed reduction column: To ruggedise the packed reduction column and eliminate the conditions which can lead to trapped air bubbles, a prototype plastic bodied column was constructed as follows:

A piece of 10 mm diameter clear acrylic rod was machined to a length of 60 mm with a 2 mm central bore. Each end was counter bored to a depth of 8 mm and threaded to accept standard 1/4 inch flange connectors. The reduction column internal bore was polished using a proprietary plastics polish and thoroughly cleaned. Fine Nylon® mesh filter inserts were cut to size using a 5 mm punch. Four filter inserts were placed in the outlet followed by a stainless steel washer to press the filter inserts hard against the outlet counterbore to prevent leakage of the copperised-cadmium as shown in Fig. 3.12.

71
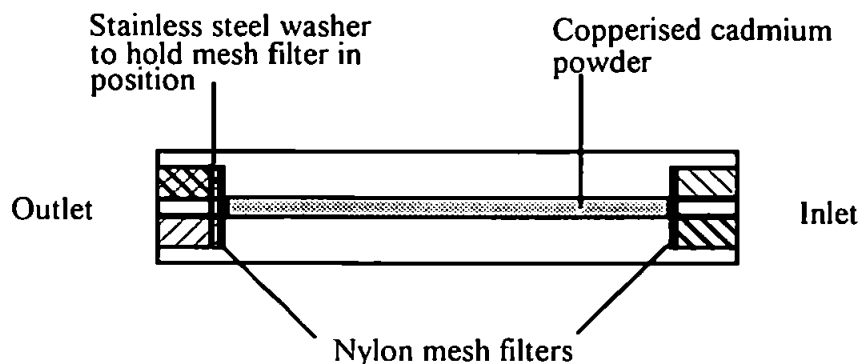
Figure 3.12. Prototype plastic bodied packed reduction column.

A length of flanged 0.8 mm ID PTFE tubing was fitted to the outlet using a standard 1/4 inch flange connector. The copperised-cadmium powder was prepared as described earlier and mixed with a small amount of ammonium chloride carrier solution (10 g l $^{-1}$) to form a slurry. This slurry was injected into the column from the inlet end using a disposable Pasteur pipette. When full, the inlet area was cleaned to remove any copperised-cadmium particles and two filter inserts were fitted. A flanged 0.8 mm ID PTFE inlet tube was then fitted to the inlet using a standard 1/4 inch flange connector. The reduction column was fitted to the instrument and carrier solution was immediately pumped through it.

3.1.4. Reaction coil

To ensure uniform mixing and reaction time, a standard length reaction coil was produced. The coil support was constructed from 25 mm diameter rigid PVC rod using a lathe to produce a coil support of dimensions as shown in Fig. 3.13.

A 1.1 metre length of 0.8 mm ID PTFE tubing was then coiled around the support and the free ends were pushed through the 2 mm holes at each end of the support as shown in Fig. 3.14. A flanged connection was made at each end of the reaction coil.
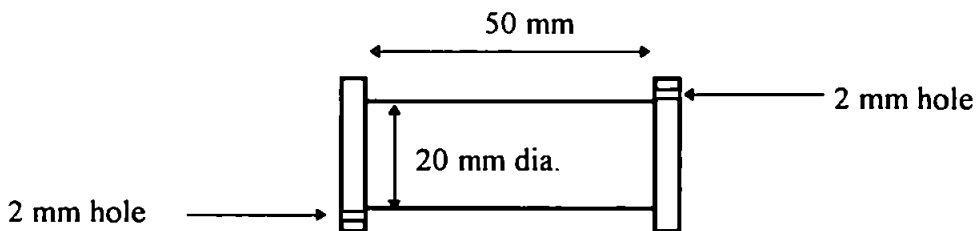
Figure 3.13. Diagram of reaction coil support before PTFE tubing fitted
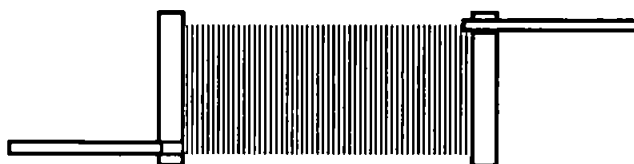
Figure 3.14. Diagram of reaction coil after PTFE tubing fitted

3.1.5. Flowcell

For ease of field maintenance a low cost, 'disposable,' solid-state flowcell was considered to be an essential component of the TON sensor. This section describes the design and manufacture of a such a device.

Reagents: All solutions were prepared from ultra-pure water produced by a 'Milli-Q' system (Millipore Corporation), and all reagents were AnalaR® (BDH) unless otherwise stated. The carrier solution was prepared by dissolving 10.0 g of ammonium chloride in 1 l of water. The N-(1-naphthyl)ethylenediamine dihydrochloride (NINED, Sigma Chemicals) and sulphanilamide reagents were prepared by dissolving 0.5 and 25.0 g respectively in 1 l of water containing 10 % ($^v/_v$) orthophosphoric acid. The mixed colour reagent was subsequently prepared by mixing equal volumes of the NINED and sulphanilamide reagents in a brown glass bottle. A stock 100 mg l^{-1} nitrate solution was prepared by dissolving 0.7220 g of potassium nitrate in water. Working standards were prepared by serial dilution with water. A stock 1000 μM Nitrite-N solution was prepared by dissolving 0.0690 g of

sodium nitrite in 1 l of water. Working Nitrite-N standards were produced by serial dilution with water.

Flowcell construction: The first prototype flowcell was designed around a 'Z' cell configuration [167] and operated in the analyte absorption region of 540nm. The photo-optic components selected for use in the flowcell were a water-clear ultrabright green LED (Radio Spares stock No. 590-496) as the source and a photodiode with peak response at 560 nm (RS stock No. 303-719) as the detector. The manufacturers' specification for the green LED was 250 mcd at 563 nm. The first prototype was machined from 20 mm diameter clear acrylic rod to assist in the manufacture and to observe liquid flow. Firstly, a piece of 20 mm dia. acrylic rod was machined in a lathe to a length of 30 mm. A 1.5 mm diameter central bore was then drilled using extreme care to prevent overheating which would otherwise cause roughening of the internal finish, resulting in light scattering and flow disruption within the finished cell. Whilst in the lathe, the centre line of the flowcell body was marked as a reference point for the drilling of the inlet and outlet bores. As stated above, the cell was based on the 'Z' cell configuration as shown in Fig. 3.15. To achieve the 'Z' configuration a special drilling jig was constructed to correctly position the body blank to drill the inlet and outlet bores at the correct angles. The drilling jig fitted into the drill vice and held the flowcell body blank at an angle of 45°. The body blank was marked in two positions on the centre line (on opposite sides of the blank) so that a 10 mm path length would be produced when the inlet and outlet bores were drilled. Each bore was counter drilled to 3.0 mm and a depth of approximately 4 mm to accept the 3.0 mm OD flexible tubing which was used to make the push-fit connections to the flowcell. The inlet and outlet bores were both 1.0 mm which was considered acceptable at the time as 0.8 mm ID PTFE tubing was to be used for the manifold. In order to dissipate any heat generated by the LED, which may have affected the kinetics of the diazotisation and coupling chemistry

(an increase of 10 °C typically doubles the reaction rate), a small aluminium heat sink was incorporated in the design. The LED was bonded into the 8.1mm OD (same OD as photodiode) aluminium heat-sink using a waterproof liquid epoxy adhesive so that the lens of the LED protruded at one end. When the adhesive had fully cured, the assembly was carefully placed in the lathe chuck and the lens was machined flush with the heat-sink face. The newly machined face of the LED was ground flat using progressively finer abrasive papers and finally polished with a small amount of a proprietary plastics polish to produce a clear, flat cell window. The flowcell body was placed back into the lathe chuck so that the photodiode and LED bores could be machined. The bores for the photodiode and LED were started using a normal 8.1 mm drill bit. Final machining of both bores was achieved by using another 8.1 mm drill bit with the point ground to produce a square end.
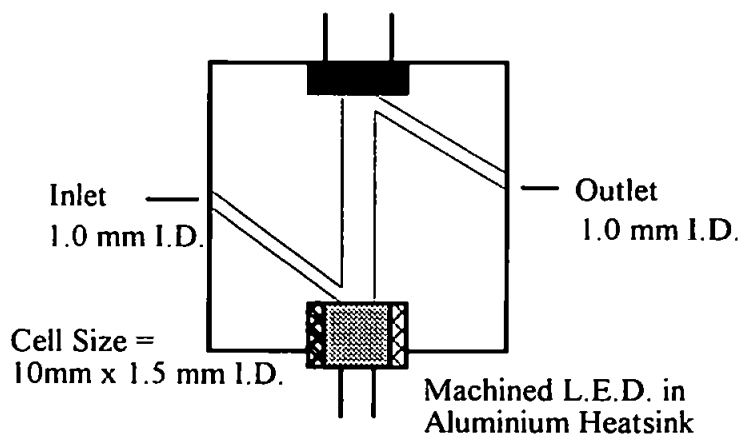
Figure 3.15.   Diagram of first prototype flowcell constructed from clear acrylic rod

The bores were carefully drilled out until the square end drill bit just started to break through into the inlet/outlet bores to produce flat-bottomed recesses in which the photodiode and LED/heatsink would fit and produce good seals. Final machining of the flowcell body involved removing material from one end of the body so that the flange on the

photodiode can would be clear of the flowcell body and therefore allow it to seat correctly.

All burrs were removed and the completed flowcell body was thoroughly cleaned by

soaking in 20 % 'Decon' 75 solution at 60 °C for 20 minutes, rinsed in clean water and

dried. The photodiode and LED/heatsink were bonded into the flowcell body using a

waterproof liquid epoxy adhesive. When the adhesive was fully cured, clean water was

flushed through the cell to check for blockages and leaks. The component leads were

soldered to the photodiode and the LED and the whole assembly was finally painted black

to eliminate the effects of external light.

For initial proof of principle, the first prototype flowcell with a 10 mm path length was

tested by connecting it to the flowcell outlet of a 'FIAstar' 5020 during the chemistry

optimisation experiments [107]. Response from the photodiode in the prototype flowcell

was measured using a custom built operational amplifier (op-amp) connected to a

millivoltmeter as shown in Fig. 3.16.   A constant current 5 volt D.C. power supply to the

LED was provided by including a 120Ω resistor connected in series to the supply. The

baseline output (carrier and mixed colour reagent) and the change in absorption of the

nitrate standard range was measured as they exited from the 'FIAstar'.
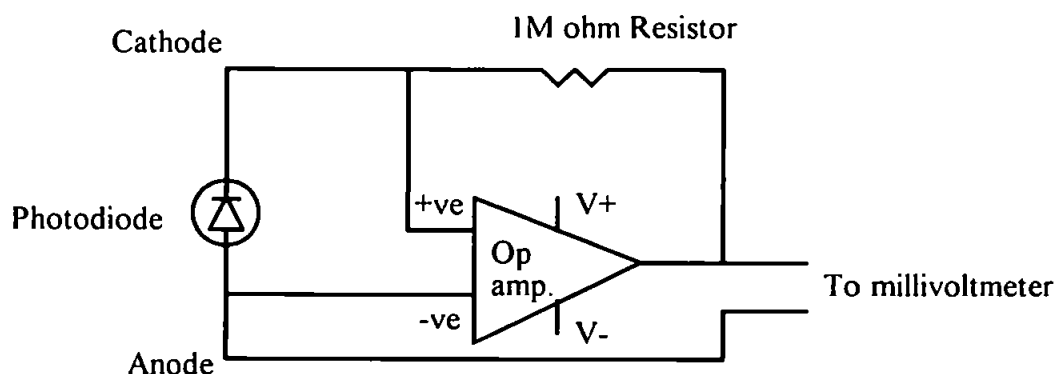
(Amplifier PCB R.S. Stock No. 434-065, Op. Amp. R.S. Stock No. 307-058)

Figure 3.16.   Circuit diagram of custom built detector operational amplifier used in initial flowcell tests

A prototype 20 mm cell was constructed from 20 mm diameter rigid PVC rod in the same way as for the acrylic bodied flowcell. From initial tests the overall response from the PVC bodied flowcell was much better. However, the problem of trapped air bubbles continued to affect the reliability of the design. A series of modifications were made to the original design in an attempt to alleviate this problem. Inlet and outlet bore diameters were increased to 1.5 mm and the angle of the inlet was changed to 90°. Due to the low sample residence time in the cell and the negligible heat generated by the LED the heatsink was considered unnecessary and therefore omitted. The LED was fitted directly into the flowcell body with the curved lens protruding into the inlet stream so that the sample flow impinged on the lens to provide additional mixing as shown in Fig. 3.17.

Photodiode, Peak Response at 560nm
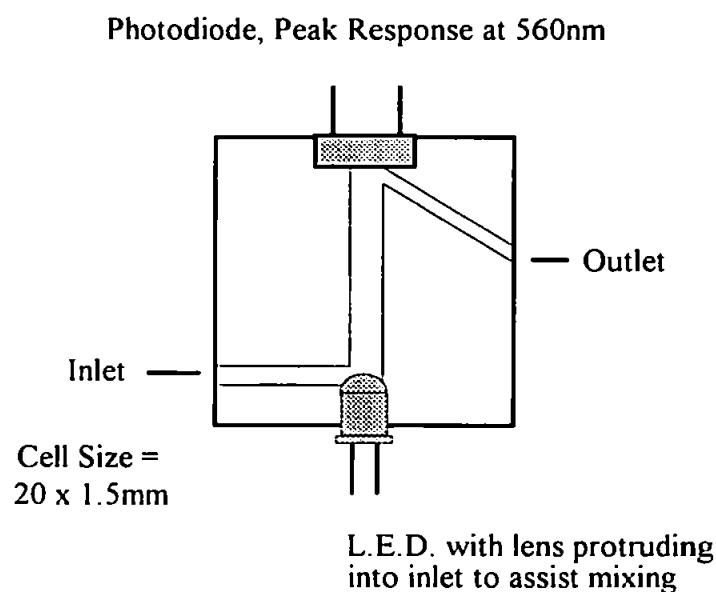
Figure 3.17.   Diagram of prototype 20 mm flowcell showing modified inlet
               configuration

This additional mixing within the cell helped to reduce refractive index gradients along the axis of the flowcell which has been reported by other workers using similar cells [168]. Retaining the LED lens also focused the beam straight down the bore of the flowcell. The

77

modified LED bore was produced in much the same way as before except that a 4.9 mm drill bit was used instead of the 8.1mm drill bit used for the combined LED/heatsink bore. The performance of the modified flowcell was assessed using a more powerful 3 stage amplifier, Fig. 3.18., a manifold as shown in Fig. 3.19. and a series of nitrite standards (in 'Milli Q') for simplicity of testing, i.e. no reduction column fitted at this stage.
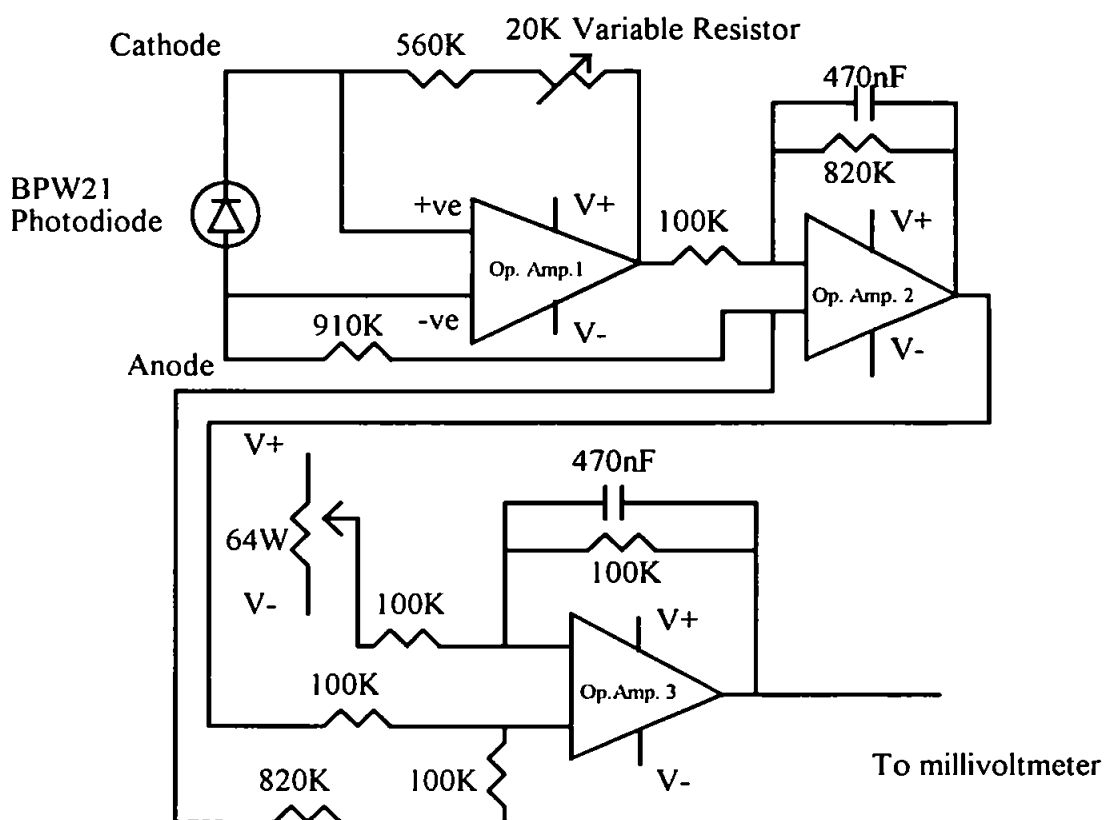
Figure 3.18. **Circuit diagram of the custom built three stage detector amplifier used in flowcell trials**

(Op. Amp. 1 & 2: R.S. Stock No. 308-887. Op. amp. 3: R.S. Stock No. 308-8930)

Flowcell design was further improved in order to eliminate the problem of air bubbles which occasionally became trapped within the flowcell. After several modifications this was eventually attributed to the acute angle of the outlet so the angle of the outlet was also increased to 90° as shown in Fig. 3.20.
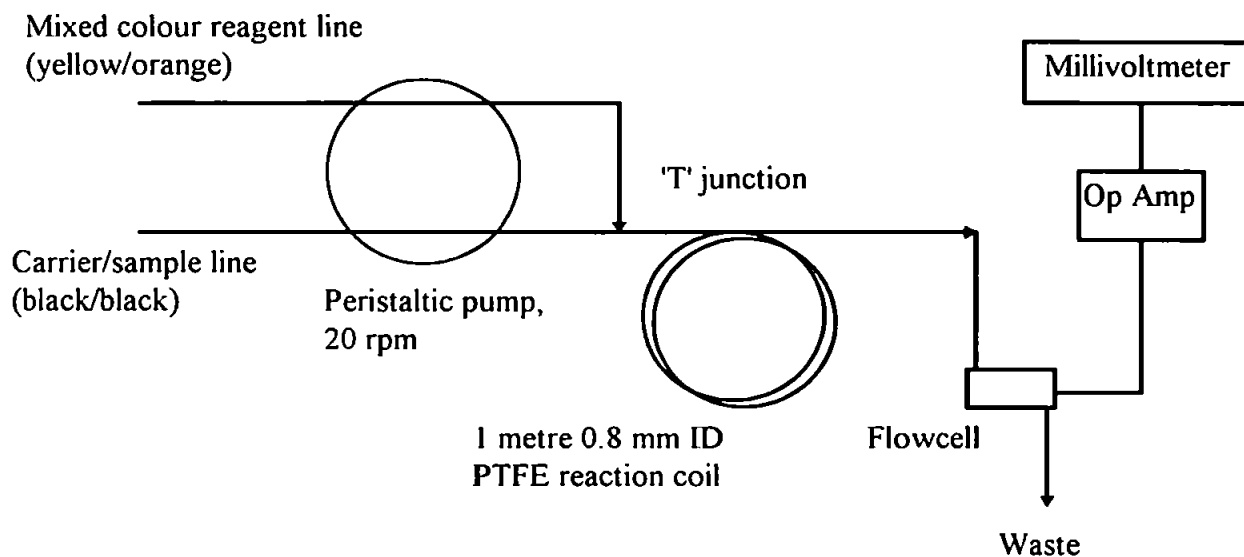
Figure 3.19. Schematic diagram of the test rig used in conjunction with nitrite standards (NO_2-N) and custom built amplifier to bench test prototype flowcells
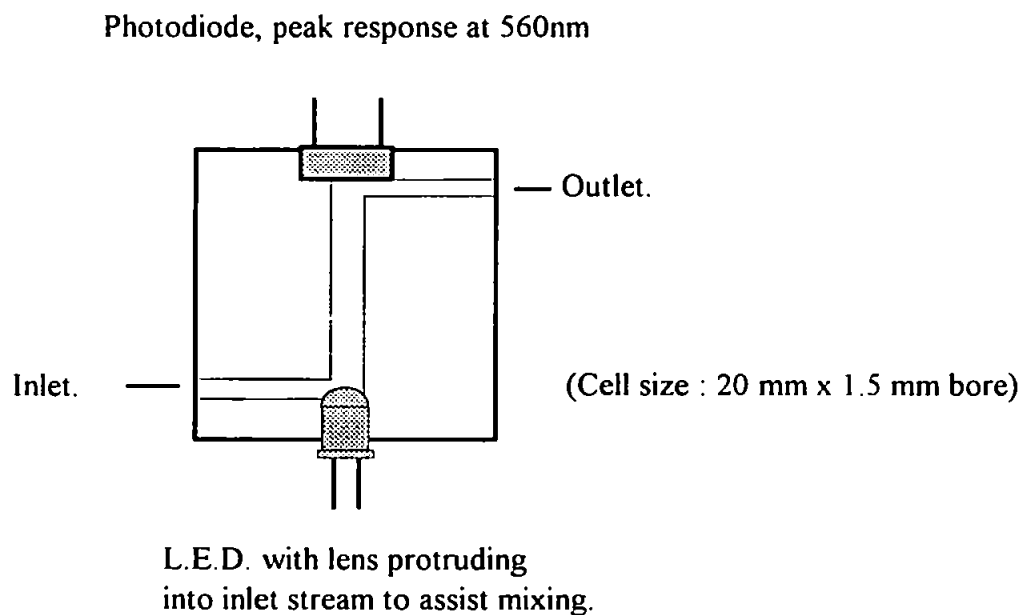
Figure 3.20. Diagram of the final flowcell configuration constructed from opaque rigid PVC

For convenience during development, all flowcells constructed up to this point had simple push fit inlet and outlet connections and the terminals legs of the LED and photodiodes

were left exposed. Therefore, a ruggedised field version of the final prototype was required. This was constructed in the same way as before except that the inlet and outlet bores were drilled and threaded to accept standard 1/4" flanged connectors. The LED and photodiode terminal legs were cropped shorter and protected by the addition of rigid PVC ring fitted around the terminal legs; bonded to the flowcell body using a waterproof PVC adhesive. After the leads were soldered to the terminal legs and the flowcell tested, the protection rings were filled with a two-part polyurethane potting compound for final protection. The final field version of the flowcell is shown in Fig. 3.21.
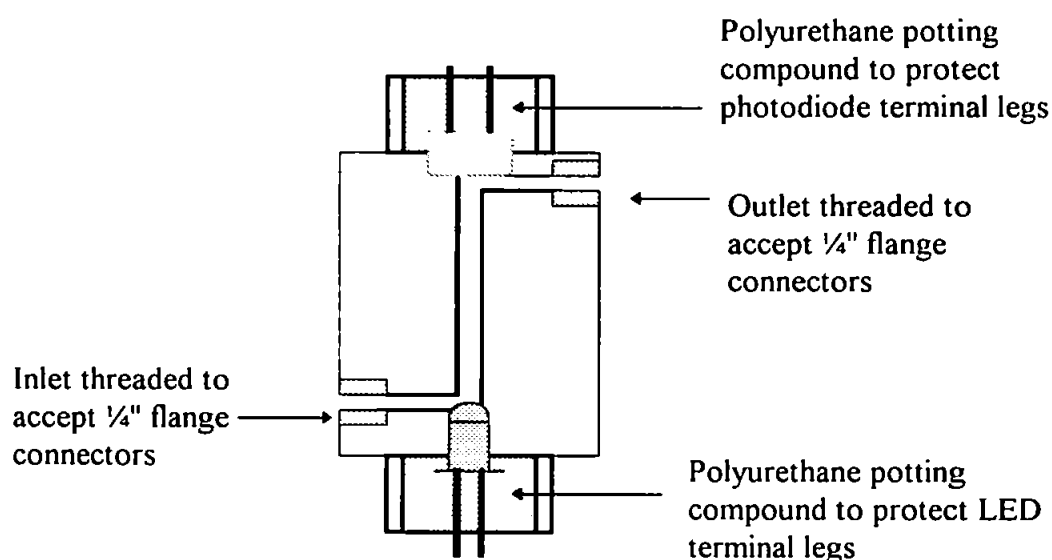
Figure 3.21. Diagram of the final field version of the 20mm flowcell showing threaded inlet and outlet connections and LED/photodiode protection

3.1.6. Control system

This section describes the design, construction and function of the on-board computer system used to control the operation of the nutrient sensor. The on-board control system is based on the system found in the terrestrial nutrient monitor developed at UOP [139] Several design changes were incorporated to improve performance, system and component

reliability, power consumption and provide an overall size reduction. At the heart of the on-board computer is the well proven Intel® 80C32 microprocessor with MCS®-BASIC v1.1 interpreter and an external 8K EPROM. This arrangement provides the following functions essential to automatic control systems.

- BASIC programmable
- EPROM programming capability
- Internal clock
- Auto boot on power up
- Floating point arithmetic
- Internal and external interrupts

The processor board is connected to the I/O board by 40-way edge connectors and ribbon cable. This board contains a central 82C55 peripheral interface adapter (PIA), configured as three 8-bit TTL output ports. Port A is connected to a network of eight 12 volt supply relays to the drive pumps, switching valves and injection valve. Port B provides TTL signals to a 14 bit analogue to digital converter (ADC), the 8 channel analogue switch and the injection valve to toggle between fill and inject positions. Port C provides the input to the 8-bit analogue to digital converter (ADC). A schematic representation of the I/O board is shown in Fig. 3.22. BASIC control programmes are executed from the on-board *EPROM* which can be modified on-line by transferring *ROM* to the 80C32's internal *RAM* by using the *XFER* command. The system can also be configured to autoboot when powered up, i.e. programme will automatically start when the system is switched on. A system operating routine, 'ROM1', was written in the MCS®-BASIC v1.1 language and is described in Chapter 4. Development and testing of the nutrient sensor was effected by direct serial connection to a PC. ADC data from each analysis was captured directly as a text file by the communications software Crosstalk® for Windows® labelled and saved to floppy disk.
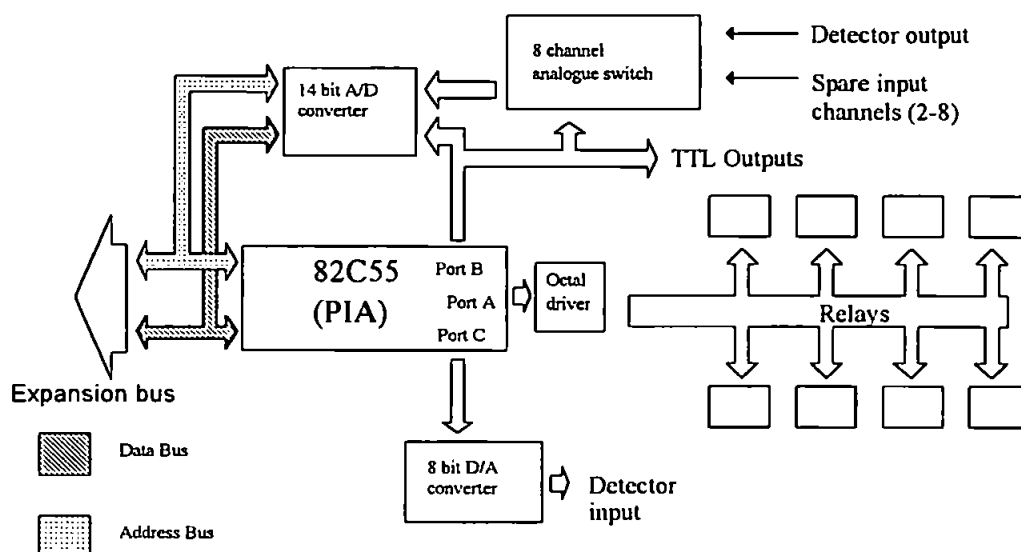
Figure 3.22.   Schematic diagram of the control systems I/O board

The saved ADC data from each analysis run was imported into spreadsheet software where it was plotted to show the peak profile. The spreadsheet analysis tools were then used to determine the range values for each standard/sample which were later used for calibration plots and the determination of analyte in the samples.

3.1.7.   Integrated System

This section describes the design, construction and configuration of the final integrated system used in field experiments to investigate the use of FI techniques in a submersible sensor.

Materials of construction: For ease of machining, durability and availability, all major components of the prototype system were constructed from rigid PVC. The pressure housing and reagent modules utilised 270 mm OD water pipe which had a wall thickness of 13 mm. This material was readily available at reasonable cost and had the required chemical resistance and physical strength for the construction of a field instrument which was to be deployed in a marine environment [169]. It is also used extensively for prototyping work

such as this. To prevent problems that could have arisen from thermal expansion/contraction, all other components in contact with the PVC tubing, e.g. pressure housing end caps, were machined from rigid PVC plate. All fasteners and metal components were constructed from 18/8 corrosion resisting steel [170].

Instrument Module: The instrument module was designed to allow good access to all major components for ease of field maintenance. The first system consisted of a pressure housing constructed from 273 mm OD rigid PVC tubing, with a wall thickness of 13 mm, which contained two separate inner sealed compartments as shown in Fig. 3.23.
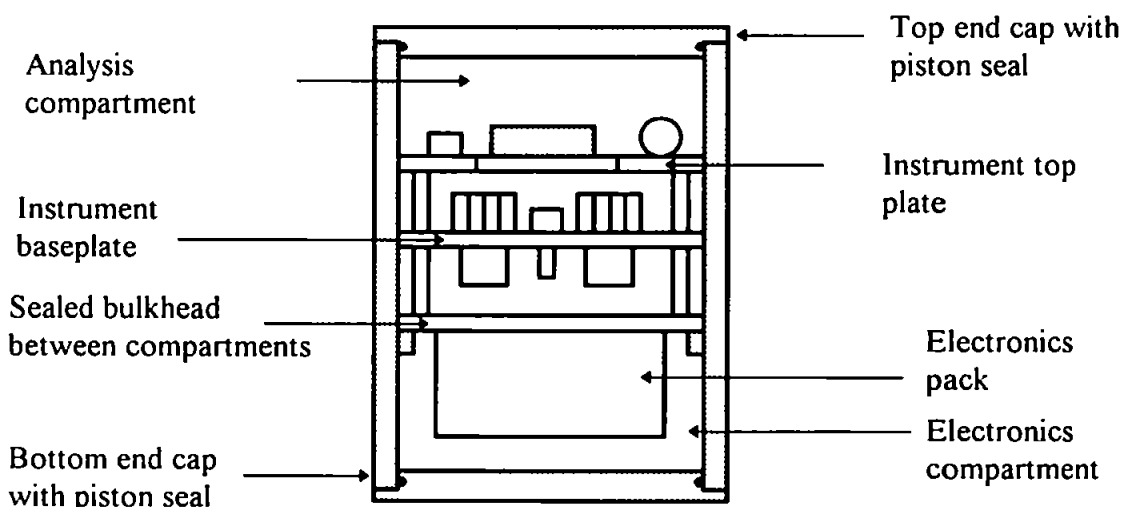
Figure 3.23. Diagram of the first instrument configuration showing separate analysis and electronics compartments

The analysis compartment contained a circular rigid PVC baseplate to which the two 4 channel 12 volt DC peristaltic pumps, switching valve and the modified four-way injection valve were fitted. The custom built reduction column, reaction coil and flowcell were fitted to a second circular PVC plate which was fitted to the baseplate using PVC spacers, internally threaded to allow fixing with stainless steel screws. A large opening was machined in this second plate to allow access to the pumps and valve situated below. The FI manifold was configured in the analysis compartment as shown in Fig. 3.24. The second

compartment contained the system electronics, consisting of single-board computer and I/O board in a specially constructed board holder. The electronics compartment was completely sealed from the analysis compartment to limit damage should a leak occur. In order to guarantee some level of reliability the on-board computer and I/O boards were finished to military specifications [171] using the following procedure. Both circuit boards were cleaned to remove all traces of solder flux residues and other organic and inorganic residues and tested using a 'Protonique' CM-2D Contaminometer [172]. This instrument flushes the circuit board/s undergoing test with a 50:50 mix of de-ionised water and propanol. It then measures surface contamination as a function of the wash solution conductivity.

Sample   Standard   Carrier   Colour Reagent

```
  |         |                          |            |
┌─────────┐    ┌─────────┐        ┌─────────┐              Waste
│Switching│    │ Pump 2  │        │ Pump 1  │                |
│  Valve  │────│         │        │         │        ┌──────────────┐
└─────────┘    └─────────┘        └─────────┘        │   Flowcell   │
                    │                  │             │              │
              ┌──────────────┐         │             └──────────────┘
              │Injection Valve│────────┘                    │
              └──────────────┘                       ┌──────────────┐
                    │                                │Reaction Column│
              ┌──────────────┐                       │              │
              │ Reaction coil │──────────────────────└──────────────┘
              └──────────────┘
                    │
                  Waste
```
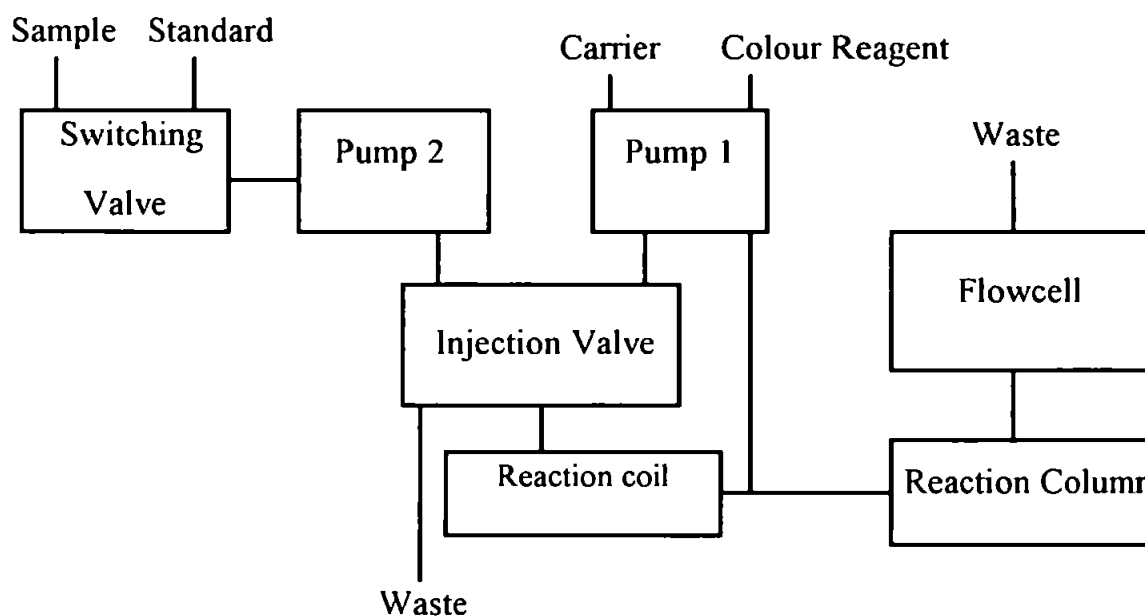
Figure 3.24.   Schematic diagram of the FI manifold layout used in the instrument

   module

After drying in a fan-assisted oven for 4 hours at 80 °C, the boards were then protected by the application of a single part acrylic conformal coating (Humiseal 1B31) [173, 174]. After the conformal coating had fully cured, the larger and more delicate components on the circuit boards were supported by applying a non-corrosive silicone RTV compound

(Dow Corning RTV 3145) [175] between the component and circuit board. This prevented damage to component legs from vibration or shock. Prior to submersed deployment, this system was laboratory tested and field bench tested aboard a research vessel (*RVS Tamaris*). During this period, the peristaltic pumps were changed as described in section 3.1. The use of two separate compartments for the FI manifold and the electronics proved awkward to use, especially during field trials on a research vessel in bad weather. The system was therefore re-configured as a chassis mounted system, as shown in Fig. 3.25, so that the complete instrument could be removed from the pressure housing.

Instrument
top plate

25 mm dia.
PVC spacers

Instrument
baseplate

Electronics pack
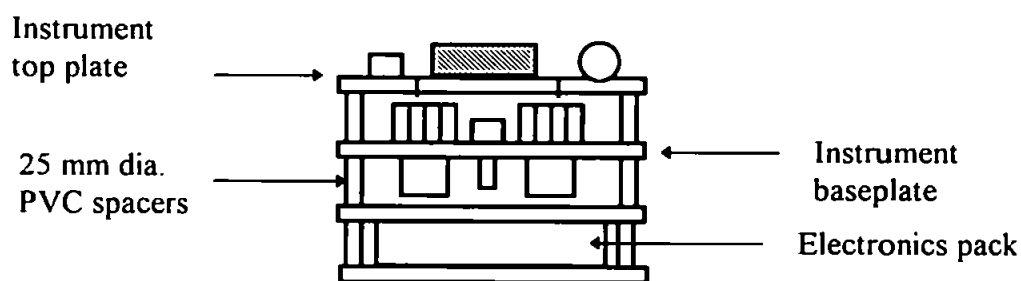
Figure 3.25.   Diagram of chassis mounted instrument configuration

A larger pressure housing for the instrument was also constructed so that an internal battery could be fitted. Unlike the first pressure housing which had two removable end caps, the second pressure housing had one removable end cap. The lower end cap was permanently sealed to the tube walls using a waterproof PVC adhesive. The pressure housing was fitted to the cage assembly as shown in Fig. 3.26., and pressure tested to a depth of 45 m in Plymouth Sound aboard the research vessel 'Squilla'. After successful completion of the housing depth/pressure test, the removable end cap of the pressure housing was modified to allow entry and exit of sample and reagents. This consisted of a machined circular rigid PVC tube holder with six 3 mm OD flexible PVC tubes running through it as shown in Fig. 3.27. A corresponding hole was machined in the instrument module removable end cap

85

for the tube holder to fit. To facilitate direct serial communications and external power supply/switching, an 'Impulse' 8-pin waterproof socket was fitted to the cover.
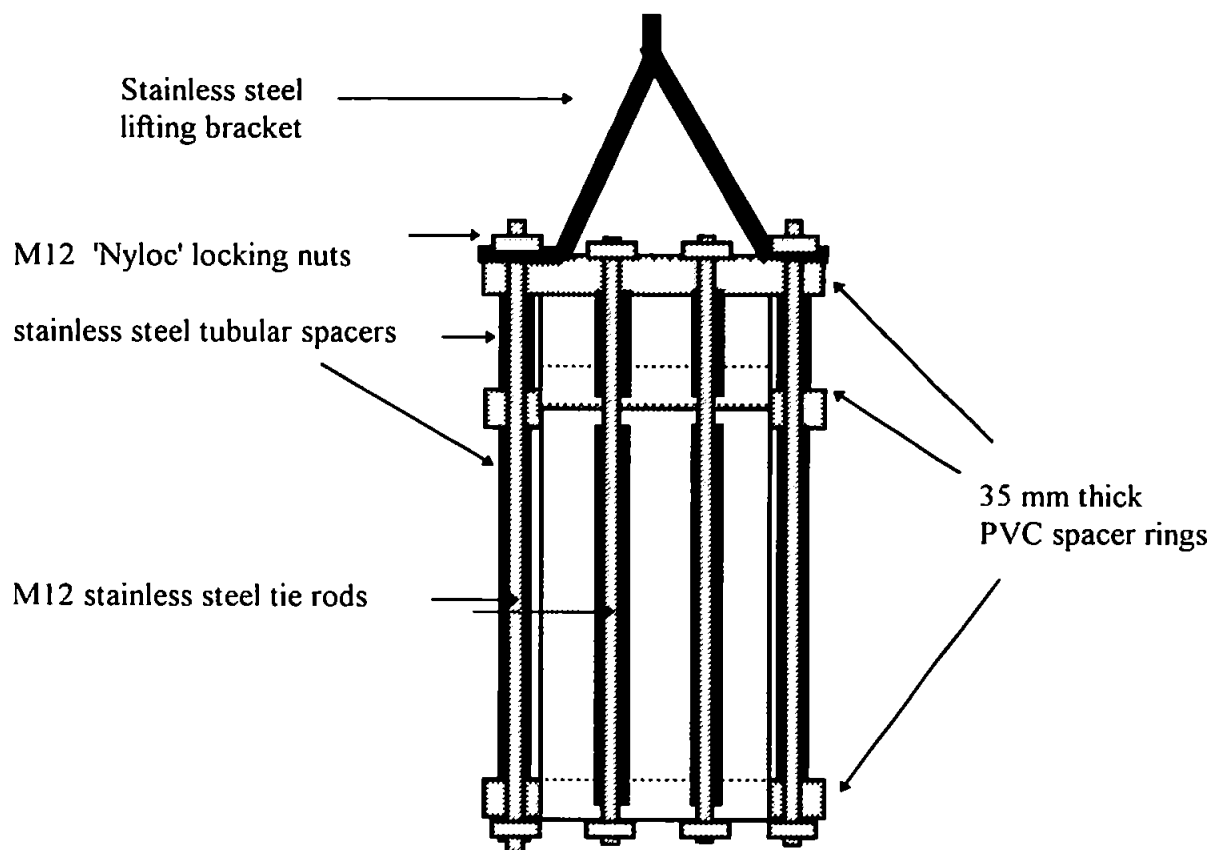
Figure 3.26.   **Diagram of the cage assembly used to lift and protect integrated system during deployments**
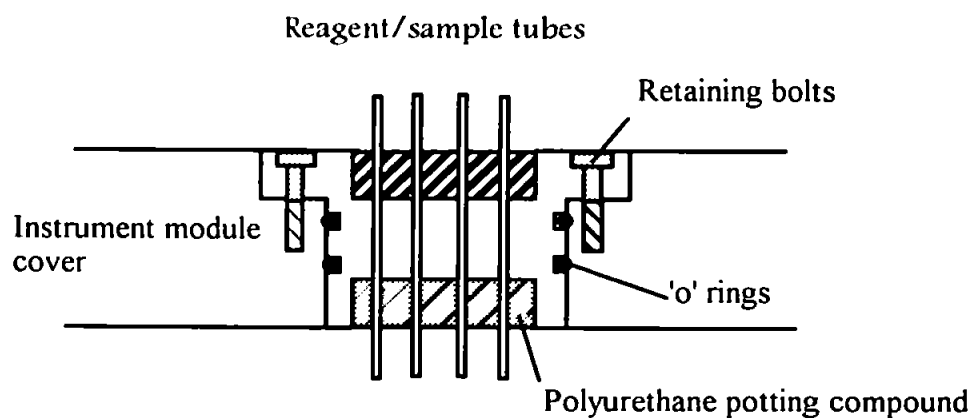
Figure 3.27.   **Diagram of the Reagent /sample inlet and outlet system fitted to pressure housing end cap**

Reagent module: A reagent module was constructed from 270 mm diameter PVC tubing as shown in Fig. 3.28., to hold the reagent bags at ambient temperature and pressure outside the instrument pressure housing.

Reagent module ⟶

Custom made umbilical cable

Reagent bags

Waterproof plug

Sample/reagent inlet

Instrument module pressure housing
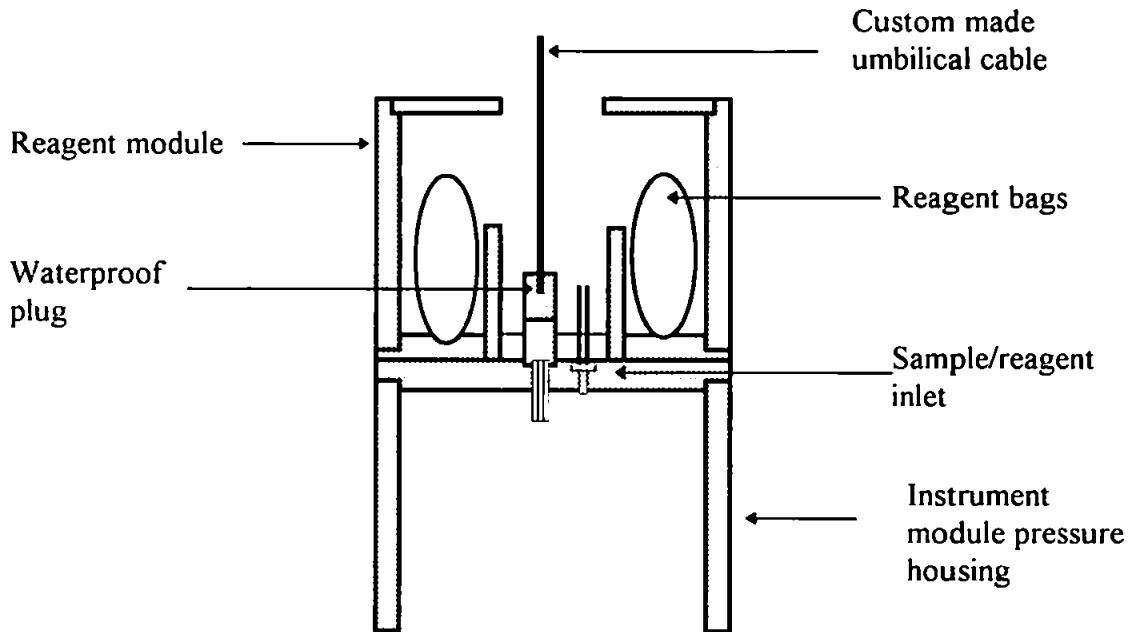
Figure 3.28. Side view of reagent module in position on instrument housing showing waterproof plug and tube inlet/outlet positions

Cage assembly: The cage assembly as shown in Fig. 3.26. was constructed to hold the various modules in position and to provide a method of attachment for deployments. This consisted of two end caps and one spacer ring machined from solid 35 mm thick rigid PVC. Six lengths of M12 stainless steel studding form the tie rods over which tubular stainless steel tube spacers were fitted to correctly position the PVC end caps and spacer ring. The stainless steel lifting bracket fitted on two of the tie rods and the whole assembly was held together with M12 stainless steel 'Nyloc' locking nuts.

Power supply and external controls: For submersed deployments the integrated system was powered internally by a 12v DC 15 amp/hour sealed lead-acid battery, type Yuasa NP15-12 which fitted into the lower part of the instrument housing as shown in Fig. 3.29.

Instrument
module pressure ——————→
housing

Instrument in position
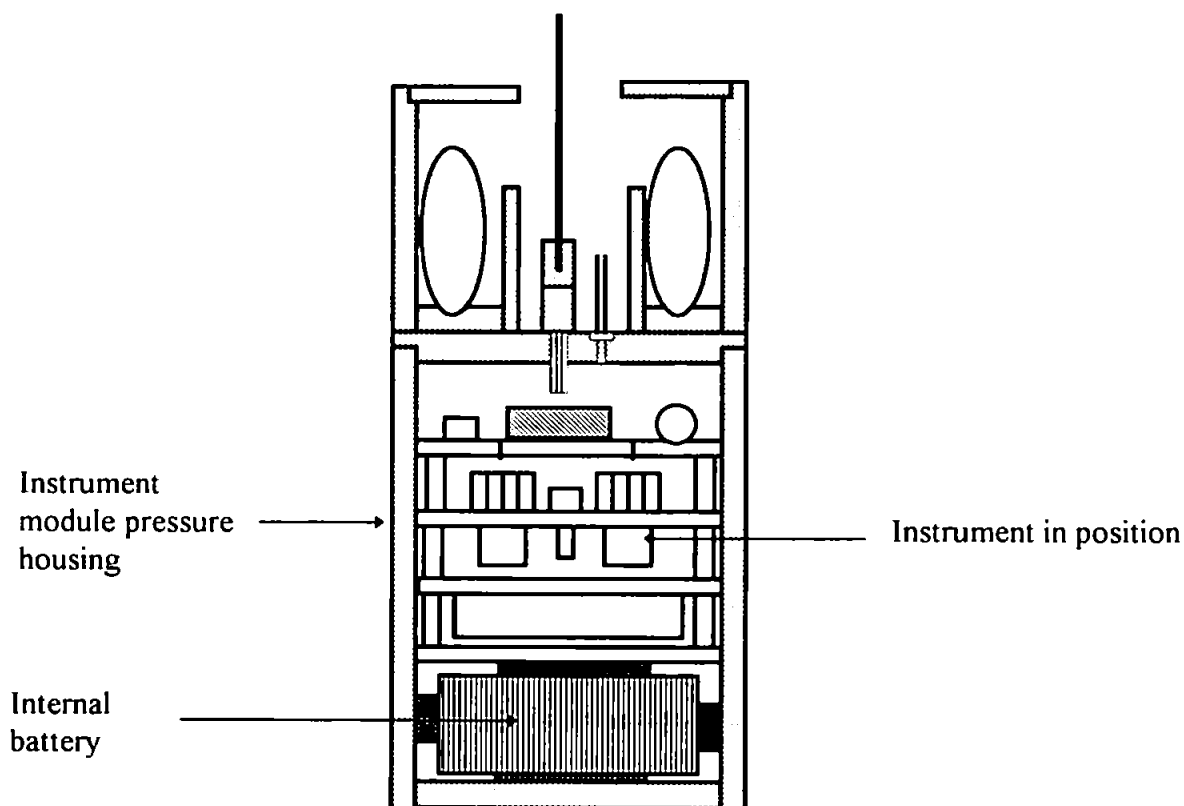
Internal
battery

Figure 3.29. Position of instrument module and internal battery in instrument module pressure housing

The battery was protected from shock using high density self-adhesive foam rubber pads. The system was configured so that it could be powered using internal batteries or an external supply via the umbilical cable.

Umbilical cable: The 50 m 8-core umbilical cable terminated at the instrument end with an 8 pin 'Impulse' waterproof plug. The surface end of the cable fed into an interface box which enabled the system to be switched on and off from the surface or powered from an external battery. The interface box also contained two coloured LED's which indicated the position of the injection valve, i.e. when in the fill and inject position. Direct serial communication

with a PC was also effected through the interface box. A schematic representation of the deployed system is shown in Fig. 3.30.
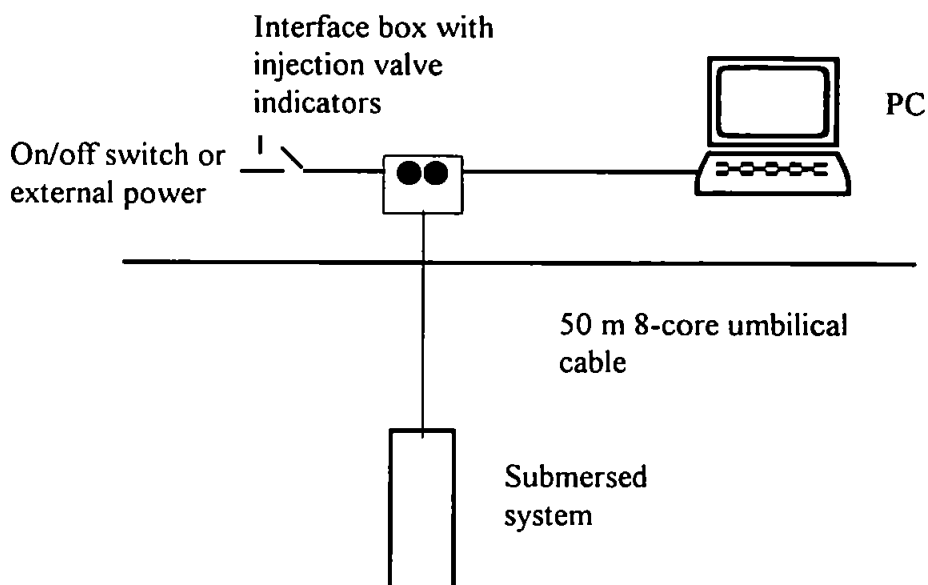
Figure 3.30. **Schematic representation of the deployed system and control interface**

Fitted to the end cap of the instrument pressure housing was the corresponding 8-pin 'Impulse' waterproof socket which was connected internally to the instrument to provide the power control, data communications and indicate the injection valve position. When connected, this arrangement allowed full external control and data communications for the development work. In addition to the on-board control programme, a small operating routine was written for the 'Crosstalk' for Windows® communications software so that all the instrument functions could be controlled manually using a Graphical User Interface.

3.2.   RESULTS AND DISCUSSION

3.2.1.   Reagent and sample delivery

Pump tubing: For a field instrument, component reliability is as much a concern as the stability of the system chemistry. FI instruments usually use peristaltic pumps to deliver

sample and reagents [117]. Generally peristaltic pumps are very reliable but the method of initiating and sustaining flow depends on physical contact between the pump rollers and pump tubing. This will eventually cause wear to the pump tubes and therefore has a direct influence on long-term reliability. Table 3.1. shows the pump tubing selected for test based on manufacturers published data.

Table 3.1. Manufacturers published data on pump tubing performance [165]

Trade Name	Material	Temperature range	Resistance to 50 % Phosphoric Acid	Service life pumping water @ 100 rpm
		° C		hours @ 21 ° C
Tygon Yellow	Modified flexible PVC	- 12 to + 65	excellent	250
Tygon	Flexible PVC	- 45 to + 65	excellent	200
-	Silicone	- 62 to + 205	*	620
Ismaprene	Butyl rubber	- 50 to + 135	excellent	1350

* no specific data available - tubing included in tests as it has been used extensively in this application with no reported deterioration.

The results from the examination of the tubing samples supplied is shown in Table 3.2., the tube bore, as measured with a shadowgraph, varied by approximately ± 3 % from the manufacturers data which was considered to be acceptable for use in a field instrument. The results of the long-term pumping experiments carried out on selected pump tubing are shown in Table 3.3. A slight fluctuation in the measured flow rates was observed for all tubes which was probably due to slight variations in room temperature during the test period.

Table 3.2. Measured physical properties of tubes purchased for reliability trials

Material.	Specification ID	Measured Mean ID	Measured ID Range	Measured Mean OD	Measured OD Range	Mean hardness	Visual
	mm	mm	mm	mm	mm	IRHD*	
Flexible Modified PVC	1.020	0.9987	1.0240 to 0.9750	2.7950	2.767 to 2.8430	44.5	Good bore profile.
Flexible PVC	1.020	1.0095	0.9900 to 1.0240	2.7440	2.7080 to 2.7830	51.9	Good bore profile.
Silicone.	1.020	0.9875	0.9620 to 1.0140	2.9543	2.9170 to 3.0000	41.7	Good bore profile.
Butyl.	1.016	1.0068	0.9750 to 1.0450	2.7198	2.6410 to 2.7960	55.0	Irregular bore profile.

* I.R.H.D. - International Rubber Hardness Degrees. used for comparison purposes only.

There is a significant difference in flow rates between the flexible PVC tubes and the silicone and butyl rubber tubes despite all having the same internal bore diameter. This suggests that when a FI manifold is optimised using a particular tubing material it must not be changed for another type without recalibration.

Table 3.3. Measured flow rates from pump tube trials over 40 days at room temperature

Time	Flexible Modified 'Tygon' Yellow	Flexible PVC 'Tygon'	Silicone Rubber.	Butyl Rubber. 'Ismaprene'
Days	ml.min^{-1}	ml.min^{-1}	ml.min^{-1}	ml.min^{-1}
3	1.0	1.0	0.7	1.2
5	1.0	1.0	0.8	1.1
20	0.9	0.9	0.8	1.0
33	0.9	0.9	0.7	1.0
40	0.9	0.9	0.8	1.0

Examination of the tube/pump roller contact area, as shown in Table 3.4., identified potential reliability problems with silicone tubing which was almost completely worn through by the end of the test period. Therefore, it cannot be recommended for extended use. However, the use of the recommended silicone lubrication spray may have caused premature deterioration as silicone fluids can penetrate the structure of silicone elastomers.

Table 3.4   Assessment of wear at pump/tube contact area after 40 days at room temperature

Flexible Modified PVC	Flexible PVC	Silicone Rubber.	Butyl rubber.
Negligible deformation and abrasion.	Very slight deformation and abrasion.	Severe deformation and abrasion, tube almost completely worn through.	Very slight deformation and abrasion.

To determine the effects of temperature on the different pump tubing samples, a similar test was carried out at controlled temperature and the results from this are shown in Table 3.5. The flow rates were reduced by as much as 30% for the flexible PVC types but the flow rate for the silicone tubing remained constant throughout the temperature range.

Table 3.5.   Measured flow rates at constant temperatures over 17 days

Temperature	Modified Flexible PVC	Flexible PVC	Silicone Rubber.	Butyl Rubber.
° C	ml.min^{-1}	ml.min^{-1}	ml.min^{-1}	ml.min^{-1}
22	1.0	1.1	0.9	1.1
5	0.8	0.9	0.8	1.0
10	0.9	0.9	0.9	0.9
5	0.7	0.8	0.9	0.9

Examination of the tube/pump roller contact spot found similar results to the room temperature test, as shown in Table 3.6., where the silicone tubing had a small flat spot worn in the contact area after only 17 days.

Table 3.6.   Assessment of wear at tube/pump contact area after 17 days running at constant temperatures

Flexible Modified PVC	Flexible PVC	Silicone Rubber.	Butyl Rubber.
No visible signs of wear	No visible signs of wear	Small flat spot worn at tube/pump contact point	No visible signs of wear

From these tests it was concluded that both forms of the flexible PVC tubing would be suitable for use in an *in situ* FI system for long term deployment. However, the temperature effect on flow rate would require appropriate calibration routines throughout the deployment period.

Pumps: The multi-roller peristaltic pump is by far the most widely used FI propulsion system and is capable of delivering a constant volumetric flow that results in highly reproducible sample residence times. Peristaltic pumps do not however, produce an entirely pulseless flow and in order to reduce the pulsations 8 - 10 closely positioned rollers are recommended. Half the rollers should be in permanent contact with the tubing, through sufficient, but not excessive, compression from the tensioner [176]. The main problem with single tensioner peristaltic pumps is the way the tensioning force is applied to the pump tubing. When different diameter tubes are used, the force required to initiate and sustain flow in the smallest diameter tube is also applied to the larger diameter tube. This effectively applies a 'brake' to the system as well as applying excessive lateral force to the pump bearings. The observed effects of this were:

i).   Poor pump start-up and flow initiation, particularly at temperatures lower than 25 ° C.

ii).   Premature wear of pump bearings; causing further flow problems.

iii).   Pump motors could be stalled under certain conditions; causing excessive current drain from the power supply.

This in turn had dramatic effects on the performance of the detection system, particularly at low analyte levels $(0.01 - 0.1$ mg $l^{-1})$ where, in the worst case situation, the sample signal was completely lost in the pulsations. One of the main aims of the project was to design an efficient and reliable propulsion system that produced accurate and precise raw data and required little or no electronic or software correction, i.e. to 'engineer out' inherent problems rather than rely on software smoothing routines. A comparison of performance of the worn original single tensioner pump and a new twin tensioner pump is shown in Fig. 3.31. Experience has shown that the twin tensioner pump provides a much smoother flow rate and has greater long-term reliability.
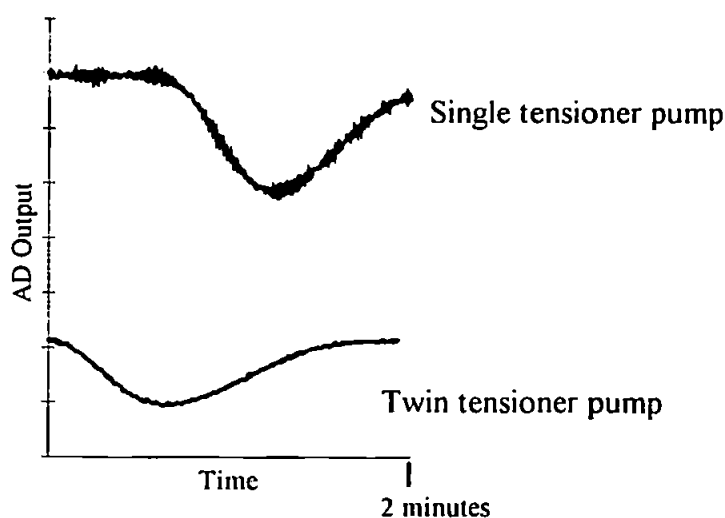
Figure 3.31. Flowcell output comparisons between single tensioner and twin tensioner peristaltic pumps, 0.5 mg l $^{-1}$ Nitrate-N

Tube connections: The adhesive bonded push fit tube connection failed to provide any significant advantage over a plain dry push-fit connection so this method was not pursued. Pull-off tests using a spring-balance showed that the push fit joint and adhesive lined heatshrink sleeving offered definite performance advantages and was relatively easy to use in the field. Pull-off tests on a joint made with heat-shrink over a push-fit connection typically required a force of 4.5 kg to break the joint compared to 0.1 kg for a standard push-fit joint. The method was used successfully for several months during submersed field trials. However, it became increasingly difficult to produce good joints in the field due to silicone grease contamination from the pressure housing seal so an alternative method of connecting the dissimilar tubing materials was investigated.

Reliable PTFE to PTFE joints were produced using the standard flanging method so it was then decided to make a similar connector for the flexible pump tubing. This could then be connected to the PTFE manifold tubing using an in-line connector. Tests on the ABS flange connectors found them to be extremely strong. The adhesive bond between the PVC tubing and the flanged ABS connector did not fail during the pull-off tests. The spring-balance used for the test went off-scale at 5 kg and there was no indication of the bond failing at that point. The spring-balance was removed from the test rig and the tube was pulled directly by hand until the PVC tubing itself broke at the point of maximum extension. The PVC to ABS bond was still intact after this test.

This method was then be used to connect the pump tubing to the PTFE manifold tubing using standard FI in-line connectors. Since developing the method, it has been successfully used in several submersed deployments to 30 metres depth. This procedure can be used in the field although it is better to prepare spare tubes in advance in clean laboratory conditions in order to guarantee reliability.

The ABS flange method of joining two dissimilar tubing materials has been shown to be the most reliable method of connecting the flexible pump tubing to the PTFE manifold.

3.2.2.   Injection valve

The original gearbox grease used was a heavy duty grade and consequently considerable effort was required to overcome the initial drag caused by the grease. This affected the operational speed of the valve and caused excessive current drain on the power supply. The grease was replaced with a mixture of grease and oil, known as a 'groil' and is often used where a grease or a lubricating oil is not suitable on its own. By mixing various amounts of oil and grease a 'custom' grade of lubricant can be produced so that unlike oil the lubricant stays in position, but is not too heavy to cause excessive drag. Prior to the change of lubricant, the gearbox could only just be turned by hand but after the change it could be rotated freely. The injection valve components were manufactured from PTFE which has excellent chemical resistance and a low coefficient of friction making it ideal for rotating valves in contact with aggressive fluids. However, PTFE tends to 'creep' under load, i.e. dimensions can alter under compression and at different temperatures so it is a difficult to hold close engineering tolerances using this material. This, coupled to the large gap between the end cap and body of the valve head, had the overall effect of causing the valve head to leak occasionally. The valve head required just the right amount of tension in the retaining screws; too tight and the valve stalled, too loose and the valve leaked. The retaining screws would also work loose soon after they had been correctly set causing a leak, a problem which had to be rectified before the nutrient sensor could be deployed remotely. Fitting the packing shim as shown in Fig. 3.8. cured the problem of leaking and

stalling and the injection valve was totally reliable after the modifications described in section 3.1.2.

3.2.3. Reduction column

Packed reduction column: Figure 3.32 shows the position of the glass wool plugs and the copperised-cadmium when in use, i.e. the carrier flow pushed the reductor material towards the outlet forming a small air pocket between the front face of the reductor and the glass wool plug on the inlet side. This caused gradual oxidation of the reduction column from that end. However, experience showed that this type of reduction column performed well for periods in excess of eight weeks of bench testing when fitted to the nutrient sensor. Performance remained constant during these periods with no observed deterioration until approximately 50% of the total length of column had oxidised.
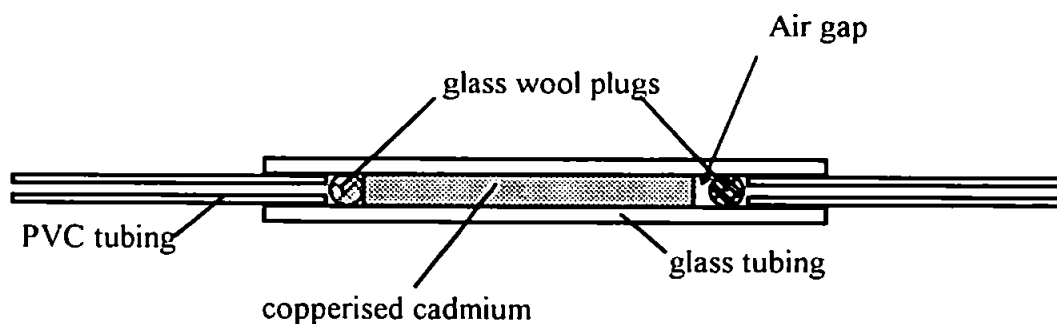
Figure 3.32. Packed reduction column with push-fit connections showing air gap formed between glass wool plug and reduction column

A more rapid deterioration was observed when the packed column was broken in several places and the larger air pocket at the front face was allowed to form smaller air pockets that remained trapped within the column. This usually happened when the column was subjected to severe shock.

Wire Reduction column: The main drawback with the packed column is that it takes considerable care to produce standard reduction columns. For this reason the wire reduction column appeared to offer distinct advantages in that the wire and tubing used would be relatively uniform, thus producing a column of standard dimensions. Table 3.7. shows the dimensions of wire reduction columns successfully used by previous workers. When fitted to the nutrient sensor manifold, the wire column did not perform as well as the packed columns, see Chapter 4, section 4.2. The long term stability of the wire column was reduced if they were not removed from the system and stored correctly when not in use. In both cases when wire columns were permanently fitted to the instrument, the columns deteriorated to a point where they were not fit for purpose within one week. It was observed that oxidation of the wire column was initiated at the areas of untreated cadmium that are present at the wire to tube wall contact points. The flow characteristics of the wire column were not suited to the instrument; the time from injection to commencement of the ADC count increased from 1.5 minutes for the packed column to 3 minutes for the wire column.

Table 3.7. Previous use of cadmium wire reduction columns

Wire Type	Wire OD	Tube ID	Reference
	mm	mm	
Cadmium	1.0	1.59	100
Cadmium	1.0	1.5	101
Cadmium	1.0	1.3	166
Cadmium	1.0	1.5	177
Cadmium / Silver (95% / 5%)	1.27	1.59	60
Cadmium/Silver (95% / 5%)	1.6	2.0	102

It was therefore decided to concentrate on optimising and ruggedising the packed reduction column for use in the nutrient sensor.

Optimised packed column: The flow characteristics of the acrylic bodied packed reduction column were found to match that of the manifold. There was no significant delay observed after the reduction column was fitted, i.e. by comparing the times taken for a nitrite and nitrate sample peak to reach the flowcell. The use of Nylon$^{\circledR}$ mesh filters eliminated the air bubbles associated with the original glass bodied reduction column. Examples of this reduction column have been used successfully in submersed deployments to depths of 30 metres and for cumulative periods of up to 6 weeks before needing to be replaced. During system shut-down, no deterioration of the reductor was observed as long as carrier solution was flushed through the manifold.

3.2.4. Reaction coil

The use of the support coil as described in section 3.1.4. enabled the reaction coil tubing to be easily replaced when soiled. This also maintained coil dimensions and bend radius which gave uniform mixing of the reagents and sample and a standardised reaction time.

3.2.5. Flowcell

UV/visible spectrophotometry continues to be the most commonly used detection method for FI analysis due to the diverse range of analytes which can be determined [116]. Low-cost light emitting diode (LED) - photodiode detectors or more sophisticated one and two dimensional photodiode array detectors offer the additional advantage of being rugged, and

therefore suitable for incorporation in FI field instrumentation. The application of LED and photodiodes in detection systems was first discussed in 1973 by Flaschka *et al.* [178]. Since then, several applications of LED - photodiodes as spectrophotometic detectors have been reported [179, 180, 181, 182]. Table 3.8. illustrates the range of LEDs which are now commercially available and the range covered, i.e. visible to NIR region. A LED is a rectifying semi-conductor device that converts electrical energy into light or infra-red radiation. For example, a red LED consists of gallium arsenide-phosphide on a gallium arsenide substrate. A *p-n* junction is created within the diode which allows passage of an electrical current in one direction only. The *p-n* junction is the boundary between the negatively charged semi-conductor material (*n-region*) containing excess unbonded electrons and, the positively charged area (*p-region*) which contains 'holes'. The 'holes' are areas of positive charge caused by the liberation of electrons from the crystal lattice. When the *p* and *n* regions are connected to a direct current (DC) source with a forward bias, i.e. *p* to positive and *n* to negative, excess electrons from the *n* region travel to the electron deficient *p* region. Light is emitted at a *p-n* junction when electrons and holes recombine [184,185].

Table 3.8.   Characteristics of commercially available LEDs [183]

Typical emitter material	Colour	Typical peak wavelength, nm.
SiN	Blue	470
GaP	Emerald Green	558
GaAsP on GaP substrate	Green	565
GaAsP on GaP substrate	Yellow	590
GaAsP on GaP substrate	Orange	620
GaAsP on GaP substrate	Red	654
GaAlAs	Near IR	880
GaAs	IR	940

Photodiodes provide a very linear and fast response to transmitted light. These semi-conductor devices are constructed from e.g. silicon which is partially 'doped' with a group V element such as arsenic to produce excess electrons in the n region and with a group III element such as gallium to produce excess holes in the p region. When connected to a reverse biased direct current, photons falling on the photodiode will liberate additional electrons which will create additional 'holes' in the p-n junction depletion layer. This results in an increased conductivity which is directly proportional to the light falling on the photodiode [184,186]. With the appropriate circuitry, photodiodes can therefore be used to detect the light emitted from LEDs [167,179]. The photodiodes investigated are shown in Table 3.9., but the final choice, the BPW21 type, was considered to offer the best performance characteristics.

Table 3.9.   Characteristics of suitably sized photodiodes [183]

Type	Can diameter	Peak spectral response	Operating temperature	R.S. product. No
	mm	λ nm	°C	
BPW21	8.12	560	-25 to +70	303-719
BPX65	4.70	850	-25 to +70	304-346
Integral Amp.	8.30	900	0 to +70	308-067
Gen. Purpose	4.70	750	0 to +70	305-462

The manufacturers data sheet [183] stated that the 'eye-response' type BPW21 photodiode would operate at approximately 95 % efficiency at 540 nm, as shown in Fig. 3.33. The other devices initially considered all had peak responses in the region of 750 - 900 nm which meant that in the region of interest they were operating at approximately 50% efficiency.
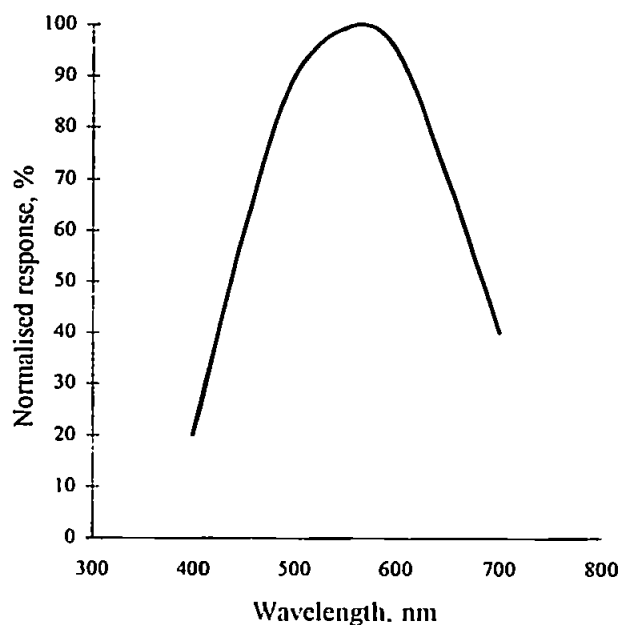
Figure 3.33. Spectral response of type BPW21 photodiode [183]

Using the effluent from the 'FIAstar' analyser used in the chemistry optimisation tests [107], which was fitted with a 260 µ l sample loop, the first prototype flowcell gave good response and was extremely stable as shown in Table 3.10. and Fig. 3.34.

Table 3.10.   Typical results from the first prototype 10 mm flowcell.

Nitrate-N	Mean Output (Baseline - Standard)	n	RSD
mg l^{-1}	mV		%
0.0	0.0	4	0.0
0.1	3.0	4	0.0
0.5	14.0	4	0.0
1.0	24.5	4	2.0

$$y = 25x + 0.6$$
$$R^2 = 0.99$$
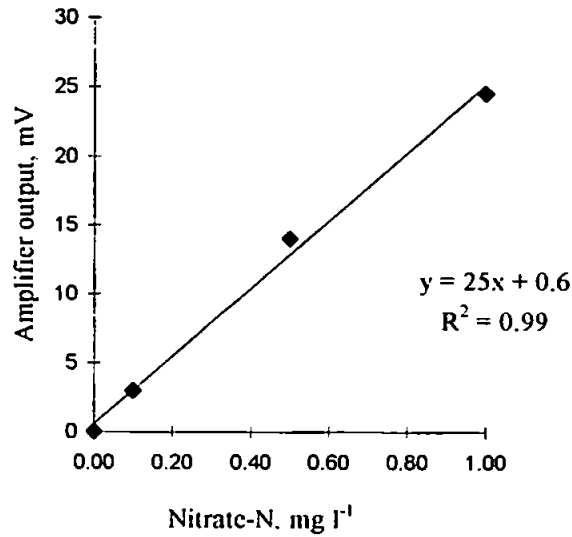
Nitrate-N, mg l^{-1}

Figure 3.34. Calibration graph of response (mV) vs Nitrate-N concentration (mg l^{-1}) using data from table 3.10.

Linearity was also found to be good over the 0 - 1 mg l^{-1} range. Although the performance was acceptable for a first prototype rugged flowcell, it required a certain amount of 'operator assistance' in order for it to operate correctly. Occasionally the cell trapped air bubbles from the manifold which could easily be dislodged by pinching the flexible outlet tube. This was not acceptable for use in a remotely deployed system. However, as the manifold cleared of bubbles and the internal surfaces began to wet, the occurrence of trapped air bubbles diminished. Further examples were constructed with different path lengths to determine the full performance range of the design. Flowcells of path length 5 mm and 20 mm were constructed but both were found to be unsatisfactory when tested using the same method. Response and stability from both versions proved unacceptable so no useful results were obtained. Close examination of the design and construction however, confirmed that the use of clear acrylic rod was not suitable. In addition to the natural internal reflection and diffraction which was thought to occur in the

material, which is used for light guides, the flat cell window produced by the addition of the heatsink may have contributed to the poor performance. The removal of the LED lens may have produced excessive scatter by increasing the angle of incidence of the LED source, which for some reason was worse in the shorter and longer length flowcells. Therefore, a suitable alternative material to the clear acrylic rod was identified as grey rigid PVC. The change to an opaque material and the retention of the LED lens supported the theory of internal reflection and diffraction affecting the performance of the cell. The results from the experiments using a series of Nitrite-N standards are shown in Table 3.11. and Fig. 3.35.

Table 3.11.   Typical results from the PVC 20 mm modified 'Z' cell

Nitrite-N Standard		Mean Output	n	RSD
μM	mgl^{-1}	Baseline - Standard mV		%
0.1	0.0014	6.3	17	7.24
1.0	0.0140	53.7	3	3.70
2.0	0.0280	109.7	3	1.87
3.0	0.0420	148.3	3	1.15
5.0	0.0700	186.7	3	0.91

Other materials were considered for the flowcell construction, but rigid PVC was finally chosen for the following properties:

o Opaque

o Good chemical resistance

o Good machinability

o Good surface wetting and adhesive bonding
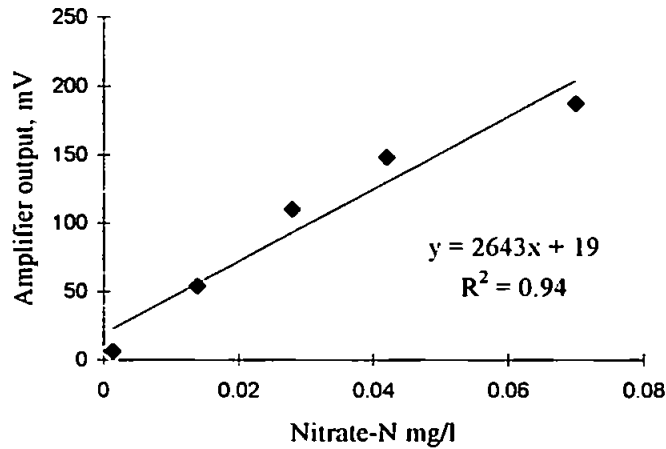
Figure 3.35. Calibration graph of response vs Nitrite-N (mg l^{-1}) using the data from table 3.11.

Materials such as PTFE (polytetrafluoroethylene) and PEEK (polyetheretherketone) are considered to have better chemical resistance than rigid PVC [169,187] but they are extremely difficult to wet and therefore adhesive bond. Therefore, they were not considered to be suitable in this application. The final flowcell design, as shown in Fig. 3.21., has proved to be very reliable and been successfully used for over 18 months of laboratory and field testing. In all cases the flowcell performance was considered acceptable for the application, giving good linearity over the ranges tested and did not suffer from trapped air bubbles.

3.2.6. Control system

The control system provided total and flexible control for the sensor and proved to be reliable during field trials. The application of the conformal coating and RTV to provide environmental protection was also extremely beneficial. Conformal coatings are essentially special purpose varnishes which are applied to circuit boards to provide a hermetic seal

against moisture and contamination, therefore reducing the risk of corrosion. Ideally, a two-part polyurethane conformal coating system would have been used in this application as this offers better protection in humid environments [173,174]. However, polyurethane coatings are difficult to remove to allow for repair or modification. They also contain isocyanates which require specialised handling during application and removal operations. Single-part acrylic conformal coatings provide a good compromise between moisture resistance and ease of application and handling. Such coatings can easily be removed using an organic solvent such as trichloroethane. Non-corrosive room temperature vulcanising (RTV) compounds cure with the liberation of alcohol whereas normal RTV compounds cure with the liberation of acetic acid which can have deleterious effects on circuit boards The use of the conformal coating and the RTV compound was actually put to the test during one submersed deployment. One of the heat-shrink tubing joints failed and caused the instrument pressure housing to flood with sea water. This unfortunately occurred as the system was being deployed so it was not discovered until it was powered up at 30 m depth. The system was immediately retrieved and the instrument pressure housing opened and washed out with clean freshwater. The only damaged sustained was a blown *EPROM* which could not be protected as it had to be removable for programming. The boards were thoroughly cleaned and a new *EPROM* was fitted and the system worked perfectly.

3.2.7. Integrated system

Materials: The materials of construction are important due to the harsh and corrosive environment in which the sensor will be deployed. The physical forces that can be encountered during deployments, particularly in bad weather, required the material to be resistant to impact damage throughout the temperature range. The prototype system was

constructed from rigid PVC and corrosion resisting steel. Both these materials were selected for ease of machining and availability. Rigid PVC is extremely tough and is extensively used for water pipes and tanks, it has low water absorption, good chemical resistance and good thermal stability over the operational range expected for the sensor [169], i.e. dimensions are expected to remain stable during deployments. Corrosion resisting steel is not the ultimate choice for the sensor as it is relatively expensive and will eventually corrode. Commercially pure titanium would be the best choice but machining can be problematic and although it is relatively inexpensive compared to some of the higher grades of corrosion resisting steel, it is not generally available. Therefore, all fasteners and external metal components were made from class 18/8 corrosion resisting steel which provides a good balance between cost and availability, machining characteristics and corrosion resistance [170].

Construction: The construction of the first instrument module provided separate manifold and electronics compartments which required two sea seals and two internal seals. Initially this design was thought to offer better protection to the instrument internals by separating the 'wet' side from the electronics so in the event of a internal leak the electronics compartment would be dry and salvageable. In practice this meant that four good seals had to be made for this arrangement to work. This was later considered to be an over complicated design and could in fact increase the chances of a leak which was another good reason for having a single compartment instrument module. The final instrument pressure housing was permanently sealed at one end and therefore only required one sea seal and no internal seals. The FI instrument was chassis mounted so that it could be completely removed from the instrument pressure housing for better maintenance and adjustment. This also allowed it to be used as a bench instrument without the additional weight of the pressure housing. The overall modular concept has also been applied to the instrument in

that all components can easily be replaced or upgraded. The second instrument pressure housing was increased in size to house sufficient battery power for a deployment of one complete tidal cycle.

Battery: The type selected was a sealed lead-acid YUASA NP15-12, 12 volt DC 15 ampere h^{-1} which proved to be sufficient for several days deployment without recharging. Portable battery operated equipment have been typically powered by primary cells, i.e. non-rechargeable batteries. However, in the last ten years the development of small, rechargeable, maintenance-free sealed nickel-cadmium and lead-acid secondary cells has made it possible for this type of cell to be used more often. The comparison between primary cells and advanced secondary cells, Table 3.12. illustrates how the high performance advanced rechargeable cells offer significant performance advantages over primary cells.

Table 3.12.   Performance comparisons between primary and advanced secondary cells [161]

	Primary cells	Secondary cells	Advanced secondary cells
Energy density	2	3	1
Power density	3	2	1
Charge retention	1	2	2
Flat discharge profile	3	1	1
Operating temperature	2	1	-

1 = best, , 3 = worst.

The initial cost of primary cells is generally lower than for secondary cells and this could be advantageous in a single use application. However, the cost advantage is soon lost when it is considered that some types of secondary cells can be recharged up to 700 times. Having decided to use a secondary cell for this application, a decision then had to be made on the

type of secondary cell to be used. For this situation it is a choice between nickel-cadmium and sealed lead-acid batteries. Both offer good performance at a reasonable cost and are readily available. Table 3.13. lists the characteristics of sealed lead-acid and nickel-cadmium rechargeable batteries. Lead-acid cells do not suffer from a 'memory' effect which means they are not susceptible to poor charging procedures, making them much more rugged and therefore more suitable for a field instrument. Extreme care has to be taken when charging and discharging nickel-cadmium cells to prevent a 'memory' effect and obtain optimum performance. Therefore, the sealed lead-acid cells were considered to be the most suitable for this application.

Table 3.13.   Performance characteristics of Ni/Cd and Pb/acid batteries [161]

	Nickel-Cadmium	Sealed Lead-Acid
Nominal cell voltage, V	1.2	2.0
Energy Density, WH/kg	35	35
Charge retention @ 20 °C	3 - 6 months	6 - 9 months
Calendar Life, years	3 - 5	3 - 8
Life cycles	300 - 500	200 - 250
Operating Temperature, °C	- 20 to + 45	-40 to + 60
Relative Initial Cost, kWH	20	10
Memory effect	yes	no

Cage assembly: The cage assembly provided a method of holding the various modules together without attaching fixings to the walls of the modules which would otherwise create stress points. The cage assembly also provided substantial protection to the sensor and attachment points for lifting brackets. For simple drop deployments from a boat a single bracket was attached to the top of the cage assembly. For tethered buoy deployments, brackets can be attached to both ends of the cage assembly so that the sensor fits between

the buoy and its anchor as described in Chapter 2. The physical dimensions of the completed integrated system are shown in Table 3.14.

Table 3.14. Physical dimensions of completed integrated system

Module	Weight	Dimensions
	kg	mm
Reagent (including reagents)	4.6	270 dia. x 190 h
Instrument housing	8.6	270 dia. x 445 h
Instrument	4.5	240 dia. x 215 h
Cage assembly	12.8	370 dia. x 700 h
Yuasa battery	5.45	180L x 165h x 75w

All modules were well below the target weight of 15 -25 kg and the combined weight of the cage assembly, empty reagent module and empty instrument module was 25 kg .

Photographs: To further illustrate the results of the development of the integrated system photographs were taken of the first and second prototype systems at various stages of development. The first prototype system to the original design concept as described in Chapter 2, Fig. 2.1. is shown in Fig. 3.36. in the early stages of construction. The instrument module was constructed with two separate compartments, i.e. the analysis compartment and the electronics compartment. Also shown are the separate battery and filtration modules which were later omitted as discussed in Chapter 2 and 3.

The manifold layout in the analysis compartment of the original two compartment system is shown in Fig. 3.37. The photograph illustrates how the various major components were positioned for ease of maintenance and repair. At this stage of development the single tensioner pumps and push-fit packed reduction column were fitted.

Removal of the four cross-headed screws in the corners of the top plate would allow the whole top plate to be removed from the compartment to gain access to the pumps and injection valve if required. For normal operation, the cut out section of the top plate, shown at the bottom of the photograph, allowed access to the pump tensioner screws when the top plate was in position.

The change to a single compartment and the chassis mounted instrument as described in Chapter 3, section 3.2.7., is shown in Figs. 3.38. and 3.39. The manifold layout was unchanged from the original design but the change to a chassis mounted system enabled the whole instrument to be split into separate components by removing eight screws. The close-up view of the manifold, Fig. 3.39., shows the twin tensioner peristaltic pumps and the ruggedised packed reduction column as discussed in sections 3.2.1. and 3.2.3.

Fig. 3.40. shows the reagent module in position with the lid removed. The central hole in the lid allowed the umbilical cable to be connected waterproof plug on the instrument module which is shown in Fig. 3.41. Also shown in this photograph is the custom built tube entry/exit system fitted to the removable end cap which enabled reagents, sample and waste to be pumped in and out of the instrument module pressure vessel. The pressure vessel is in position in the cage assembly as described in section 3.1.7. and this photograph shows the detail of how the PVC spacer rings, stainless steel tie rods and stainless steel spacer tubes were assembled. The internal connections for the umbilical cable and tubing, i.e. on the internal side of the instrument housing removable end cap, are shown in Fig. 3.42. The tube entry/exit device is shown in greater detail in Fig. 3.43. where one of the 'O' seals has been removed for clarity. Also shown in this photograph are some of the custom built tubing connectors fitted to the flexible tubing as described in section 3.2.1. Fig. 3.44. shows the instrument module pressure housing with the end cap removed to show the internal battery in position. Also shown is the machined internal surface of the pressure housing which was

required to provide a good seal with the end cap. The cage assembly was designed to give protection to the instrument and to hold the various modules together without resorting to attaching fastening devices directly to the pressure housing. This photograph illustrates how the interface between the instrument module and the reagent module was protected by the 35 mm thick PVC spacer ring. The final photograph, Fig. 3.45., shows the instrument module and the reagent module in the cage assembly. Attached to two of the tie rods at the top of the integrated system is the custom made stainless steel lifting bracket. This arrangement was used for the simple drop deployments from the research vessels. For tethered buoy deployments as discussed in Chapter 2, section 2.8., a second bracket could be attached to the underside in the same way as shown in Fig. 2.3.
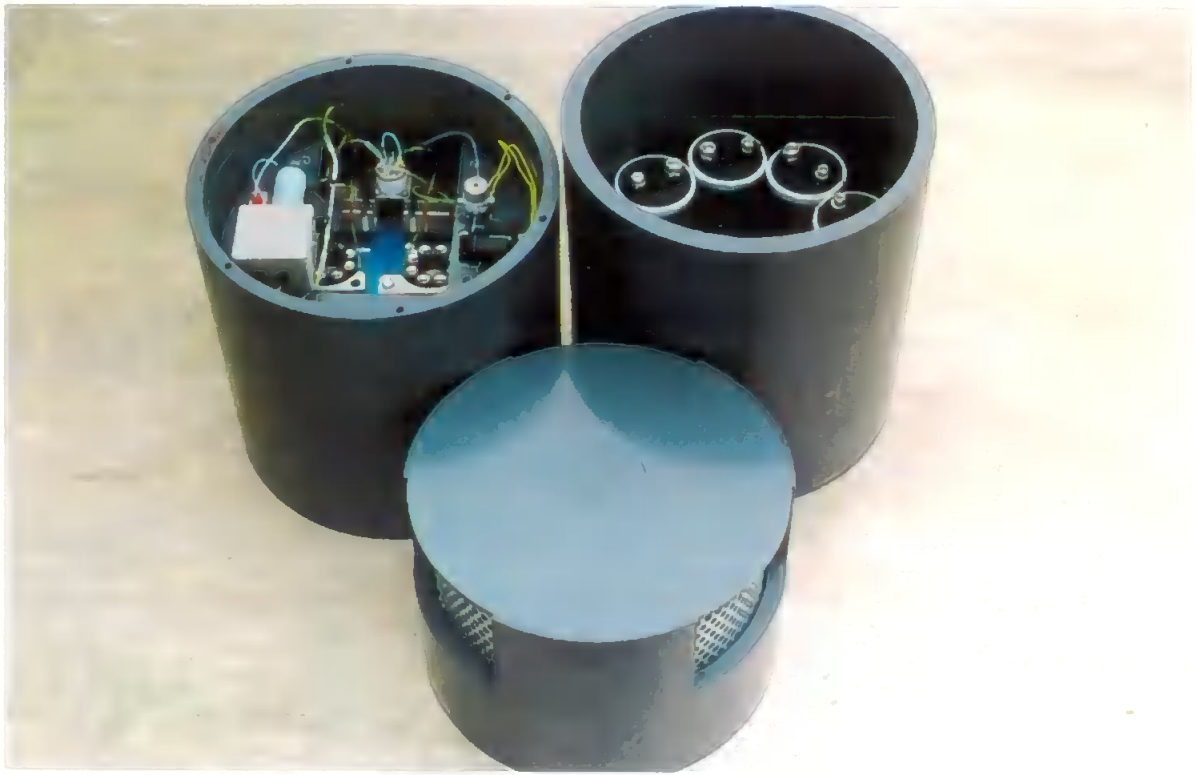
Figure. 3.36.   View of original design concept showing separate modules and instrument module with separate analysis and electronics compartments
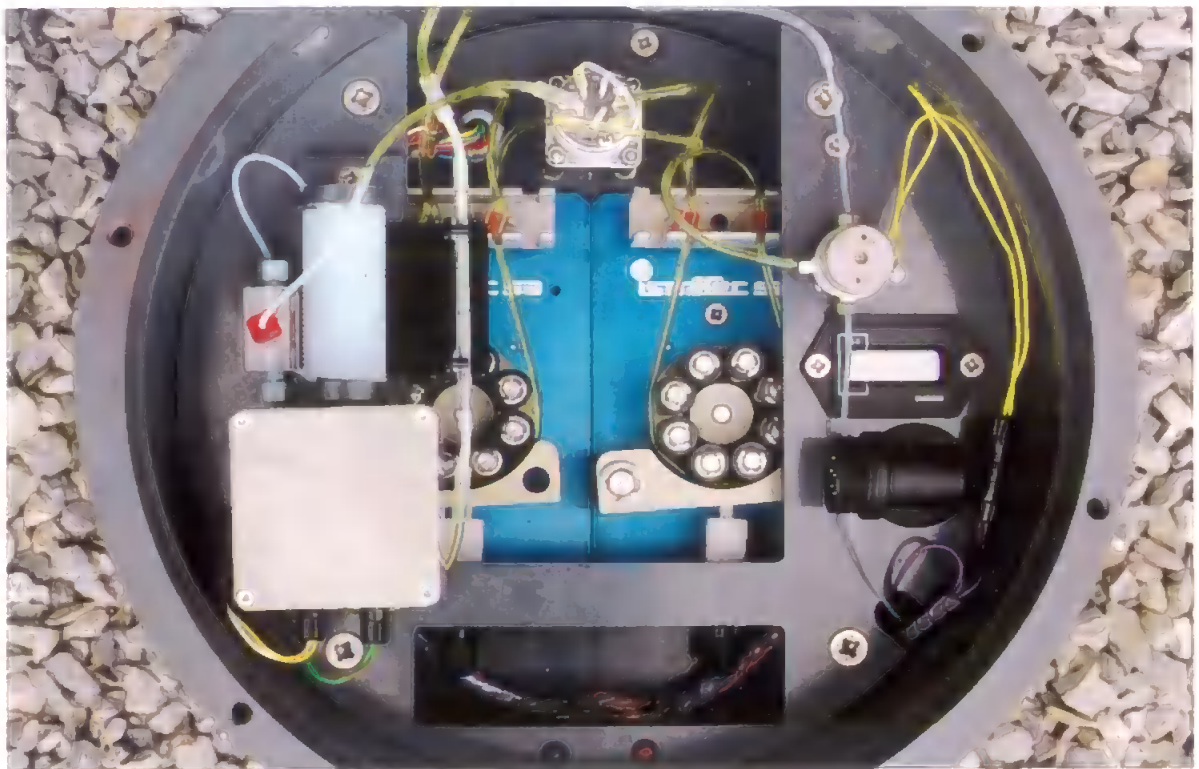
Figure 3.37.   View of original system analysis compartment showing single tensioner pumps and push-fit packed reduction column
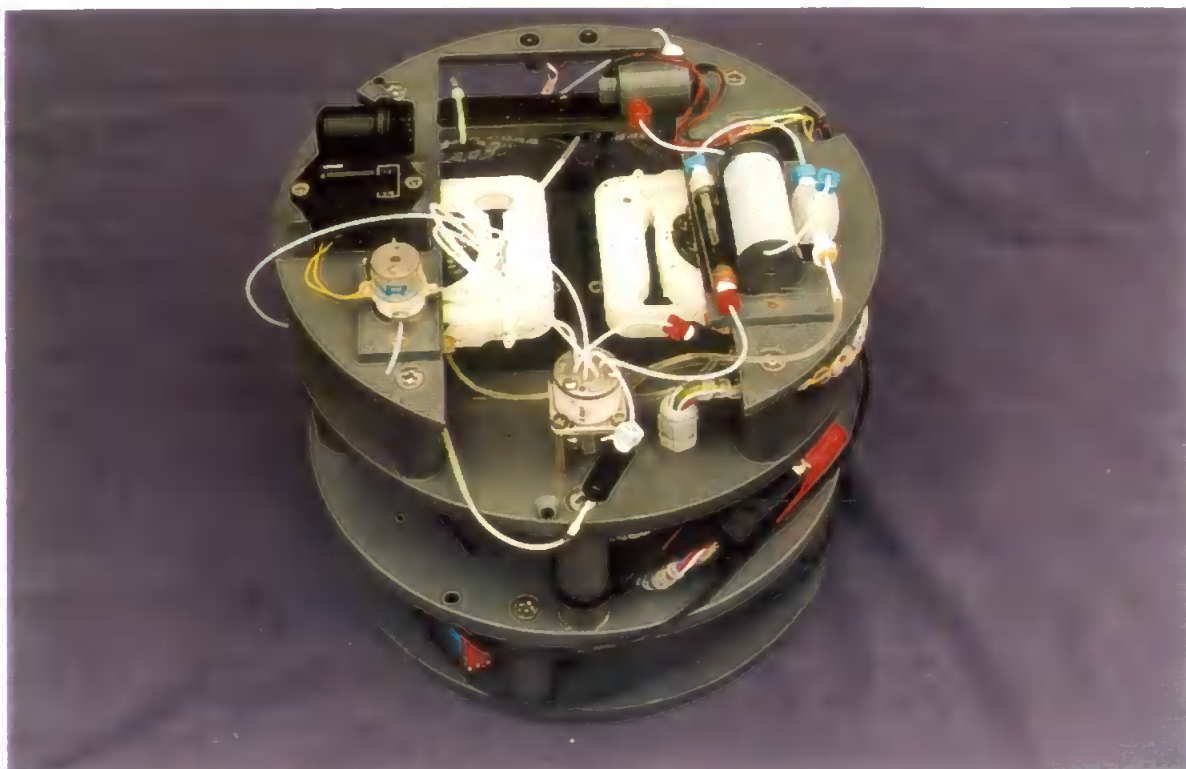
Figure. 3.38.   View of chassis mounted instrument
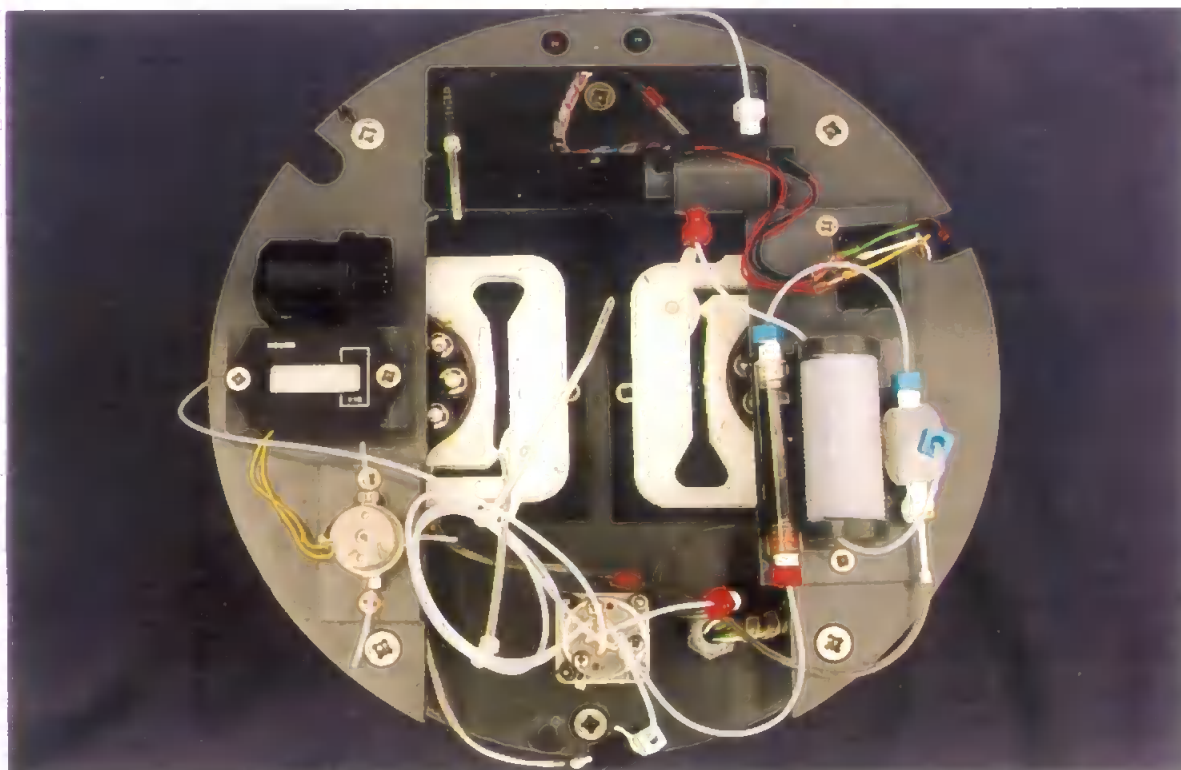
Figure 3.39.   View of chassis mounted instrument showing twin tensioner pumps, acrylic bodied packed reduction column, reaction coil and final design flowcell

Figure. 3.40. View of reagent module in position
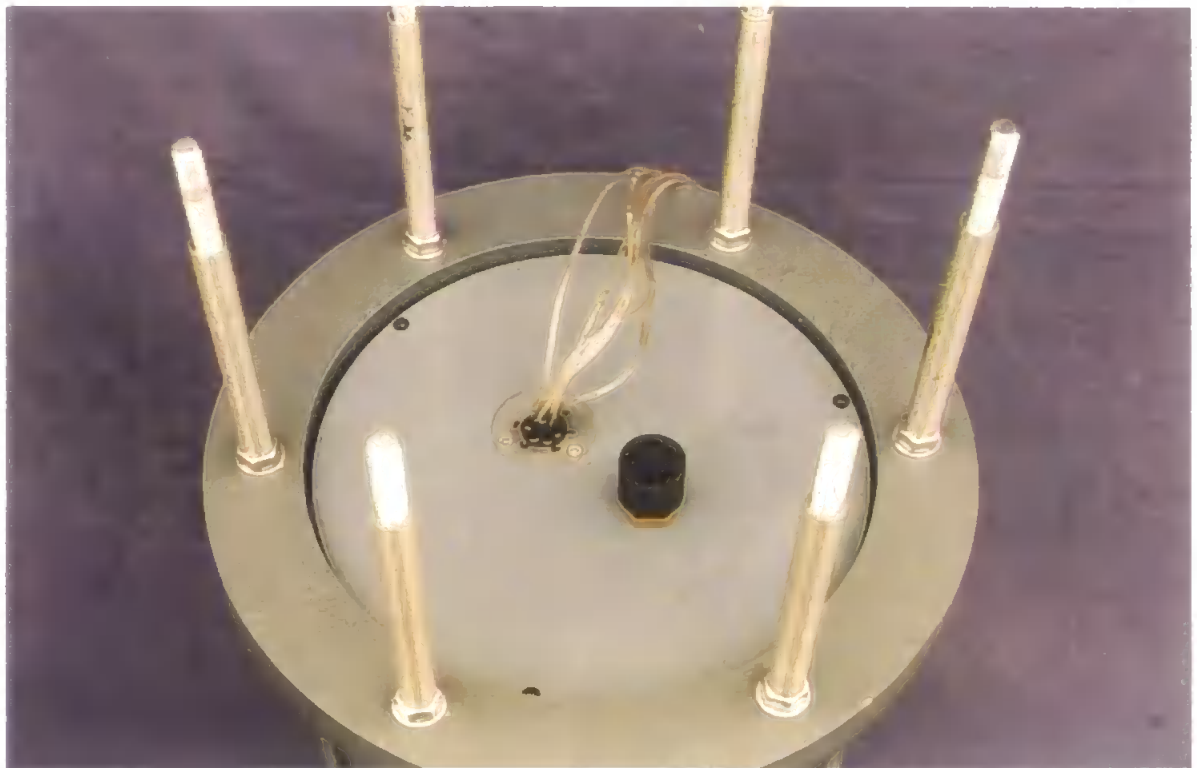
Figure 3.41. View of instrument housing end cap with detail of waterproof
socket and tube entry system

Figure. 3.42. View of underside of instrument housing end cap showing detail of internal connections for cable and tubes

Figure 3.43. Detail of tube entry device showing 'O' seals
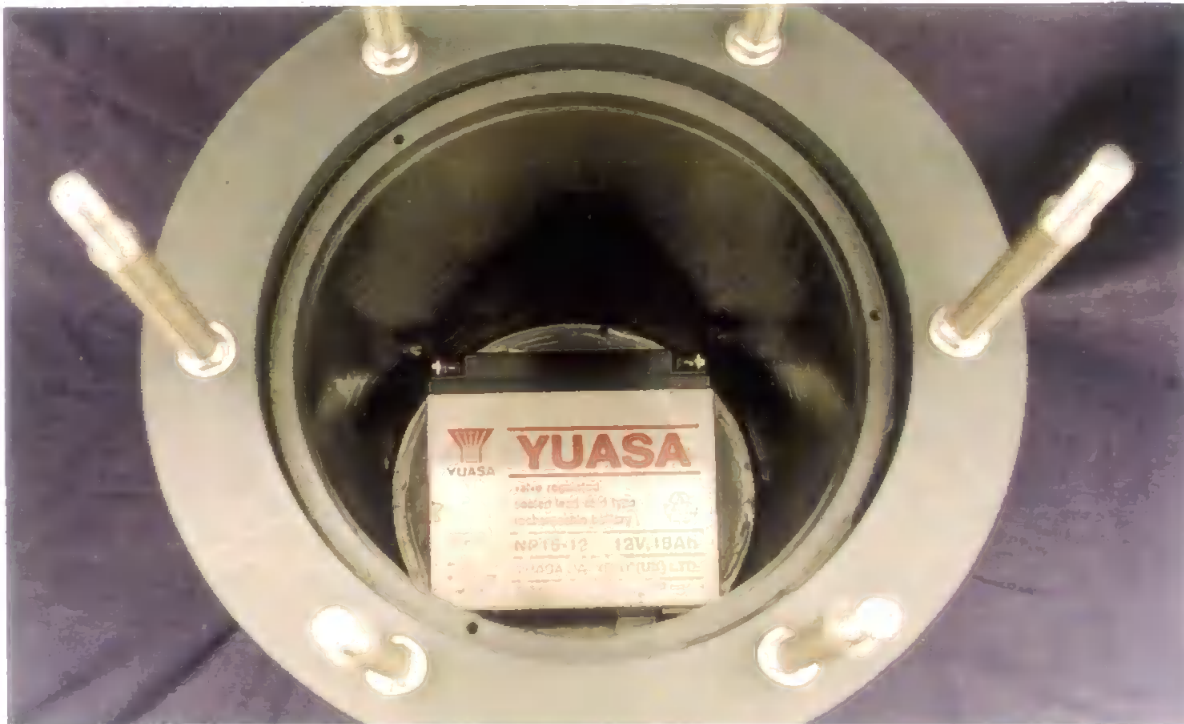
Figure. 3. 44. View of the internal battery in position in the instrument module

Figure 3.45. View of instrument and reagent modules in cage assembly

3.3.   CONCLUSIONS

The key individual components of the submersible FI based nutrient sensor were meticulously investigated in order to provide the final integrated system with the capability of operating under the conditions specified in Chapter 2.

The final integrated system was of modular construction and the weight of each module was less than the specification 15 kg. The design enabled the sensor to be used in a simple ship-borne drop deployment mode by attaching a lifting cable to the lifting bracket. With the addition of a second bracket attached to the underside of the cage assembly the sensor could be tethered to a surface buoy and anchor.

The construction materials used throughout the system were corrosion resistant and capable of withstanding the harsh physical conditions expected during deployments.

The FI instrument was designed and constructed to permit simple field maintenance and repair. The final chassis mounted FI instrument could be stripped down and re-assembled within one hour using a screwdriver.

Power could be provided using an internal battery or via an umbilical cable which also enabled direct serial communication with a PC on the surface. This allowed the system to be used in a manual mode as well as the normal fully automatic mode which was effected by the on-board control system.

Chapter Four
Laboratory Trials

4. LABORATORY TRIALS

This chapter describes the optimisation and analytical performance of the FI instrument under laboratory conditions for the determination of nitrite and nitrate. The key operational parameters e.g. flowcell path length, injection volume and LED intensity are investigated. The development of the operating routine for on-board control is also described in this chapter.

4.1. EXPERIMENTAL

4.1.1. Reagents

All solutions were prepared from ultra-pure water produced by a 'Milli-Q' system (Millipore Corporation), and all reagents were AnalaR® (BDH) unless otherwise stated. The carrier solution was prepared by dissolving 10.0 g of ammonium chloride in 1 l of water. The N-(1-naphthyl)ethylenediamine dihydrochloride (N1NED, Sigma Chemicals) and sulphanilamide reagents were prepared by dissolving 0.5 and 25.0 g respectively in 1 l of water containing 10 % ($^v/_v$) orthophosphoric acid. The mixed colour reagent was subsequently prepared by mixing equal volumes of the N1NED and sulphanilamide reagents in a brown glass bottle. A stock 1000 μM Nitrite solution was prepared by dissolving 0.0690 g of sodium nitrite in 1 l of water. A stock 1000 μM nitrate solution was prepared by dissolving 0.1011 g of potassium nitrate in 1 l of water. Working standards were prepared by serial dilution of the stock solutions with water.

4.1.2. Manifold configuration

The chemical manifold of the FI instrument, as shown in Fig. 4.1., was set up with a 260 μl sample loop [107], a push-fit connection packed reduction column (Chapter 3, Fig. 3.11.),
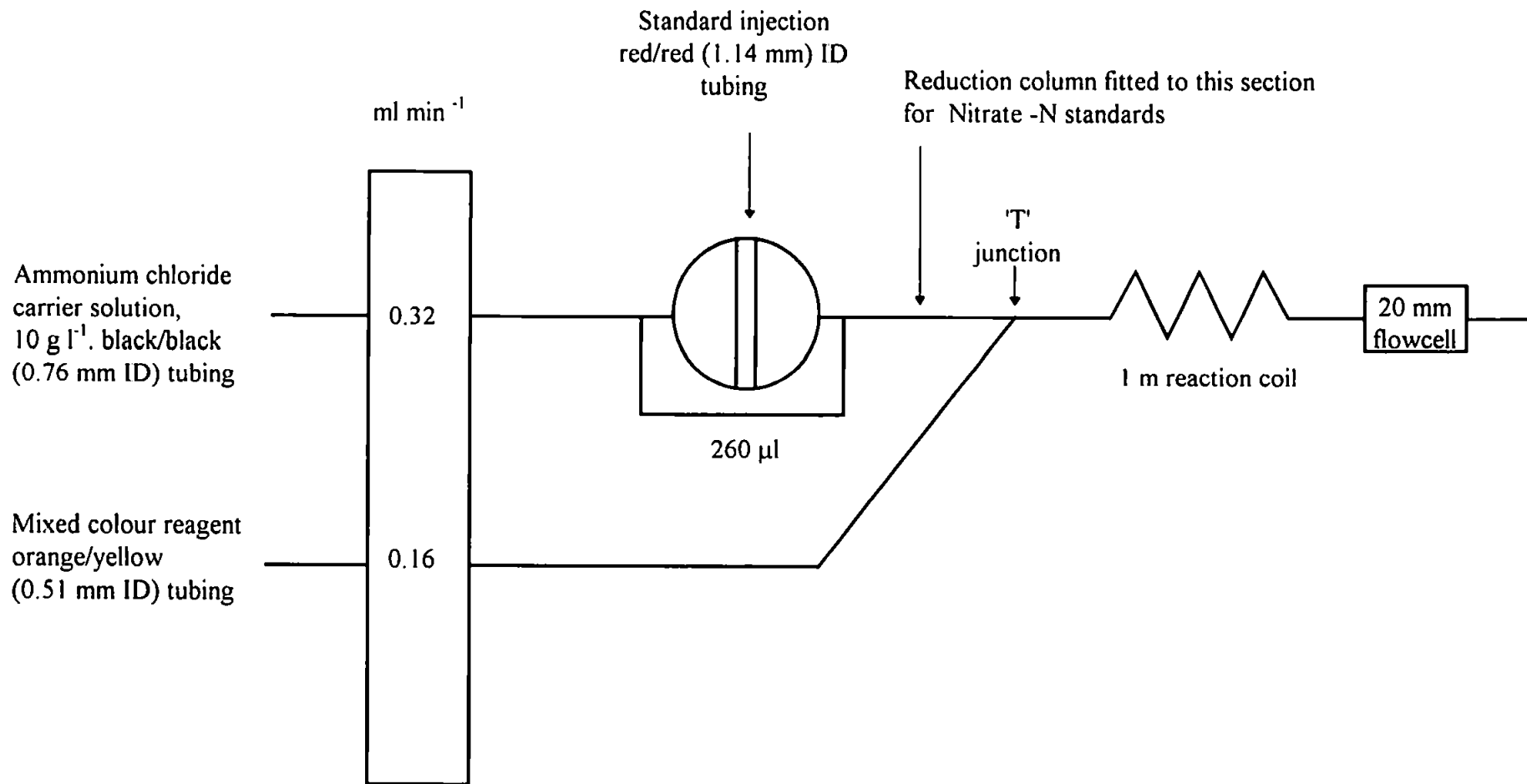
Figure 4.1. Schematic diagram showing the FI instrument manifold configuration for the determination of Nitrite-N

and the position where the reduction column was fitted for Nitrate-N determinations

a 1 metre reaction coil (Chapter 3, Fig. 3.14.) and 20 mm flowcell (Chapter 3, Fig. 3.17.). During the initial stages of the laboratory experiments the original single tensioner pumps were fitted , (Ismatec Mini - S/8/12VDC/60:1) as described in Chapter 3, section 3.1.1. and shown in Fig. 3.37. After approximately 300 hours use these pumps were replaced with the twin tensioner pumps (Ismatec CA1-E/8/12VDC/100:1) as discussed in Chapter 3, section 3.2.1. The flowcell development experiments overlapped with the earlier stages of the FI instrument development. Therefore, for approximately 2 months, the laboratory experiments using the completed FI instrument were carried out with the modified 'Z' cell fitted. The flowcell was then changed to the final version for the remainder of the laboratory experiments. The various reduction columns, as discussed in Chapter 3, section 3.2.3., were fitted to the manifold in the position as shown Fig. 4.1. The FI instrument was interfaced with a PC and a 12 volt DC power supply for the laboratory experiments as shown in Fig. 4.2.
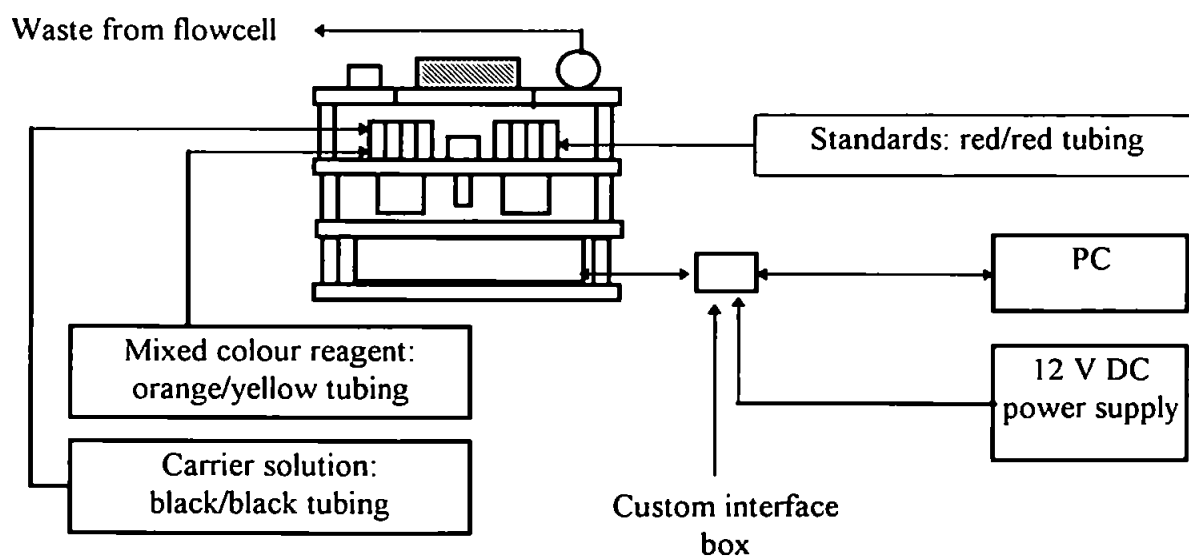
Figure 4.2. Schematic diagram showing how the FI instrument was interfaced with a PC and power supply for the laboratory experiments

4.1.3. Communications and data transfer

Using a short custom made interface cable, the instrument was connected to a desktop PC and 12 volt DC power supply via the interface box as described in Chapter 3, section 3.6. This enabled direct serial data communications with the PC for data transfer and operational control. 'Crosstalk' for Windows® communication software was used in terminal mode to provide the necessary top level control and data transfer. The standard PC communication settings used are shown in Table 4.1.

Table 4.1. F1 instrument/PC communications and file transfer settings

Property	Setting
Comms Port	2
Baud speed	9600
Data bits	8
Parity	None
Stop bits	1
Protocol	Z modem
Xmit buffer	2 K
Receive buffer	2 K
Terminal emulation	DEC VT320

4.1.4. Instrument control program

An instrument operating routine, '*ROM1*', was written in the MCS®-BASIC v1.1 language on the PC and transferred to the on-board *RAM* using the file transfer routine. When the final version of this was completed, it was programmed onto the *EPROM* fitted to the on-

board computer. When executed using the RUN command at the terminal, 'ROM1' controlled the instrument as shown in Table 4.2.

Table 4.2.   'ROM1'- nutrient sensor control program

Line	Software Command	Action
5	REM control programme	None
10	xby(58371)=128:xby(58368)=5	Initiates system : starts pump 1
15	XBY(58370)=88	Sets LED power
20	DELAY=4 : GOSUB 140 : XBY(58368)=21	4 second delay : pump 2 on
30	DELAY=10:GOSUB 140 : XBY(58369)=24	10 second delay : injection valve to fill position
40	DELAY=90 : GOSUB 140 : XBY(58369)=16	90 second delay : injection valve injects
50	DELAY=10 : GOSUB 140 : XBY(58368)=5	10 second delay : pump 2 off
55	GOTO 160	Starts ADC loop
140	CLOCK 1 : TIME = 0	Sets internal clock
150	DO : UNTIL TIME >= DELAY	Sets delay command
155	RETURN	Completes action
160	DELAY=90 : GOSUB 140: GOTO 170	sets ADC delay
170	XBY(58369)=16 : XBY(58369)=0 : XBY(58369)=16	sets ADC
180	A=XBY(60416) : B=XBY(60417)	ADC control
190	IF B>31 THEN D=8191 : IF B<32 THEN D=-8191	ADC control
200	C=A+(B*256)	ADC control
210	PRINT C-D	prints ADC output to terminal
220	FOR T=0 TO 500 : NEXT	ADC count frequency
230	RETURN	completes loop

Changes to the *BASIC* control program loaded on to the *EPROM* could be modified on-line by transferring the *ROM* to the 80C32's internal *RAM* by using the *XFER* command. Running in real-time and in terminal mode, the analogue to digital converter (ADC) sampled the detector response approximately 100 times per minute and 'printed' the output to the PC screen. The ADC print-out was allowed to run for approximately 2 minutes before it was terminated using the *Control-C* command from the PC.

4.1.5.   Procedures

To run the FI system on the bench, approximately 250 mm of 0.8 mm ID PTFE tubing was attached to each of the three pump tubes. The pump tube tensioners were tightened and the reagent lines were placed in the respective bottles of carrier and mixed colour reagent. The sample line was initially placed in a beaker containing water in order to flush the sample line out prior to running the standards. The system was then switched on and the control program *ROM 1* was selected and set to run. When satisfied with the operation of the system, the sample line was removed from the water and placed in a standard solution and the system was set to run. Standards were analysed in order of increasing strength to eliminate carry over. During the operation, the colour development of the standards was timed so that the appropriate delays could be written into the control programme for commencement of data capture. During the method development, the system was set to start print ADC data to the PC immediately after the sample injection and this was observed in real-time as the standard progressed through the manifold. When an operational pattern developed, the appropriate delays were incorporated in the control programme. When satisfied that the standard peak had gone through the flowcell (the resultant chromophore could be observed flowing through the reaction coil) the program was terminated by executing the *CONTROL-C* command on the PC. This action stopped the on-board

computer 'printing' the ADC data to the PC screen and allowed direct PC control over the FI system. The data from the ADC was displayed as a single column of numeric values which was saved as a text file by the communications software. The text files were imported into spreadsheet software where the peak heights were calculated and the peak profiles plotted. For convenience during the laboratory and subsequent field trials, the Crosstalk for Windows® communications software was programmed to allow the use of 'Quickpads' to be used. This meant that the code for particular command could be assigned a 'button'. When a command 'button' was clicked using the PC mouse the code was sent to the on-board computer and the action was executed. This facility allowed the FI instrument to be used in a manual mode, i.e. by directly controlling the various instrument functions using the PC.

Extended range experiments: Experiments were also carried out to investigate extending the analytical range of the instrument. The first part of this work investigated the effect of sample size on the instrument's performance using different size sample loops. Sample loops of 40, 80, 150, 260 and 450 μl were investigated using a 20 mm flowcell. Similar experiments were carried out using a 10 mm flowcell.

Wire reduction column experiments: The effects on the FI instruments performance characteristics of using a cadmium wire reduction column, as described in Chapter 3, section 3.1.3, were also investigated.

LED intensity experiments: During the laboratory experiments, the effect of LED input power on flowcell response was investigated. This was done using a second control programme *ROM2* resident on the *EPROM*, as shown in Table 4.3. The routine was transferred to *RAM* using the *XFER* command where it was modified on-line using the PC

in terminal mode. Once in *RAM*, the LED intensity could be altered by changing the end value of the code in line 15 of the program, i.e. the value after the main address and = sign. When executed, the programme ran pump 1, (carrier and mixed colour reagent) and set the LED to the new intensity and the routine printed the ADC output on the PC screen. The programme continued to run until terminated by the *CONTROL- C* command.

Table 4.3. *ROM2* **LED Test Routine**

Line	Code	Action
5	REM LED Test Routine	None
10	XBY(58371)=128 : XBY(58368)=5	Sets system : starts pump 1
15	XBY(58370)= n	(n = 0 - 255) Sets LED power
20	XBY(58369)=16 : XBY(58369)=0 : XBY(58369)=16	ADC control
25	a = XBY(60416) : b = XBY(60417)	ADC control
30	IF B > 31 THEN D = 8191: IF B < 32 THEN D = - 8191	ADC control
35	C=A+(B*256 : print C-D: FOR T=0 to 500: NEXT	Prints data from ADC to PC
40	GOTO 30	Completes loop

4.1.6.   Anglo-Russian Interdisciplinary Estuarine Study (ARIES) project flowcell

During the early development of the flowcell design, and in conjunction with Plymouth Marine Laboratory (PML), a prototype flowcell was incorporated in a portable system for nutrients that was deployed in an arctic estuary in the White Sea [188]. The flowcell

supplied was the modified 'Z' cell with a 20 mm path length, as described in Chapter 3, Fig. 3.17. PML provided the manifold and custom built amplifier and the system was set-up and tested as shown in Fig. 4.3. using a series of Nitrite-N standards.
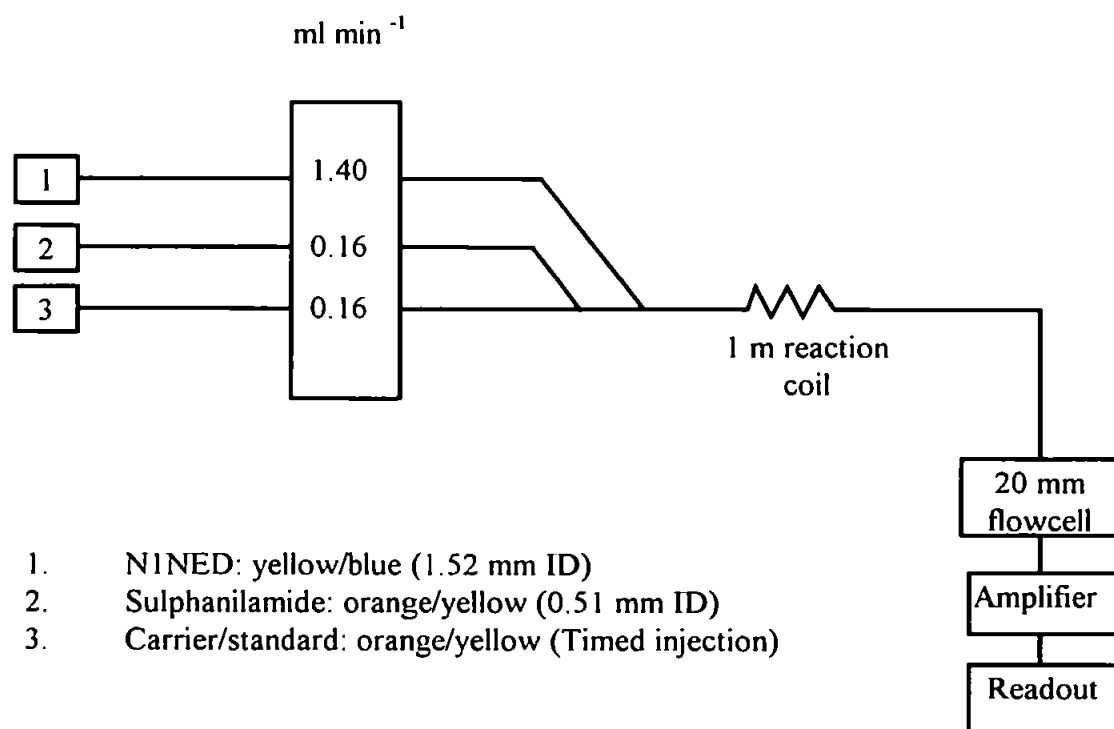
Figure 4.3. **Manifold used for ARIES project flowcell experiments**

Reagents: All solutions were prepared from ultra-pure water ('Milli-Q') and all reagents were AnalaR® (BDH) unless otherwise stated. All reagents and standards were supplied by PML in accordance with their internal nutrient procedures document [166]. The N1NED was prepared by dissolving 0.5 g of N-(1-naphthyl) ethylenediamine dihydrochloride (Sigma) in 1 litre of water. The sulphanilamide reagent was prepared by dissolving 5 g of sulphanilamide in 500 ml of water. 50 ml of concentrated hydrochloric acid was added and the solution was made up to 1 litre with water. The carrier solution was prepared by dissolving 10 g of ammonium chloride in 1 litre of water. A stock 100 mM Nitrite-N solution was prepared by dissolving 6.90 g of sodium nitrite in 1 litre of water. Working standards were prepared by serial dilution of the stock solution.

4.2.   RESULTS AND DISCUSSION

4.2.1.   Nitrite Standards

Modified 'Z' Flowcell: For each standard injection the ADC output consisted of approximately 200 readings over a 2 minute period which were taken during the progress of each standard/sample through the flowcell; commencing and terminating at the baseline value. These values were saved as a text file for each injection and imported into spreadsheet software to determine the peak height and examine the peak profile.

Analytical performance from the integrated system was found to be good. Fig. 4.4. shows a typical sample peak from a 1.0 μM (0.014 mg l^{-1}) Nitrite-N injection. The detector LED was set at 100 % power. Fig. 4.5. shows a typical peak from a 2.0 μM Nitrite-N injection with the LED set at maximum power. At this stage the LED intensity and delays to control the injection valve flush through time had not been finalised and therefore a day to day comparison was not possible at this stage. The next standard injections were made using a 5.0 and 10.0 μM Nitrite-N with the LED set at 50% power to examine the effect on detector response. This lowered the detector response and typical peaks for 5.0 and 10.0 μM Nitrite-N are shown in Fig. 4.6. and 4.7. respectively. The results from this early series of experiments are shown in Table 4.4.

Table 4.4.   Results from a series of Nitrite-N standard injections, 7.3.94.

Nitrite-N	n	Mean peak height	RSD	Comments
μM		ADC Count	%	
1.0	4	1505	0.4	LED @ maximum power
2.0	2	2704	2.5	LED @ maximum power
5.0	4	1515	1.7	LED @ 50% power
10.0	3	2122	1.0	LED @ 50% power

Figure 4.4. Typical peak from a 1.0 μM Nitrite-N standard injection (LED set at maximum power)

Figure 4.5.   Typical peak from a 2.0 μM Nitrite-N standard injection (LED set at maximum power)
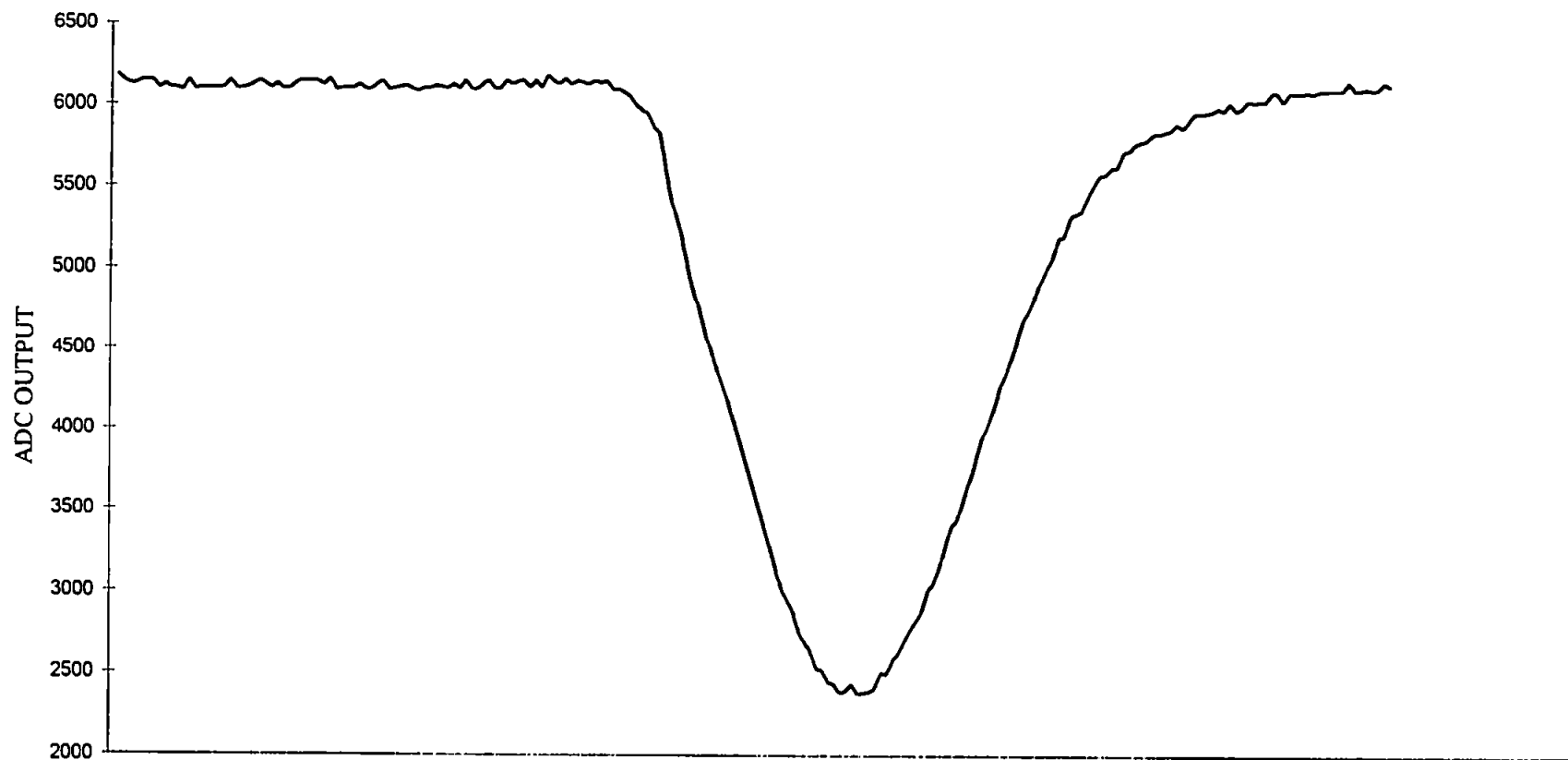
Figure 4.6. Typical peak from a 5.0 μM Nitrite-N standard injection (LED set at 50 % power)

131
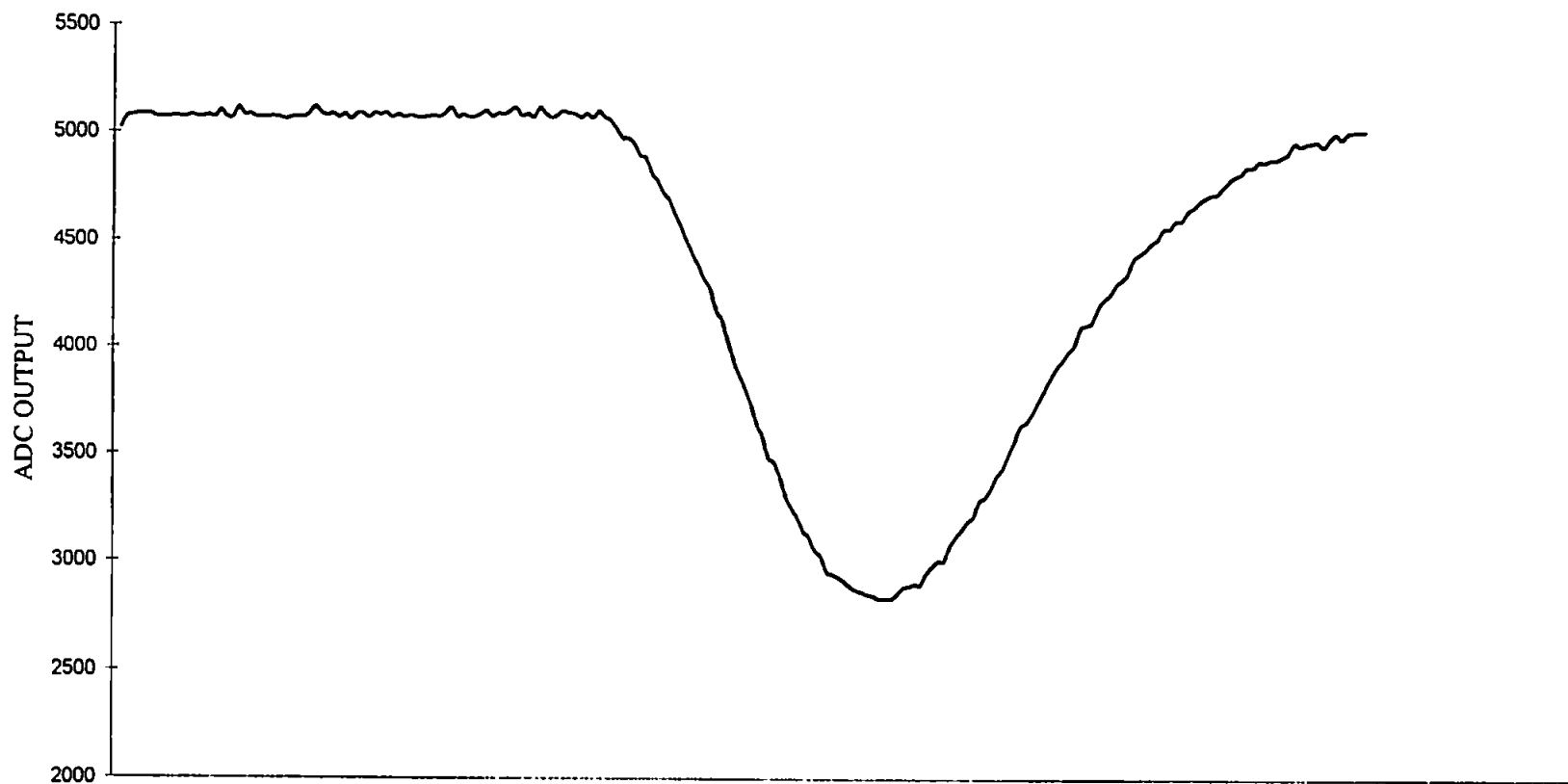
Figure 4.7. Typical peak from a 10.0 µM Nitrite-N standard injection (LED set at 50 % power)

Experiments were carried out on a daily basis and Table 4.5. show the results from a similar set carried out 9 days later using the same set of standards and reagents.

Table 4.5. **Results from a series of Nitrite-N standard injections, 16.3.94**

Nitrite-N	n	Mean peak height	RSD	Comments
μM		ADC Count	%	
1.0	4	1682	0.4	LED @ maximum power
2.0	9	2396	2.5	LED @ maximum power
5.0	6	3943	1.7	LED @ maximum power
10.0	9	2395	1.0	LED @ 50% power

The injection valve flush-through time was increased to 90 seconds to eliminate any sample carry over. Baselines were very stable and peak shapes were very similar with low RSD values for peak height. At this stage an operational pattern for the system was observed and this is shown in Fig. 4.8.

Injection
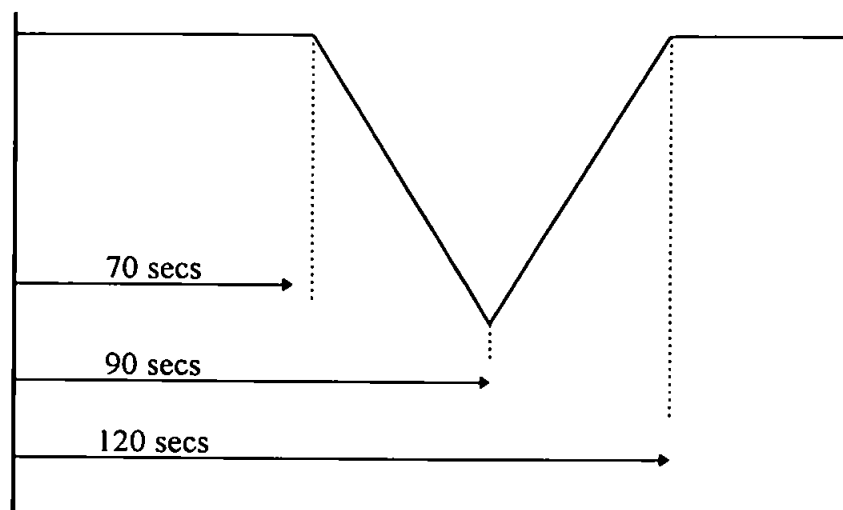
Figure 4.8. Observed operational pattern of FI instrument during laboratory experiments

New design flowcell: At this stage the analytical performance of the FI instrument was reliable except for the occasional trapped bubble in the flowcell which required manual assistance to purge the system. This only required pinching the flowcell outlet pipe to create a back-pressure so that when the restriction was released a surge in the flow dislodged the bubble. In a stable laboratory environment the occurrence of bubbles in the system would probably be minimal once the manifold had been flushed through and all internal surfaces thoroughly wetted. In this situation it would not suffer from shocks likely to cause disruption to the flow pattern and thereby cause bubble formation. However, during field deployment it is much more likely that the occasional bubble will form so it was essential for the FI system to be able to cope with this situation. Therefore, the flowcell design was further improved to eliminate detector noise due the presence of the occasional trapped bubble in the light path. The final flowcell design, as described in Chapter 3, Fig. 3.20., was therefore incorporated at this stage of the development. After fitting the new flowcell, any bubbles which formed in the manifold passed straight through the flowcell without any manual assistance. Even though the result from an individual injection would be void, the system baseline was quickly restored as Figs. 4.9. and 4.10. illustrate. After incorporation of the new design of flowcell, there were no instrumental problems caused by trapped bubbles during the subsequent 18 months of laboratory experiments, field trials and the North Sea cruise experiments.

After the new design of flowcell had been fitted the FI instrument was evaluated with a series of Nitrite-N standards using the same procedures as described section 4.1.5. The LED was set at 50% power for the complete series of experiments so that all standards would be in the same range. By varying the LED power setting, the detector response was changed and was an effective method of attenuating the signal for a particular range of absorbencies.
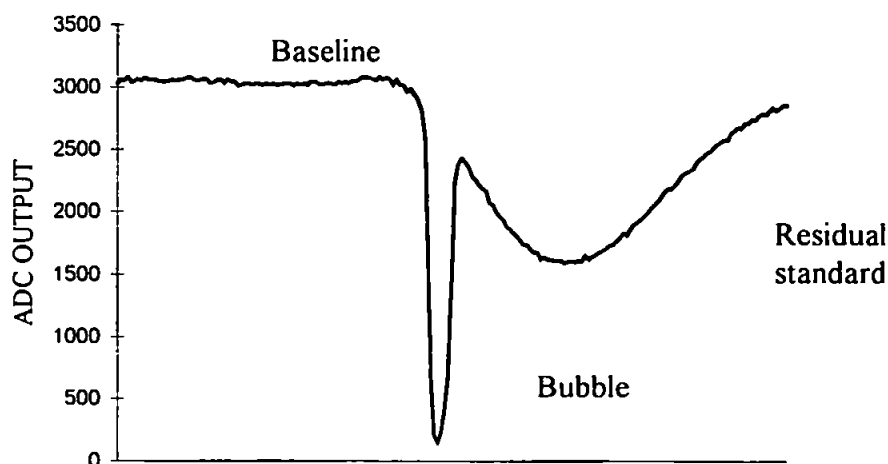
Figure 4.9. Peak profile from the new flowcell (10.0 μM Nitrite-N) with a bubble moving through the system
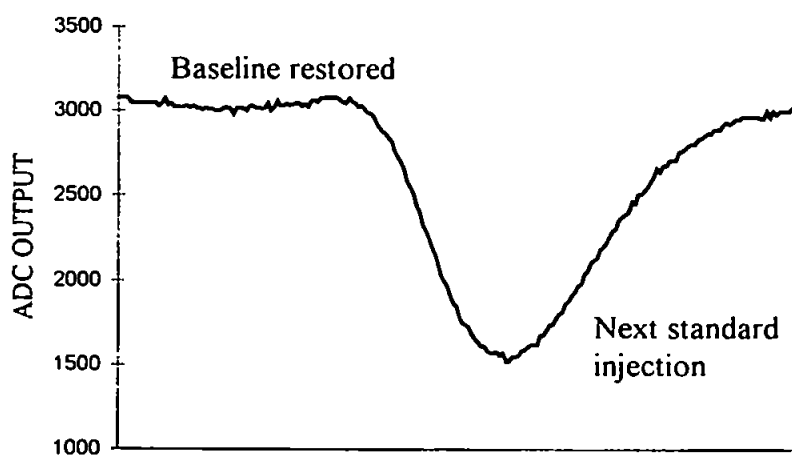
Figure 4.10. Peak profile from the new flowcell (10.0 μM Nitrite-N) immediately after bubble cleared the system with no manual assistance

It was found that for lower concentrations, e.g. 0 - 5 μM, a power setting of 100 % for the LED gave better response and a larger peak height and therefore enhanced the performance of the instrument in this region.

Figs. 4.11., 4.12. and 4.13. show typical peaks for 1.0, 5.0 and 10.0 μM Nitrite-N respectively. The baseline for the 1.0 μM standard appears to be noisier than for the 5.0 and 10.0 μM standards but this is due to the expanded scale used on the y-axis. Tables 4.6. and 4.7. show the results from two series of experiments carried out 4 days apart. The results for the 1.0 , 5.0 and 10.0 μM standards over the period were within the ± 5 % target for day to day reproducibility.

Table 4.6.   Results from a series of Nitrite-N injections with the improved design flowcell fitted, 21.3.94.

Nitrite-N	n	Mean peak height	RSD	Comments
μM		ADC Count	%	
1.0	4	457	3.1	LED @ 50% power
5.0	4	1016	4.1	LED @ 50% power
10.0	4	1572	2.4	LED @ 50% power

Table 4.7.   Results from a series of Nitrite-N injections with the improved design flowcell fitted, 25.3.94.

Nitrite-N	n	Mean peak height	RSD	Comments
μM		ADC Count	%	
1.0	4	435	3.4	LED @ 50% power
5.0	4	975	4.5	LED @ 50% power
10.0	4	1577	4.1	LED @ 50% power
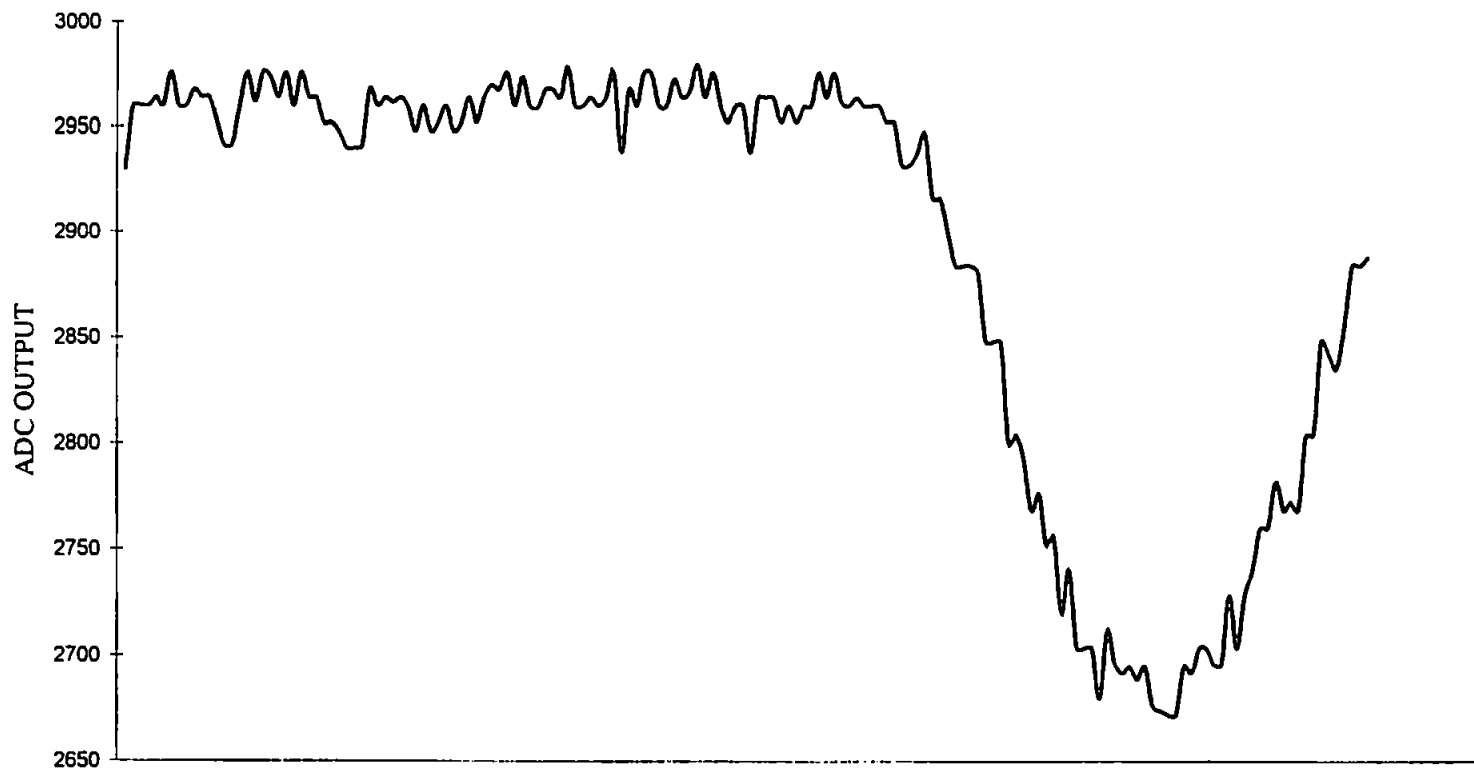
Figure 4.11.   Typical peak from the new flowcell with a 1.0 μM Nitrite-N standard injection

137

Figure 4.12. Typical peak from the new flowcell with a 5.0 μM Nitrite-N standard injection

138
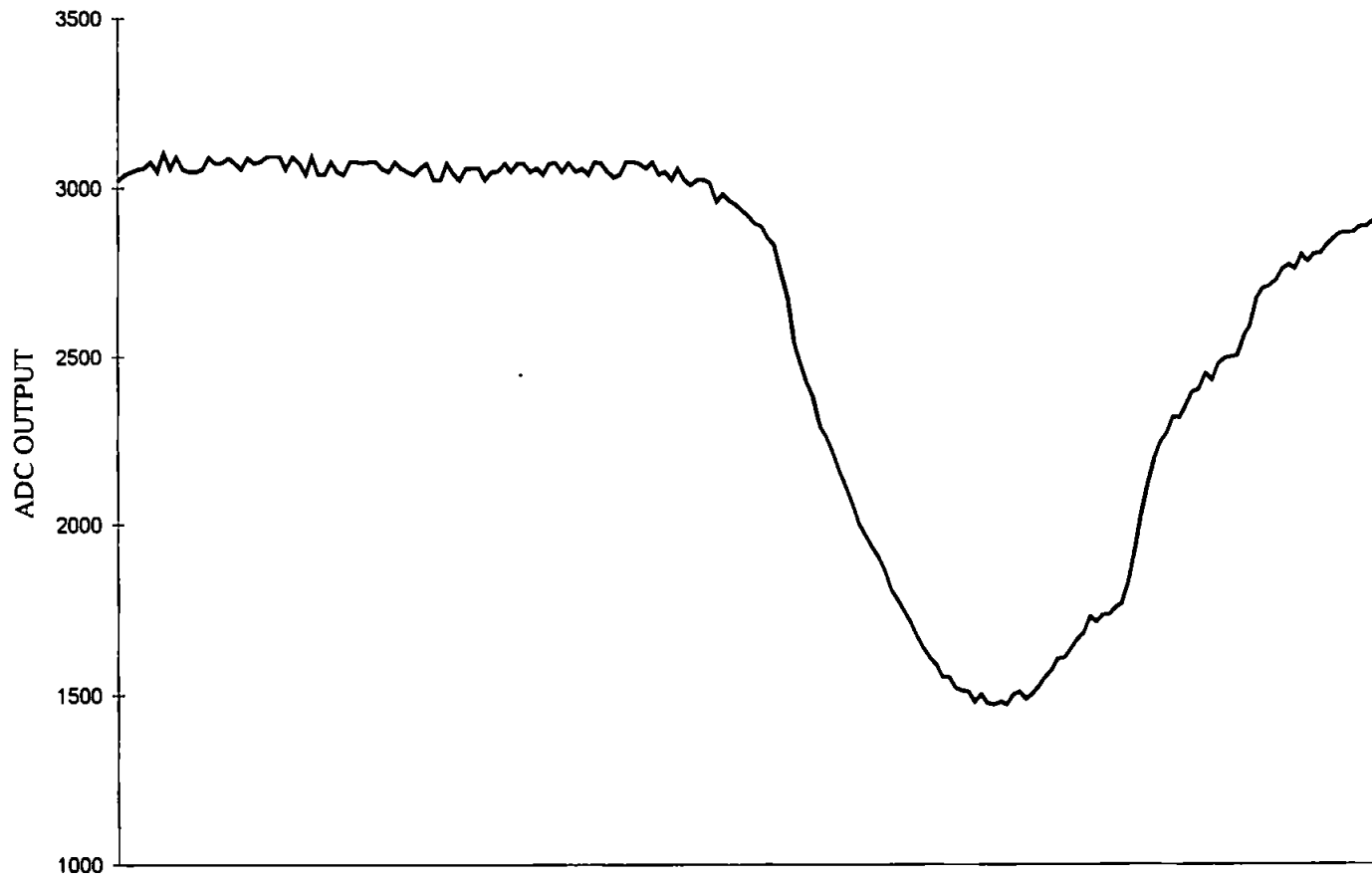
Figure 4.13.   Typical peak from the new flowcell with a 10.0 µM Nitrite-N standard injection
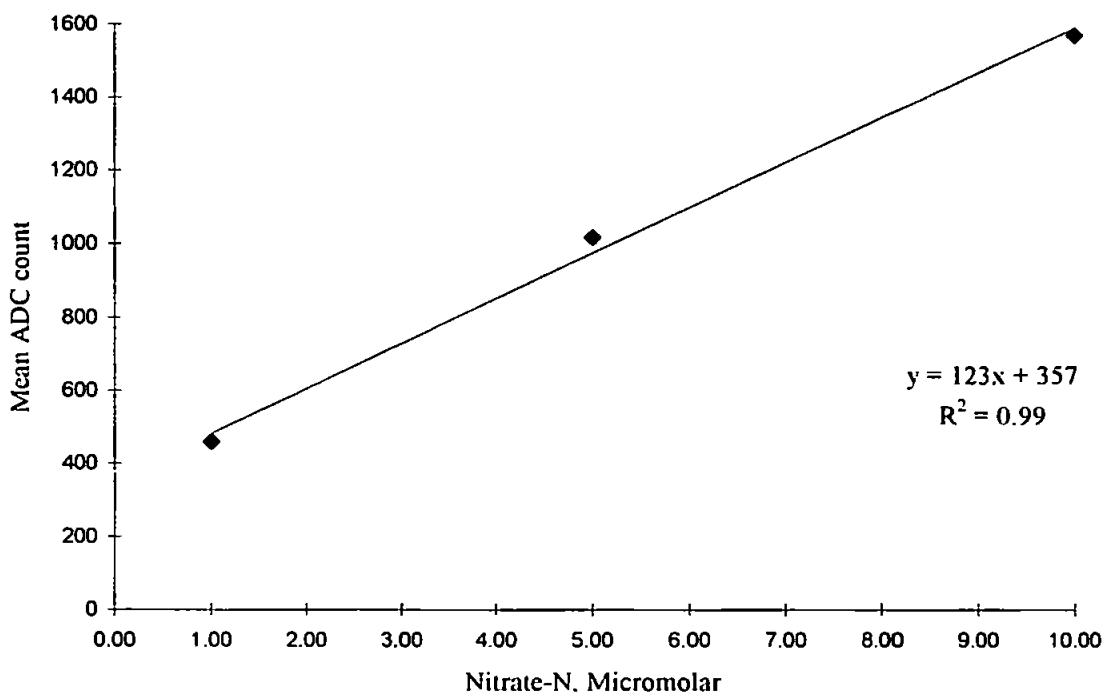
Figure 4.14. Calibration graph using data from Table 4.6.

Graph with y-axis "Mean ADC count" (0 to 1600) and x-axis "Nitrate-N, Micromolar" (0.00 to 10.00), showing:

$$y = 123x + 357$$
$$R^2 = 0.99$$
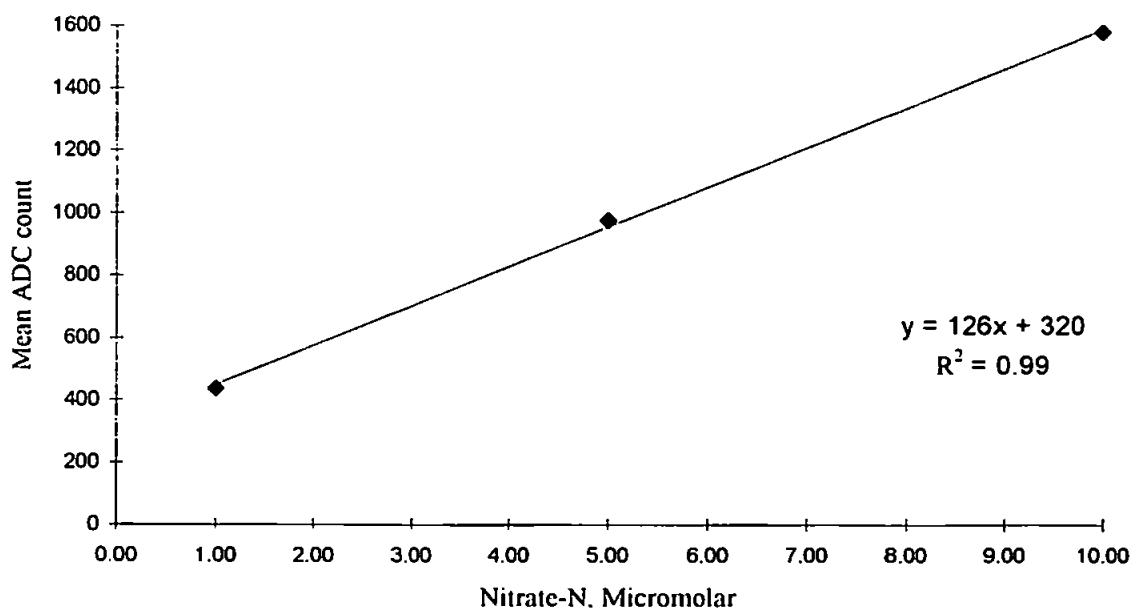
Figure 4.15. Calibration graph using data from Table 4.7.

Graph with y-axis "Mean ADC count" (0 to 1600) and x-axis "Nitrate-N, Micromolar" (0.00 to 10.00), showing:

$$y = 126x + 320$$
$$R^2 = 0.99$$

Subsequent laboratory experiments carried out 4 days later, i.e. 29.03.94., suffered from very unstable baselines regardless of the LED power setting used and the tests had to be

aborted. The cause of the problem was eventually traced to a faulty power transistor in the detector circuitry which was replaced with a new item.

4.2.2. Nitrate-N standards

At this stage the analytical performance of the FI instrument was within the target specification of ± 5 % for within batch repeatability and day to day reproducibility and was therefore considered acceptable. The instrument was then configured for nitrate determinations by incorporating a push-fit packed copperised-cadmium reduction column as described in Chapter 3, section 3.1.3. A series of Nitrate-N standards were analysed using the same procedures as described in section 4.1.5. Typical results for Nitrate-N determinations are shown in Table 4.8. It can be seen from the table that the new power transistor produced a different response from the detector.

Table 4.8.   Typical results from Nitrate-N determinations

Nitrate-N	n	Mean peak height	RSD	Comments
μM		ADC Count	%	
1.0	3	771	1.7	LED @ 75% power
5.0	3	1323	0.3	LED @ 75% power
10.0	3	1644	4.7	LED @ 75% power
20.0	3	2936	1.9	LED @ 75% power
30.0	3	3690	1.7	LED @ 75% power

The results shown in Table 4.8. were plotted to give a calibration graph as shown in Fig. 4.16. which was linear over the range 1 - 30 μM NO_3 - N and within the ± 5 % batch repeatability target.

$$y = 102x + 730$$
$$R^2 = 0.99$$
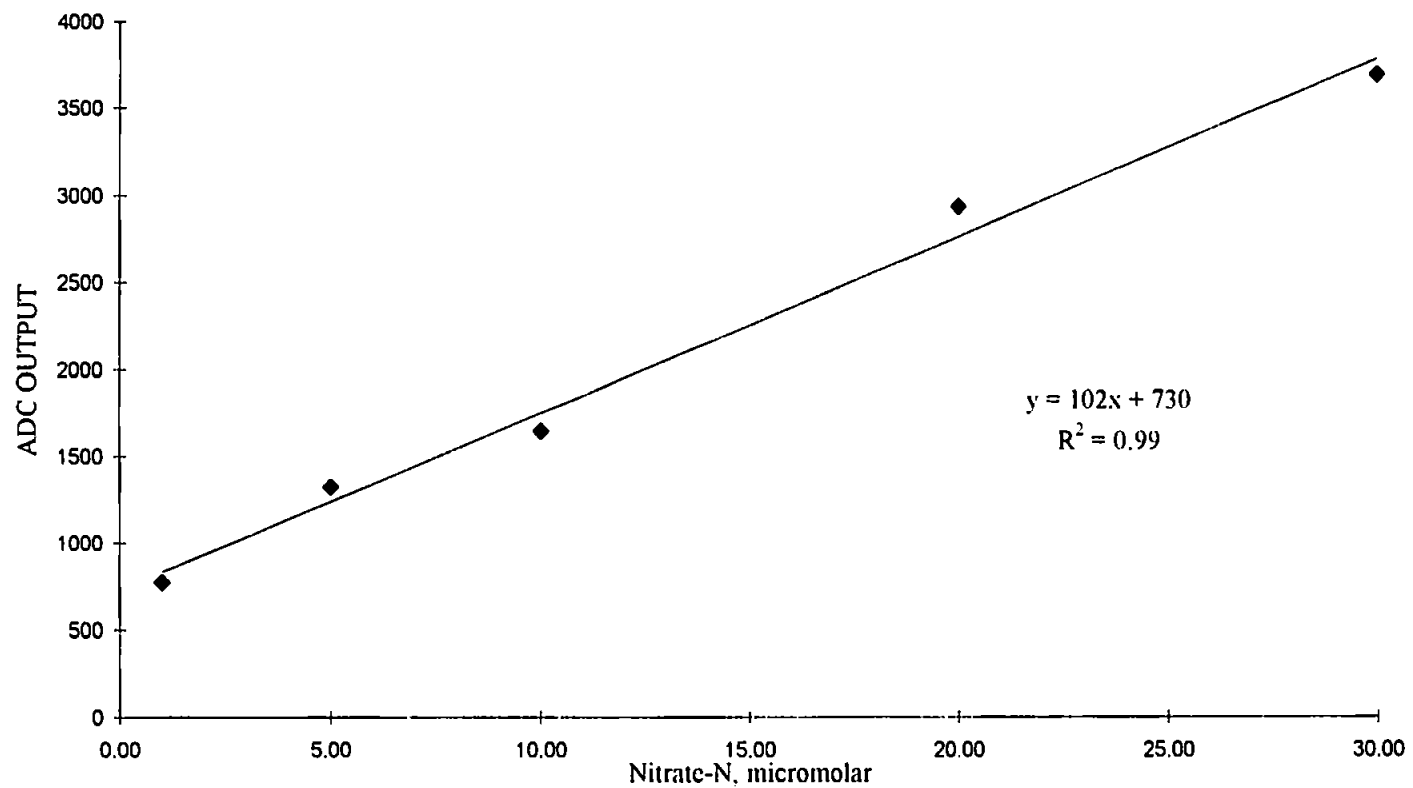
Figure 4.16.   Calibration graph from integrated system with new flowcell and Nitrate-N standards

4.2.3. Extended range experiments

To determine the full range of the instrument, additional Nitrate-N standards were prepared over the range 0 - 100 µM Nitrite-N and analysed. Fig. 4.17. shows the full range for the instrument configured with a 20 mm flowcell and a 260 µl sample loop. The graph shows how the absorbance starts to plateau at approximately 55 µM Nitrate-N, the point at which the cell starts to go out of range due to the very intense colour formation.

Sample loop experiments: At this stage different sample loop sizes were experimented with to determine the effect of sample size reduction on the upper range system performance and therefore the optimum sample loop size/s for the instrument. Sections of the peak profiles obtained using a 60 µM Nitrate-N standard with the 20 mm flowcell and sample loops of 40, 80, 150 and 260 µl are shown in Fig. 4.18. The results from this series of experiments illustrates the importance of optimising the sample volume and flow properties of a FI system. The 40 and 80 µl sample loops introduced pulsations superimposed on the recorded peak. This suggests that a Schlieren effect is present, caused by the intermittent presence of concentrated and diluted portions of the sample zone in the flowcell. The frequency of the modulations in this situation is normally determined by the pulsation of the peristaltic pump. The 150 and 260 µl sample loops produced well defined peak profiles without the presence of any superimposed pulsations and can therefore be considered optimum sample loop sizes for the system when fitted with a 20 mm flowcell. Fundamental instrumental parameters such as injection volume, reduction column design, diazotisation reactor length, mixing geometry and flowcell design have a marked effect on the Schlieren signal in a FI system.
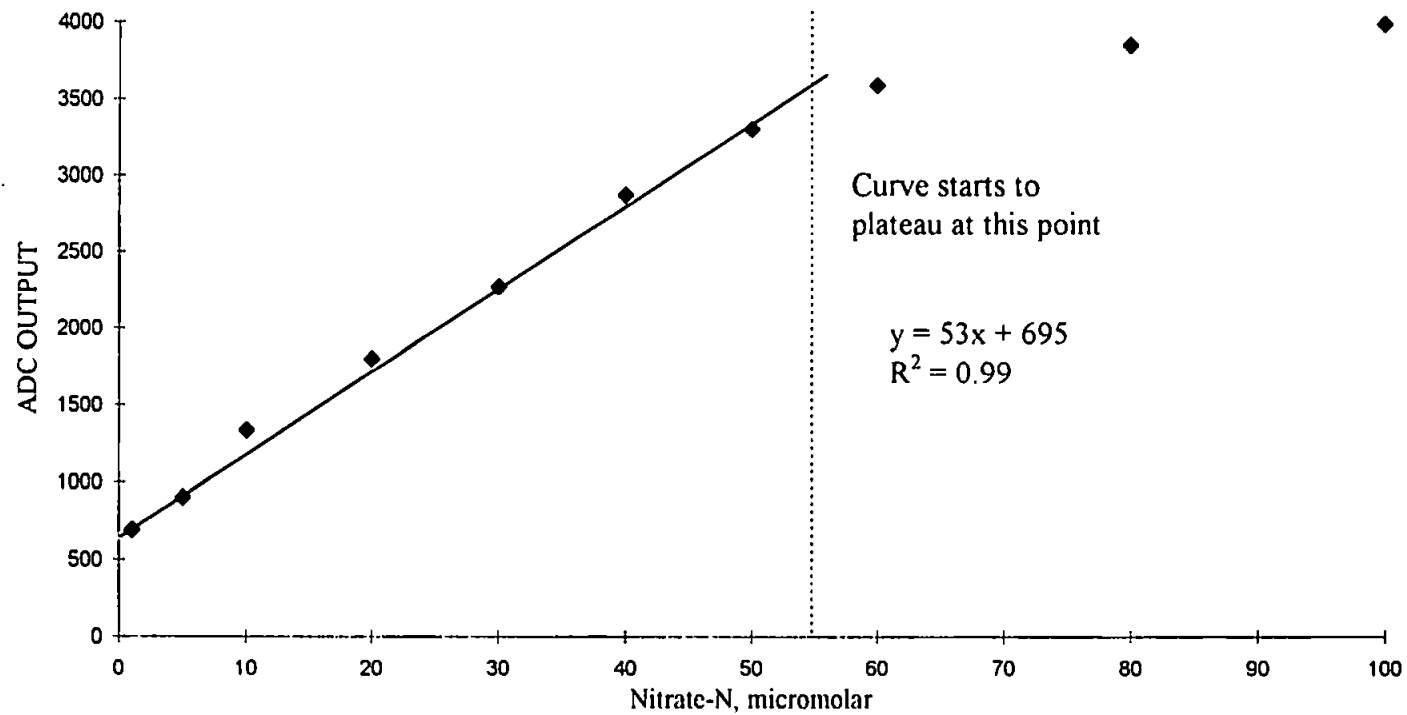
Figure 4.17.   Results from the extended range experiments using a 20 mm flowcell and 260 µl sample loop

144

40μl sample loop

80 μl sample loop

150 μl sample loop

260 μl sample loop
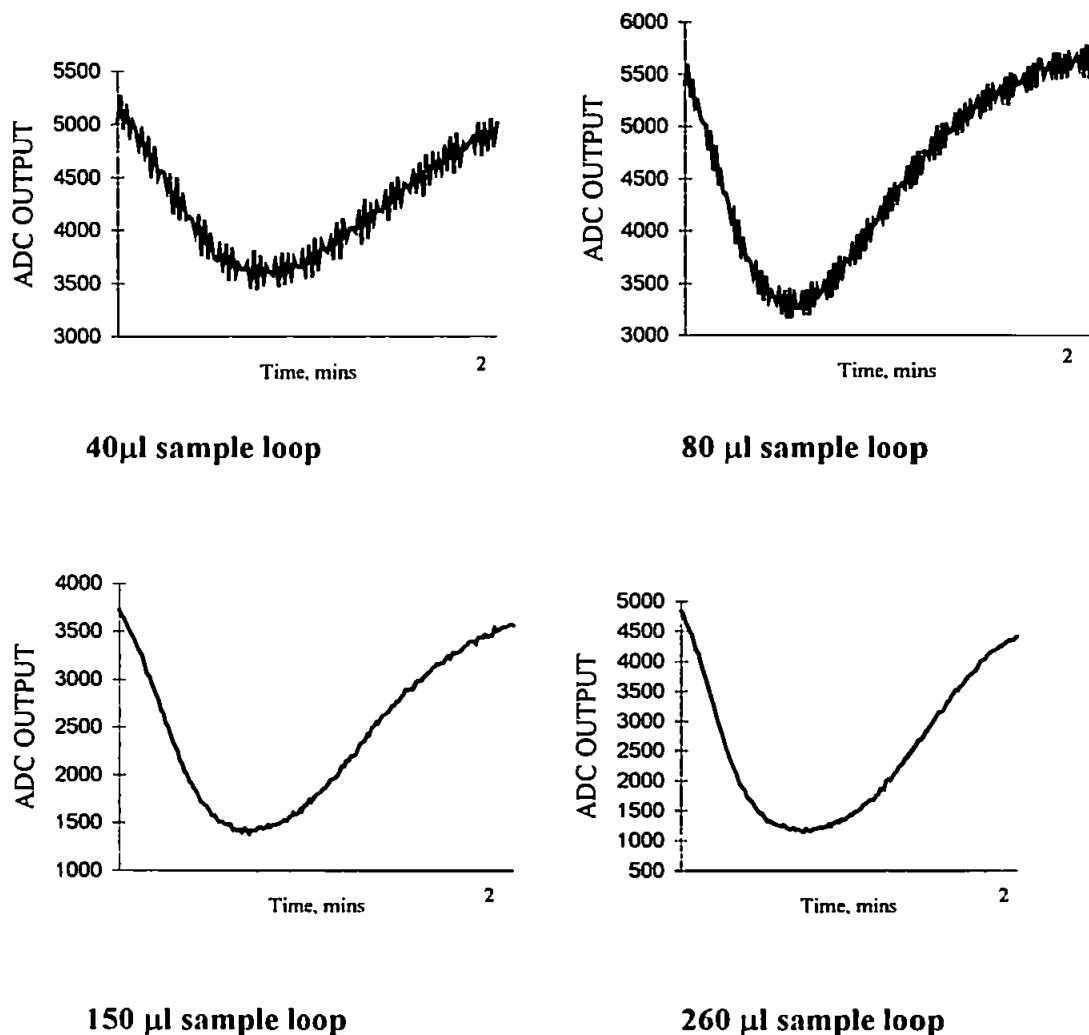
Figure 4.18.   Effects of sample loop size on FI instrument when fitted with a 20 mm flowcell using a 60 μM Nitrate-N standard

When the sample loop is increased the Schlieren signal also increases due to the formation of two distinct regions at the front and tail regions of the peak where the RI gradients are highest. Therefore, by increasing the sample volume a better separation between these regions is achieved. If the sensitivity of the technique is limited by the Schlieren effect and sampling rate is not critical, then by increasing the sample volume a sample peak with a large central zone that is less affected by the light scattering will be produced. Therefore, the approach adopted to overcome the Schlieren effect in a single channel system was to

concentrate on the design and performance of the following aspects of the FI system; simple design with good flow characteristics, good sample/carrier mixing, sufficient sample to produce large central zone, pulse-free pumping and data treatment of central part of sample peak only.

10 mm flowcell/150 µl sample loop experiments: To continue the extended range experiments and to improve the upper limit of linear range, a 10 mm flowcell and a 150 µl sample loop were fitted to the instrument. Based on the results of the sample loop experiments, this configuration was considered to be an effective method of reducing the chromophore intensity without changing the chemistry and therefore allow higher concentration samples to be analysed. Nitrate-N standards of 60, 80 and 100 µM were analysed and the peak profiles are shown in Fig. 4.19.
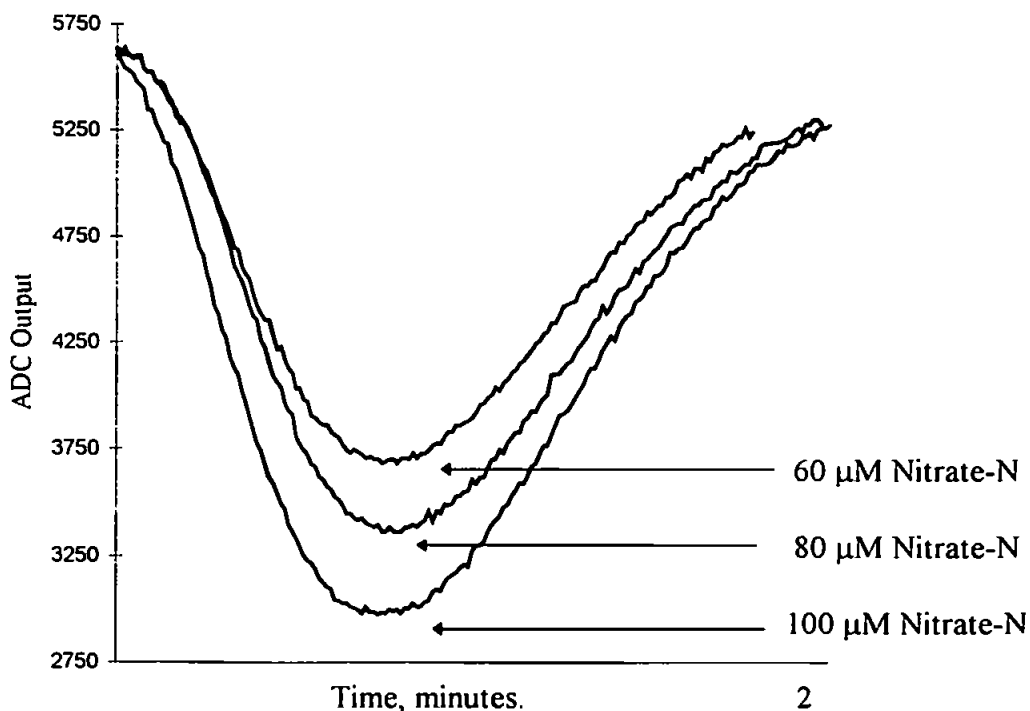
Figure 4.19. **Peak profiles from extended range experiments with the FI instrument fitted with a 150 µl sample loop and 10 mm flowcell**

Peak heights were calculated and these are shown in Table 4.9. from which a calibration graph was plotted and is shown in Fig. 4.20.

Table 4.9.   Extended range experiment results, 60 - 100 μM Nitrate-N, 10 mm flowcell and a 150 μl sample loop

Nitrate-N	n	Peak Height	Comments
μM		ADC Output	
60	1	1952	LED at 75% power
80	1	2278	LED at 75% power
100	1	2630	LED at 75% power

$y = 17x + 931$

$R^2 = 0.99$
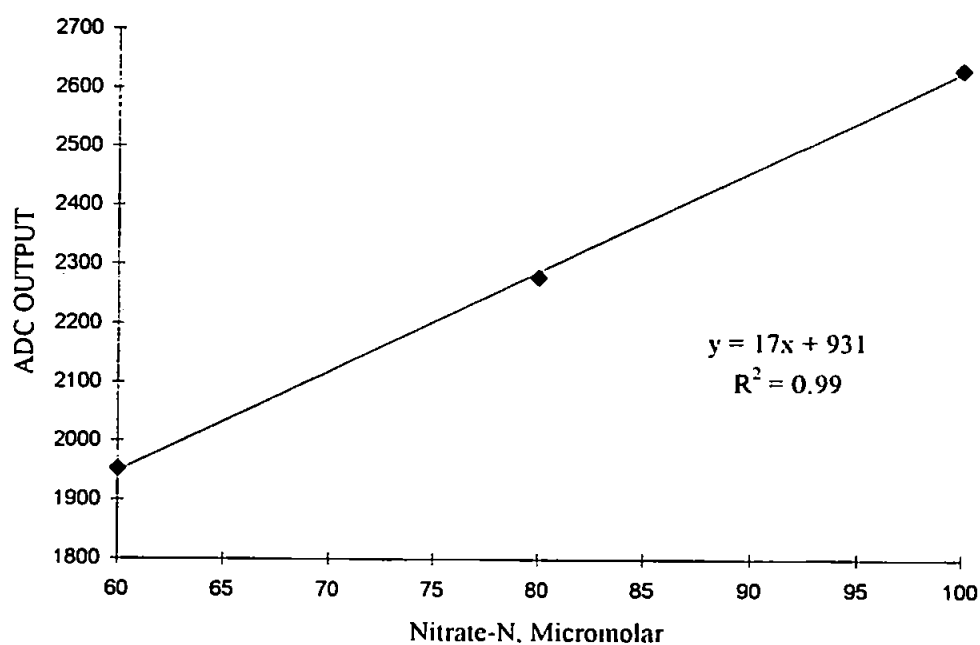
Figure 4.20.   Calibration graph from extended range experiments data in Table 4.9.

A second series of extended range experiments were then carried out with the same instrument configuration. This time 60, 80, 100, 120, 140 and 160 μM   Nitrate-N standards were analysed and the results from this series of experiments are shown in Table 4.10.

Table 4.10.   Results from second series of extended range experiments using a 150 μl
sample loop and a 10 mm flowcell

Nitrate-N	n	Peak Height	Comments
μM		ADC Output	
60	1	1983	LED at 75% power
80	1	2398	LED at 75% power
100	1	2789	LED at 75% power
120	1	3136	LED at 75% power
140	1	3398	LED at 75% power
160	1	3514	LED at 75% power

The results were then plotted to give the calibration graph shown in Fig. 4.21. indicating

that the linear range for the instrument with a 150 μl sample loop and a 10 mm flowcell was

60 to 140 μM Nitrate-N.

$$y = 18x + 957$$
$$R^2 = 0.99$$
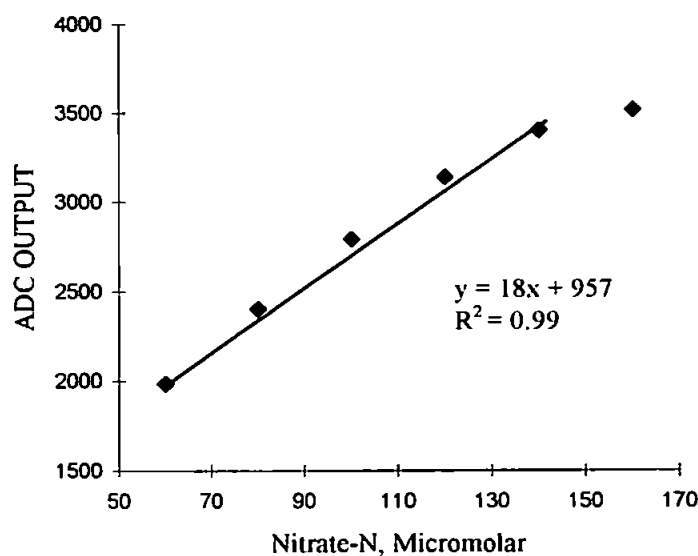
Figure 4.21.   Calibration graph of extended range data from Table 4.10.

Calibration protocol: For simplicity of design and build, the instrument operated using

transmittance. This results in a narrower analytical range and hence a slight curvature on the

calibration graph is observed. To convert the instrument to absorption would require a log

scale and baseline subtraction which would have required a more complicated system. The positive intercept observed throughout the calibrations is possibly due to a background colour formation caused by a slight nitrite contamination of the 'Milli-Q' water used to produce the mixed colour reagent. The azo dye formation has been shown to be sensitive down to 0.3 nM Nitrite-N [189] and this means that when working at the lower ranges, i.e. 0 - 0.1 µM Nitrate-N, it is essential that particular attention is paid to the calibration protocol. For example, it may be necessary to use separate sulphanilamide and NINED reagents and to use low nutrient sea water for the preparation of the reagents and standards instead of 'Milli Q' water. It is also essential to ensure that any plastic containers used are appropriate for nutrient work [154] and suitably washed before use [107].

4.2.4.   Reduction column experiments

Figs. 4.22. and 4.23. illustrate the effects of fitting a 1 metre cadmium wire reduction column as described in Chapter 3. Section 3.1.3. In both cases a Schlieren (mixing) effect was observed.
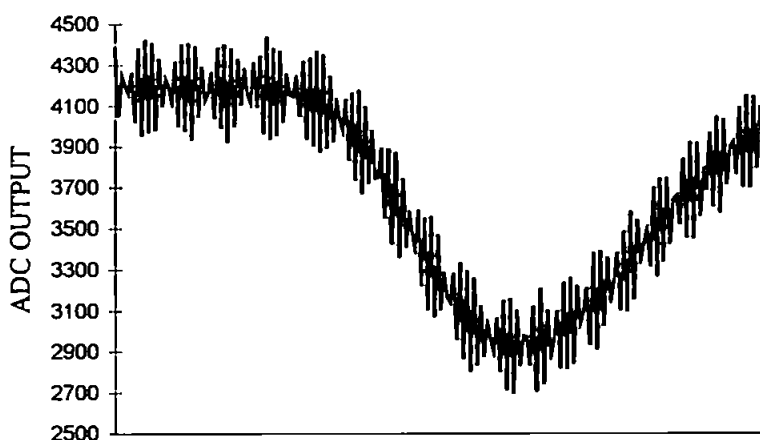
Figure 4.22.   Cadmium wire column, 10 mm flowcell, 150 µl loop, 1.0 mg l^{1} Nitrate-N
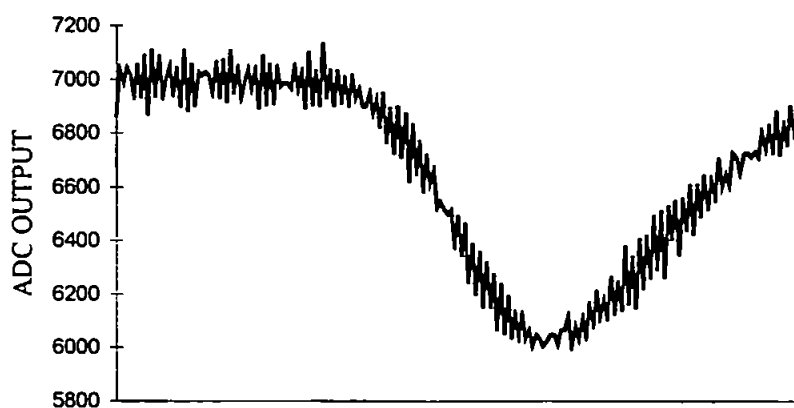
Figure 4.23. Cadmium wire column, 20 mm flowcell, 260 µl loop, 0.1 mg l^{-1}

Nitrate-N

Slightly better results were obtained when the flow rates were increased to approximately

0.5 ml min^{-1} but the effect was still too great to meet the required specification. The overall

effect was to make the system particularly temperamental and decreased the sampling rate

as discussed in Chapter 3, section 3.2.3. For a Nitrite-N standard sample, the typical time

from injection to the point of peak commencement was 70 seconds as previously shown in

Fig. 4.8. The fitting of a packed reduction column for the Nitrate-N standards increased this

time to approximately 90 seconds. The wire column increased this time to 3 minutes which

effectively reduced the sampling rate of the instrument to 6 minutes and therefore did not

meet the specification. Therefore, this reduction method was not pursued any further as

satisfactory performance and flow rates were achieved using the ruggedised packed

reduction column [107] as described in Chapter 3, section 3.2.3.

4.2.5.   LED power settings

Baseline observations during actual analysis and a series of experiments determined the

typical baseline expected for a given LED power setting as shown in Table 4.11. and Fig.

4.24.

Table 4.11   Typical detector response to LED power settings

Approximate LED Power	LED Setting : xby (58370) = n	Baseline
%	n	ADC Output Range
100	0	6000 ± 20 %
75	64	4900 ± 20 %
50	128	3200 ± 20 %
40	32	2300 ± 10 %
30	64	1700 ± 10 %
20	144	1200 ± 10 %
10	176	1000 ± 10 %
0	255	300 ± 10 %
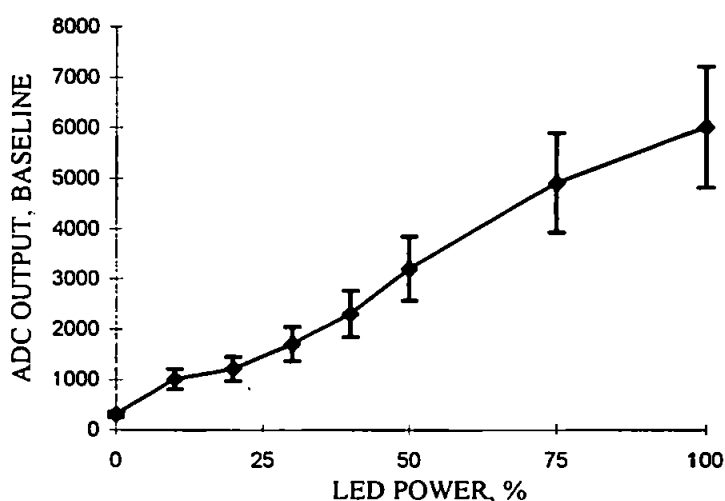
Figure 4.24.   Detector baselines at various LED power settings

The results, coupled with the ability to use various configurations of flowcell and sample loop sizes, illustrates the flexibility of the system to analyse over 0 - 140 μM   ranges of analyte concentrations. To produce a low-cost 'disposable' the components used in the flowcell were general commercially available components which typically had performance tolerances of ± 5 % [186]. Therefore, each flowcell would have slightly different

characteristics so the LED setting for different ranges of analyte concentration would generally be optimised during the calibration as described in section 4.1.5. The typical system settings for a particular range of Nitrite/Nitrate concentration are shown in Table 4.12.

Table 4.12. **Typical FI instrument settings for the range of 0 - 140 μM Nitrite/Nitrate**

Range	LED power setting	Flowcell path length	Injection volume
μM	%	mm	μl
0 -1	100	20	260
1 - 55	50	20	260
60 - 140	75	10	150

4.2.6. ARIES Project flowcell

The results from the series of experiments on the flowcell specially constructed as described earlier in this chapter are shown in Table 4.13. and Fig. 4.25.

Table 4.13. **ARIES project flowcell results**

Nitrite-N	n	Mean	RSD
μM		mV	%
0.0	3	0	0
0.1	17	6	4.9
1.0	3	54	3.1
2.0	3	110	1.5
3.0	3	148	1.1
4.0	3	187	0.9
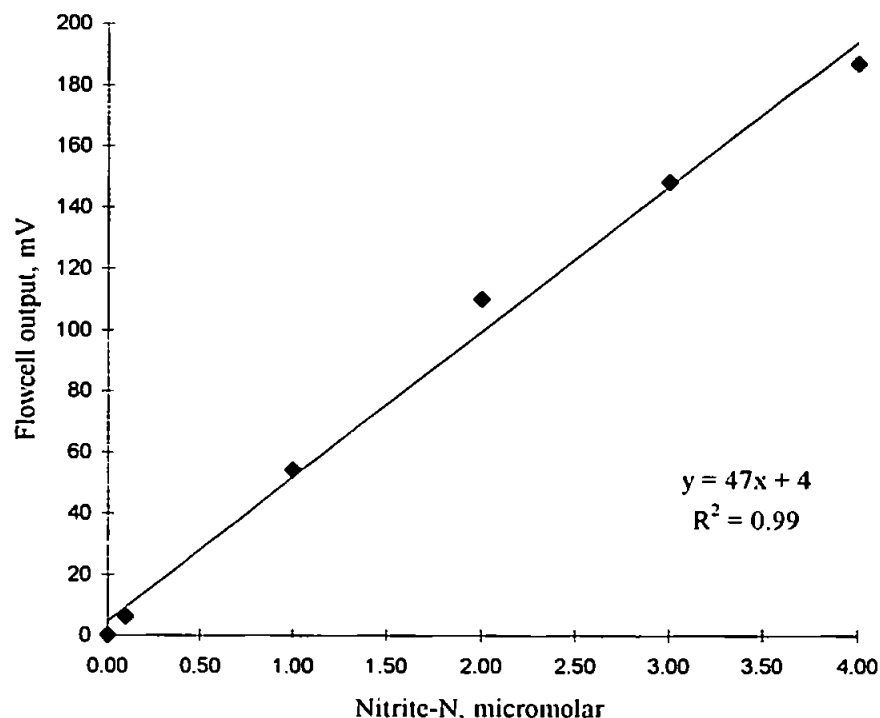
Figure 4.25. ARIES project flowcell calibration graph from Table 4.13. data

The results confirm that a LOD of 0.1 μM is achievable with the flowcell design. No field data was obtained using the system as the op-amp suffered transit damage and was therefore unserviceable. However, the results from this series of laboratory experiments showed that the flowcell design could be used in another system and was capable of achieving low limits of detection.

4.3. CONCLUSIONS

The results from the laboratory experiments have shown the potential of the system, i.e. there are several key operational parameters which can be optimised to achieve maximum performance for a given deployment. For example, in separate experiments it has been shown that the 20 mm flowcell can achieve a LOD of 0.1 μM Nitrite-N and has a linear range of up to 55 μM Nitrate-N using a 260 μl sample loop. A 10 mm version of the flowcell was shown to be linear over the range of 60 to 140 μM Nitrate-N. It is therefore

reasonable to expect that additional combinations of flowcell length and sample volume could extend the performance range of the system even further. It has also been shown that once the manifold configuration has been set further performance enhancements can be achieved by modifying the detector response via the LED power setting.

The instrument was fully compatible with a PC and capable of direct serial communications using standard PC communication software and settings. This would enable industry standard communication methods to be utilised, e.g. cellular telephone network and portable satellite platforms [163].

The target analytical performance of ± 5 % in-batch repeatability, ± 5 % day to day reproducibility and a LOD of 0.1 μM was achieved.

The sampling rate was one every 2 minutes which was the time from sample injection to when the baseline was restored after the sample zone had passed through the flowcell. This sampling rate is sufficient to monitor estuarine changes and was within the sampling rate specification of < 3 minutes. If a greater frequency is required, e.g. during storm conditions, and depending on the sample flush-through time required to prevent carry over, this could be increased to approximately one sample every minute.

Chapter Five
Field Experiments

5. FIELD EXPERIMENTS

This chapter describes the field evaluation of the integrated nutrient sensor. In the initial stages of the field work, the instrument pressure housing was depth tested and the analytical performance of the submersible sensor was compared to that of a modified commercial laboratory instrument [107] during river Tamar cruises on the research vessel 'Tamaris'. The research work culminated in full submersed trials of the integrated system in Plymouth Sound. The use of a cellphone for remote data acquisition and diagnostic information was also investigated.

5.1 EXPERIMENTAL

5.1.1. Tamar field trials

Reagents: All solutions were prepared from ultra-pure water produced by a 'Milli-Q' system (Millipore Corporation), and all reagents were AnalaR® (BDH) unless otherwise stated. The carrier solution was prepared by dissolving 10.0 g of ammonium chloride in 1 l of water. The N-(1-naphthyl)ethylenediamine dihydrochloride (N1NED, Sigma Chemicals) and sulphanilamide reagents were prepared by dissolving 0.5 and 25.0 g respectively in 1 l of water containing 10 % (v/v) orthophosphoric acid. The mixed colour reagent was subsequently prepared by mixing equal volumes of the N1NED and sulphanilamide reagents in a brown glass bottle. A stock 100 mg l^{-1} nitrate solution was prepared by dissolving 0.7220 g of potassium nitrate in 1 l of water. Working standards were prepared by serial dilution of the stock solution with water. For all field experiments, units for Nitrate-N determinations were in mg l^{-1}. A conversion chart between micromolar and mg l^{-1} is shown in Table 5.1. based on 1 μM $\equiv$ 14 x 10^{-3} Nitrate-N / 1 mg l^{-1} $\equiv$ 71.43 μM Nitrate-N.

Table 5.1. Conversion chart for micromolar to mg l^{-1} Nitrate-N

μM Nitrate-N	mg l^{-1} Nitrate-N
1	0.014
2	0.028
3	0.042
4	0.056
5	0.070
6	0.084
7	0.098
8	0.112
9	0.126
10	0.140
11	0.154
12	0.168
13	0.182
14	0.196
15	0.210
16	0.224
35.72	0.5
71.43	1.0
107.15	1.5
142.86	2.0
178.58	2.5
214.29	3.0

Manifold configuration: The instrument was set up with a 150 μl sample loop, a packed reduction column, a 1 metre reaction coil and 20 mm flowcell (LED set at 75 % power) as shown in Fig. 5.1. A 5.0 μm syringe filter was placed in the sample line. Mixed colour reagent pump tubing was orange/yellow (0.508 mm ID) the carrier black/black (0.762 mm ID) and the sample/standard line on pump 2 was red/red (1.143 mm ID)
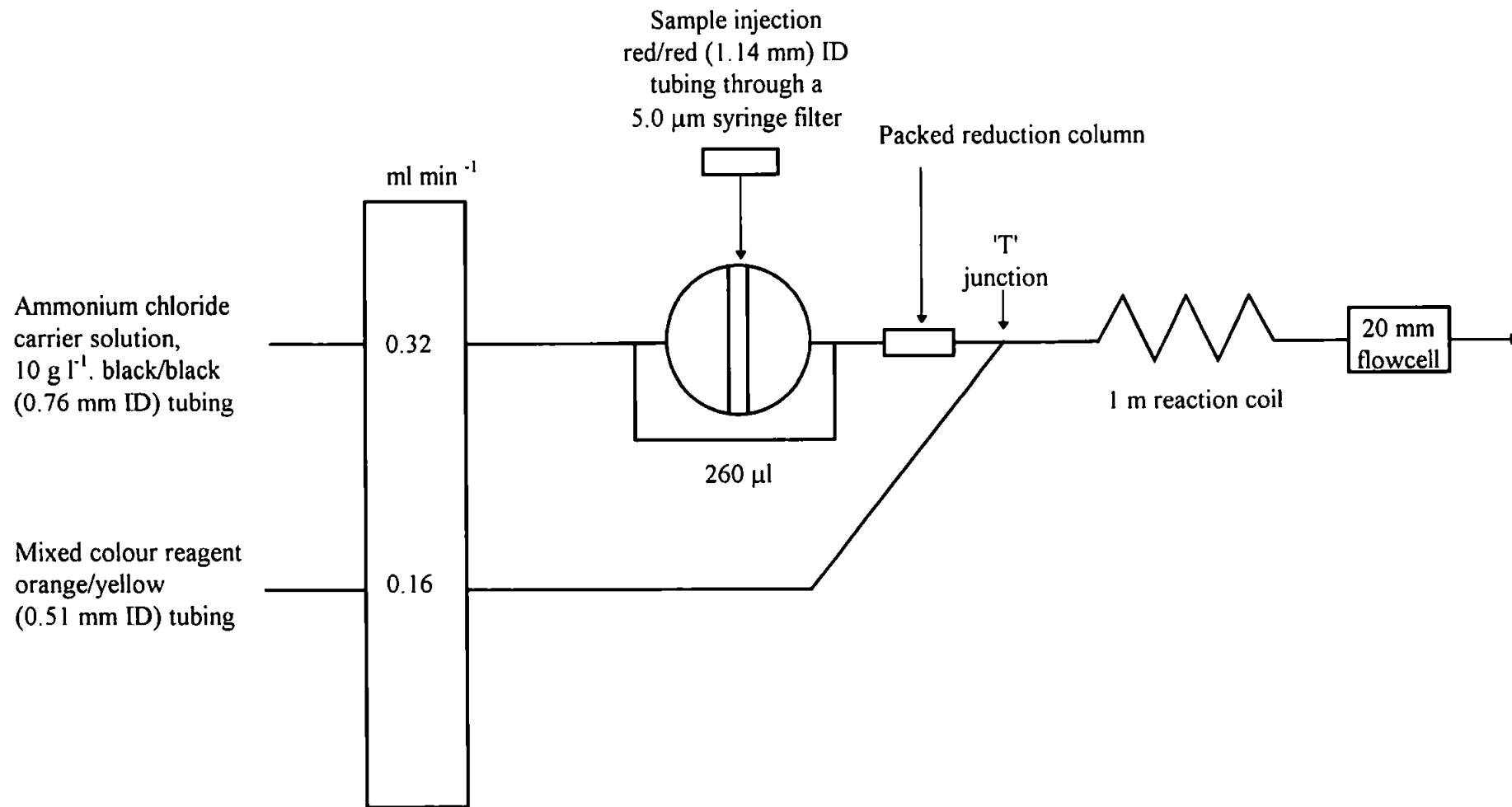
Figure 5.1. **Schematic diagram of manifold configuration for the determination of Nitrate-N used on Tamar field trials**
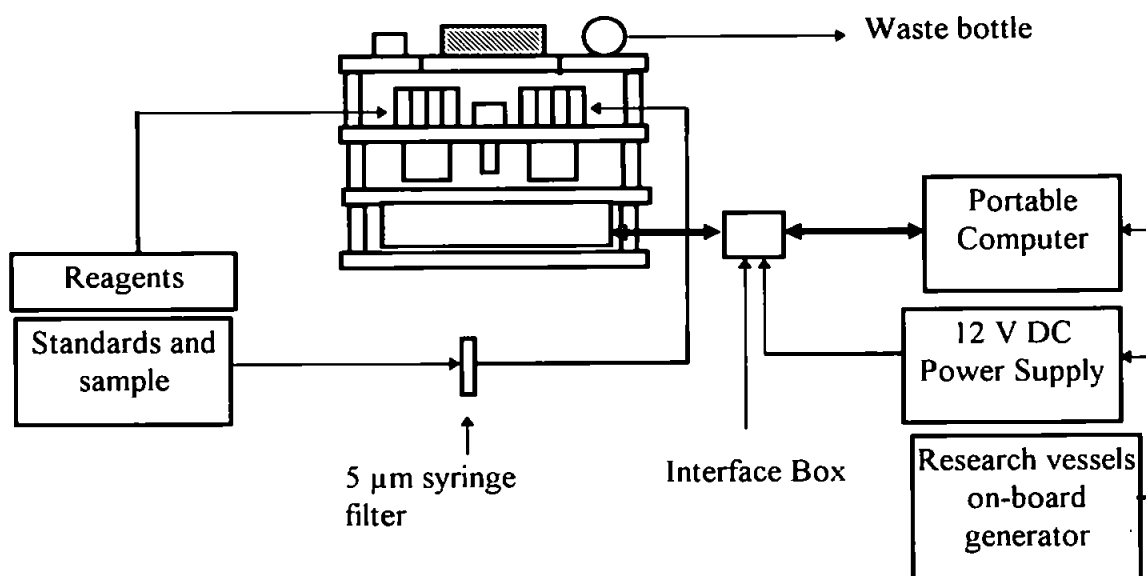
Figure 5.2. Schematic diagram showing instrument bench set-up for Tamar cruises

Data transfer: Using a custom made interface cable, the instrument was connected to a portable PC and 12 volt DC power supply via the interface box as described in Chapter 3, section 3.6. This enabled direct serial data communications with the PC for data transfer and operational control. 'Crosstalk' for Windows® communication software was used in terminal mode to provide the necessary top level control and data transfer. The communication settings used are shown in Chapter 4, Table 4.1.

Cruise track: The cruises were carried out aboard a Rotork Sea Truck (*R.V.S. Tamaris*) and commenced at Sutton harbour on or around high tide and followed the course of the river to Calstock, pausing to take samples from a submersible pump at a depth of 0.5 metre at various points along the way as shown in Table 5.2. and Fig. 5.3.

Table 5.2.   Sampling points on Tamar cruises

Sampling Station Number	Name	Position
1	Drakes Island	50° 21.0' N. 4° 8.2' W
2	Skinham Point	50° 25.6' N. 4°11.8' W
3	Weir Quay	50° 27.5' N. 4° 12.3' W
4	Tinnel	50° 27.3' N. 4° 13.6' W
5	Whitsam	50° 28.4' N. 4° 13.0' W
6	Museum	50° 29.8' N. 4° 13.1' W
7	Calstock	50° 29.7' N. 4° 12.4' W

Operating routine: The instrument was controlled using the operating routine, *'ROMI'*, which was programmed onto an *EPROM* and fitted to the instruments on-board computer, as described in Chapter 4. The system was run in real-time by direct serial communication with a portable PC running in the terminal mode through Crosstalk for Windows communication software.   The analogue to digital converter (ADC) monitored the detector response and printed the output to the PC. The ADC print-out was allowed to run for 2 minutes before it was terminated by the *Control-C* command from the PC. The ADC output consisted of approximately 200 measurements which were taken as each sample progressed through the flowcell; commencing and terminating at the baseline value.

Sampling procedure: Water samples were taken at the sampling points shown in Fig.5.3. from a pumped supply on the research vessel. The samples taken for the nutrient sensor were analysed immediately before reaching the next sample station. The Tamar cruises took place approximately every month over a period of 8 months from 19.04.94 to 09.11.94.
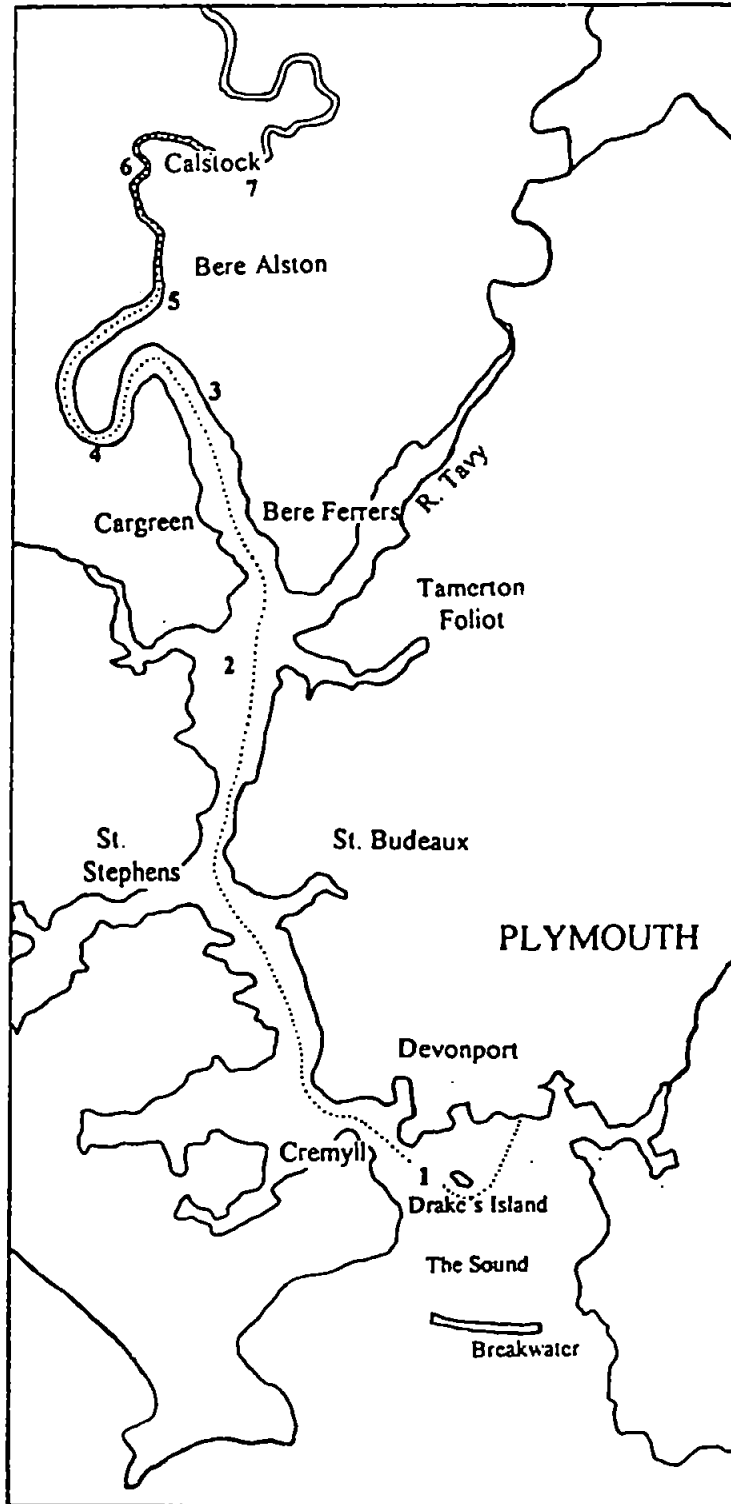
Figure 5.3. Map of Tamar cruise track showing sampling points

5.1.2. Submersed trials

Depth tests: The completed instrument pressure housing and cage assembly, as described in Chapter 3, section 3.6, was subjected to depth/pressure testing aboard the research vessel 'Squilla' on 07.10.94. The housing was weighted with approximately 20 kg of lead and lowered to a depth of 45 m just off Rame Head, as shown in Fig. 5.4., reference 50° 18.0' N. 4° 13.1' W, and held there for 1 hour.
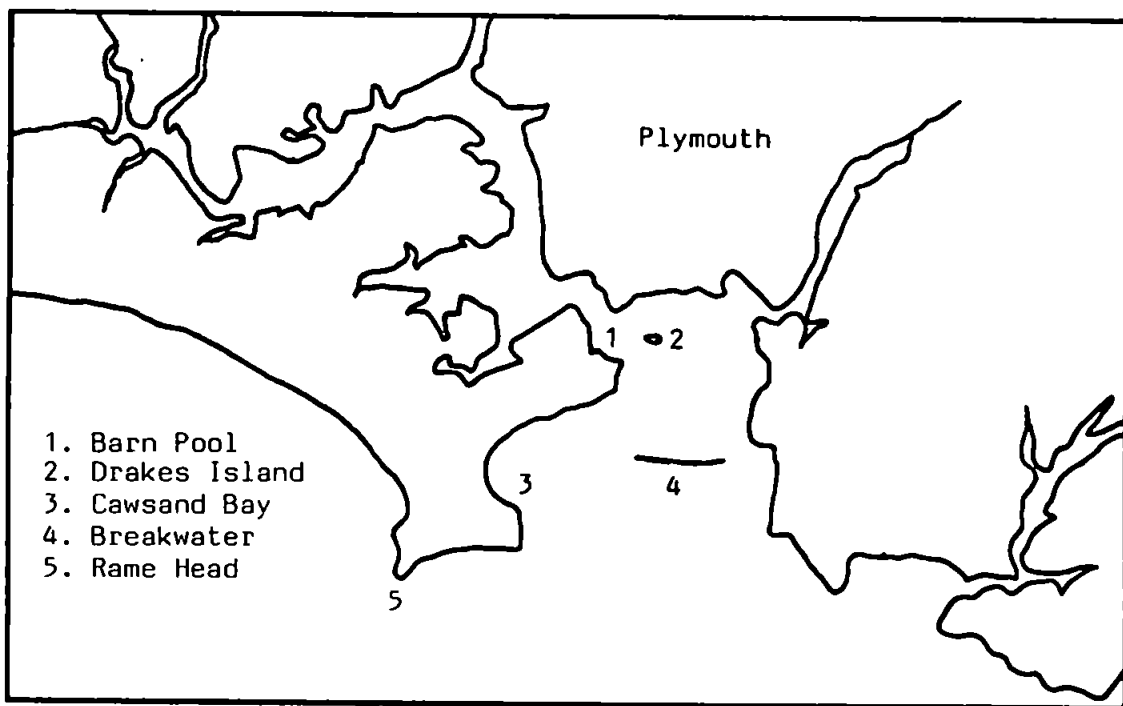
Figure 5.4.   Map showing positions of Rame Head, Cawsand Bay and Barn Pool

To determine the instrument housing temperature equilibration time, a temperature logger, type "Tiny Talk Temp' (RS Stock No. 213 - 436), was placed inside the housing to record the internal temperature and a second temperature logger was attached to the outside of the housing in a sealed container to monitor the water temperature.

First series submersed experiments: After successful completion of the housing depth/pressure experiments, the manifold was set up as shown in Fig. 5.1. with a 260 μl

161

sample loop. The complete integrated sensor system was then fitted into the housing and

cage assembly as shown in Fig. 5.5. for full submersed trials. Two new 600 ml reagent bags

were filled with mixed colour reagent and carrier solution respectively. Stopcocks were
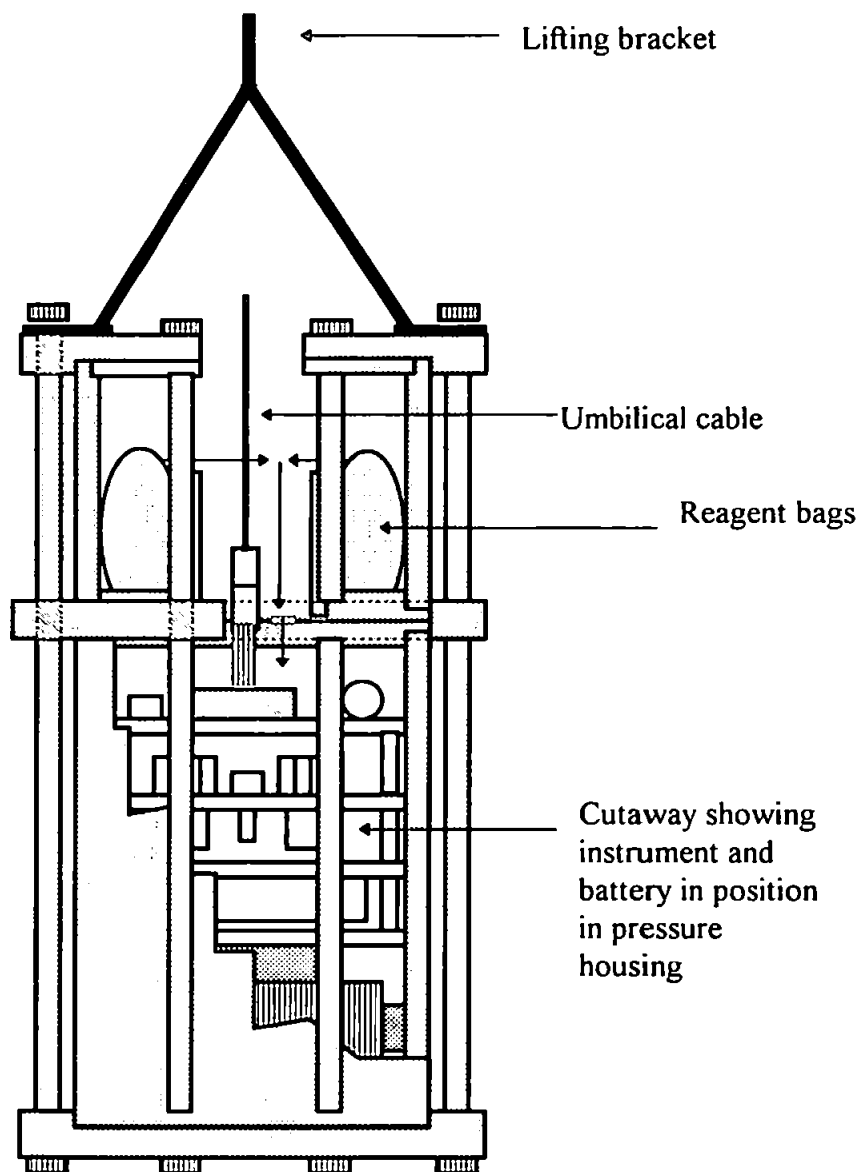
Figure 5.5. **Diagram showing configuration of integrated system used for**

submersed deployments

fitted and left in the open position so that the air could be squeezed out to minimise solution oxidation and to prevent air entering the system. The stopcocks were closed immediately after this operation and the reagent bags were placed in the reagent module. The fully charged battery was placed in the housing and connected to the instrument and placed in position at the bottom of the pressure housing. The internal cables and tubes were connected and the pressure housing end cap was rested on top of the housing. The external cable and tubes were connected and the system was switched on and reagents allowed to flush through. The sample line was flushed through with water. When satisfied with the operation, the end cap 'O' seal was lubricated with silicone grease and fixed in position with M4 stainless steel socket head screws. A series of submersed deployments were carried out over a number of weeks to test the operation of the integrated system before environmental data was collected. The first submersed deployment was made from the research vessel 'Squilla' in Cawsand Bay, as shown in Fig. 5.4., reference 50° 19.8' N. 4° 11.6' W, but all subsequent submersed deployments were made from the research vessel 'Tamaris' in Barn Pool which is also shown in Fig. 5.4. The first submersed deployment was at depth of 5 metres but had to be abandoned due to the severe weather conditions. Subsequent deployments in Barn Pool, grid reference 50° 21.3' N. 4° 10.0' W, started at 5 metres depth and eventually reached 30 metres depth. This first series of submersed trials concentrated on achieving successful operation at varying depths. Towards the end of this series of experiments it was decided to calibrate the instrument and obtain submersed data.

Second series submersed experiments: For this series of submersed experiments the integrated system was compared against a 'FIAstar' using bottles samples taken at the same depth as the submersed sensor. Bottle samples were taken using a National Institute of Oceanography (NIO) pattern sampling bottle as shown in Fig. 5.6. The bottle was lowered

to the same depth as the nutrient sensor with both ends open. When at the required depth, a water sample was obtained by closing both ends of the bottle by sending a weight called a 'messenger' down the line which triggered the spring mechanism of the bottle. The bottle was retrieved and the water sample was drained from the bottle and filtered to 5 µm. A Corning colorimeter set at 540nm for absorbance/transmission determinations, pH meter, thermometer, refractometer and a conductivity meter were also used to collect various physical parameters of the filtered water.

Figure 5.6.   Photograph of NIO pattern sampling bottle ready for deployment from

the research vessel Tamaris

To investigate the optical effects of sample and reagents on the flowcell components, i.e. how the LED/photodiode combination responded to solutions of different refractive index,

a light-tight static cell, as shown in Fig. 5.7., was constructed. The static cell had the same 20 mm path length and was fitted with the same LED and photodiode as used in the instrument flowcell.

The static cell was connected to a 5 V DC power supply, an op-amp and a millivoltmeter. The effects of the optical properties of the 5 μm filtered sea water samples, reagents and carrier solution could then be compared using the cell.
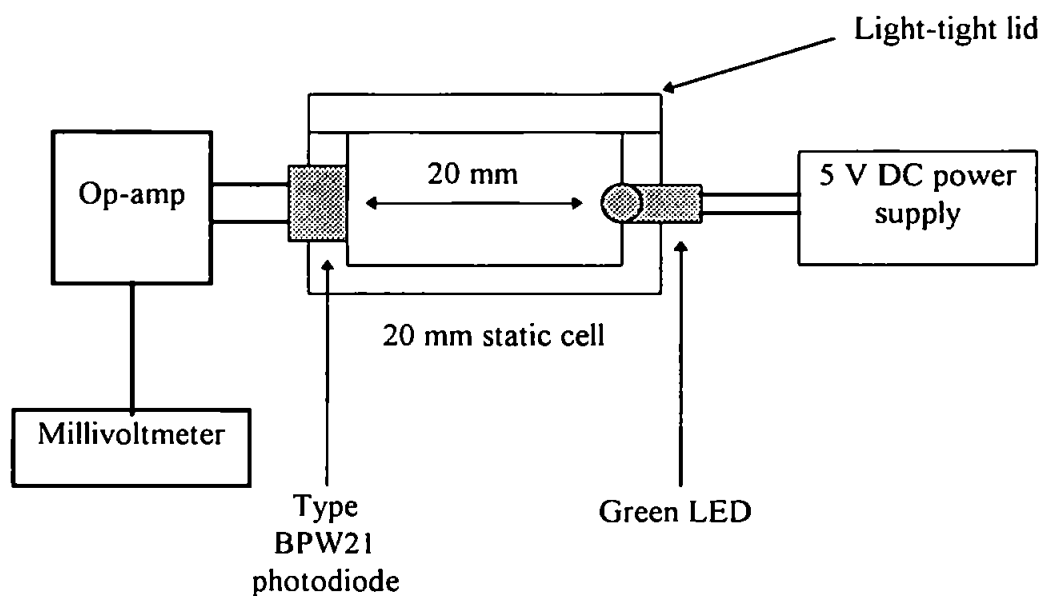
Figure 5.7.   **Schematic diagram of the static cell used for matrix effects investigation**

5.1.3.   Communications

Cellphone range checks: Signal strength experiments were carried out at the various sampling stations on the Tamar cruises, as shown in Fig. 5.3., and in coastal waters off Plymouth, as shown in Fig. 5.8., using a Class 4 handportable cellphone.
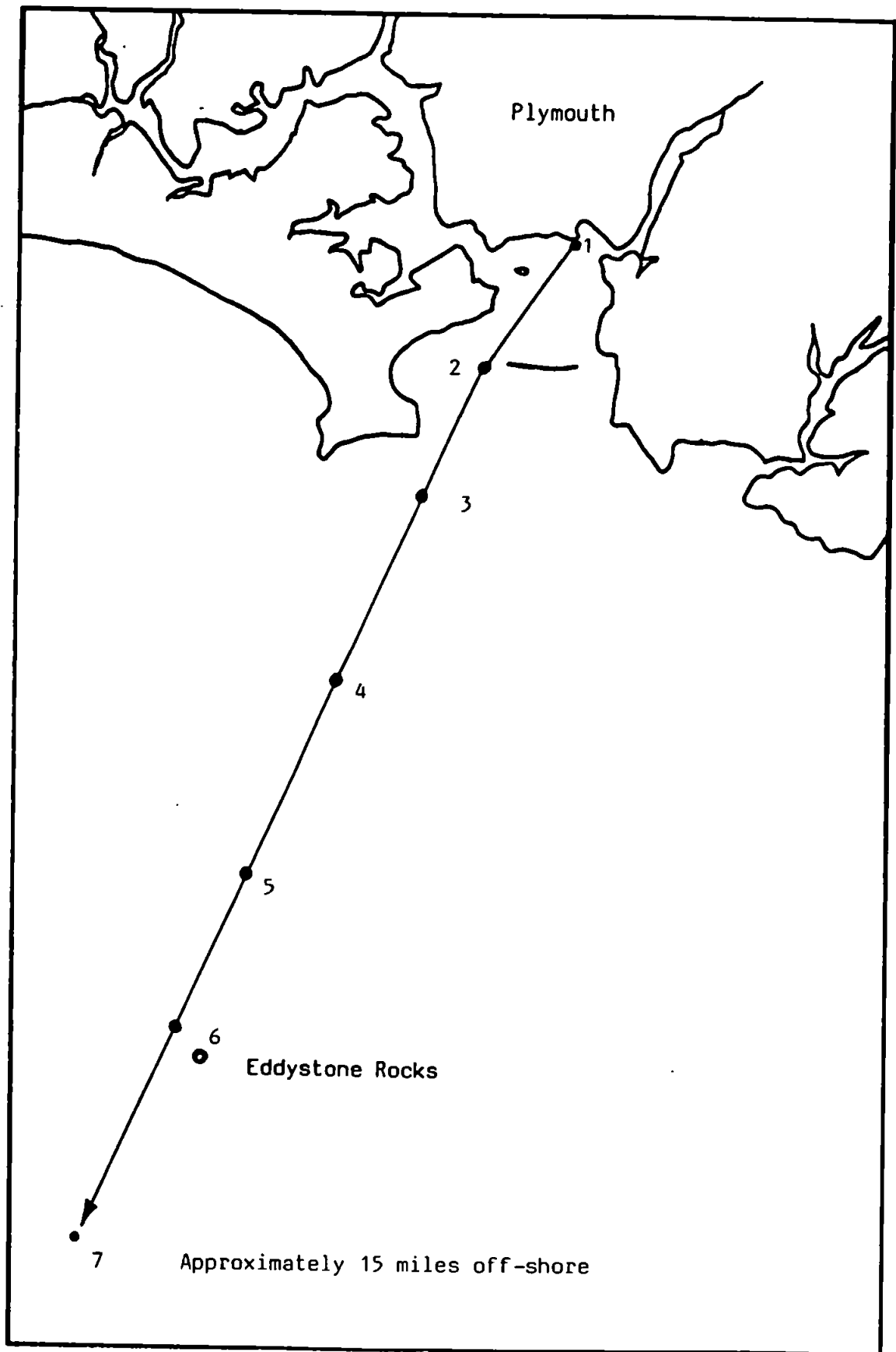
Figure 5.8.   Map showing approximate positions of cellphone coastal range checks

The labels on the map read:

Plymouth

1

2

3

4

5

6

Eddystone Rocks

7   Approximately 15 miles off-shore

5.2. RESULTS AND DISCUSSION

5.2.1. Tamar field trials (19.04.94 - 09.11.94)

The manifold was set-up with a 20 mm flowcell and a 150 μl sample loop. Although no laboratory experiments were carried out using this combination, previous experience suggested that it offered a good compromise between detection limit and linear range for the Nitrate-N levels expected in the Tamar estuary. The 150 μl sample loop produced approximately 50 % decrease in detector response compared to a 260 μl sample loop for the same 60 μM Nitrate-N standard as discussed in Chapter 4, section 4.2.3, i.e. due to increased sample dispersion. The FI manifold was calibrated over the range 1 - 2 mg l^{-1} for this series of experiments and therefore the riverine end-member (0 ‰ salinity) and the sea water end-member (34.1 ‰ salinity) nitrate concentrations were outside the operating range. Early trials were generally unsuccessful, mainly due to problems associated with the transfer of the support equipment from a stable laboratory environment to the field. There was also a steep learning curve in what was required by way of set-up procedures for a successful trial. However, analytical performance in a field environment continuously improved over the eight month period to a point where, for a particular range, the instrument produced results very close to those of the 'FIAstar' 5020, as shown in Table 5.3., which shows field data from the final Tamar cruise. Conditions on the day of this particular trial were extreme in that it immediately followed 4 days of heavy rainfall which had produced flood conditions in the river. The water was highly coloured with suspended material which at one point blocked the research vessels intake filters to the engine cooling water system. During the river Tamar field trials, a 5 μm syringe filter, type Gelman

Science's 'Acro Disc', was fitted to the sample inlet. This level of filtration was found to be sufficient in all situations.

Table 5.3. Comparison of field data obtained from the nutrient sensor FI instrument and a FIAstar during the final Tamar cruise on 09.11.94

Sample Station	Position	Nutrient Sensor	FIAstar
		Nitrate-N mg l^{-1}	
1.	Drakes Island	< range	0.33
2.	Skinham Point	1.89	1.93
3.	Weir Quay	> range	2.79
4.	Tinnel	1.96	2.14
5.	Whitsam	1.72	1.60
6.	Museum	1.56	1.54
7	Calstock	1.66	1.55

A paired *t*-Test [190] on the available data was carried out to determine the agreement between the two methods:

Sample	Nutrient sensor	FIAstar	Difference
2	1.89	1.93	- 0.04
4	1.96	2.14	- 0.18
5	1.72	1.60	+ 0.12
6	1.56	1.54	+ 0.02
7	1.66	1.55	+ 0.11

The mean difference ($\bar{x}_d$) = 0.006 and the standard deviation (S_d) of the differences =

0.123. Therefore, by substituting for the equation: $t = \bar{x}_d \sqrt{n} / S_d$

$t = 0.006 \sqrt{5} / 0.123 = 0.11$

Assuming a P level of 0.05 and n -1 degrees of freedom the critical value for t = 2.78. Therefore, the null hypothesis has been retained which shows that the two methods did not give significantly different values for the TON concentration. The FIAstar method had been validated by participation in two inter-laboratory exercises (EU Community Bureau of Reference (BCR) and International Council for Exploration of the Sea) for nitrates in river water and sea water respectively [157]. Resulting from the good correlation between the two systems the submersible FI system was therefore considered ready to commence submersed deployment experiments.

5.2.2.   Submersed trials

Depth tests: It was considered that an *in situ* depth/pressure test would be more valuable than a tank pressure test as it would also provide an opportunity to assess the handling characteristics of the housing. On retrieval of the instrument pressure housing and cage assembly from a depth of 45 metres after 1 hour, no leaks into the instrument housing were observed. Shortly after deployment, the pressure housing and cage assembly had to be retrieved for a short period to allow the boat to change position slightly. The effect of this can be seen on the temperature plots, i.e. a rise in temperature before a steady decrease. The temperature sensors indicated that after 25 minutes the instrument module attained a temperature of within 2 °C of the water temperature as shown in Fig. 5.9. This suggests that a delay of approximately 30 minutes would be required for the full system to equilibrate

before analysis commences. The handling characteristics of the housing and cage assembly during deployment and retrieval were good.
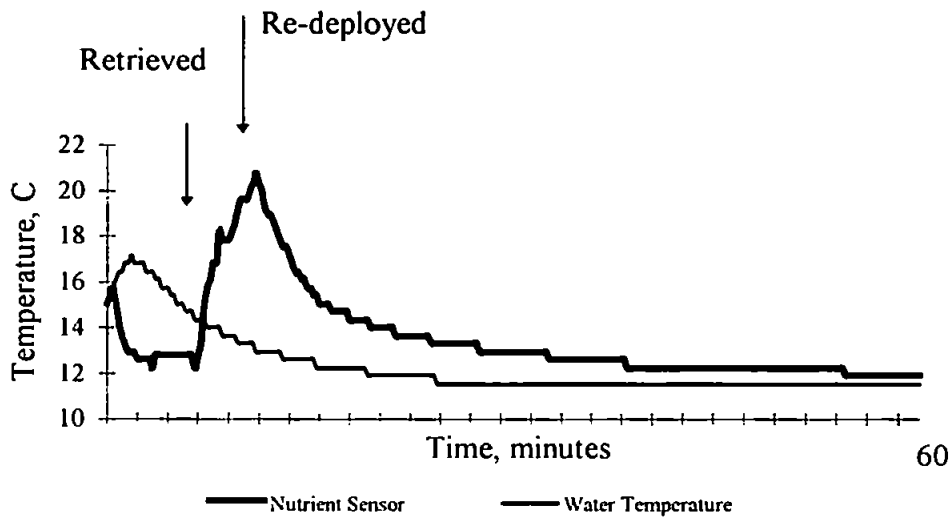
Figure 5.9.   **Output from temperature loggers during depth test on pressure housing**

First series submersed experiments: The first series of submersed deployments, as shown in Table 5.4., concentrated on achieving successful submersed operation only, i.e. actual field data was not be collected apart from obtaining a 'satisfactory' analyte signal from a sample injection when submersed.

Submersed Deployment 1: The system was deployed at a depth of 5 m in Cawsand Bay, (see Fig 5.4.), which is outside the breakwater, and set to run. The weather conditions on the day of the first submersed trials were far from ideal. Force 7 winds created a severe sea swell which made the final on-board adjustments very difficult. Reagents and sample were successfully pumped through the system and the instrument was in communication with the PC. The system was retrieved soon after as weather conditions deteriorated even further so

the remainder of the trial was aborted. However, the severe sea conditions did test the overall construction of the integrated system.

Table 5.4.   **First series of submersed deployments to test operation of integrated system**

Deployment	Date	Research vessel	Depth	Successful Operation
			m	
1	02.12.94	Squilla	5	yes
2	10.01.95	Tamaris	5	no
3	06.02.95	Tamaris	5	yes
4	15.02.95	Tamaris	5, 10	yes
5	20.02.95	Tamaris	12, 17, 20	yes
6	02.03.95	Tamaris	20	yes
7	07.03.95	Tamaris	10, 20	yes

On several occasions it was thrown hard against the side of the vessel as it rolled, and, during set-up before deployment, the heavy sea caused the instrument module to fall off the bench. Despite the adverse weather conditions which prematurely halted the testing, this first full system submersed trial was considered a partial success. Sample and reagents were pumped through the system and full control and communications were effected from the surface. The construction of the instrument had been tested in harsh conditions and considered to be adequate for the purpose and therefore fulfilled the requirements of the specification.

Submersed Deployment 2: Barn Pool was chosen for the next and all subsequent submersed deployments due to its location. It is in a sheltered position well inside the breakwater and has 30 to 40 metres depth of water depending on the tidal conditions and was within easy reach from Sutton harbour where the research vessels were berthed. It was

also at the mouth of the Hamoaze channel into which the Tamar, Lyhner and Tavy rivers flow and was therefore a good position to test the submersed system prior to the North Sea/Humber Plume cruise. The first submersed deployment off 'Tamaris' was unsuccessful as the system was unable to pump the colour reagent. This was traced to the stiffening and contraction of the pump tubing caused by the cold weather (the effects of temperature on pump tubing performance were investigated in Chapter 3) and the dimensions of the tube bed in the pump tensioner. The tubing tensioner was unable to initiate or sustain flow in the colour reagent line. Close examination found the tube bed was slightly too deep for the pump tubing at low temperatures. A combination of lowered flexibility and a slight decrease in diameter required additional tensioning force to initiate flow. This additional force could not be applied as the tensioner fouled the pump rollers due to the depth of the tube bed. The situation was rectified by reducing the depth of the tube bed, as shown in Fig. 5.10., by approximately 50% using a file.

Tube bed
tensioner
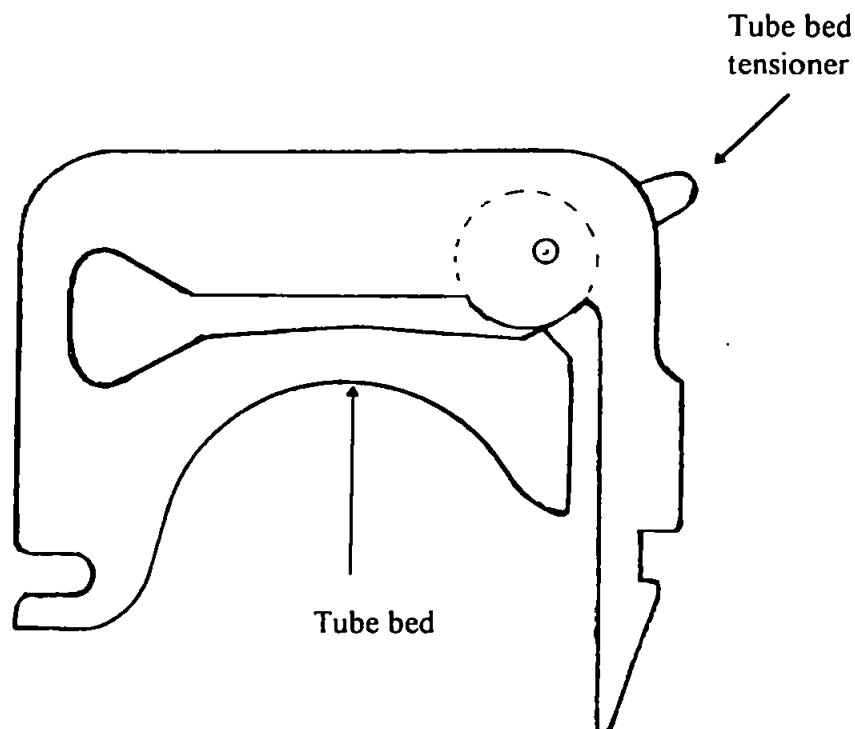
Tube bed

Figure 5.10.   Peristaltic pump tube holder

After this modification, as shown in Fig. 5.11., no further problems with flow initiation were observed.
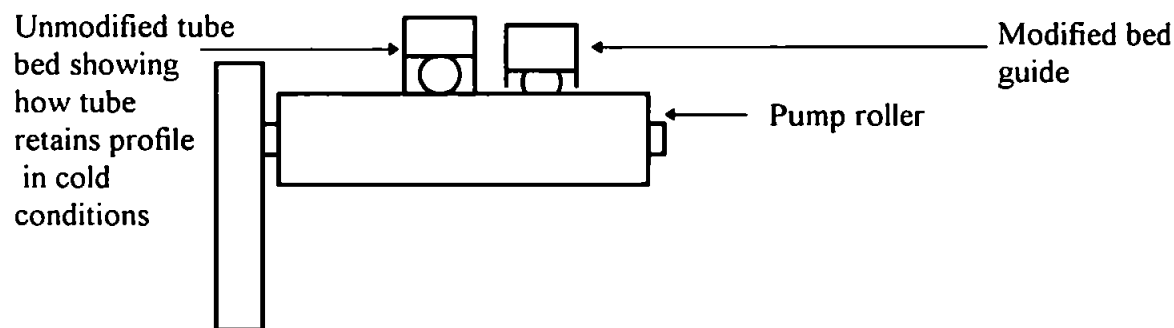
Figure 5.11.   Cross section of tube bed before and after modification

Submersed Deployment 3: The integrated system operated successfully during this submersed deployment to produce well defined analyte peaks at a depth of 5 metres. The result from the first sample injection is shown in Fig. 5.12. The time taken for the sample to progress through the system was shortened due to the pressure differential assisting the pumping operation. The delay before the start of the ADC count was shortened from 90 seconds (as used for bench set-up) to 70 seconds.
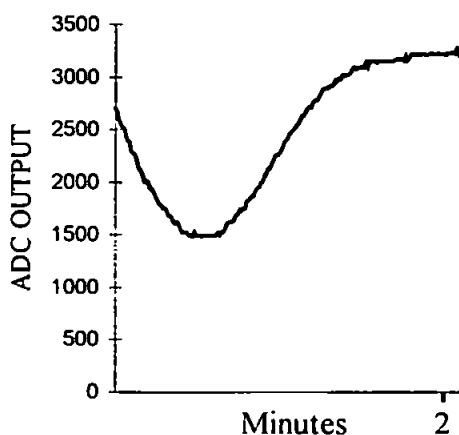
Figure 5.12.   Submersed deployment 3: first sample peak at 5 metres depth

173

Submersed Deployment 4: The integrated system was successfully deployed at 5 metres depth for approximately 2 hours. The first sample injection is shown in Fig. 5.13. The system worked faultlessly during this period until the portable PC used for direct serial communications overheated and crashed.
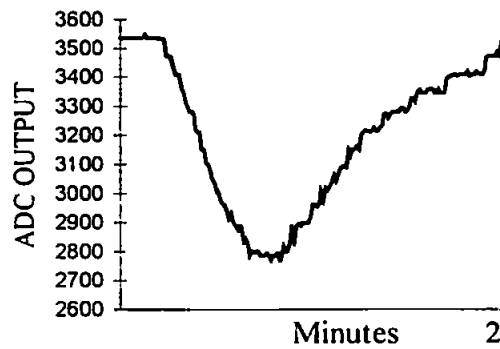
Figure 5.13. Submersed deployment 4: first sample peak at 5 metres depth

The PC was allowed to cool for approximately 1 hour before resuming submersed trials at a depth of 10 metres. The system was operated at this depth for about 1 hour and worked well. The first sample injection at 10 metres depth and after the system shutdown due to PC failure is shown in Fig. 5.14.
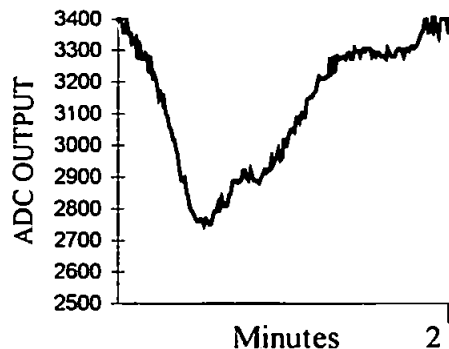
Figure 5.14. Submersed deployment 4: first sample at 10 metres after system shut down

One of the main problems encountered during the field trials was the unreliability of the portable PC, especially on the Tamar cruises during the summer months when the air temperature was high. An earlier fault with the power supply had caused the re-chargeable batteries to overheat and cause further damage to the internal power circuitry. As a result of this, the PC could only be operated from a mains supply. During the field experiments it was not unusual for the PC to run for only 1 hour before it overheated and crashed. In addition to this, there were problems in saving data from the instrument to disk which was caused by the vibration from the research vessel. In the worst case the PC would not write to the hard drive or to the floppy drive and when it did, it would create a file name without saving the data, i.e. the ADC count data was occasionally lost or corrupted. Therefore, in the event of total PC failure, an alternative means of communicating with the instrument was sought. This was achieved using a Psion Organiser® II configured to run in terminal mode. Using a Psion proprietary serial interface cable connected to a custom made interface cable, the instrument could be controlled and communicated with in much the same way as with a PC. The only drawback with this system was the size of the screen and the keypad layout which made the operation slightly awkward in heavy weather conditions. However, the Psion did prove to be a useful backup system and did not take up a great deal of space in the field support kit.

Submersed deployment 5: This deployment was the first of the this series of experiments in which the integrated system was calibrated so that environmental data could be collected. A new reduction column was fitted, the reagent bags were filled with fresh reagents and a series of Nitrate-N standards prepared. The system was calibrated against the series of Nitrate-N standards on board the 'Tamaris' immediately before the pressure housing end cap was sealed and the system was deployed. The results of the pre-deployment calibration are

shown in Table 5.5. and Fig. 5.15. The field data obtained from submersed deployments 5

at depths ranging from 12 to 17 metres is shown in Table 5.6.

Table 5.5.   **Calibration data for submersed deployment 5**

Nitrate-N Standard	Peak height
mg l $^{-1}$	ADC count
0.00	390
0.10	630
0.25	781
0.50	1442
0.75	1775
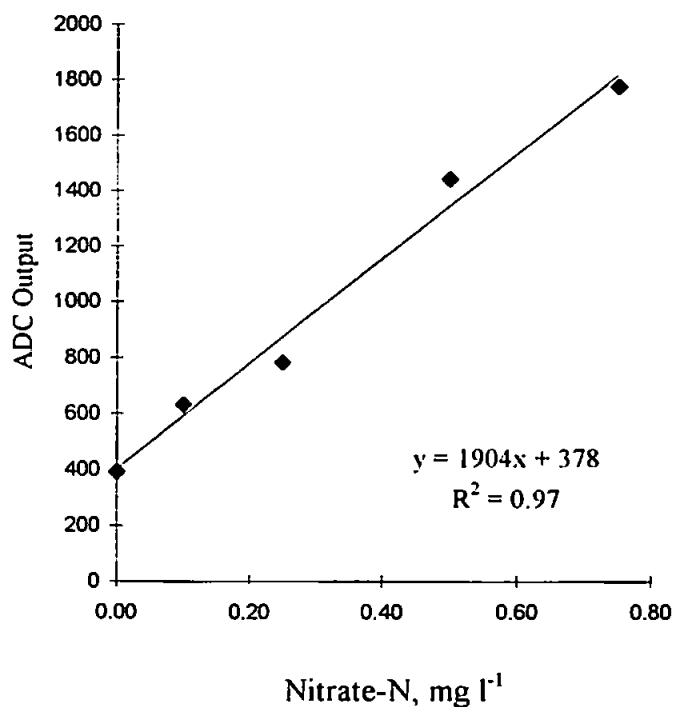
Figure 5.15.   Calibration graph for submersed deployment 5

176

Table 5.6.   Field data from deployment 5 : High tide 0850 hrs

Sample	Time	Depth	Nitrate-N
		m	mg l^{-1}
1	1000	17	0.47
2	1010	17	0.50
3	1020	17	0.37
4	1030	17	0.47
5	1040	17	0.46
6	1050	17	0.51
7	1100	17	0.56
8	1105	16	0.61
9	1135	16	0.60
10	1140	15	0.64
11	1150	15	0.76
12	1200	14	0.48
13	1205	14	0.45
14	1210	13	0.67
15	1220	13	0.62
16	1230	12	0.63
17	1240	12	0.68
18	1250	12	0.49

The integrated system operated reliably and was in direct serial communication with a PC for the duration of the submersed deployment. The measured TON values show an upward trend as the tide receded due to the increasing influence of riverine nitrate and the influence of changing position.

177

Submersed deployment 6:   The integrated system was calibrated as for deployment 5 using the same series of standards apart from the blank ('Milli-Q' water) which was prepared the day before the deployment. The calibration data for the deployment is shown in Table 5.7. and Fig. 5.16. The field data obtained from the submersed deployment is shown in Table 5.17.

Table 5.7.   Calibration data for submersed deployment 6

Nitrate-N	Peak Height
mg l^{-1}	ADC count
0.00	350
0.10	673
0.25	784
0.50	1237
0.75	1817

$y = 1857x + 368$
$R^2 = 0.98$
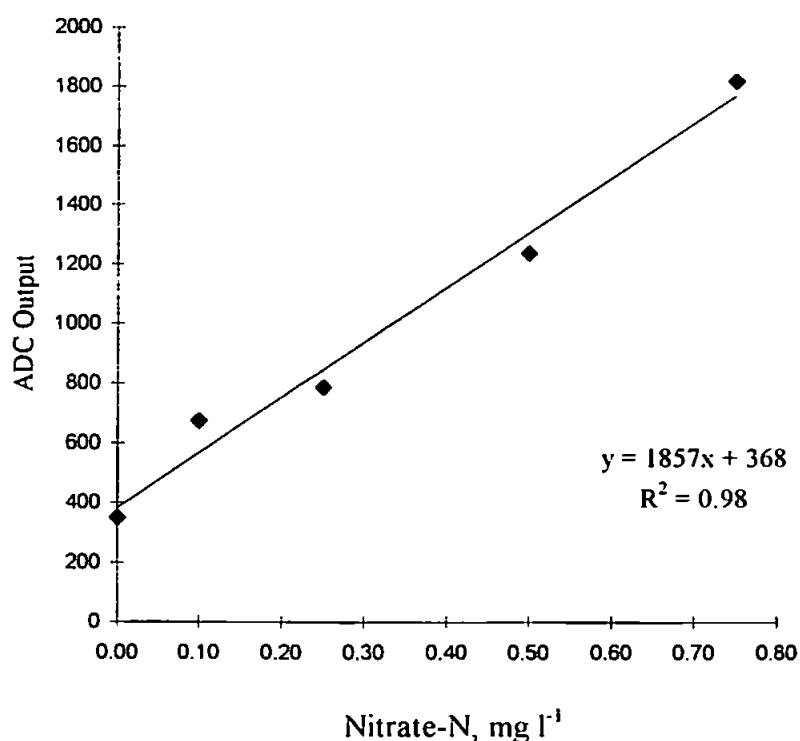
Nitrate-N, mg l^{-1}

Figure 5.16.   Calibration graph for submersed deployment 6

178

Table 5.8. Field data from submersed deployment 6: High tide 0706 hrs

Sample	Time	Depth	Nitrate-N
		m	mg l^{-1}
1	1040	20	0.53
2	1050	17	0.52
3	1100	17	0.51
4	1110	17	0.53
5	1120	17	0.54
6	1130	17	0.55
7	1200	20	0.50
8	1210	20	0.48
9	1220	20	0.53
10	1230	20	0.52
11	1240	20	0.52
12	1250	20	0.52
13	1300	20	0.51

The integrated system operated reliably and was in direct serial communication with the surface throughout the deployment and remained submersed when the position of the vessel changed at 1130 due to tidal conditions. The measured TON concentrations appear to be relatively stable throughout the depth range and time period. This was probably due to the fact that it was almost low tide by the time the analysis had commenced so the riverine input of nutrients into the area was being observed.

Submersed deployment 7: The integrated system was calibrated as for deployment 6 and

the calibration data is shown in Table 5.9. and Fig. 5.17. The system was deployed at 10

and 20 metre depths and the field data obtained is shown in Table 5.10.

Table 5.9.   **Calibration data for submersed deployment 7**

Nitrate-N	Peak Height
mg l $^{-1}$	ADC count
0.00	377
0.10	637
0.25	845
0.50	1321
0.75	1617

$$y = 1644x + 433$$
$$R^2 = 0.99$$
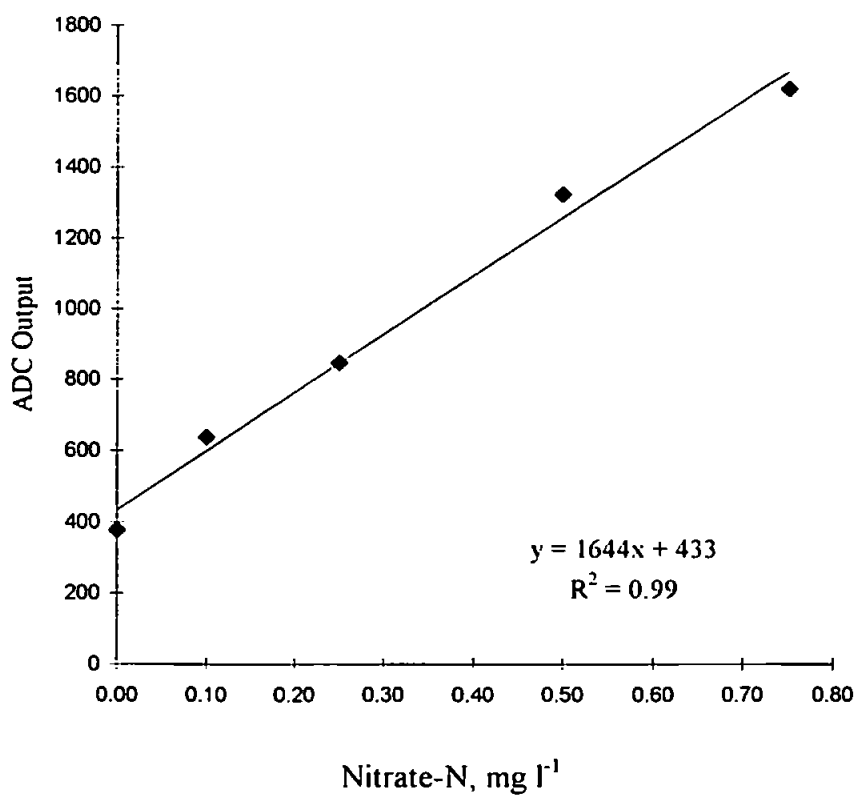
Nitrate-N, mg l^{-1}

Figure 5.17.   **Calibration graph for submersed deployment 7**

Table 5.10. **Field data from submersed deployment 7: High tide 0927 hours**

Sample	Time	Depth	Nitrate-N
		m	mg l^{-1}
1	1105	10	0.34
2	1115	10	0.45
3	1125	10	0.37
4	1130	10	0.40
5	1140	10	0.32
6	1150	10	0.45
7	1155	10	0.46
8	1240	20	0.64
9	1250	20	0.58
10	1255	20	0.65
11	1300	20	0.62
12	1305	20	0.65
13	1310	20	0.58
14	1320	20	0.64
15	1325	20	0.68
16	1330	20	0.58
17	1340	20	0.56

The integrated system worked reliably and was in direct communication with the surface for the duration of the submersed deployment. The measured TON levels show a gradual increase as the tide recedes and the riverine nutrient input increases.

Overview of 1st series of submersed deployments: The reagents for the diazotisation and coupling reaction had been confirmed as stable for a 30 day period [107]. Therefore, apart

from the blank ('Milli-Q') the same reagents and standards were used for submersed deployments 5, 6 and 7. The same reduction column was also used. The stock reagents were kept in dark glass bottles and these were used to refill the reagents bags on the evening prior to deployment. On completion of the submersed deployment the system was completely flushed through with 'Milli-Q' water and carrier solution. The Fl system manifold was kept full of carrier solution by joining the disconnected ends of the various tubes and it was stored in this way until the next deployment. By following this procedure at the end of each deployment the reduction column was preserved which resulted in no observed deterioration of the column over a 30 day period. The column was routinely changed after being fitted to the instrument for one month. By comparing the reproducibility of calibration for the 17 day period, as shown in Table 5.11., it can be seen that the rsd values are within the target specification ± 5 %. This suggests that a single calibration prior to deployment could be used over a 17 day period. If greater precision was required on-board standards would be used to compensate for electronic drift during deployment. However, depending on the number of on-board standards, this would add a degree of complexity which may have a detrimental affect on the sampling frequency.

Table 5.11.   Comparison of integrated system calibration data from submersed deployments 5, 6 and 7

Nitrate-N	5	6	7	Mean	rsd
mg l $^{-1}$	20.02.95	02.03.95	07.03.95		%
0	390	350	377	372	5.5
0.1	630	673	637	647	2.9
0.25	781	784	845	803	4.5
0.50	1442	1237	1321	1333	7.7
0.75	1775	1817	1617	1736	6.1

At this stage, the operation of the integrated system was totally reliable when submersed. It was therefore decided to move on to the next phase by collecting additional supporting field data from the Barn Pool study area as described in section 5.1.2. To achieve this the second series of submersed deployments was carried out.

Second series of submersed experiments: The details of the second series of submersed deployments are shown in Table 5.12.

Table 5.12. Second series of submersed deployments in Barn Pool from the research vessel Tamaris

Deployment	Date	Depth	Successful deployment
		m	
8	16.03.95	30	yes
9	23.03.95	20	yes
10	30.03.95	15	yes
11	06.04.95	10	yes
12	12.04.95	10	yes
13	27.04.95	30	no
14	25.05.95	10	yes

As an initial precautionary measure, new standards reagents and reduction column were used each time for deployments 8 and 9. For subsequent deployments the same new reagents, standards and reduction column were used for the duration of the remaining successful submersed deployments, i.e. deployments 10, 11 and 12.

Submersed Deployment 8: A new reduction column was fitted and fresh reagents and standards prepared. The instrument was calibrated and the results from the calibration are shown in Table 5.13. and Fig. 5.18. The results from deployment 8 and the additional tests carried out on the bottle sampled water at 30 metres are shown in Table. 5.14.

Table 5.13.   Calibration data for submersed deployment 8

Nitrate-N mg l^{-1}	Peak Height ADC count
0.00	339
0.10	656
0.25	1029
0.50	1585
0.75	1898

$$y = 1644x + 433$$
$$R^2 = 0.99$$
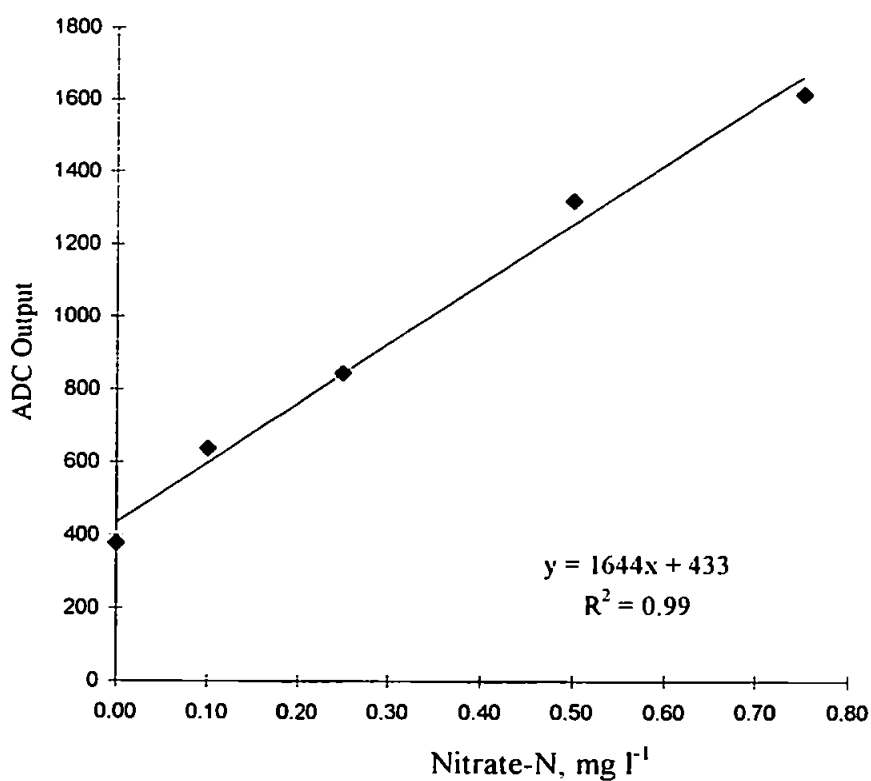
Figure 5.18.   Calibration graph for submersed deployment 8

The system operated reliably at 30 metres which was the final target depth and was in direct communication with the surface. During this deployment, the FIAstar developed a fault which could not be rectified at the time and this meant that comparison nutrient data was not available so the field experiment was aborted after one hour. The additional tests on the 5.0 μm filtered seawater, bottle sampled at the same depth of deployment, found that there were no absorbing species at 540 nm and there were no significant refractive index effects on the static cell when the seawater sample and reagents were measured. The data from the static cell was considered essential in support of the approach taken to minimise the Schlieren effect, i.e. by optimising the key manifold parameters as discussed in Chapter 4, section 4.2.3. This data showed that the cell configuration and components were not affected by solutions of differing refractive index and therefore would not contribute any additional signal.

Table 5.14. Submersed deployment 8: results from submersed nutrient sensor, bottle samples and reagents: High tide 1526 hrs.

				5 µm filtered bottle samples and reagents							
Sample	Time	Depth	Nitrate-N Submersed nutrient sensor	Nitrate-N FIAstar	Temp	Conductivity	pH	R.I.	Absorbance at 540 nm	Transmittance at 540 nm	Static 20 mm cell
		m	mg l^{-1}	mg l^{-1}	°C	µmhos				%	mV
1	1240	30	0.23	-	10.5	45000	7.9	4	0	100	290
2	1255	30	0.31	-	10.0	45000	7.9	4	0	100	291
3	1315	30	0.23	-	10.0	42500	7.4	4	0	100	291
4	1330	30	-	-	10.0	46000	7.5	4	0	100	290
5	1345	30	-	-	10.0	44000	7.2	4	0	100	286
				Carrier	15.0	13400	5.4	1.25	0	100	280
				Standards							
				0.00	15.0	0.1	7.0	0	0	100	289
				0.10	15.0	2.6	7.0	0	0	100	293
				0.25	15.0	4.2	7.0	0	0	100	290
				0.50	15.0	7.4	7.0	0	0	100	291
				0.75	15.0	9.0	7.0	0	0	100	292

Submersed Deployment 9: New standards, reagents and reduction column were used and the integrated system was calibrated prior to deployment. The calibration data is shown in Table 5.15. and Fig. 5.21. The results from the submersed sensor and the FIAstar gave good correlation as shown in Table 5.16.

Table 5.15.   Calibration data for submersed deployment 9

Nitrate-N	Peak Height
mg l $^{-1}$	ADC output
0.00	312
0.10	501
0.25	1057
0.50	1335
0.75	1588

$y = 1713x + 410$
$R^2 = 0.93$

Figure 5.19.   Calibration graph for submersed deployment 9

Table 5.16. Submersed deployment 9: results from submersed nutrient sensor, bottle samples and reagents: High tide 0803 hrs.

				5 µm filtered bottle samples and reagents							
Sample	Time	Depth	Nitrate-N Submersed nutrient sensor	Nitrate-N FIAstar	Temp	Conductivity	pH	R.I.	Absorbance at 540 nm	Transmittance at 540 nm	Static 20 mm cell
		m	mg l^{-1}	mg l^{-1}	°C	µmhos				%	mV
1	1055	20	0.17	0.19	10.0	47500	7.5	4	0	100	289
2	1110	20	0.25	0.25	10.0	50000	7.9	4	0	100	290
3	1135	20	0.22	0.26	10.0	47500	7.9	4	0	100	290
4	1145	20	0.22	0.19	10.0	50000	7.8	4	0	100	288
5	1205	20	0.16	0.17	11.0	52500	7.9	4	0	100	288
6	1230	20	0.20	0.18	10.5	50000	8.0	4	0	100	289
7	1240	20	0.21	-	-	-	-	-	-	-	-
8	1245	20	0.21	-	-	-	-	-	-	-	-
				Carrier	14.5	13400	5.4	1.25	0	100	290
				Standards							
				0.00	14.5	0.2	7.1	0	0	100	289
				0.10	14.5	2.5	7.0	0	0	100	290
				0.25	14.5	4.2	7.0	0	0	100	291
				0.50	14.5	7.3	7.0	0	0	100	291
				0.75	14.5	9.0	7.0	0	0	100	290

To examine the correlation between both methods, a paired t - Test was carried out on the nutrient data obtained from the integrated system and the bottle samples analysed using the FIAstar. From Table 5.16. :

Sample	Nutrient sensor	FIAstar	Difference
	mg l^{-1}	mg l^{-1}	
1	0.17	0.19	- 0.02
2	0.25	0.25	0.00
3	0.22	0.26	- 0.04
4	0.22	0.19	+ 0.03
5	0.16	0.17	- 0.01
6	0.20	0.18	+ 0.02

The mean difference ($\bar{x}_d$) = - 0.0033 and the standard deviation (S_d) of the differences = 0.026. Therefore, by substituting for the equation: $t = \bar{x}_d \sqrt{n} / S_d$

$$t = - 0.0033 \sqrt{6} / 0.026 = - 0.31$$

Assuming a P level of 0.05 and n - 1 degrees of freedom the critical value for t = 2.57. Therefore, the null hypothesis has been retained which shows that the two methods did not give significantly different values for the TON concentration.

Submersed Deployments 10, 11 and 12: For these deployments, the same new reagents, standards and reduction column were used for the duration of the three deployments. The calibration data for deployments 10, 11 and 12 is shown in Tables 5.17., 5.19. and 5.21. respectively and in Figs. 5.20., 5.21. and 5.22. respectively. Due to a persistent fault, the FIAstar was not available for the remainder of the deployments. The additional data from the 5.0 μm filtered sea water and reagents using the static cell was not collected after deployment 10 as there was no significant change observed throughout the previous deployments. The field data collected from deployments 10, 11 and 12 is shown Tables 5.18., 5.20. and 5.22. respectively.

Table 5.17.   Calibration data for submersed deployment 10

Nitrate-N	Peak Height
mg l $^{-1}$	Range
0.00	365
0.10	552
0.25	1107
0.50	1400
0.75	1744

$$y = 1818x + 457$$
$$R^2 = 0.96$$
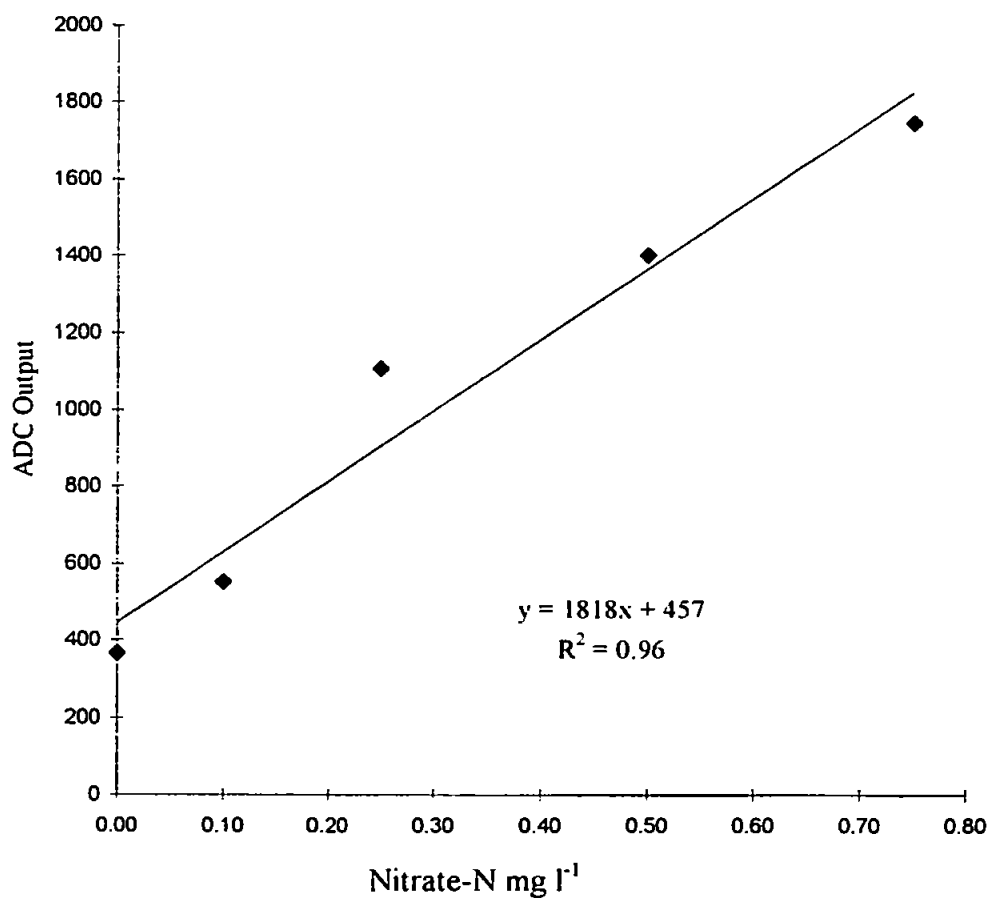
Figure 5.20.   Calibration graph for submersed deployment 10

Table 5.18.   Submersed deployment 10: results from submersed nutrient sensor, bottle samples and reagents: High tide 1537 hrs.

					5 μm filtered bottle samples and reagents						
Sample	Time	Depth	Nitrate-N Submersed nutrient sensor	Nitrate-N FIAstar	Temp	Conductivity	pH	R.I.	Absorbance at 540 nm	Transmittance at 540 nm	Static 20 mm cell
		m	mg l^{-1}	mg l^{-1}	°C	μmhos				%	mV
1	1125	15	0.29	*	12.5	45000	8.0	3.8	0	100	283
2	1140	15	0.24	*	10.5	50000	8.0	3.8	0	100	287
3	1155	15	0.18	*	11.0	50000	8.0	3.8	0	100	287
4	1215	15	0.18	*	12.0	50000	8.0	3.5	0	100	285
5	1245	15	0.13	*	11.0	45000	8.0	3.5	0	100	282
6	1300	15	0.18	*	10.5	50000	8.1	3.5	0	100	282
7	1315	15	0.13	*	10.5	50000	8.0	3.5	0	100	283
8	1330	15	0.15	*	10.5	50000	8.1	3.8	0	100	287
9	1345	15	0.21	*	10.5	50000	8.1	3.8	0	100	286
10	1400	15	0.25	*	10.0	45000	8.0	4.0	0	100	287
				Carrier	15.0	13500	5.4	1.25	0	100	289
				Standards							
				0.00	15.0	0.2	7.0	< 0	0	100	287
				0.10	15.0	2.4	7.0	< 0	0	100	288
				0.25	15.0	4.2	7.0	< 0	0	100	288
				0.50	15.0	7.2	7.0	< 0	0	100	289
				0.75	15.0	9.0	7.0	< 0	0	100	290

Table 5.19. Calibration data from submersed deployment 11

Nitrate-N	Peak Height
mg l^{-1}	ADC count
0.00	330
0.10	576
0.25	948
0.50	1326
0.75	1578

$$y = 1658x + 421$$
$$R^2 = 0.97$$
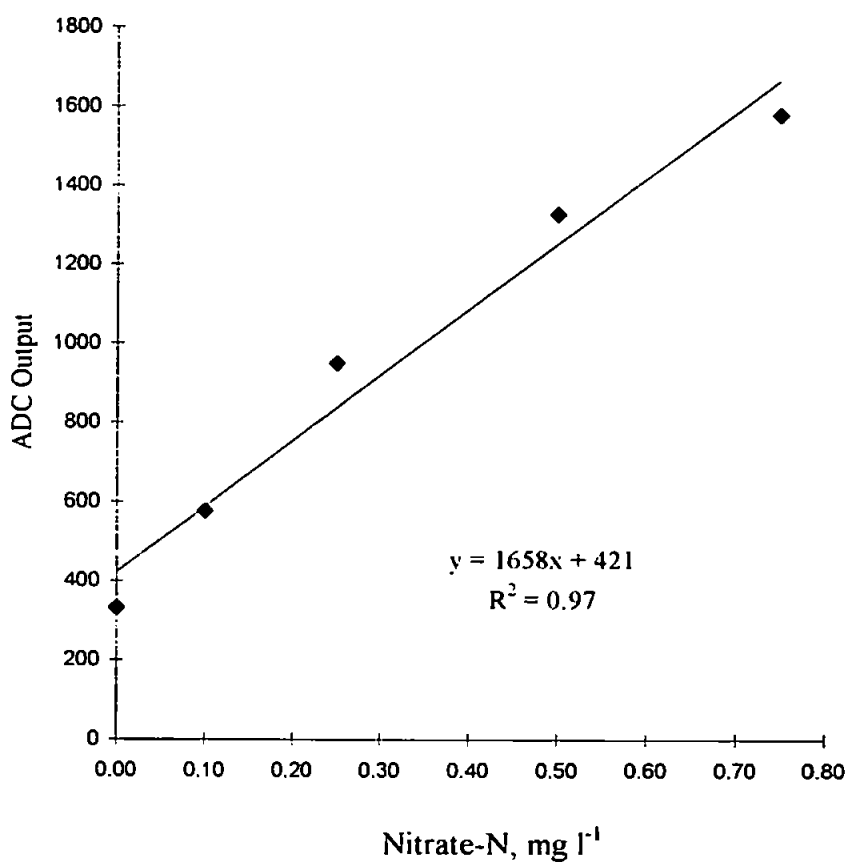
Figure 5.21. Calibration graph for submersed deployment 11

Table 5.20. Submersed deployment 11: results from submersed nutrient sensor and bottle samples: High tide 0708 hrs.

Sample	Time	Depth	Nitrate-N Submersed nutrient sensor	Temp	Conductivity	pH	R.I.	Absorbance at 540 nm	Transmittance at 540 nm
		m	mg l^{-1}	°C	µmhos				%
1	1145	10	0.23	11.5	46000	8.2	4.0	0	100
2	1200	10	0.23	11.5	47500	8.3	4.0	0	100
3	1215	10	0.23	12.0	49000	8.2	4.0	0	100
4	1230	10	0.23	12.0	50000	8.2	4.0	0	100
5	1245	10	0.25	12.0	50000	8.3	4.0	0	100
6	1300	10	0.28	12.5	47500	8.3	4.0	0	100
7	1315	10	0.30	12.0	47500	8.3	4.1	0	100
8	1330	10	0.30	12.0	47500	8.3	4.0	0	100
9	1345	10	0.30	12.5	47500	8.2	4.0	0	100
10	1400	10	0.32	12.0	47500	8.2	4.0	0	100

Table 5.21. Calibration data for submersed deployment 12

Nitrate-N mg l^{-1}	Peak Height Range
0.00	350
0.10	609
0.25	1024
0.50	1380
0.75	1780

$$y = 1952 + 384$$
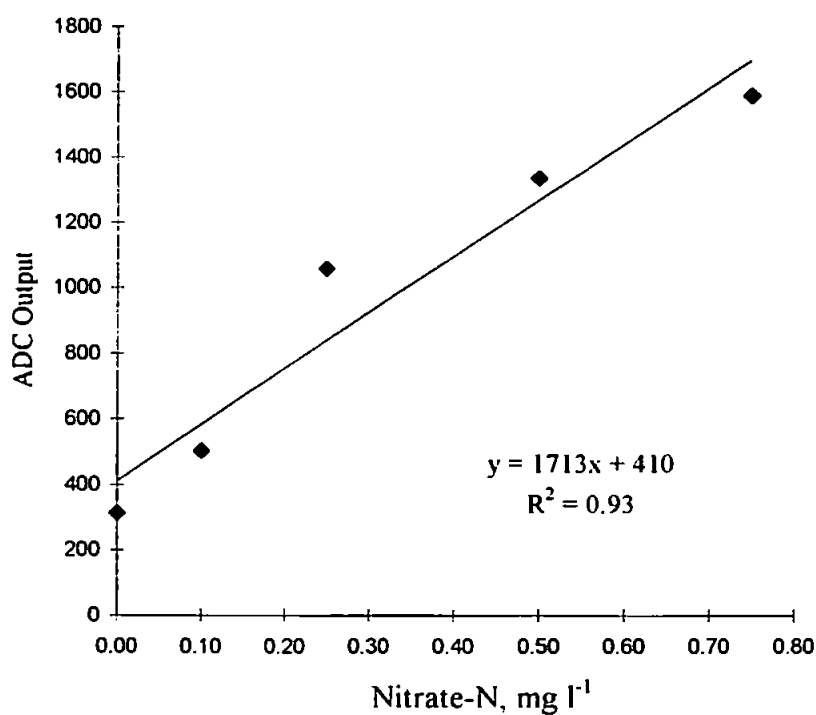$$R^2 = 0.97$$

Nitrate-N, mg l^{-1}
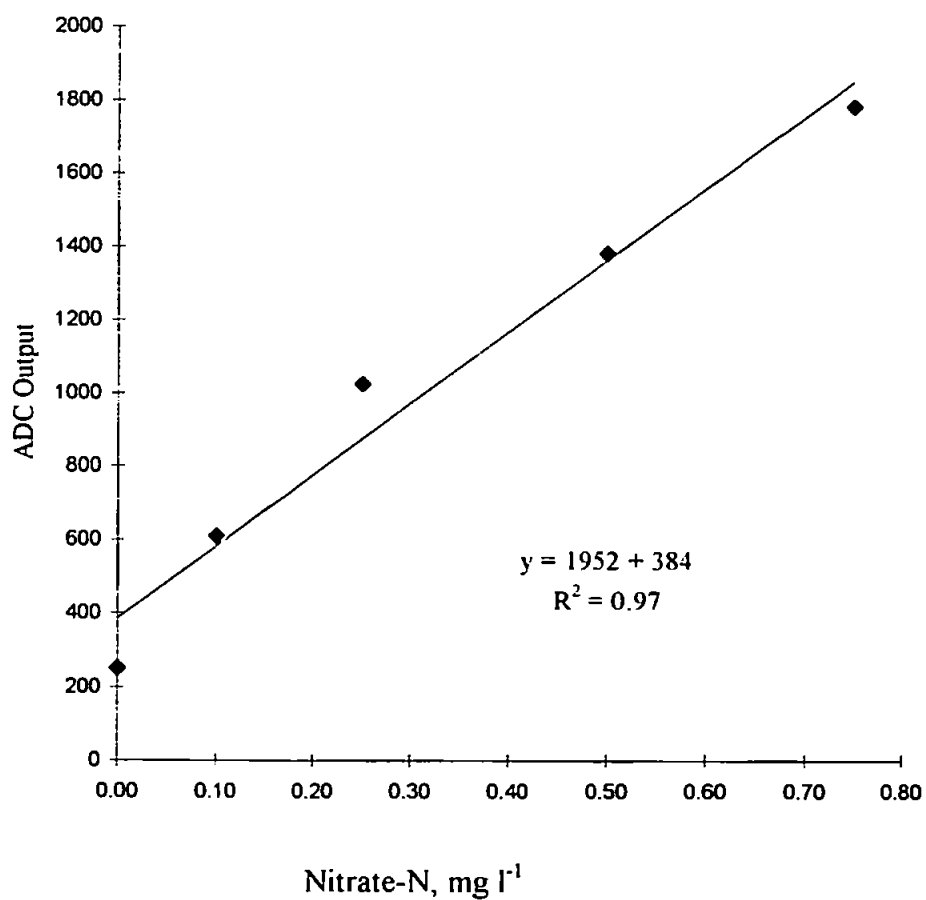
Figure 5.22. Calibration graph for submersed deployment 12

Table 5.22.　Submersed deployment 12: results from submersed nutrient sensor and bottle samples: High tide 1332 hrs.

Sample	Time	Depth	Nitrate-N Submersed nutrient sensor	Temp	Conductivity	pH	R.I.	Absorbance at 540 nm	Transmittance at 540 nm
		m	mg l $^{-1}$	°C	µmhos				%
1	1045	10	0.17	12.0	47500	8.2	4	0	100
2	1100	10	0.16	12.0	49000	8.1	4	0	100
3	1115	10	0.20	12.0	50000	8.2	4	0	100
4	1130	10	0.18	11.5	50000	8.2	4	0	100
5	1145	10	0.17	12.0	47500	8.2	4	0	100
6	1200	10	0.21	12.5	47500	8.2	4	0	100
7	1215	10	0.21	12.0	52500	8.1	4	0	100
8	1230	10	0.17	12.0	50000	8.2	4	0	100
9	1245	10	0.16	12.0	50000	8.2	4	0	100
10	1300	10	0.15	12.0	50000	8.2	4	0	100

Barn Pool was chosen as the location for the submersed experiments with the integrated system because of its sheltered location, depth of water and was within easy reach of the shore base. This meant that regular sea trials could continue throughout the winter thus enabling a profile of the area to be developed. However, the latter was to prove more difficult than first anticipated. The location of Barn Pool is at the entrance of the Hamoaze channel, into which the tidal reaches of the Tamar, Tavy and Lyhner rivers flow. Therefore, there is considerable turbulence in Barn Pool caused by the tidal flow in and out of the Hamoaze. This turbulence was on occasions so strong that the Tamaris dragged its anchor or was spun around on the anchor point. Table 5.23. shows the measured TON concentration ranges for the study area for the period 20.02.95 to 12.04.95.

Table 5.23. **Measured TON concentration ranges in Barn Pool for the period 20.02.95 to 23.04.95**

Submersed deployment	Date	TON Range
		mg l^{-1}
5	20.02.95	0.37 - 0.67
6	02.03.95	0.48 - 0.55
7	07.03.95	0.32 - 0.68
8	16.03.95	0.23 - 0.37
9	23.03.95	0.16 - 0.25
10	30.03.95	0.13 - 0.29
11	06.04.95	0.23 - 0.32
12	12.04.95	0.15 - 0.21

A gradual decrease in concentration is shown which is probably due to the start of the spring bloom when there is an increased uptake of nutrients. To be absolutely certain of this

however, further studies would be required using the submersed sensor moored in the same position and depth. Figure 5.23. shows the positions of sewage outfalls in the Tamar and Plymouth region and shows the volume discharged based on population served, and whether the sewage is untreated, partially treated or fully treated [191,192].
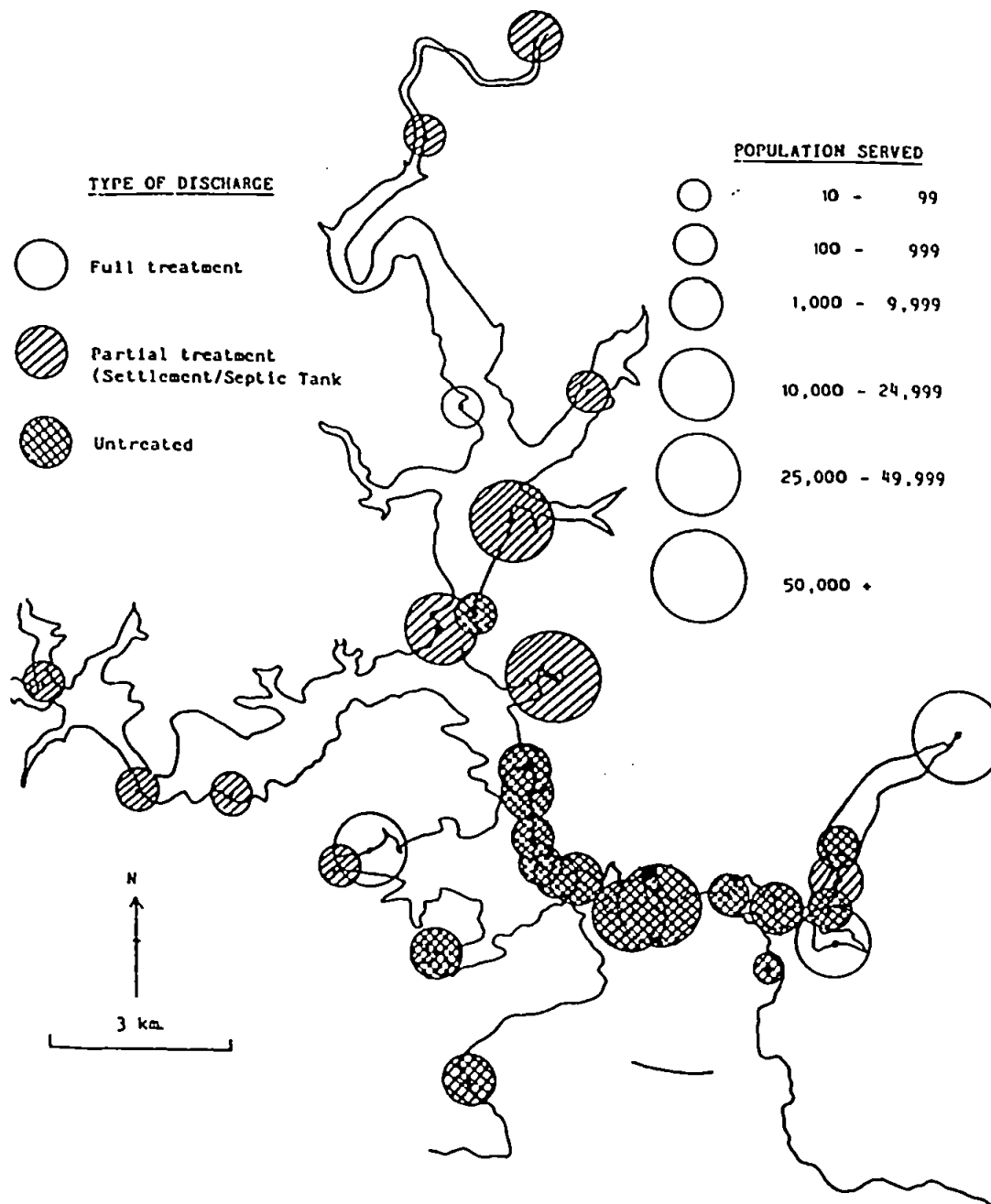
Figure 5.23.   Map showing sewage outfall positions, population served and type of discharge in the Plymouth coastal area [191, 192]

In addition to this, large river systems which flow through agricultural land drain into the area and will therefore contribute to the overall nutrient concentration. It can therefore be seen that depending on the seasonal agricultural activity, weather, tidal conditions and sewage outfall patterns, the whole area would be expected to have a complex nutrient pattern and a wide range of concentrations. This is where the submersible nutrient sensor or a number of strategically placed systems would enable the fate of nutrients to be determined in such an area , particularly when there are several popular beaches in the area.

Reproducibility: The calibration data for deployments 10, 11 and 12 were compared to determine the day to day reproducibility over the 14 day period in which the deployments were carried out. It can be seen from the results as shown in Table 5.24. that the rsd values are within the ± 5 % target specification.

Table 5.24. Comparison of calibration data for deployments 10, 11 and 12

Nitrate-N	10	11	12	Mean	rsd
mg l^{-1}	30.03.95	06.04.95	12.04.95		%
0	365	330	350	348	5.0
0.1	552	576	609	579	4.9
0.25	1107	948	1024	1026	7.8
0.50	1400	1326	1380	1369	2.8
0.75	1744	1578	1780	1701	6.3

Submersed deployment 13: After calibration, the integrated sensor was sent to 20 m depth and set to run. During the first sample injection, the ADC print-out on the PC was unusual so the system was retrieved immediately. Closer examination of the pressure housing found that the waste outlet heat-shrink tube connection had pulled off inside the

pressure housing allowing sea water to enter the system. The system was immediately switched off and flushed with fresh water. The instrument was later dismantled and thoroughly cleaned again with 5% detergent solution in de-ionised water and finally flushed with copious amounts of de-ionised water. When dry, the circuit boards were tested but it was found the *EPROM* containing the operational code had been damaged. No other damage to the boards and components was observed. The electronics had been conformally coated as described in chapter 3 for protection in the event of a flood such as this. This precaution had obviously worked except for where the conformal coating could not be applied on the removable *EPROM* holder. A new *EPROM* was obtained, re-programmed and fitted to the instrument which restored the operation of the system to normal. The system was repaired and ready for use within one month and was deployed from the 'Tamaris' on the 25.05.95. All heat-shrink connections were replaced with the custom made ABS plastic flange connectors as described in Chapter 3, section 3.1.1.

Submersed deployment 14: The system was first sent to 10 metres depth and set to run to test the operation and integrity of the pressure housing and tube connections. The first few injections were acceptable but the output from the Tamaris' generator became erratic which appeared to cause a similar effect on the portable PC and submersed instrument. This effect was attributed to a 'dirty' power supply sending transient power spikes down the RS232 lead of the PC to the instrument. Eventually the generator became completely unserviceable and the trial was aborted. The integrated system was started up in the laboratory later the same day using mains power for the portable PC. No similar problems were observed.

5.2.3. Communications

Tamar cellphone range tests: The results from the Tamar cellphone range tests, as shown in Table 5.25., showed that in all but one location there was network coverage. Additional transmitters were planned for installation in the area so it most likely that there is now better coverage.

Table 5.25.   Results from Tamar cellphone signal strength trials

Sample Station	Name	Position	Signal Strength 0 -5 (max.)
1	Drakes Island	50° 21.0' N. 4° 8.2' W	5
2	Skinham Point	50° 25.6' N. 4° 11.8' W	4
3	Weir Quay	50° 27.5' N. 4° 12.3' W	2
4	Tinnel	50° 27.3' N. 4° 13.6' W	1
5	Whitsam	50° 28.4' N. 4° 13.0' W	1
6	Museum	50° 29.8' N. 4° 13.1'W	0
7	Calstock	50° 29.7' N. 4° 12.4' W	1

Coastal cellphone range tests: The coastal range tests, as shown in Table 5.26., showed that there was network coverage to at least 15 miles line of sight which was the point at which the research vessel turned around. The signal strength had reduced to 60 % at this point so depending on weather conditions it is reasonable to expect 5 - 10 miles additional range. The range tests were carried out using a Class 4 handportable which limits power output to 0.6 Watts for personal safety. However, for a remotely deployed instrument a Class 2 system, similar to a fixed carphone, with a 3 watts power output would be used.

This would typically give 10 miles additional range and therefore, based on the UK cellphone coverage map [164], this would cover approximately 98 % of the UK's coastal waters.

Table 5.26.   Results from cellphone coastal range checks

Position (Fig. 5.8.)	Approximate distance from shore	Signal strength
	miles	0 - 5 (max.)
1	1	5
2	2	3
3	4	5
4	7	5
5	10	4
6	12	2
7	15	3

5.3.   CONCLUSIONS

When used as a bench instrument during the Tamar cruises, the custom built FI system was found to give good correlation with the validated FIAstar method. A paired t - Test carried out on the final cruise results showed that the null hypothesis had been retained and therefore shows that the two methods did not give significantly different results. The same was found for submersed deployment 9 where the FIAstar was used to analyse seawater samples taken at the same depth as the submersed nutrient sensor. Day to day variance over a 14 day period was found to be within the ± 5 % target specification.

Apart from deployments 2 and 13, as discussed in section 5.2., all submersed deployments were successful and the integrated system operated reliably and achieved the target depth of 30 metres. Deployment 13 did however prove that the precautions taken to protect the on-board computer worked, i.e. by the application of a conformal coating, by minimising the damage caused by sea water flooding the pressure housing. The integrated system did not suffer any corrosion or physical damage throughout the deployments and therefore achieved the target specification for a rugged and corrosion resistant construction. It was also easy to handle during deployment and retrieval.

Chapter Six
North Sea Cruise

6.   NORTH SEA CRUISE

The final objective of the research was to deploy the completed submersible nutrient sensor sub-surface for complete tidal cycles to obtain *in situ* nutrient data. This work was carried out off the North East coast and in the Humber Plume as part of the Land Ocean Interface Study (LOIS) cruise aboard the *RRS Challenger*. The cruise was split into three legs during 1995: Leg A, 1st - 12th June, Leg B, 13th - 29th June and the final leg, Leg C, 30th June - 13th July. The work described in this chapter was carried out during of Leg A of the cruise.

6.1.   EXPERIMENTAL

6.1.1.   Cruise details

The completed integrated system, reagents and standards and support equipment for the cruise was securely packed and loaded on the transport on the 30th May 1995 at PML, Plymouth. All equipment and scientific personnel joined the *Challenger* at Grimsby on the 31st May, as shown in Fig. 6.1., and set sail on the 1st June at 0830 hrs.

Figure 6.1.   *RRS Challenger* **being loaded at Grimsby on 31st May 1995 prior to the LOIS cruise.**

The *RRS Challenger* is a 54.3 m research vessel with accommodation for up to 14 scientific staff, the full details for which are given in appendix A. For leg A of the cruise, continuous underway monitoring was undertaken along the Humber/Wash grid, as shown in Table 6.1. and Fig. 6.2., and the North East Coast Grids, Table.6.2. and Fig. 6.3. Sea water was pumped to the on-board instruments at a separate sampling point via the ships non-toxic supply which had its take-up point at 4 metres depth at the bow of the vessel. Continuous monitoring of the physical parameters, e.g. turbidity, salinity, and nutrient determinations using Continuous Flow Analysis (CFA) techniques were carried out by the ships scientific staff throughout the cruise. These instruments were directly linked to the ships scientific log which was interfaced with the navigational system so that accurate positions could be obtained for the locations sampled.

Table 6.1.   Map reference details for the Humber/Wash area grid stations

Station number	Latitude	Longitude
1	53°51.50'N	00°02'W
2	54°02.00'N	00°31'E
3	53°43.50'N	00°08'E
4	53°53.50'N	00°41'E
5	53°33.00'N	00°08'E
6	53°46.00'N	00°50'E
7	53°26.00'N	00°17'E
8	53°39.00'N	00°58'E
9	53°18.50'N	00°21'E
10	53°25.00'N	00°46'E
11	53°29.00'N	01°00'E
12	53°15.00'N	00°39'E
13	53°00.00'N	00°24'E
14	53°00.00'N	01°04'E
15	53°17.50'N	01°21'E
16	52°54.00'N	01°21'E
17	52°43.00'N	01°49'E
18	52°47.00'N	02°12'E
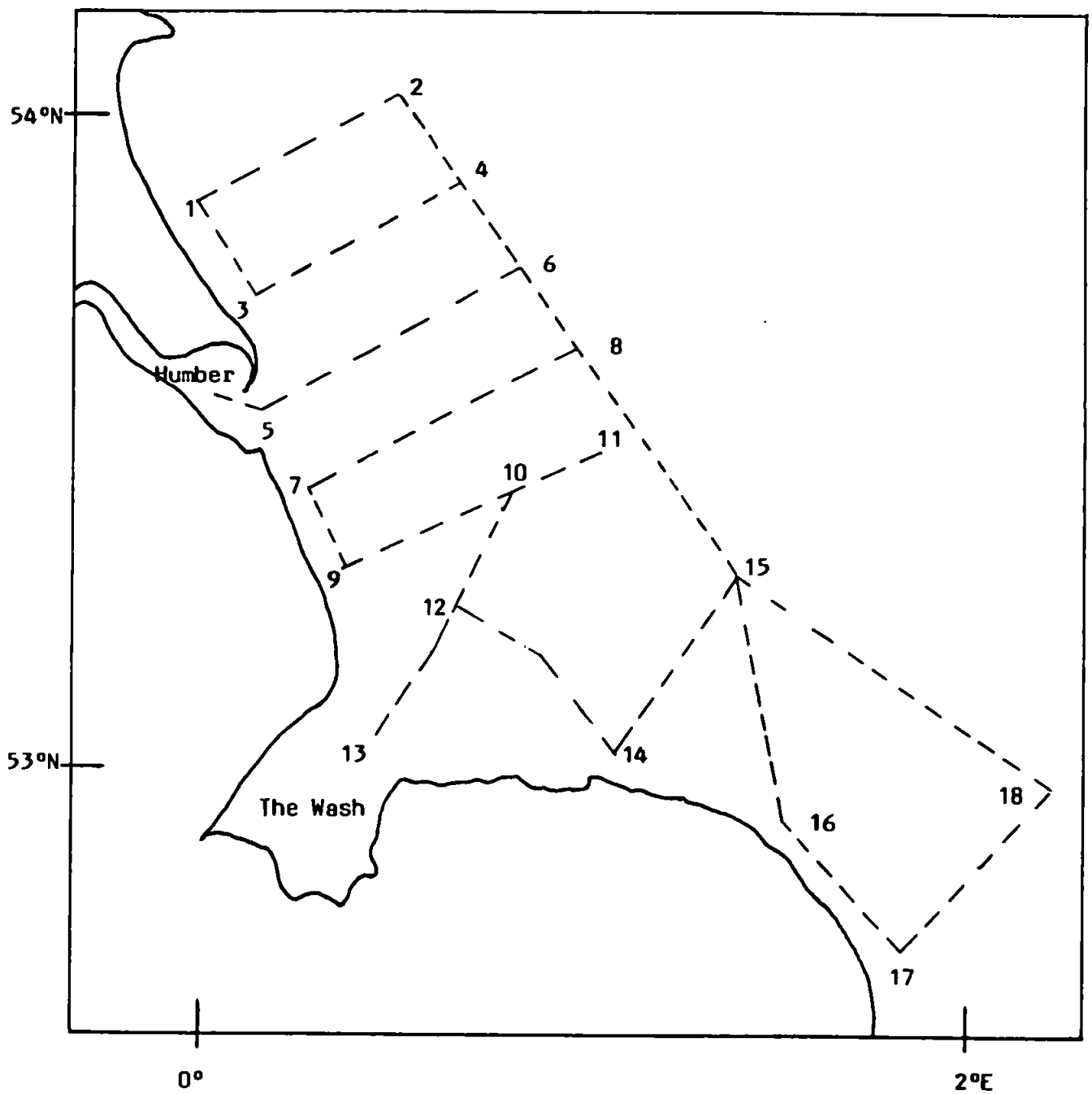
Figure. 6.2. Map showing the approximate positions of the Humber/Wash grid track stations

Part of the overall cruise objectives were to perform detailed surveys of the Humber mouth and its immediate coastal area, for the vertical profiling of physical variables which were to be used for the calculation of fluxes and boundary data for modelling. These particular studies were carried out over complete tidal cycles, i.e. for 13 hours from high tide to low tide, and at three anchor stations, the positions of which are shown in Table 6.3. and Fig. 6.4. It was during these times at anchor that the nutrient sensor was deployed.

205

Table. 6.2.   Map reference details of the Humber/Tweed coastal track stations

Station Number	Latitude	Longitude
1	53°45.00'N	00°24.40'E
2	53°51.80'N	00°04.00'E
3	54°02.20'N	00°18.40'E
4	54°03.00'N	00°03.00'W
5	54°07.50'N	00°14.00'E
6	54°11.50'N	00°13.00'W
7	54°23.00'N	00°03.00'W
8	54°23.20'N	00°27.00'W
9	54°38.50'N	00°13.00'W
10	54°33.50'N	00°45.00'W
11	54°48.00'N	00°36.00'W
12	54°38.50'N	01°02.00'W
13	54°52.50'N	00°50.50'W
14	54°41.40'N	01°08.50'W
15	54°57.00'N	00°55.00'W
16	54°56.00'N	01°19.00'W
17	55°05.00'N	01°03.00'W
18	55°00.80'N	01°22.00'W
19	55°12.50'N	01°01.50'W
20	55°12.50'N	01°27.00'W
21	55°20.50'N	01°03.50'W
22	55°23.50'N	01°30.00'W
23	55°29.50'N	01°04.00'W
24	55°34.00'N	01°33.00'W
25	55°45.00'N	01°15.00'W
26	55°47.50'N	01°56.00'W
27	55°55.00'N	01°35.00'W
28	51°55.00'N	02°05.00'W
29	56°00.00'N	02°17.00'W
30	56°00.00'N	01°36.00'W
31	55°42.00'N	01°03.05'W
32	54°53.50'N	00°45.00'W
33	54°45.00'N	00°18.00'W
34	54°31.50'N	00°02.50'E
35	54°00.00'N	00°23.00'E
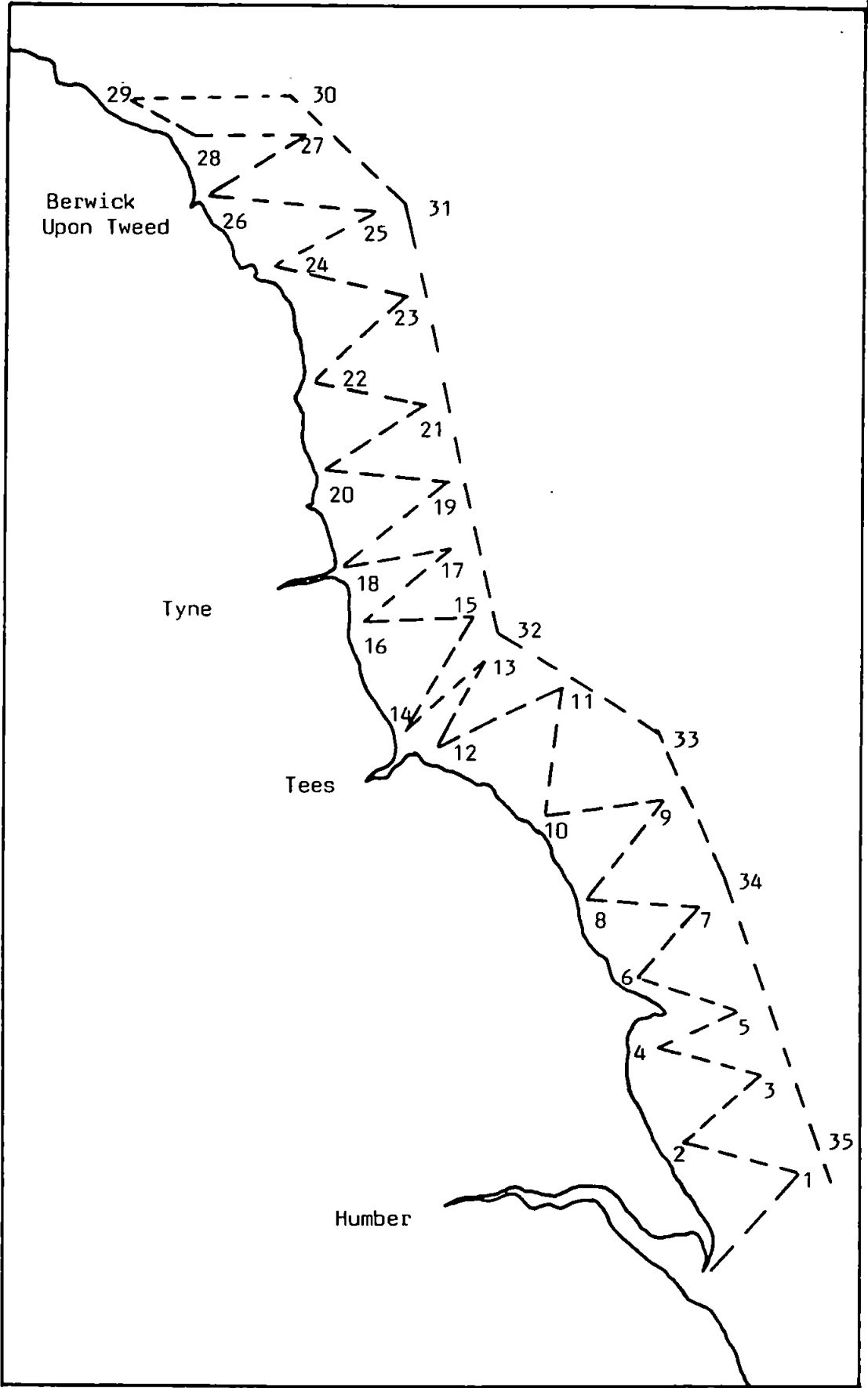
Figure 6.3. **Approximate positions of the Humber/Tweed coastal track stations**

Table 6.3. Map reference details for the positions of the anchor stations where the submersed nutrient sensor was deployed

Date	Anchor Station	Latitude	Longitude
03.06.95	13	53°35.19'N	00°13.09'E
04.06.95	24	53°32.06'N	00°15.29'E
07.06.95	10	53°36.57'N	00°11.39'E
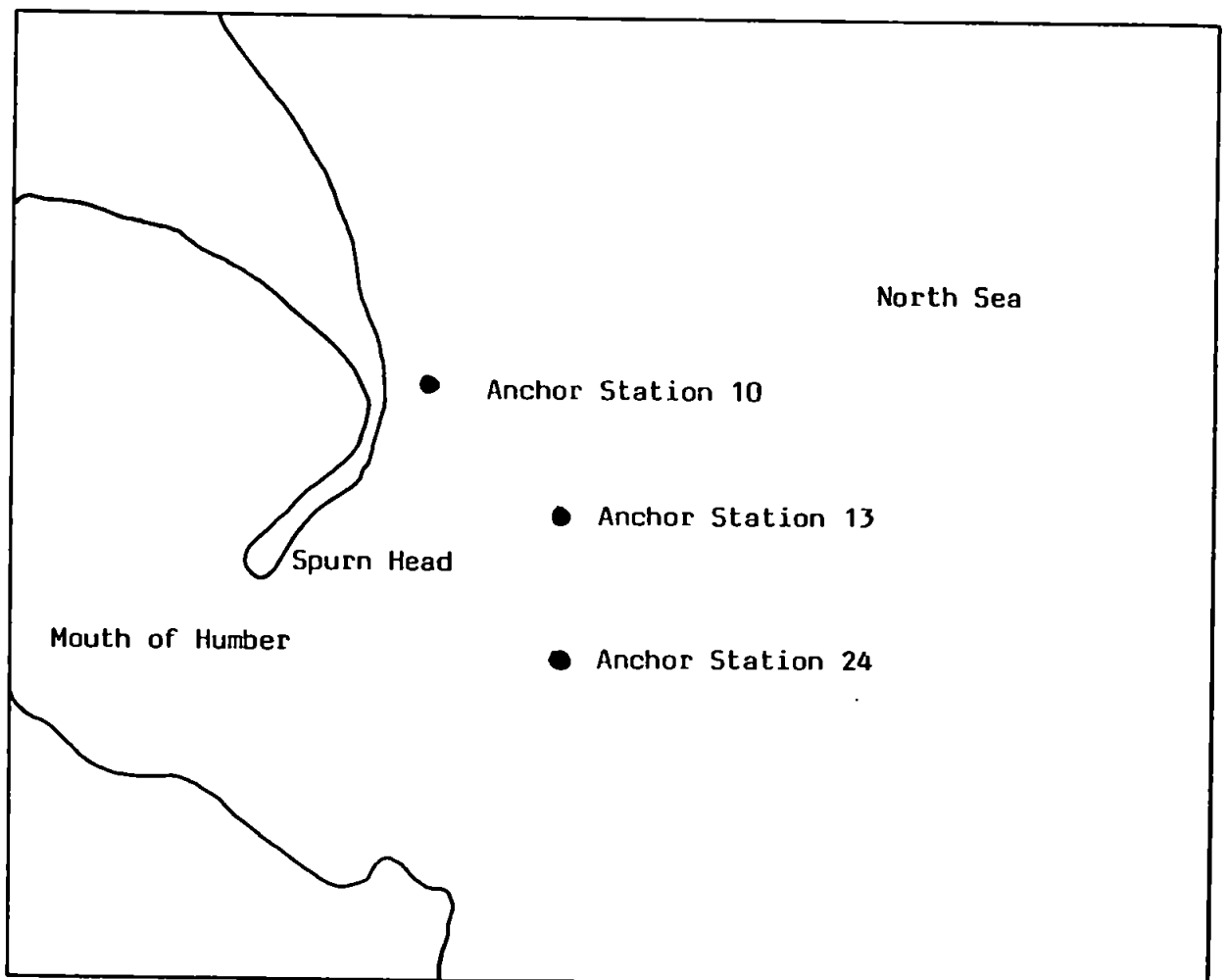
Figure 6.4. Map showing the approximate positions of the anchor stations where the submersed nutrient sensor was deployed

6.1.2.   Procedures

Reagents: All reagents and standards were prepared at the UOP the day before travelling to join the Challenger at Grimsby, i.e. 30th May 1995. All solutions were prepared from ultra-pure water produced by a 'Milli-Q' system (Millipore Corporation), and all reagents were AnalaR® (BDH) unless otherwise stated. The carrier solution was prepared by dissolving 10.0 g of ammonium chloride in 1 l of water. The N-(1-naphthyl)ethylenediamine dihydrochloride (N1NED, Sigma Chemicals) and sulphanilamide reagents were prepared by dissolving 0.5 and 25.0 g respectively in 1 l of water containing 10 % ($^v/_v$) orthophosphoric acid. The mixed colour reagent was subsequently prepared by mixing equal volumes of the N1NED and sulphanilamide reagents in a brown glass bottle. A stock 100 mg l^{-1} Nitrate-N solution was prepared by dissolving 0.7220 g of potassium nitrate in 1 l of water. Working standards were prepared by serial dilution of the stock solutions with water.

Manifold configuration: The FI manifold as shown in Fig. 6.1., was set up with a 260 µl sample loop, a screw connection packed reduction column and a 20 mm flowcell.

Filtration: Based on the Tamar cruise experiences as discussed in Chapter 5, the 5.0 µm syringe filters provided adequate protection to the system without impairing flow properties of the FI system. However, due to the high suspended solids loading which was observed at the outlet of the non-toxic supply, additional pre-filtration was considered necessary. A cartridge type depth-media pre-filter was then constructed using a 10 ml syringe body. Due to the non-availability of glass wool for the filter media, a suitable alternative had to be improvised. This was achieved by using some packaging cord and stripping out the sisal fibres. These were tightly packed into the syringe body as shown in Fig. 6.6. and flushed through with 'Milli-Q' water. A new 5.0 µm syringe filter was used for each submersed deployment.
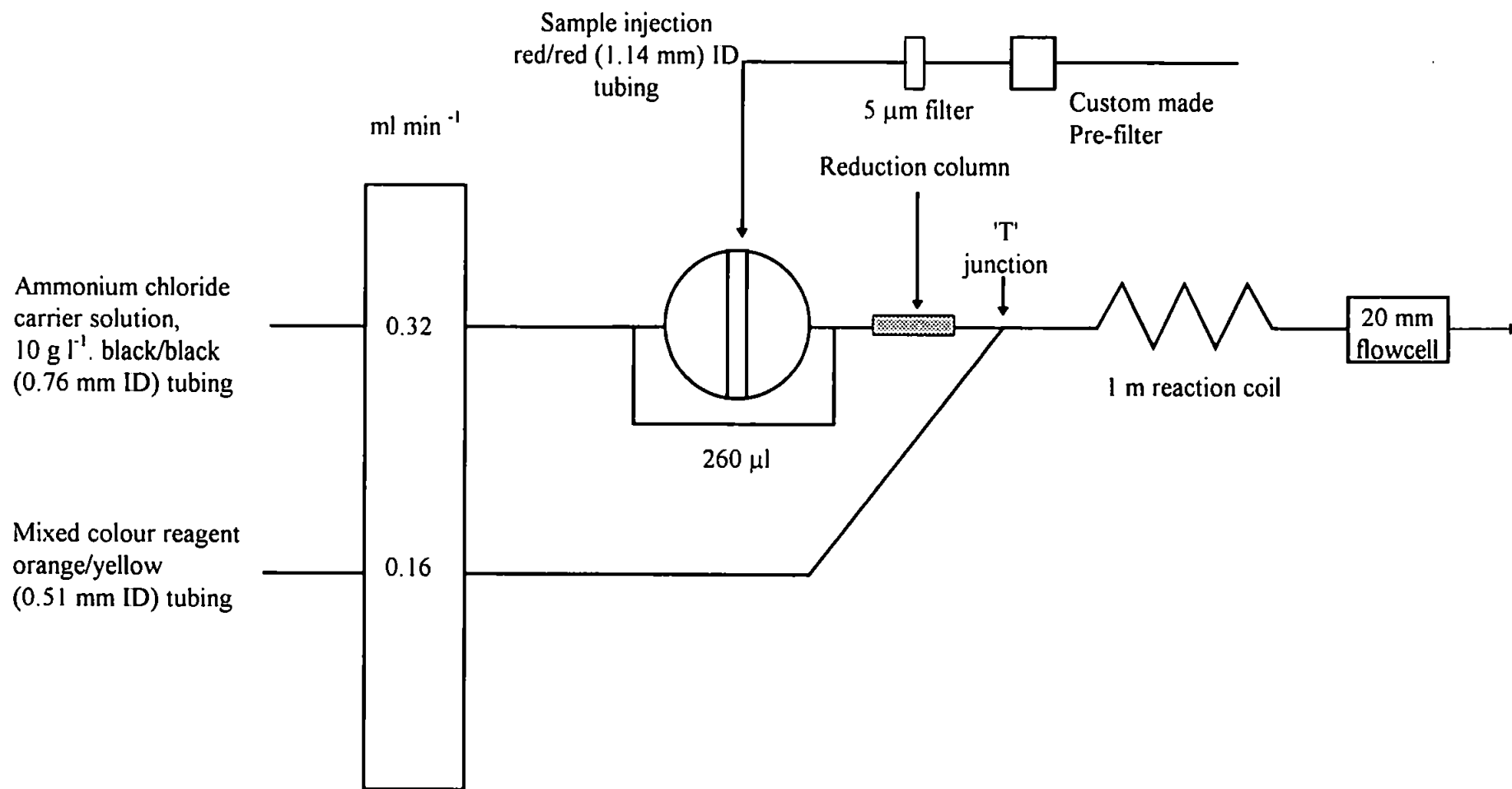
Figure 6.5. Schematic diagram showing the FI instrument manifold configuration used for nitrate determinations during the North Sea cruise

Sample out ←——— Sample in

Syringe body containing
packed fibres

5.0 μm Syringe filter
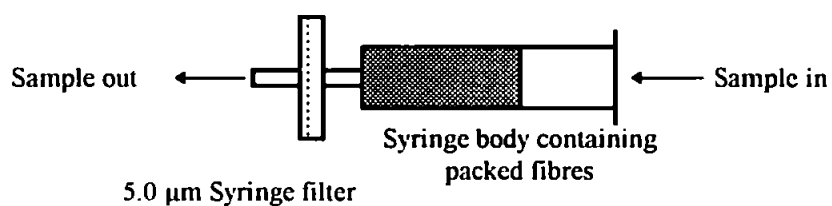
Figure 6.6.   Filtration system used on the submersed nutrient sensor during the North sea cruise

System settings: To determine the correct sample loop size, the FI instrument was set-up for bench running and was initially configured with a 20 mm flowcell with the LED set at 50 % intensity and a 150 μl sample loop. A sample of sea water from the ship's non-toxic supply was analysed whilst steaming between grid points 17 and 18 on the Humber/Wash study area. There was negligible response from the system which suggested low levels of nutrients so a 260 μl sample loop (as used for the Plymouth Barn Pool area) was fitted and the test repeated. A good response from the detector was observed so this configuration was retained for the duration of the cruise. The nutrient sensor was configured to run on internal batteries and have direct serial communications with a portable PC via the custom built umbilical cable. This enabled real-time study of the systems performance and respond immediately should there be a problem. To prevent sample memory effects, the instrument was set to allow a 90 second sample flush-through of the sample loop prior to injection. A 70 second delay was set between injection and data capture. To conserve reagents and power, the system was also set to shut down between samples.

Submersed deployments: When on station, the nutrient sensor was assembled, calibrated and deployed at 4 metres depth which was the same depth as the non-toxic supply which fed the on-board continuous flow AutoAnalyzer to allow comparisons of the two

instruments. Additional salinity and turbidity data from the ships log was also collected for each anchor station.

6.2. RESULTS AND DISCUSSION

6.2.1. Bench set-up

The results from the initial bench calibration used to check the system operation after the transport are shown in Table 6.4. and Fig. 6.7.

Table 6.4. Results from the initial calibration run used to check system operation after transport

Nitrate-N	Peak height
mg l $^{-1}$	ADC Range
0.00	230
0.10	600
0.25	1070
0.50	1701
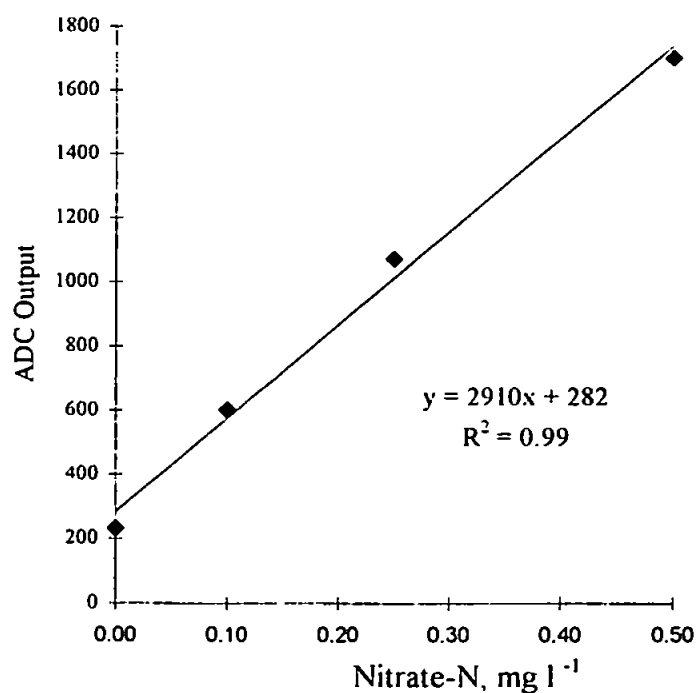
Figure 6.7. Calibration graph for initial bench calibration after transportation

212

The sample of sea water taken from the ship's non-toxic supply and analysed when at station number 8 on the Humber/Wash grid gave a value of 0.005 mg l $^{-1}$. The results from this system bench test showed that the instrument was capable of being transported considerable distances without any detrimental effect on the analytical performance.

Filtration: The custom made pre-filter was tested using a 1 litre sample from the non-toxic supply and was found to retain all large suspended particulate material so the same item was used for the duration of the cruise. New membrane filters were fitted for each deployment and retained for examination. The pre-filter was also retained for examination. The membranes were removed from the plastic housings and examined using a microscope set at 30X magnification. In all cases, the 5.0 μm membrane filters were not heavily loaded and had retained particulate material in the size range of 5 - 25 μm. The pre-filter used for the duration of the cruise had retained particulate material in the size range of 10 - 250 μm. Further investigation found that the majority of the particulates were a hard, sand-like material and therefore would have caused serious damage or a blockage if allowed into the FI manifold.

Data collection: The data from the ship's AutoAnalyzer chart recorder was reported to be unreliable so the raw data sent directly to the ship's log was collected daily for each anchor station. This data was subsequently processed using spreadsheet software as it was reported by the ship's scientific officer that by the time the data was processed there may be an error factor of ± 10 %. This was not considered acceptable for true comparison purposes so the data sets were processed independently on a daily basis. The salinity and turbidity data sets for each anchor station were also obtained from the ships log on the day of the deployment.

6.2.2.   Submersed deployments

Anchor station 13 (03.06.95) : After calibration, the integrated system was deployed at a depth of 4 metres at 0855 hours BST. After sampling every 10 - 15 minutes during the tidal cycle, the system was retrieved at 1900 hours. The results from the calibration are shown in Table 6.5. and Fig. 6.8.

Table 6.5.   Anchor station 13: calibration data for submersible nutrient sensor

Nitrate-N	Peak height
mg l $^{-1}$	ADC output
0.00	250
0.10	618
0.25	1008
0.50	1776

$$y = 3001x + 275$$
$$R^2 = 0.99$$

Nitrate-N, mg l $^{-1}$
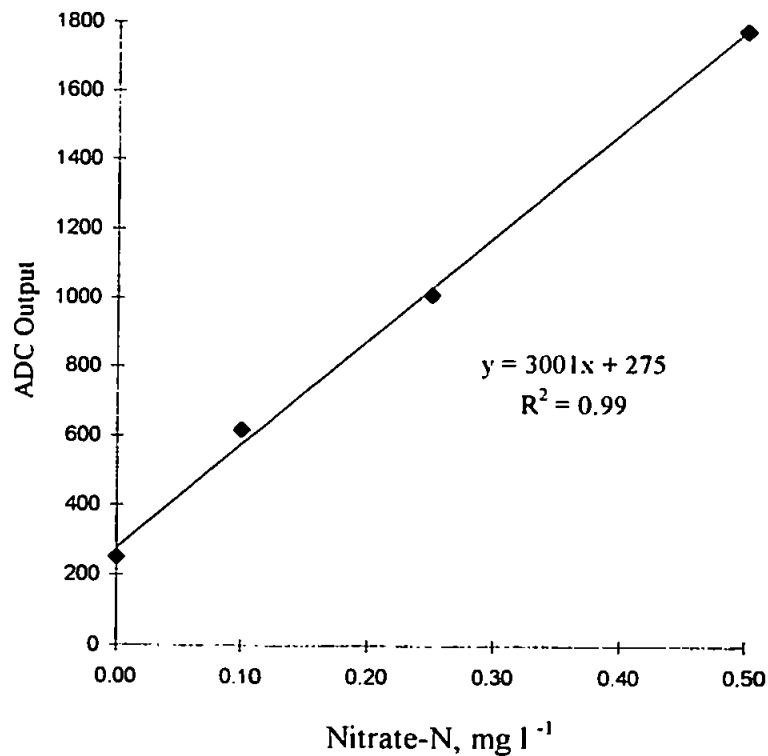
Figure 6.8.   Anchor station 13: calibration graph for submersible nutrient sensor

The nutrient sensor operated without any problems during the deployment. No leaks or mechanical wear were observed when the system was retrieved. Reagent consumption was in the order of 250 ml carrier solution and 150 ml of mixed colour reagent for the 56 samples analysed during the deployment, i.e. approximately 4.5 ml of carrier solution and 2.8 ml of colour reagent per sample. Therefore, extended deployments, e.g. 30 days at the same sampling rate would require in the order of 20 litres of carrier solution and 12 litres of colour reagent. Larger reagent bags are commercially available, e.g. 'Nalgene Flexboy', and are offered in 5, 10 and 20 litre sizes [193]. Based on the carrier solution consumption and the stability of the reagents [107], these would therefore provide sampling capacities over a 30 day period in the order of 1000, 2000 and 4000 samples respectively.

The AutoAnalyzer Nitrate-N, turbidity and salinity data sets for the tidal cycle were obtained from the ships scientific log and these are shown with the data from the submersed nutrient sensor in Table 6.6. The smoothed data from the submersed nutrient sensor is shown in Fig. 6.9. and clearly shows an increase in Nitrate-N concentration as the tide recedes. The results from the submersed nutrient sensor and the AutoAnalyser are shown together in Fig. 6.10. There was good correlation between the methods until the point at which the AutoAnalyzer went out of its calibration range of 0 - 0.28 mg l^{-1} (0 - 20 µM) Nitrate-N. The submersed sensor was calibrated for the range of 0 - 0.5 mg l^{-1} (0 - 35 µM) Nitrate-N and was therefore in range for all data points apart from the one at 1820 hrs. If the system was to be used for true environmental monitoring and to obtain absolute Nitrate-N values then the calibration protocol and precautions described in Chapter 4 must be observed. To examine the relationship between salinity, turbidity and nitrate levels for the deployment, the data sets for salinity, turbidity and the submersed nutrient sensor were plotted on the same graph as shown in Fig. 6.11. Where the salinity decreases as the tide recedes, the freshwater influence correspondingly increases turbidity and the nitrate level.

Table 6.6.   Anchor station 13: results from submersed nutrient sensor and AutoAnalyzer with turbidity and salinity data:

High tide 0930 hrs (BST)

Time	Nutrient Sensor	On-Board AutoAnalyzer	Turbidity	Salinity
hrs. (BST)	mg l^{-1}	mg l^{-1}	ppm	
08 55	0.050	-	2.0	33.8
09 00	0.050	-	-	33.8
09 30	0.055	-	3.0	33.8
09 45	0.050	-	1.0	33.8
10 00	0.050	-	-	33.8
10 15	0.045	-	3.0	33.9
10 30	0.040	0.011	-	34.1
10 45	0.043	0.011	3.0	34.1
11 00	0.060	0.011	-	34.1
11 15	0.060	0.000	3.0	34.1
11 45	0.035	0.000	6.0	34.1
12 00	0.045	0.000	-	34.0
12 15	0.065	0.021	12.0	33.7
12 30	0.090	0.102	-	33.7
12 45	0.140	0.120	14.0	33.6
12 55	0.155	0.154	-	33.5
13 05	0.180	0.160	-	33.5
13 15	0.195	0.190	19.0	33.4
13 25	0.225	0.210	-	33.3
13 35	0.230	0.220	20.0	33.3
13 45	0.250	0.230	-	33.3
13 55	0.270	0.260	-	33.3
14 05	0.270	0.260	-	33.2
14 15	0.275	0.270	24.0	33.3
14 25	0.270	0.290	-	33.2
14 35	0.275	0.290	-	33.2
14 45	0.285	0.300	29.0	33.1
14 55	0.295	0.340	-	33.1
15 05	0.315	0.350	-	33.0
15 15	0.320	0.360	31.0	32.9
15 25	0.330	0.400	-	32.9
15 35	0.335	0.410	-	32.8
15 45	0.340	0.430	29.0	32.8
15 55	0.350	0.460	-	32.7
16 05	0.330	0.470	-	32.7
16 15	0.345	0.480	28.0	32.3
16 25	0.395	0.500	-	32.2
16 35	0.440	0.510	-	32.2
16 45	0.445	0.640	34.0	32.1
16 55	0.415	0.660	-	31.9
17 05	0.430	0.670	-	31.9
17 20	0.475	0.760	40.0	31.7
17 35	0.460	0.790	-	32.2
17 50	0.420	0.360	27.0	32.4
18 20	0.465	0.100	24.0	32.6
18 35	0.585	0.560	17.0	32.9
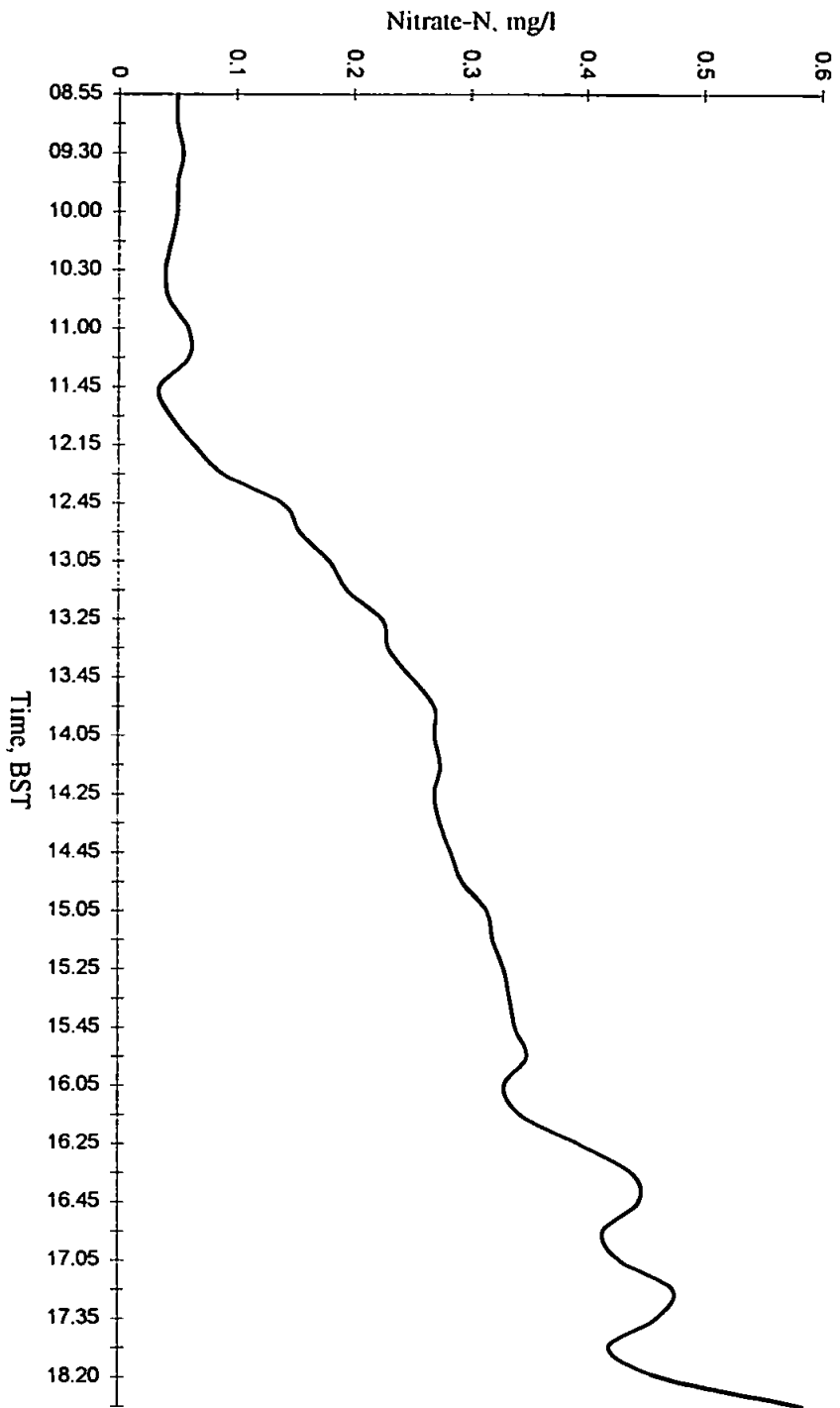
Figure 6.9.   Anchor station 13: smoothed data plot from submersed nutrient sensor results

217
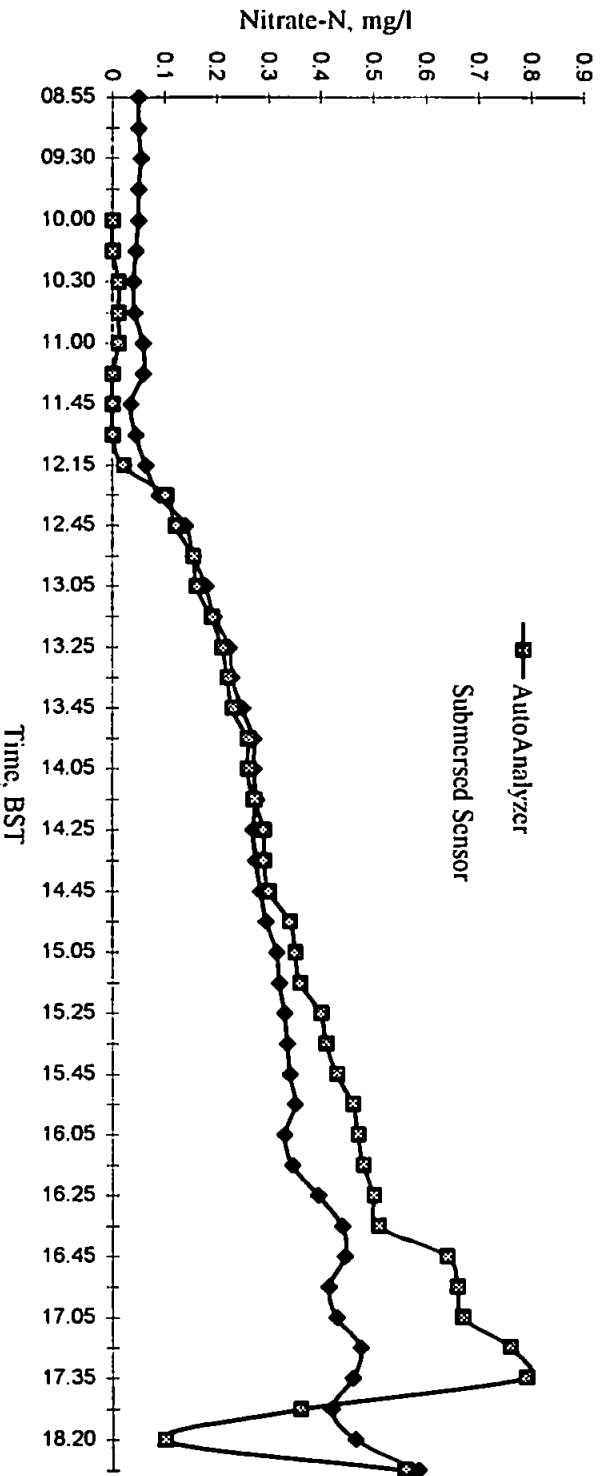
Figure 6.10. Anchor station 13: graph showing results from the submersed nutrient sensor and the AutoAnalyzer

Figure 6.11.   Anchor station 13: graph showing submersed nutrient sensor results with salinity and turbidity data

Anchor station 24 (04.06.95) : Immediately prior to deployment, the nutrient sensor

was calibrated using a series of nitrate standards and the results are shown in Table 6.7. and

Fig. 6. 12.

Table 6.7.   **Anchor station 24: calibration data for submersed nutrient sensor**

Nitrate-N	Peak height
mg l $^{-1}$	ADC output
0.00	250
0.10	590
0.25	947
0.50	1547

$$y = 2543x + 293$$
$$R^2 = 0.99$$
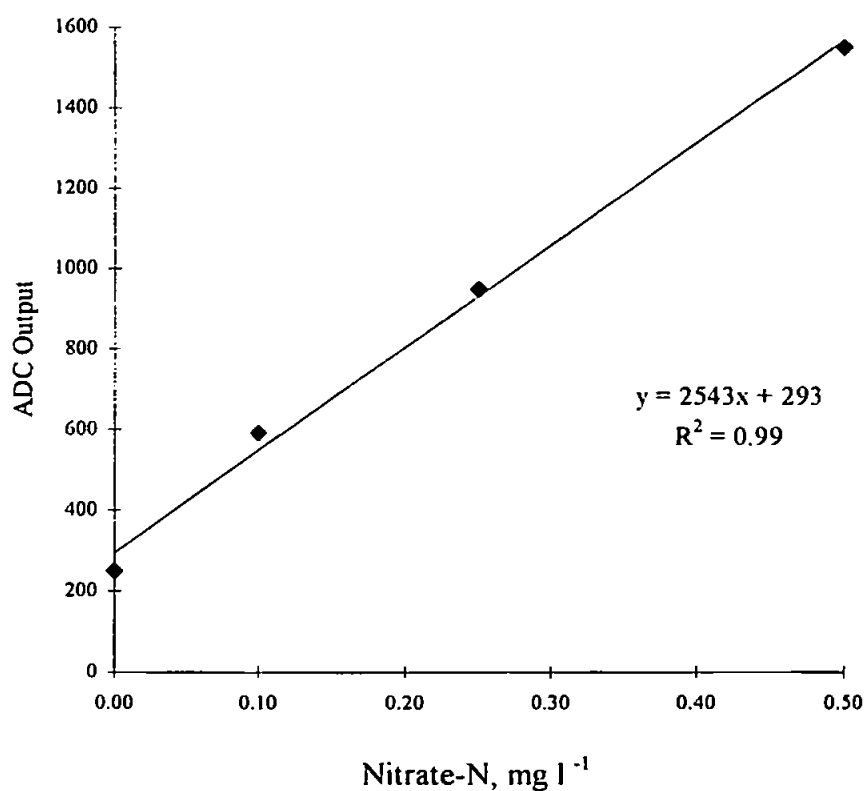
Figure 6.12.   Anchor station 24: calibration graph for submersed nutrient sensor

220

The reagent bags were re-filled and a new 5.0 μm syringe filter was fitted before the nutrient sensor was deployed at a depth of 4 metres at 0820 hours (BST). For the first 3 hours the system was working satisfactorily until the detector response became erratic. The system was shut down remotely and re-started but the fault did not clear. The LED test programme was then run, as described in Chapter 4, but there was still no response from the detector. The system was retrieved and the fault was traced to a faulty connector in the detector circuit. This was replaced and the nutrient sensor was re-deployed at 1355 hours (BST). The system worked satisfactorily thereafter until finally retrieved at 2015 hours. The various data sets were collated as before and are shown in Table 6.8. A thorough examination of the system found no evidence of leaks or deterioration of the pump tubes or pre-filter. Reagent consumption was slightly less than that of the previous deployment which was due to the system being retrieved for repair. Apart from the loss of approximately 2 hours data due to the faulty connector, the nutrient sensor performed well and the data obtained from it is shown in Fig. 6.13. The ships AutoAnalyzer also suffered a breakdown at this anchor station so the comparison between the two systems was limited to approximately 5 hours of data. However, there was good correlation between the methods and they produced similar responses to the changes in Nitrate-N concentration as shown in Fig. 6.14. The AutoAnalyzer was out of its 0 - 0.28 mg l^{-1} Nitrate-N range for most of the deployment; the submersed nutrient sensor was in range throughout the deployment. The combined plot of the submersed nutrient sensor results with the salinity and turbidity data, Fig. 6.15., shows that the submersed nutrient sensor gave a maximum nutrient concentration at minimum salinity, i.e. at the point of maximum freshwater influence.

Table 6.8. Anchor station 24: results from submersed nutrient sensor and

AutoAnalyzer with turbidity and salinity data:

High tide 1000 hrs (BST)

Time	Nutrient Sensor	On-Board AutoAnalyzer	Turbidity	Salinity
hrs. (BST)	mg l^{-1}	mg l^{-1}	ppm	
08 20	0.145	-	13.0	33.6
08 35	0.280	-	13.0	33.7
08 50	0.180	-	-	33.7
09 05	0.215	-	-	33.8
09 20	0.220	-	13.0	33.8
09 35	0.200	-	-	33.7
09 50	0.300	-	15.0	33.5
10 05	0.275	-	-	33.4
10 20	0.270	-	15.0	33.4
10 35	0.240	-	-	33.4
10 50	0.185	-	12.0	33.4
11 05	0.195	0.130	-	33.4
11 20	0.220	0.123	9.0	33.5
11 35	-	-	-	33.5
11 45	-	0.126	-	33.5
12 00	-	0.172	12.0	33.3
12 15	-	0.220	14.0	33.2
12 30	-	0.228	-	33.2
12 45	-	0.235	14.0	33.2
13 00	-	0.238	-	33.1
13 15	-	0.249	9.0	33.0
13 30	-	0.235	-	33.0
13 45	-	0.210	-	33.0
14 00	0.210	0.220	11.0	33.0
14 15	0.240	0.193	-	33.0
14 30	0.270	0.220	14.0	32.9
14 45	0.305	0.252	16.0	32.9
15 00	0.315	0.301	-	32.9
15 15	0.330	0.295	21.0	32.9
15 30	0.365	0.295	-	32.9
15 45	0.390	0.364	21.0	32.9
16 00	0.385	0.375	-	32.9
16 15	0.392	-	19.0	32.9
16 30	0.392	-	-	33.0
16 45	0.385	-	-	32.5
17 00	0.390	0.336	14.0	32.5
17 15	0.360	0.357	7.0	32.7
17 30	0.360	0.357	-	32.9
17 45	0.380	0.277	7.0	32.9
18 00	0.380	0.340	7.0	33.1
18 30	0.350	0.336	-	33.5
18 45	0.345	0.329	11.0	33.5
19 00	0.375	0.322	-	33.5
19 15	0.413	0.322	12.0	33.7
19 30	0.395	0.319	12.0	33.9
19 45	0.370	0.319	-	34.0
20 00	0.325	0.310	-	34.0
20 15	0.245	0.390	-	-

Figure 6.13. Anchor station 24: smoothed data plot from submersed nutrient sensor results

Figure 6.14. Anchor station 24: graph showing results from the submersible nutrient sensor and the AutoAnalyzer
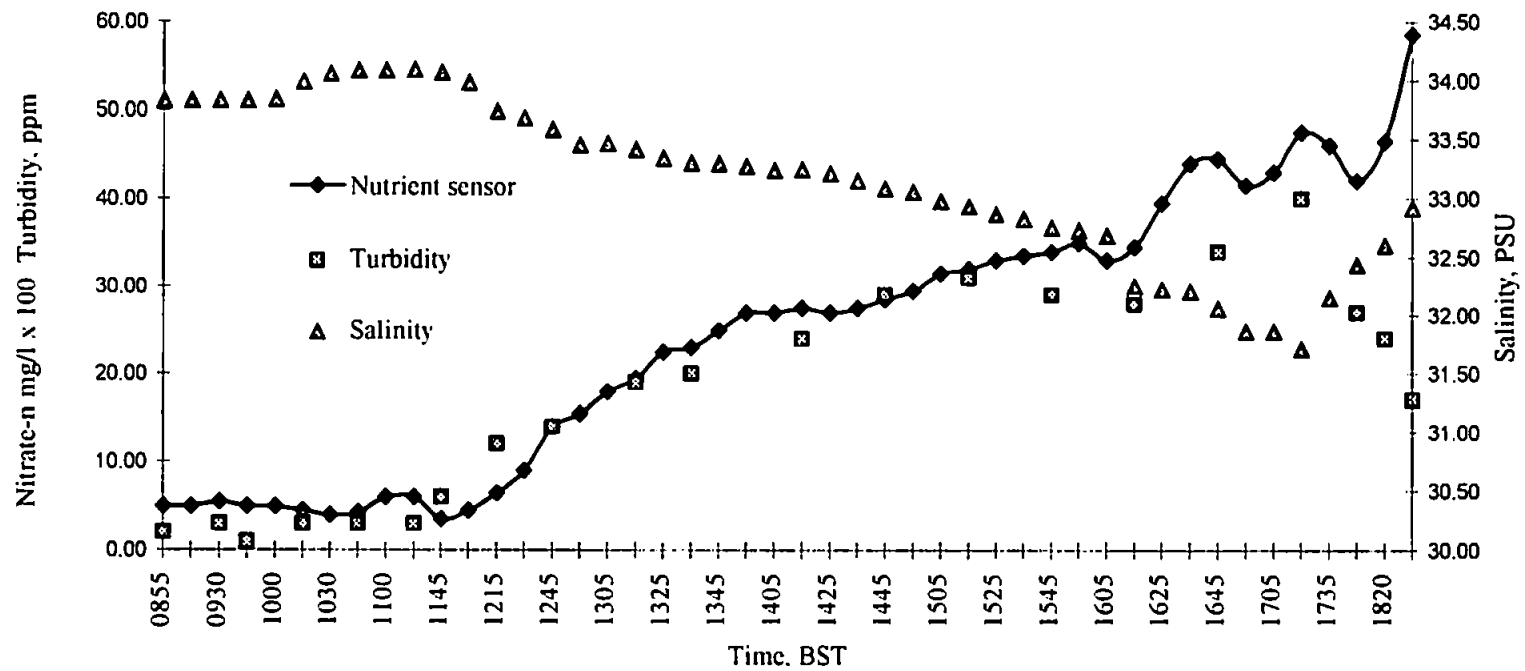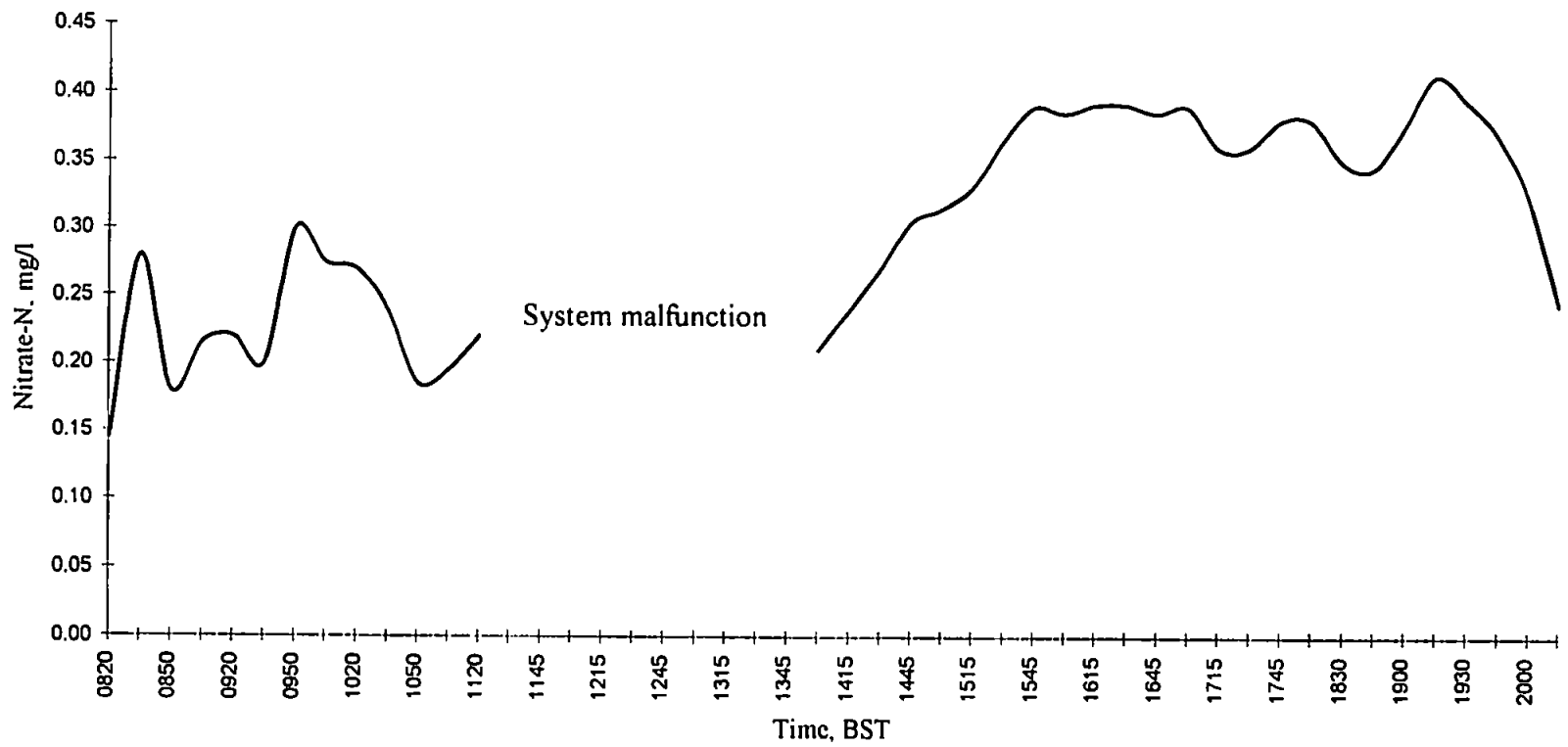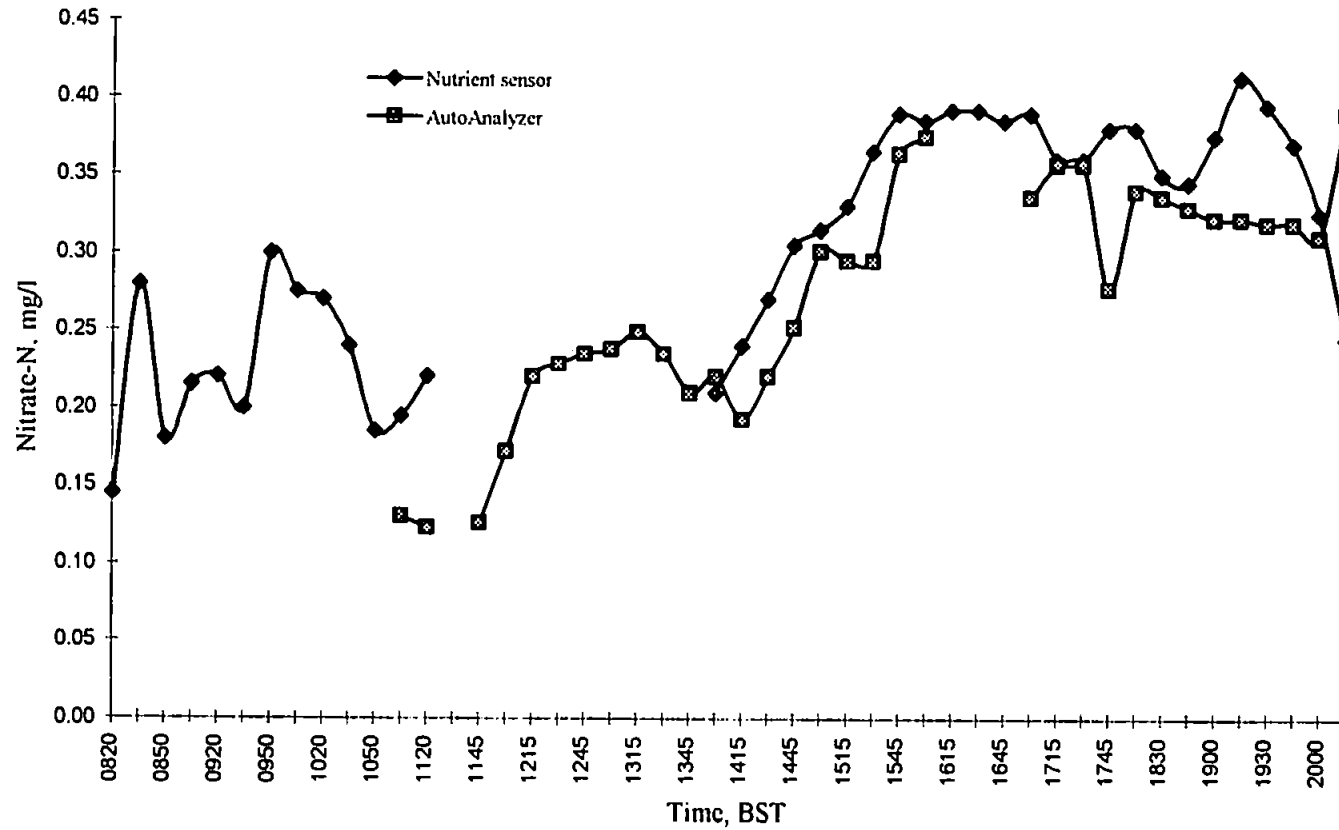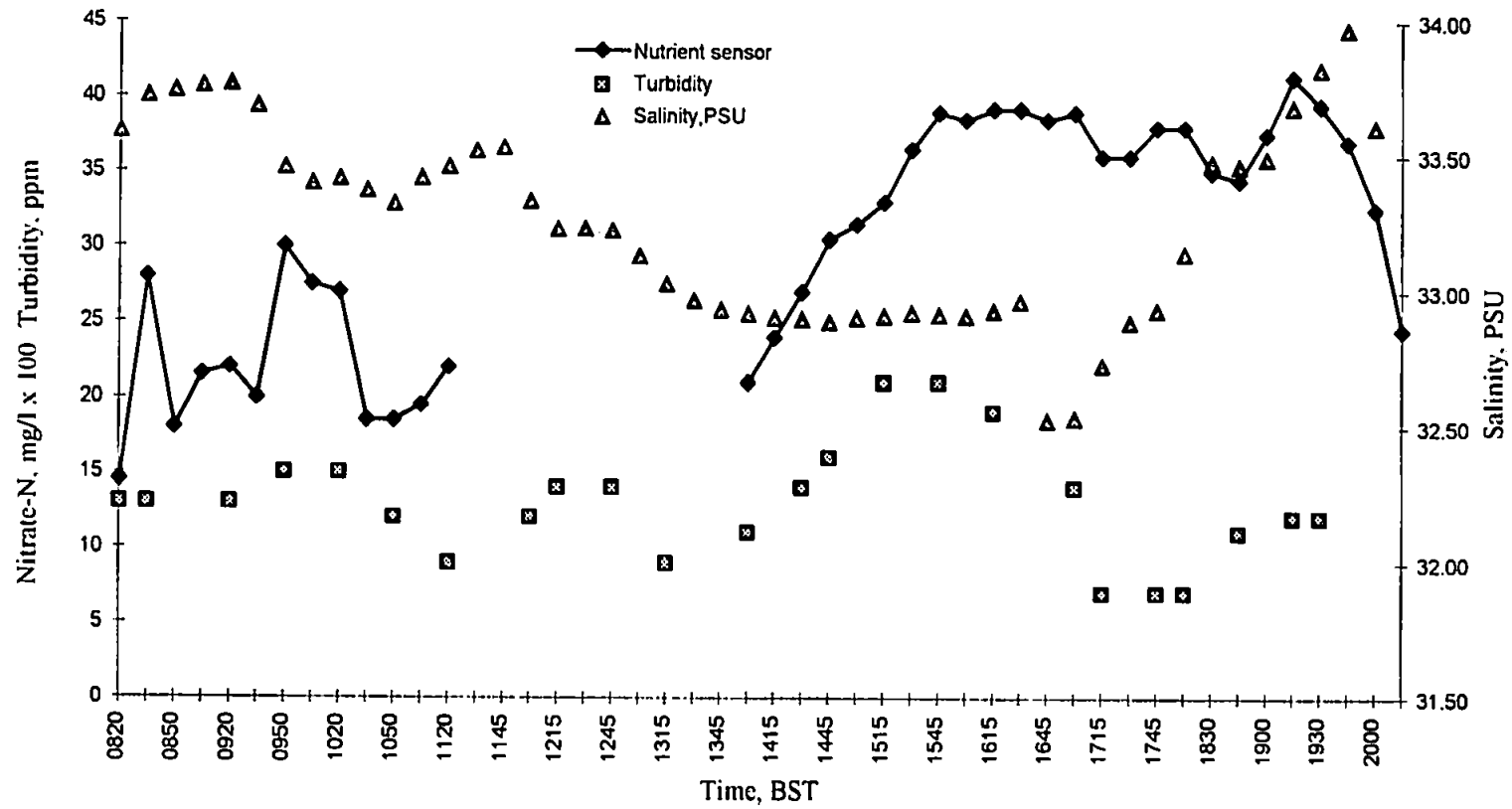
Figure 6.15. Anchor station 24: graph showing submersed nutrient sensor results with salinity and turbidity data

Anchor station 10 (07.06.95) : The reagent bags were refilled as before and a new 5.0 μm syringe filter was fitted. The first calibration run of the nutrient sensor produced a high baseline which was initially thought to be a collapsed reduction column. As a precautionary measure the column was replaced but the response from the instrument remained the same. The reagents for the cruise were prepared at UOP before joining Challenger. Two batches of carrier solution were prepared from two different sources of 'Milli-Q' water and the reagent bags for this particular deployment were refilled from the second batch of carrier solution. New carrier solution was prepared using the ships supply of 'Milli-Q' water and the problem was resolved. Post-cruise investigations discovered that a problem had developed with the water purification system that the second batch of carrier solution had been prepared from. The results from the final calibration prior to deployment are shown in Table 6.9. and Fig. 6.16. The results from the submersed nutrient sensor and the AutoAnalyzer are shown with the turbidity and salinity data for the deployment period in Table 6.10.

Both systems showed similar patterns, as shown in Fig. 6.18., in response to changes in the nitrate levels although the Autoanalyzer showed no significant response for the first 4 hours. During the same time period the submersed nutrient sensor was able to resolve differences in nitrate concentration over the 20 - 40 μg l $^{-1}$ range. Towards low tide when the freshwater influence was at a maximum and when nitrate levels were expected to be higher, both systems responded accordingly. The combined plot of submersed nutrient sensor results, salinity and turbidity data, as shown in Fig. 6.19., confirmed that the area of minimum salinity corresponded to maximum nitrate concentration, i.e. at the point of maximum freshwater influence.

Table 6.9.   Anchor station 10: calibration data

Nitrate-N	Peak height
mg l $^{-1}$	ADC count
0.00	245
0.10	565
0.25	1056
0.50	1489

$$y = 2481x + 311$$
$$R^2 = 0.97$$
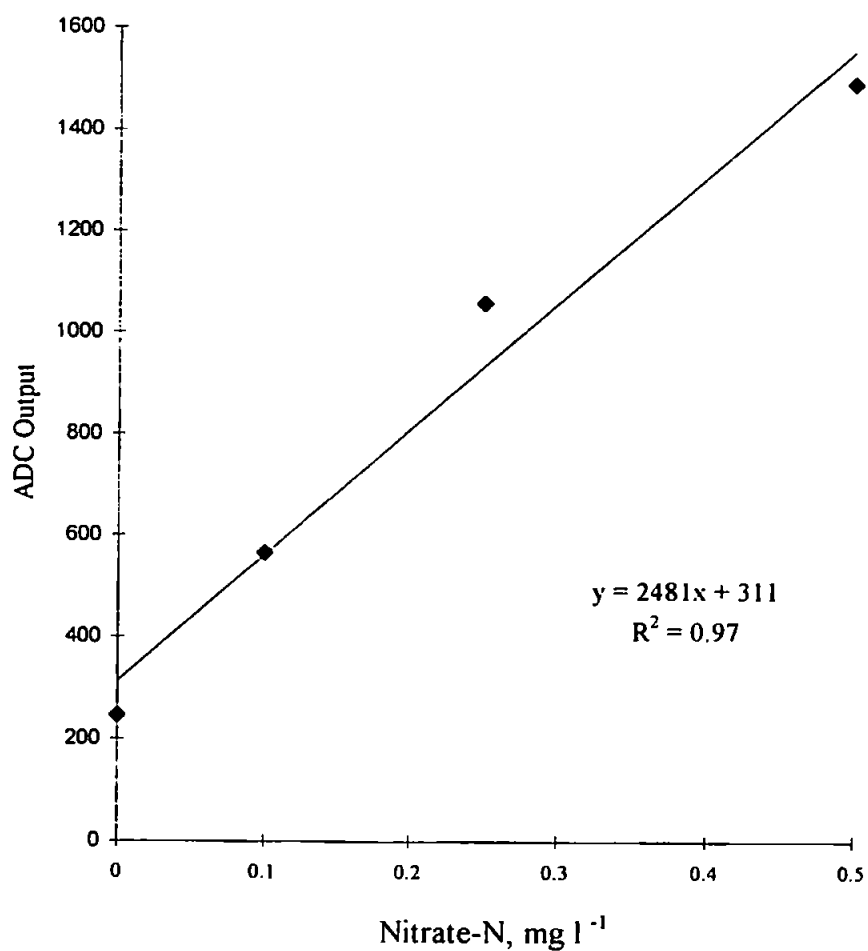
Figure 6.16.   Anchor station 10 calibration graph

Table 6.10.   Results from anchor station 10 deployment showing submersed

nutrient sensor, AutoAnalyzer, turbidity and salinity data:

High tide 1230 hrs (BST)

Time	Nutrient Sensor	On-Board AutoAnalyzer	Turbidity	Salinity
hrs. (BST)	mg l $^{-1}$	mg l $^{-1}$	ppm	
11 45	0.034	0.025	8.0	34.1
12 00	0.043	0.025	-	34.2
12 15	0.038	0.025	9.0	34.2
12 30	0.039	0.025	-	34.2
12 45	0.042	0.025	7.0	34.1
13 00	0.040	0.025	-	34.3
13 15	0.036	0.025	9.0	34.1
13 30	0.039	0.025	-	34.2
13 45	0.040	0.025	8.0	34.1
14 00	0.030	0.025	-	34.1
14 15	0.025	0.025	6.0	34.1
14 30	0.028	0.025	-	34.1
14 45	0.025	0.025	4.0	34.1
15 00	0.022	0.025	-	34.1
15 15	0.036	0.025	9.0	34.1
15 30	0.027	0.025	-	34.1
15 45	0.029	0.021	-	34.1
16 00	0.027	0.024	16.0	34.1
16 15	0.036	0.031	-	34.0
16 30	0.051	0.070	27.0	33.8
16 45	0.063	0.100	-	33.8
17 00	0.063	0.119	29.0	33.7
17 15	0.110	0.140	38.0	33.6
17 30	0.140	0.210	-	33.4
17 45	0.180	0.273	41.0	33.2
18 00	0.240	0.315	-	33.1
18 15	0.250	0.350	41.0	33.0
18 30	0.310	0.381	-	32.9
18 45	0.315	0.399	34.0	32.9
19 00	0.340	0.381	-	32.8
19 15	0.360	0.409	34.0	32.8
19 30	0.350	0.409	-	32.8
19 45	0.340	0.402	33.0	32.8
20 00	0.390	0.392	-	32.9
20 15	0.360	0.381	-	32.9
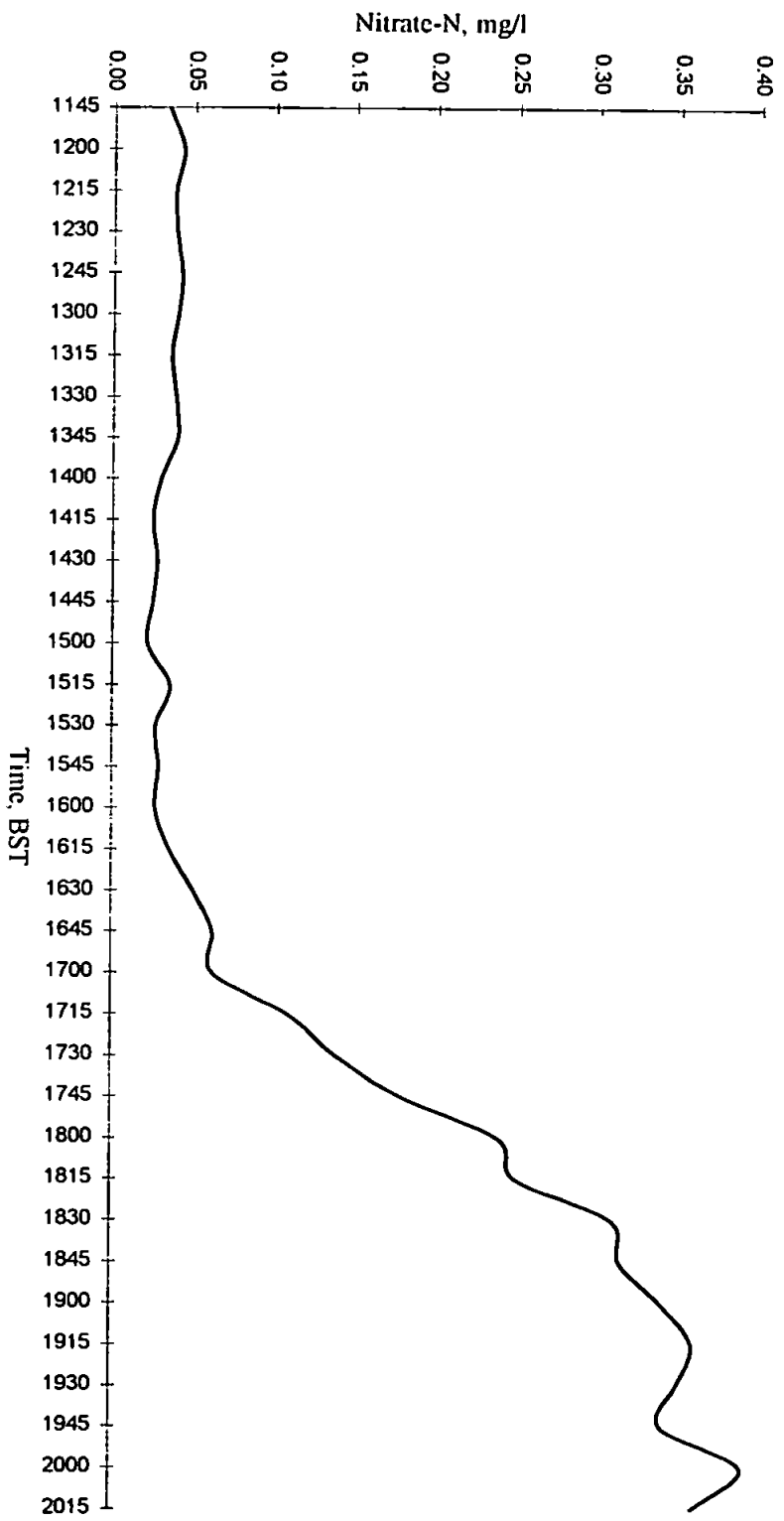
Figure 6.17. Anchor station 10: smoothed data plot from submersed nutrient sensor results
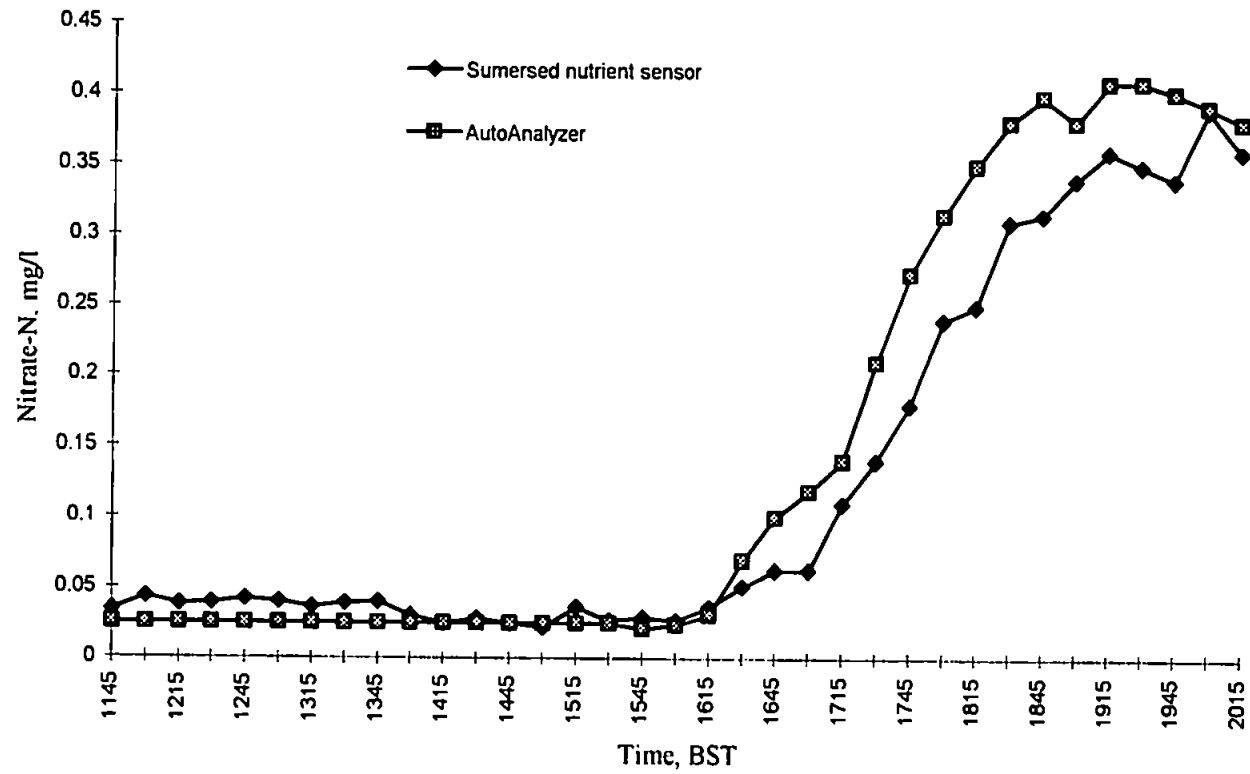
Figure 6.18. Anchor station 10: graph showing results from submersed nutrient sensor and AutoAnalyzer
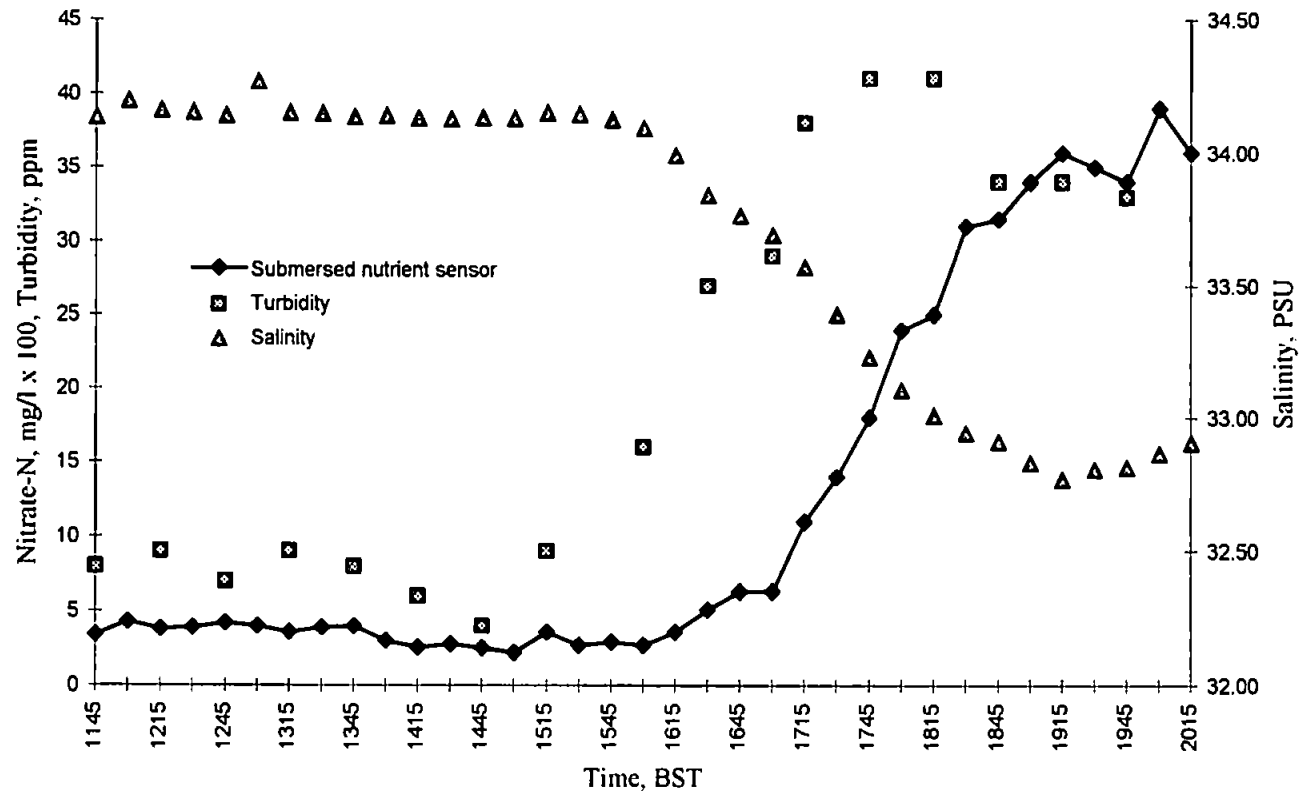
Figure 6.19. Anchor station 10: graph showing submersed nutrient sensor results with salinity and turbidity data

6.2.3.   Reproducibility

Day to day reproducibility for the entire cruise, as shown in Table 6.11., was within the

± 5 % target specification.

Table 6.11.   Comparison of calibration data for the integrated system during the North Sea cruise

Nitrate-N	Bench	Station 13	Station 24	Station 10	Mean	rsd
mg l $^{-1}$	02.06.95	03.06.95	04.06.95	07.06.95		%
0	230	250	250	245	244	3.9
0.1	600	618	590	565	593	3.7
0.25	1070	1008	947	1056	1020	5.5
0.50	1701	1776	1547	1489	1628	8.2

6.2.4.   Comparative performance

AutoAnalyzer manifold: Figure 6.20. shows the AutoAnalyzer manifold used for the determination of nitrate during the North Sea cruise. The manifold is more complicated than the FI manifold with eight streams pumped at faster flow rates. The sample stream was air-segmented prior to merging with the ammonium chloride (10 g l^{-1}) carrier stream and the bubbles were removed using a debubbler before entering the cadmium wire reduction coil. Air-segmentation was re-introduced into the sample stream before merging with the separate sulphanilamide and N1NED streams. The bubbles were finally removed by a second debubbler before entering the flowcell.

232
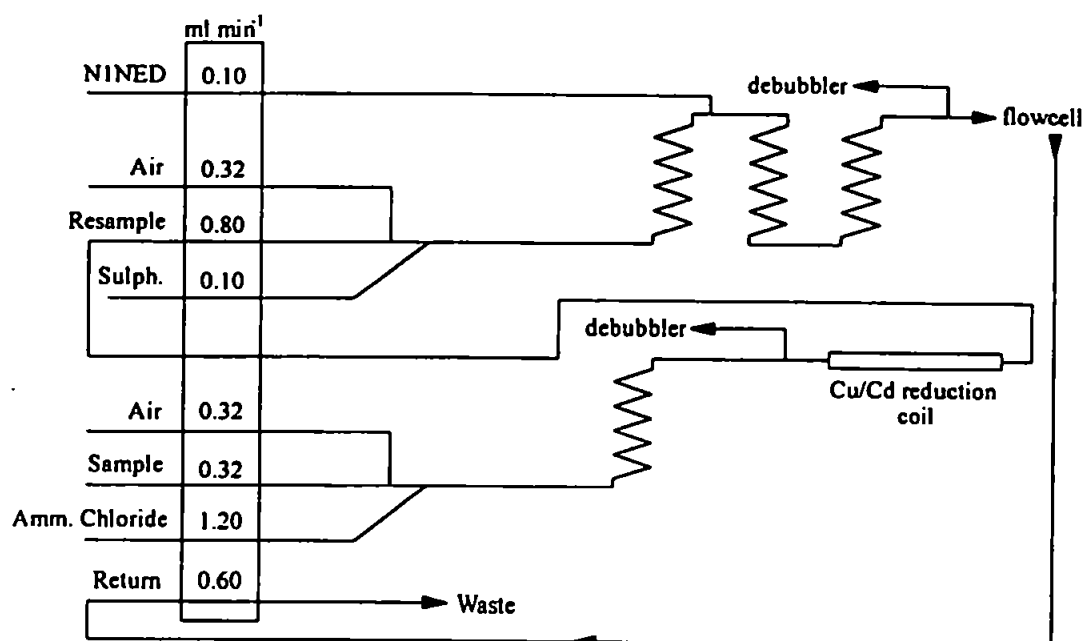
Figure 6.20. Schematic diagram of the AutoAnalyzer manifold used on the North Sea cruise

AutoAnalyzer vs FI operation: To obtain a continuous nitrate profile, a sea water sample was continuously taken from the ships non-toxic supply via a filter block [194]. Calibration required the system to be stopped, so in order to preserve the continuous profiling this was only carried out periodically. Therefore, any problems, e.g. due to drift, degradation of reagents or reduction column, would not be identified immediately. The FI method permits a continuous calibration protocol which would be equivalent to using on-board standards for the submersible instrument. Sampling every 10 - 15 minutes over the tidal cycles produced satisfactory nitrate profiles, as shown in Figs. 6.9., 6.13. and 6.17. Therefore, if a higher precision was required there would be many opportunities to perform an *in situ* calibration without affecting the continuous profiling. The submersed system was shut down between samples which conserved reagents, reduction column and power and reduced the filtration requirements, e.g. the submersed FI system typically used in the order of 250 ml of

carrier solution over a tidal cycle whereas the AutoAnalyzer used approximately 940 ml for the same period. Due to the high particulate loading found in the Humber plume region, (typically > 100 mg l^{-1}) [157], the filters of the filtration block in the non-toxic supply to the AutoAnalyzer were routinely changed every hour which could cause disruption of the flow to the AutoAnalyzer. The submersed systems on-board filtration system proved to be adequate throughout the deployments so there was no disruption in the profiling. The main drawback with air-segmented systems is the need for a reproducible bubble pattern which can be difficult to achieve when at sea in rough conditions. The air bubbles are compressible and therefore will create pulsations in the system and for most detector designs the bubbles have to be removed to avoid flow problems within the cell as discussed in Chapter 3, section 3.2.5. Therefore, the FI method gives the following distinct advantages over the air-segmented CFA method:

1.   Introduction of a reproducible sample volume by injection.

2.   Reproducible system operation.

3.   Less complicated manifold.

4.   Better control over flow of reagents.

5.   Lower reagent consumption.

6.   Simple on-line filtration requirements.

7.   Longer reduction column lifetime.

6.3.   CONCLUSIONS

The system was totally reliable throughout the cruise apart from one small breakdown resulting from a faulty bought-in connector. Most of the instrument down-time resulting from this fault was spent waiting for a qualified crane operator to become available for

retrieval and re-deployment of the system. The actual fault was traced, repaired and the system was ready for re-deployment within 1 hour. This illustrated how the design allowed easy fault diagnosis and repair which is essential for a field instrument. The ability to remotely interrogate the system, i.e. via the umbilical cable, or with a modem and cellphone in a remotely deployed situation, would enable faults to be diagnosed and repairs to be carried out quickly and efficiently.

The submersed FI system was simple to set-up and operate and its reagent consumption and filtration requirements were less than those of the ship-borne AutoAnalyzer.

Reproducibility was less than the ± 5 % target specification for the duration of the cruise and the system was shown to be capable of being used immediately after being transported a considerable distance by road, with no special precautions other than wrapping the FI instrument in 'bubble wrap' inside its transit box.

By sampling every 10 - 15 minutes the submersed system monitored the nitrate concentration during three tidal cycles and produced profiles which were in good correlation with the salinity and turbidity data.

Chapter Seven
Conclusions and Future Work

7.   CONCLUSIONS AND FUTURE WORK

7.1.   Final conclusions

The key individual components of the submersible FI nutrient sensor were meticulously investigated in order to provide an integrated system which achieved the design and operational specification stated in Chapter 2.

The following general conclusions can be drawn from the preceding chapters regarding the FI approach for a submersible nutrient sensor for the determination of TON in estuarine and coastal waters:

7.1.1.   Analytical performance

The optimised custom built FI instrument achieved the following:

i.   A limit of detection of 0.1 μM (0.0014 mg l^{-1}) Nitrate-N

ii.   A linear range of 0 - 140 μM (0 - 2.0 mg l^{-1}) Nitrate-N

iii.   In-batch repeatability < $\pm$ 5 %

iv.   Day to day reproducibility < $\pm$ 5 %

v.   Capable of operating in a salinity range of 0 - 35 ‰.

7.1.2.   Flowcell design

The final flowcell design which had 90° inlet and outlet angles eliminated the problem of trapped air bubbles in a FI manifold and was capable of being used in other systems. The opaque PVC used to construct the flowcell body produced a cell which was unaffected by stray light and unlike transparent materials, e.g. clear acrylic (Perspex®), did not suffer from internal reflection or refraction.   Despite being constructed using general commercial

236

quality electronic components in order to produce a low cost 'disposable' flowcell, the overall performance met the specification.

7.1.3. Integrated system and construction

The integrated nutrient sensor achieved submersed operation at depths of up to 30 metres and the pressure housing was tested to 45 metres depth. The use of PVC and stainless steel throughout the construction ensured that the system was rugged and not susceptible to corrosion. The cage assembly provided additional protection for the integrated system from the harsh physical conditions that were encountered during ship-borne deployments. The cage assembly also provided a means of deploying the integrated system from a ship as a simple drop deployment or tethered from a buoy. Placing a custom FI instrument inside a pressure housing was shown to work at depths of up to 30 metres. This approach eliminated many of the fundamental engineering problems associated with having the various components at ambient pressure. It also provided the additional benefit of being able to use the FI system as a bench instrument or as a terrestrial field instrument.

7.1.4. Deployment

The integrated system was found to be simple to set-up and operate and *in situ* repairs could be effected quickly and efficiently. It could be interrogated remotely via the umbilical cable using a portable PC or a PSION® hand-held computer. This allowed the raw analytical data to be processed remotely and the system operation to be assessed. This capability would allow true remote deployments using an industry standard modem and a cellphone or satellite link.

7.2. Suggestions for future work

The submersible nutrient sensor described in the preceding chapters could be developed in a number of ways. Possible areas for further investigation are summarised below:

7.2.1. Full autonomous operation

The development of on-board data processing to permit full autonomous operation and automatic transfer of data and remote diagnostics using cellphone or satellite communications. This would also permit the integrated system to be used as an early warning system for pollution incidents.

7.2.2. Integration with other systems

The system could be deployed on other platforms, e.g. CTD frames and benthic landers, and therefore interfaced with other sensors to enable simultaneous measurement of nutrient and physical parameters. Using this method of deployment would also allow an increased reagent payload which would therefore permit a higher sampling rate over a 30 day period. Communications and power could be provided by the host platform.

7.2.3. Additional chemistries

The incorporation of additional chemistries such as phosphate, silicate and trace metals would provide means of studying the relationships of these species simultaneously and at the same sample point. The sensor could also be developed for other nitrogen species e.g. ammonia and organic nitrogen species such as urea and amino acids using on-line photo-oxidation.

7.2.4. Further environmental deployments

Use of the integrated system for long-term studies of a particular area, e.g. Barn Pool in Plymouth Sound, where the field experiments as discussed in Chapter 5, have already identified a complex nitrate pattern. Deploying the system in different locations over a set period of time, e.g. in an estuarine plume, would enable the spatial distribution of nitrate to be determined. A buoy deployment over an extended period, i.e. in a fixed position, would give the temporal fluxes of nitrate for a particular location.

7.2.5. Extension of analytical range

It has been shown that the analytical range of the system can be changed by using different combinations of injection volume, flowcell size and detector response in the FI instrument. Further work would establish the absolute analytical limits of the system, particularly for the higher levels of nitrate found in freshwater systems. The system could then be used to monitor land drain-off vs the application of nitrate-based fertilisers over extended periods.

References

REFERENCES.

1. Söderlund, R., and Svensson, B.H. The global nitrogen cycle, in Svensson, B. H., and Söderlund, R., (eds.) *Nitrogen,Phosphorus and Sulphur - Global Cycles, SCOPE Report No. 7, Ecol. Bull. (Stockholm)*, **22**, 23, (1976).

2. Delwiche, C. C., (1970), *Sci. Amer.*, **223**, 137.

3. Emery, K. O., Orr, W.L., and Rittenberg, S.C. Nutrients in the ocean, in *Essays in the honour of Captain Alan Hancock*, Los Angeles, University of Southern California Press, 299, (1955).

4. Rosswall, T., The Nitrogen Cycle, in *The Major Biogeochemical Cycles and their Interactions*, Bolin, B, and Cook, R.B. (eds.) SCOPE Report No. 21, Wiley, Chichester, (1983).

5. Riley, J.P., and Chester, R., *Introduction to Marine Chemistry*, Academic Press, London, (1971).

6. Grasshoff, K., Ehrhardt, M., and Kremling, K., *Methods of Seawater Analysis*, Verlag Chemie, New York, (1976).

7. Nutman, P.S., (1959), *Symp. Soc. Exp. Biol.*, **13, 42**.

8. Dugdale, R. C., and Goering, J.J., (1964), *Limnol. Oceanog.*, **9**, 507.

9. Dugdale, R. C., and Goering, J.J.,(1967), *Limnol. Oceanog.*,**12**, 196.

10. Goering, J.J., Dugdale, R.C. and Menzel, D.W., (1966), *Limnol. Oceanog.*, **11**, 614.

11. Fogg, G.E., and Than-Tun, (1958), *Biochim. Biophys. Acta.*, **30**, 209.

12. Dugdale, R.C., Menzel, D.W., and Ryther, J.H., (1961), *Deep Sea Res.*, 7, 297.

13. Ramamurthy, V.D., and Krishnamurthy, S., (1968), *Curr. Sci.*,37, 21.

14. Jones, K, and Stewart, W.D.P., (1969), *J. Mar. Biol. Ass.* U.K., **49**, 475.

15. Jones, K, and Stewart, W.D.P., (1969), *J. Mar. Biol. Ass.* U.K., **49**, 701.

16. Carpenter, E.J., and Capone, D.G., *Nitrogen in the Marine Environment*, Academic Press, London, (1983).

17. Blackburn, T.H., and Sorensen, J., *Nitrogen Cycling in Coastal Marine Environments.*, Wiley, Chichester, (1988).

18. Parsons, T.R., in *Chemical Oceanography* , Riley, J.P., and Skirrow, G., (eds.) Vol. 2, Academic Press, London (1975).

19. Craig, H., and Gordon. L.I., (1963), *Geochem Cosmochim Acta*, **27**, 949.

20. Pomeroy, L.R., (1974), *Bioscience*, **24**, 499.

21. Malone, T.C., *Algal Size*, in Morris, I, (ed.), *The Physiological Ecology of Phytoplankton*, University of California Press, Berkeley, (1980).

22. Griffith, E.J., Beeton, A., Spencer, J.M., and Mitchell, D.T., *Environmental Phosphorus Handbook*, Wiley, Chichester, (1973).

23. Kester, D.R., and Pytkowicz, R.M., (1967), *Limnol. Oceanog.*, **12**, 243.

24. Stevenson, F.J., Origin and distribution of nitrogen in the soil, in Bartholomew, W.V., and Clark, F.E., (eds.) *Soil Nitrogen, Agronomy*, **10**, 1-42, American Society for Agronomy Inc., Madison, Wisc., (1965).

25. Donald, C.M., (1960), *J. Austr. Inst. Agric. Sci.*, **6**, 319.

26. Mopper, K., and Degens, E.T., Organic carbon in the ocean: Nature and Cycling, in Bolin, B., Degens, E.T., Kempe, S., and Ketner, P. (eds.) *The Global Carbon Cycle*, SCOPE report No. 13, 293, Wiley, Chichester, (1979).

27. Delwiche, C.C., and Likens, G.E., Biological response to fossil fuel combustion products, in Stumm, W. (ed.), *Global Chemical Cycles and their Alterations by Man*, 73, Berlin, Dahlem Konferenzen, (1977).

28. Nybakken, J.W., *Marine Biology-an Ecological Approach*, 3rd edition, Harper Collins, London, (1993).

29. The Royal Society: *The Nitrogen cycle of the United Kingdom*: A Study Group Report, (1983).

30. Saull, M., (1990), *New Scientist*, 15 September, 1.

31. Goulding, K., and Poulton, P.,(1992), *Chemistry in Britain*, December, 1100.

32. Livingstone, D.A., Chemical Composition of Rivers and Lakes, in Fleischer, M., (ed.), *Data of Geochemistry*, U.S. Geological Survey, Washington, DC, (1963).

33. Meybeck, M, (1982), *Amer. J. Sci.*, **282**, 401.

34. Van Bennekom, J,J., and Solomans, W., Pathways of organic nutrients and organic matter from land to ocean through rivers, in Burton, J.D., Eisma, D., and Martin, J.M., (eds.), *River Input to the Ocean System*, SCOR, Rome, 33, (1981).

35. Wollast, R., Interactions in Estuaries and Coastal waters, in Bolin, B., and Cook, R.B., (eds.), *The Major Biogeochemical Pathways and their Interactions*, Wiley, Chichester, 385, (1983).

36. Walsh, J.J., (1991), *Nature*, **350**, 53.

37. Owens, N.J.P., in Burt, T.P., Heathwaite, A.L., and Trudgill, S.T., (eds.), *Nitrate: Processes, Patterns and Management*, Wiley, Chichester, (1993).

38. Nitrate in Water, D.O.E. Pollution Paper 26, H.M.S.O., London, (1986).

39. Casey, H., Clarke, R.T., (1979), *Freshwater Biology*, **9**, 91.

40. Freshwater Quality, 16th Report by the *Royal Commission on Environmental Pollution*, HMSO, London, (1992).

41. UNEP/WHO Report, *Assessment of freshwater quality*, London, (1988).

42. EC Directive on Drinking Water 80/778.

43. WHO/UNEP Report, *Global pollution and health, results of health related environmental monitoring, Geneva and United Nations Environment Programme*, Nairobi, Yale Press, London, (1987).

44. Lean, G., (1990), *Observer*, 21 January.

45. EC Directive on Nitrates 91/676.

46. EC Directive on Surface Waters for Drinking 75/440.

47. House of Lords, Select committee on the European Community, session 1988-89, 16th report, *Nitrates in Water*, HMSO, London, (1989).

48. Correa, P., Haenszel, W., Cuello, C., Archer, M. and Tannenbaum, S., (1975), *Lancet*, ii, 58.

49. Preussman, R. and Stewart, B.W., N-nitroso-carcinogens, in Searle, C.E. (ed) Chemical Carcinogens, A.C.S. monographs, 182, *American Chemical Society*, Washington DC, 643, (1984).

50. Hartman, P.E., (1983),*Environmental Mutagenesis*, **5**, 111.

51. Henderson-Sellars, B. and Markland, H., *Decaying Lakes: origin and control of eutrophication*, Wiley, Chichester, (1987).

52. NRA Report: *Water Quality Series No. 2.*, *Toxic Blue-Green Algae*, (1990).

53. Robbins, J.,(1990), *New Civil Engineer*, 31 May, 5.

54. GESAMP No 39, *The state of the marine environment*, UNEP, New York, (1990).

55. Howarth, J.M., Dyer, K.R., Joint, I.R., Hydes, D.J., Purdie, D.A., Edmunds, H., Jones, J.E., Lowry, R.K., Moffat, T.J., Pomroy, A.J., and Proctor, R., (1993), *Phil. Trans. Roy. Soc. Lond.*, **343**, 383.

56. Oceanography, Summerhayes, C.P. and Thorpe, S.A., Manson Publishing Ltd., London, (1996).

57.   Brewer, P.G., and Riley, J.P., (1965), *Deep Sea Research*, **12**, 765.

58.   Wood, E.D., Armstrong, F.A.J., and Richards, F.A.,(1967), *J. Mar. Biol. Ass.(UK)*, **47**, 23.

59.   Anderson, L., (1979), *Anal. Chim. Acta.*, **110**, 123.

60.   Willis, R.B., (1980), *Anal. Chem.*, **52**, 1377.

61.   Gine, M.F., Bergamin., F., Zagatto, E.A.G., and Reis, B.F., (1980), *Anal.Chim. Acta*,**114**, 191.

62.   Johnson, K.S., and Petty, R.L., (1983), *Limnol. Oceanogr.*, **28**, 1260.

63.   Gaugush, R.F., and Heath, R.T., (1984), *Water Research*, **18**, 449.

64.   van Staden, J.F., Joubert, A.E., and van Vliet, H.R., (1986), *Fresenius Z Anal. Chem.*, **325**, 150.

65.   Clinch, J.R., Worsfold, P.J., and Casey, H., (1987) *Anal. Chim. Acta.*, **200**, 523.

66.   Oudot, C., and Montel, Y., (1988), *Marine Chemistry*, **24**, 239.

67.   Maimo, J., Cladera, Mas, F., Forteza, R., Estela, J.M., and Cerda, V, (1989), *Intern. J. Environ. Anal. Chem.*, **35**, 161.

68.   Perstorp Analytical Ltd., Application Note AN 136/91, (1992).

69.   Raimbault, P., Slawyk, G., Coste, B. and Fry, J. (1990) *Mar. Biol.*, **104**, 347.

70.   Pai, S.C., and Riley, J.P., (1994), *Intern. J. Environ. Anal. Chem.*, **57**, 263.

71.   Ebdon, L., Braven, J. and Frampton, N.C. (1991) *Analyst*, **116**, 1005.

72.   Motomizu, S., Mikasa, H. and Toei, K. (1987) *Anal. Chim. Acta.*, **193**, 343.

73.   Noufi, M., Yarnitzky, C. and Ariel, M. (1990) *Anal. Chim Acta*, **234**, 475.

74.   Fogg, A.G., Scullion, S.P. and Edmonds, T.E. (1988) *Analyst*, **113**, 979.

75.   Brown, L., and Bellinger, E.G., (1978), *Water Res.*, **12**, 223.

76.   Garside, C., (1982), *Mar. Chem.*, **11**, 159.

77.   Verma, K.K., and Verma, A., (1992), *Anal. Lett.*, **25**, 2083.

78.   Fogg, A.G., Scullion, S.P., Edmonds, T.E. and Birch, B.J., (1991), *Analyst*, **116**, 573.

79.   Doherty, A.P., Stanley, M.A., Leech, D., and Vos, J.G., (1996), *Anal. Chim. Acta.*, **319**, 111.

80.   Crompton, T.R., *Analysis of Seawater*, Butterworths, Sevenoaks, (1989).

81.   Kim, H.J. and Kim, Y. K., (1989), *Anal. Chem.*, **61**, 1485.

82.   Gennaro, M.C., Bertolo, P.L., and Cordero, A., (1990), *Anal. Chim. Acta.*, **239**, 203.

83.   Burke, E.M., Suarez, F.X., Hillman, D.C., and Helthmer, E.M., (1989), *Water Res.*, **23**, 519.

84.   Cawse, P.A., (1967), *Analyst*, **92**, 311.

85.   Morries, P., (1971), *Water Treat. Exam.*, **20**, 132.

86.   Rennie, P.J., Sumner, A.M., and Basketter, F.B., (1979), *Analyst*, **104**, 837.

87.   Montgomery, H.A.C., and Dymcock, J.F., (1962), *Analyst*, **87**, 374.

88.   Jenkins, D., and Medsker, L.L., (1964), *Anal. Chem.*, **36**, 610.

89.   Mullin, J.B., and Riley, J.P., (1955), *Anal. Chim. Acta.*, **12**, 464.

90.   Downes, M.T., (1978), *Water Research*, **12**, 673.

91.   Bower, C.E., and Holm-Hansen, T., (1980), *Aquaculture*, **21**, 281.

92.   Kempers, A.J.,and Luft, A.G., (1988), *Analyst*,**113**, 1117.

93.   Chow, J.J., and Johnstone, M.S., (1962), *Anal. Chim. Acta.*, **27**, 441.

94.   Matsunanga, K., and Nishimura, M., (1969), *Anal. Chim. Acta.*, **45**, 350.

95.   Bajic, S.J., and Jaselskis, B., (1985), *Talanta*, **32**, 115.

96.   Margeson, J.H., Suggs, J.C., and Midgett, M.R., (1980), *Anal. Chem.*, **52**, 1955.

97.   Morris, A.W., and Riley, J.P., (1963), *Anal. Chim. Acta.*, **29**, 272.

98.   Lambert, R.S.,and DuBois, R.J., (1977), *Anal. Chem.* **47**, 955.

99.   Nydahl, F., (1976), *Talanta*, **23**, 349.

100. Stainton, M.P., (1974), *Anal. Chem.*, **46**, 1616.

101. Oxidised Nitrogen in Waters: *Methods of Examination of Waters and Associated Materials*, HMSO, London, (1981).

102. Kouparis, M.A., Walczak, K.M., and Malmstadt, H.V., (1982), *Anal. Chim. Acta.*,**142**, 119.

103. Hydes, D.J., and Hill, N.C., (1985), *Estuarine, Coastal and Shelf Science*, **21**, 127.

104. van Staden, J.F., (1982), *Anal. Chim. Acta.*, **138**, 403.

105. Parsons, T.R., in Riley, J.P. and Skirrow, G., (eds.), *Chemical Oceanography*, Vol.2., Academic Press, London, (1975).

106 Bendschneider, K., and Robinson, R.J., (1952), *Journal of Marine Science*, **11**, 87.

107. McCormack, T., David, A.R.J., Worsfold, P.J., and Howland, R.J.M.,(1994), *Anal. Proc.*, **31**, 81.

108. Discrete and Air Segmented Automated Methods of Analysis including Robots, An Essay Review (2nd Edition), *Methods for the Examination of Water and Associated Materials*, HMSO, London, (1988).

109. Skeggs, L.T., (1957), *Am. J. Clin. Pathol.*, **28**, 311.

110. Strickland, J.D.H., and Parsons, T.R., *A Practical Handbook of Seawater Analysis*, 2nd edition, (1972).

111. Brewer, P.G., and Riley, (1966), *Anal. Chim. Acta*, **35**, 514.

112. Slawyk, G., and MacIsaac, J.J., (1972), *Deep Sea Research*, **19**, 521.

113. Ruzicka, J., and Hansen, E.H., (1975), *Anal. Chim. Acta.*, **78**, 145.

114. Ruzicka, J., and Hansen, E.H., (1978), *Anal. Chim. Acta.*, **99**, 37.

115. Betteridge, D., Dagless, E.L., Fields, B., and Graves, N.F., (1978), *Analyst*, **103**, 897.

116. Flow Injection Analysis, An Essay review and Analytical Methods: *Methods for the examination of Waters and Associated Materials*, HMSO, London, (1990),

117. Ruzicka, J., and Hansen, E.H., *Flow Injection Analysis*, 2nd. edition, Wiley-Interscience, Chichester, (1988).

118. Valcarcel, M.D., and Luque de Castro, M.D., *Flow Injection Analysis-Principles and Applications*, Ellis Horwood Ltd., Chichester, (1987).

119. Kalberg, B., and Pacey, G.E., *Flow Injection Analysis - A Practical Guide*, Elsevier Science Publications, B.V., Amsterdam, (1989).

120. Betteridge, D., (1978), *Anal. Chem.*, **50**, 832A.

121. Ruzicka, J., (1983), *Anal. Chem.*. **55**, 1041A.

122. Maugh II, T.H., (1984), *Science*, **224**, 45.

123. Ruzicka, J., (1994), *Analyst*, **119**. 1925.

124. Audunsson, G., (1986), *Anal. Chem.*, **58**, 2714.

125. Hirata, S., Umezaki, Y., and Ikeda, M., (1986), *Anal. Chem.*, **58**, 2602.

126. van der Linden, W.E., (1983), *Anal. Chim. Acta.* **151**, 359.

127. Li, Y., and Ma, H., (1995), *Talanta*, **42**, 2033.

128. Reijin, J.M., van der Linden, and Poppe, H., (1981), *Anal. Chim. Acta.*, **123**, 229.

129. MacDonald, R.W., McLaughlin, F.A., (1982), *Water Research*, **16**, 95.

130. Clementson, L.A., Wayte, S.E., (1992), *Water Research*, **26**, 1171.

131. U.S. EPA Method No. 353.2, *Methods for the Chemical Analysis of waters and wastes*, Washington, (1979).

132. Roman, M., Dovi, R., Yoder, R., Dias, F., and Warden, B., (1991), *J. Chrom.*, **546**, 341.

133. Andrew, K.N., Blundell, N.J., Price, D. and Worsfold, P.J., (1994), *Anal. Chem.*, **66**, 916A.

134. Clinch, J.R., Worsfold, P.J., Casey, H., and Smith, S.M., (1988), *Anal. Proc.*, **25**, 71.

135. Casey, H., Clarke, R.T., Smith, S.M., Clinch, J.R., and Worsfold, P.J., (1989), *Anal. Chim. Acta.*, **227**, 379.

136. Worsfold, P.J., Clinch, J.R., and Casey, H., (1987), *Anal. Chim. Acta.*, **197**, 43.

137. Clinch, J.R., Worsfold, P.J., and Sweeting, F., (1988), *Anal. Chim. Acta.*, **214**, 401.

138. Benson, R.L., Worsfold, P.J., and Sweeting, F., (1990), *Anal. Chem. Acta.*, **238**, 177.

139. Blundell, N.J., Hopkins, A., Worsfold, P.J, and Casey, H., (1993), *J. Auto.Chem.*, **15**, 159.

140. Blundell, N.J., Worsfold, P.J., Casey, H, and Smith, S., (1995), *Env. Int.*, **21**, 205.

141. Johnson, K.S., Beehler, C.L., and Sakamoto-Arnold, C.M., (1986), *Anal. Chim. Acta.*, **179**, 245.

142. Johnson, K.S., Sakamoto-Arnold, C.M., and Beehler, C.L., (1989), *Deep-Sea Research*, **36**, 1407.

143. Daniel, A., Birot, D., Lehaitre, M., and Poncin, J., (1995), *Anal. Chim. Acta.*, **308**, 413.

144. NAS-2 Nutrient Analyser product bulletin, (1996), W.S. Oceans Systems Ltd., Alton, UK.

145. ME APP 4002 automatic analyser data sheet, (1993), CSIP Ltd., Weymouth, UK.

146. Marine Nitrate Sensor - First Results, in *Valeport News* (Spring 1996), Valeport Ltd., Dartmouth, UK.

147. Meadows, P.S. and Campbell, J.I., *An introduction to marine science*, 2nd.edn., Blackie, London, (1988).

148. Chester, R., *Marine Geochemistry*, 322, Unwin Hyman, London, (1990).

149. Gibbs, R.J., in *Suspended solids in water*, R.J.Gibbs, (ed), Plenum, New York, (1974).

150. Chester, R.. and Stoner, J.H., (1972), *Nature*, **240**, 552.

151. Guide to filtration system design, (1986/87), in *Gelman Sciences Process Microfiltration Catalog*, Gelman Sciences Ltd., Northampton, UK.

152. Sartorious membrane filters, (1983/84) in *Laboratory Microfiltration*, Sartorious Instruments Ltd., Sutton, UK.

153. Membranes for Microfiltration, (1995/96), in *Cole-Palmer Catalogue*, CP Instrument Company Ltd., Bishops Stortford, UK.

154. Marvin, K.T., Proctor, R.R. and Neal, R.A., (1972), *Limnol. Oceanogr.*, **17**, 777.

155. Robards, K., McKelvie, I.D., Benson, R.L., Worsfold, P.J., Blundell, N.J., and Casey, H., (1994), *Anal. Chim. Acta.*, **287**, 147

156. Eutrophication study undertaken by the NRA, in *Water and Water Treatment*, (1994), October.

157. McCormack, T., *Flow injection chemistries for the in situ monitoring of nutrients in sea water*, PhD Thesis, University of Plymouth, (1996).

158. Bergamin, H., Reis, B.F., and Zagatto, A.G., (1978), *Anal. Chim. Acta*, 97, 427

159. Thomsen, J., Johnson, K.S. and Petty, R.L., (1983), *Anal. Chem.* 55, 2378.

160. Zagatto, E.A.G., Reis, B.F., Martinelli, M., Krug, F.J., Bergamin, H., and Gine, M.F., (1987), *Anal. Chim. Acta.*, **198**, 153.

161. Linden, D., (ed.), *Handbook of batteries and fuel cells*, McGraw-Hill, New York, (1983).

162. Health and Safety Executive, *Guidance on Regulations, Manual Handling Operations regulations*, HMSO, London, (1992).

163 Smart Cat© PIT Satellite platform data sheet, Seimac Ltd., Dartmouth, Canada.

164 Cellnet UK coverage map, Telecom Securicor Cellular Radio Ltd., Slough, UK, (1993).

165 Ismatec Catalogue 93/94, Ismatec UK Ltd., Carshalton, UK.

166 Nutrient Analysis Techniques, PML internal document.

167 Dasgupta, P.K., Bellemy, H.S., Liu, H., Lopez., J.L., Loree, E.L., Morris, K., Petersen, K., and Mir, K.A., (1993),*Talanta*, **40**, 53.

168 Johnson, K.S., Petty, R.L. and Thomsen, J., in *Mapping strategies in chemical oceanography*, American Chemical Society, 7, (1985).

169 *Handbook of industrial materials*, 1st edn. , Trade and Industrial Press Ltd, (1980).

170 Defence Standard 01-2 (part 1) / issue 2 , 15 March 1991, Guide to engineering alloys used in navy service: data sheets Part 1 : ferrous alloys (F)

171 MIL - STD -2000, (1989), *Standard requirements for soldered electrical and electronic assemblies.*

172 Protonique CM-2D Handbook, Protonique S.A., Switzerland, (1982).

173 Warygold, J., *How to Select Conformal Coatings for Printed Circuit Boards*, Humiseal Div., Columbia Chase Corp., Woodside, New York.

174 Naisbitt, G.K., *An Explanation of Conformal Coatings*, Concoat LTD., Alasan House, Albany Park, Frimley Road, Camberley, U.K.

175 Dow Corning RTV 3145 Product Data Sheet, Dow Corning UK Ltd., Reading, UK.

176 MacLaurin, P., Andrew, K.N., and Worsfold, P.J., *Flow injection analysis*, in, *Process analytical chemistry*, McLennan, F. and Kowalski, B.R., eds.,Blackie, London, (1996).

177 Clinch, R, *Remote spectrophotometric water quality monitoring*, PhD Thesis, University of Hull, (1988).

178 Flaschka, H., Mc.Keithan, C., and Barnes, R.M., (1973) *Anal. Lett.*, **6**, 585

179 Trojanowicz, M., Worsfold, P.J., and Clinch, J.R. (1988) *Trends Anal. Chem.*,**7**, 301.

180 Trojanowicz, M., Pobozy, E., and Szpunar, J., (1990), *Chemia Anal.*, **35**, 661.

181   Hauser, P.C., Rupasinghe, T.W.T., and Cates, N.E., (1995), *Talanta*, **42**, 605.

182   Liu, H., and Dasgupta, K., (1994), *Anal. Chim. Acta.*,**289**,347

183   R.S. Data File, (1993), *Photodiodes*, F14784.

184   Skoog, D.A., and West, D.M., *Fundamentals of Analytical Chemistry*, 5th edn. Saunders College Publishing, New York, (1988).

185   Oxford Concise Science Dictionary, Oxford University Press, Oxford, UK, (1991).

186   Giacoletto, L.J., (ed.), *Electronic Designers Handbook*, 2nd edn., Mc.Graw-Hill, New York, (1977).

187   Chemical resistance data sheets, Vol. 1, *Plastics*, RAPRA Technology, Shrewsbury, UK, (1983).

188   Anglo-Russian Interdisciplinary Estuarine Study (ARIES) Project executive summary, Plymouth Marine Laboratory, UK, Moscow State University, Russia., (1993).

189   Van Den Berg, C.M.G. and Li, H., (1988), *Anal. Chim. Acta.*, **212**, 31.

190   Miller, J.C. and Miller. J.N., *Statistics for Analytical Chemistry*, 3rd edn., Ellis-Horwood, London, (1993).

191   Field Studies Council, *Surveys of harbours, rias and estuaries in southern Britain*, 1, (1986).

192   Lewin, V.H., (1973), Water Research, 7, 55.

193   Nalgene Labware Catalogue, Nalge (Europe) Ltd., Hereford, UK, (1996).

194   Morris, A.W., Howland, R.J.M., and Bale. A.J., (1978), *Estuarine and Coastal Marine Science*, **6**, 105.
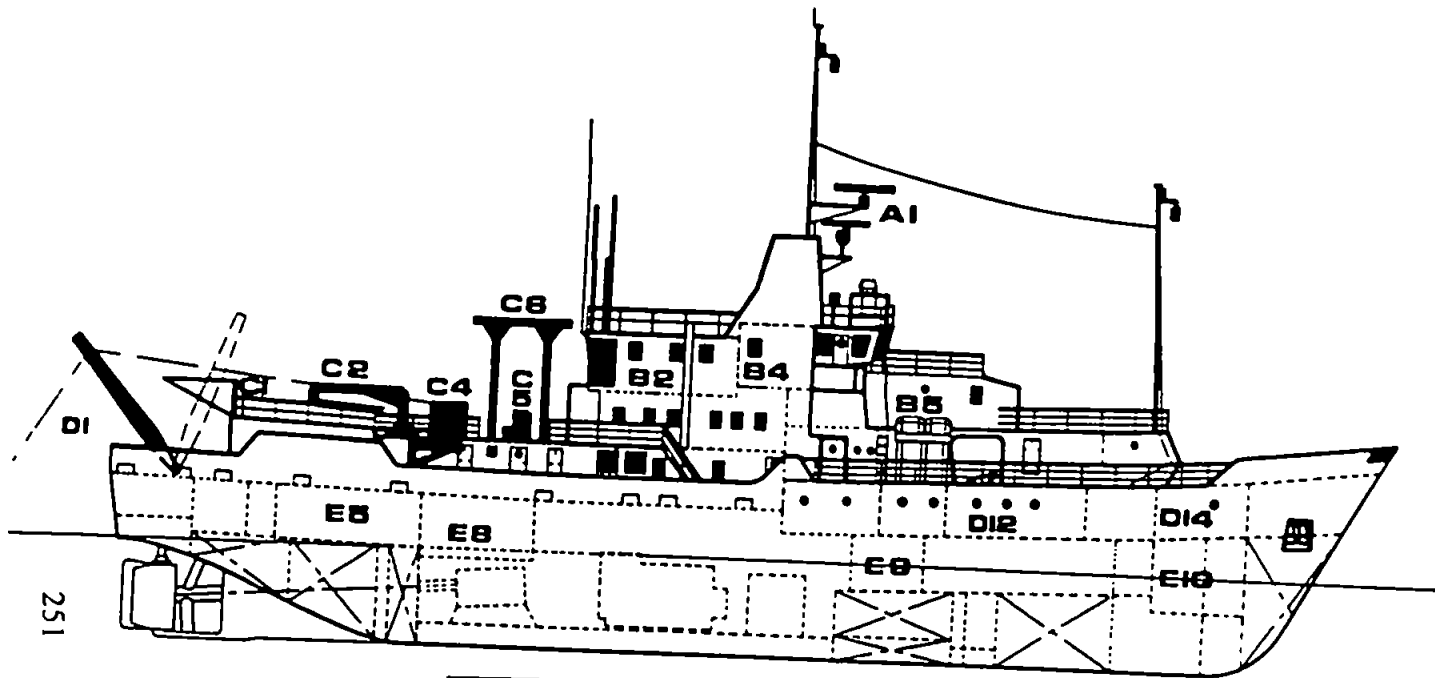
Appendices
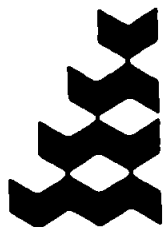
Natural
Environment
Research
Council
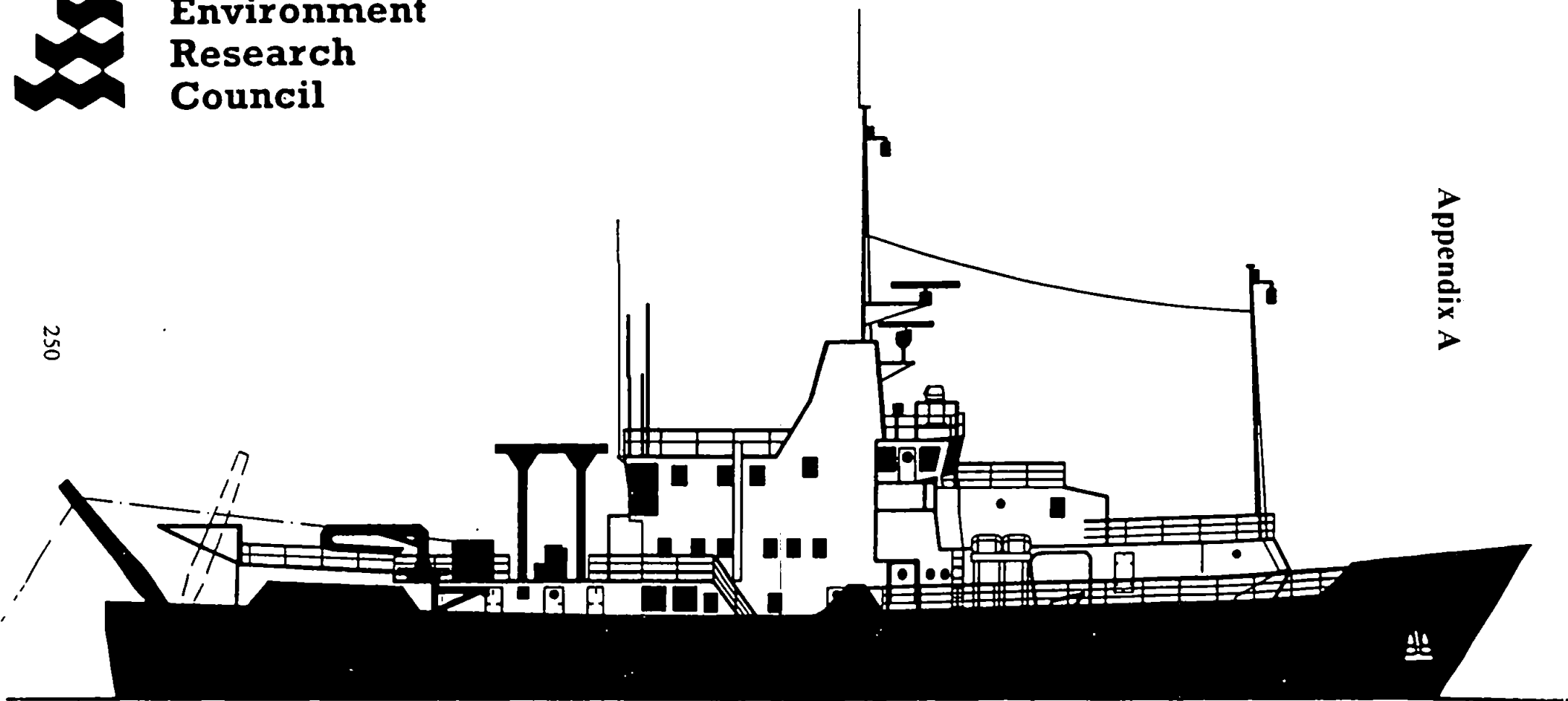
R.R.S. CHALLENGER

SCIENTIFIC SPACES

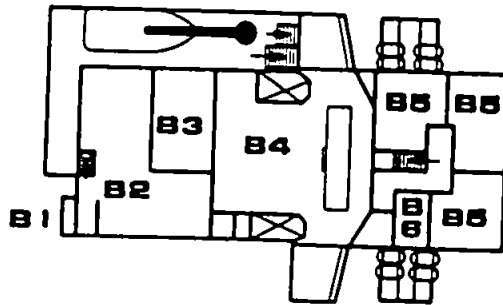**PROFILE**
A1 Radar and Signals Mast

BRIDGE DECK
B1 Winch Controls
B2 Scientific Control Room
B3 Computer Room
B4 Wheelhouse
B5 Scientists' Cabin - 2 Berth
B6 Toilet Facilities

FORECASTLE & BOAT DECK
C1 Towing Boom
C2 Atlas 6002 Hydraulic Crane
C3 Auxiliary Winch
C4 Dynamometer Sheave Frames
C5 Hydrographic Winch
C6 'A' Frame
C7 Smoke Room
C8 Scientists' Cabin - 2 berth
C9 Scientist's Cabin - 1 berth
C10 Principal Scientist's Cabin
C11 Toilet Facilities

251
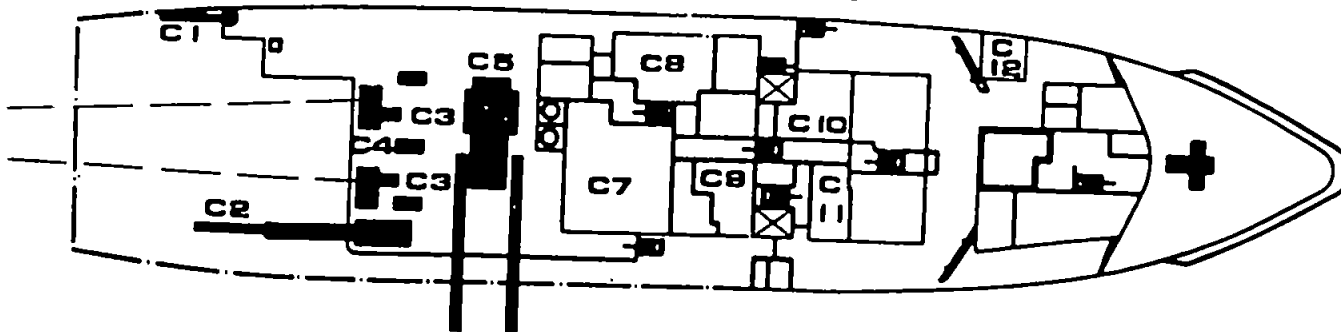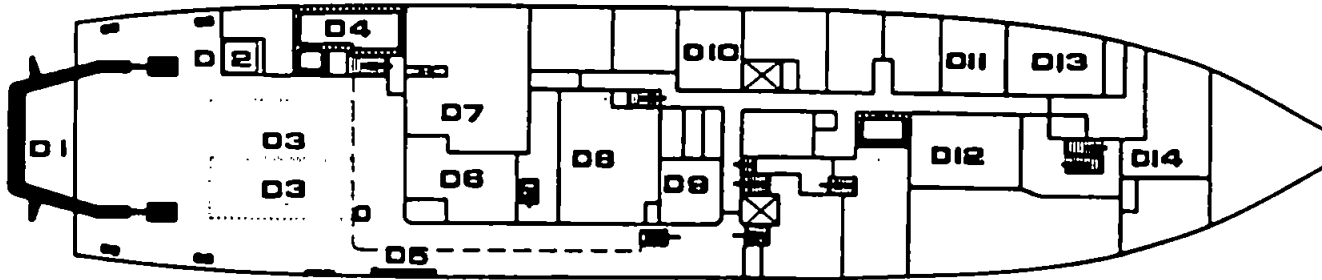
UPPER DECK

D1   'A' Frame
D2   Hatch to Scientific Hold
D3   Container Stowage Position
D4   Low Temperature Laboratory
D5   Towing Boom
D6   Fishing Laboratory
D7   General Laboratory
D8   Wet Laboratory
D9   Hospital
D10 Scientists' Cabin - 2 Berth
D11 Scientists' Cabin - 2 Berth
D12 Officers Mess
D13 Scientist's Cabin - 1 Berth
D14 Electrical Conversion Machinery Room
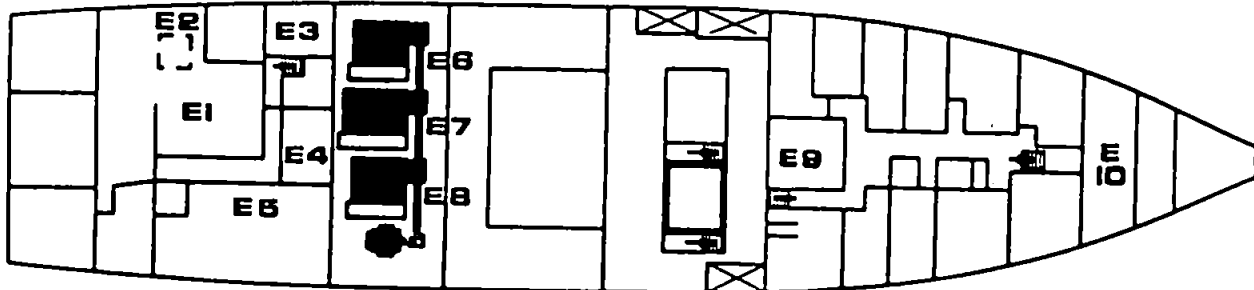
LOWER DECK

E1   Scientific Hold
E2   Hatch to Upper Deck
E3   Dark Room
E4   Scientific Workshop
E5   Laboratory
E6   Port Trawl Winch
E7   Deep Wire Winch
E8   Starboard Trawl Winch
E9   Ship's Office
E10 Bow Thruster

R.R.S. CHALLENGER

SPECIFICATIONS

SHIPS PARTICULARS

All weights in metric tonnes and given for Summer marks.

Callsign: GPTU
Official Number: 343403
RT Telex Code: 45811
Class: DTp Class VII Lloyds 100 A1
Port of Registration: Cardiff
Length Overall: 54.3 m
Beam: 11.3 m
Summer Draft: 4.48 m
FW capacity: 90 tonnes
Gross tonnage: 1050 tonnes
Nett tonnage: 350 tonnes
Displacement: 1440 tonnes
Deadweight: 350 tonnes
Registered tonnage: 350 tonnes
Speed: Nominal passage speed 10 knots
Endurance: Nominal cruise length - 32 days
Consumption: 4.28 TPD
Bunker capacity: 153 tonnes
Passive roll stabilised

Operational areas are temperate Atlantic Waters, Mediterranean and Caribbean seas.

PROPULSION
(Bridge controlled diesel-electric)

Main Engines:
2 of Mirrlees Blackstone ESL6 diesel generators delivering 550 kW each.
Lawrence - Scott 800 kW propulsion motor.

Auxiliary Engines:
Mawdsley 250 kVA Motor Generator.

Propeller:
Single controllable pitch - 4 bladed propeller with Kort nozzle.

Bow Thrust:
White Gill Azimuthing unit of 3.0 t thrust.

ELECTRICAL SUPPLIES AVAILABLE FOR SCIENTIFIC USE
2 x 415 V AC 3 phase 50 Hz 300 Kw (Diesel Generator)
240 V AC 1 phase 50 Hz 60 KVA
240 V AC Stablised 50 Hz 11 KVA (Rotary Convertor)
115 V AC Stablised 50 Hz 6.5 KVA (Rotary Convertor)
220 V DC 8 kW
24 V DC 0.6 kW (Battery)
415 V AC 3 phase Stablised

SCIENTIFIC SPACES

Scientific Compressor Room ....23.6 sq m
Scientific Workshop ....6.6 sq m
Darkroom ....6.3 sq m
Fishing Gear Store ....42.3 sq m
Refrigerated Machinery Space ....6.0 sq m
General Laboratory ....31.2 sq m
Fish Laboratory ....10.9 sq m
Wet/Chemistry Laboratory ....20.0 sq m
Constant Temperature Laboratory ....6.7 sq m
Scientific Plot ....38.0 sq m

SCIENTIFIC ACCOMMODATION
1 Single Cabin - Principal Scientist
3 Single Cabins
6 Double Cabins

SHIPS CREW
8 officers
11 crew

NAVIGATION EQUIPMENT

Bridge:
Radars: Decca Type AC1226C ⎫ Inter-
           Decca Type RM1226C ⎭ switchable
Decca Navigator: Mark 21A
                       Mark 21B
Track Plotter: 350T
Autopilot: 550GM
Gyro Compass: Arma Brown Mk10 (x 2)
Echo Sounder: Simrad EK38D
Logs: Simrad Doppler
         Electromagnetic
Weather Facsimile: Furuno Fax 108
Radio Equipment: Transocean/Pacific
              (Marconi) with Telex link
                   Sailor T128
                   VHF sets (x 2)

HANDLING EQUIPMENT

Gantries:
Stern: SWL 15 t - static load on centre lug. 12.5 t luffing. In addition 2 x 7 t on main cross-member and 2 x 10 t outboard gallows blocks and 2 x 3 t quarter blocks are fitted.
Clear distance between legs: 5.3 m at base, 4.0 m at block.
Clear distance under block: 6 m
Maximum over stern: 2 m under block.
Time from full inboard to fully outboard: 2 minutes

Starboard: SWL 6t - static load on centre lug, 3 t - luffing.
Clear distance between legs: 3 m
Clear distance under blocks: 6 m
Maximum outreach overside: 2 m under block

Crane:
Main Crane (amidships):
Atlas 6002 hydraulic crane, SWL 6 t at 2 m radius.

Winches:
Main Deep Wire Winch:
13,000 m tapered wire 13 mm - 10 mm.

Port and Starboard Trawl Winches:
3400 m of 22 mm wire. These wires run via scrolling gear and dynamometer sheaves with displays mounted in the scientific plot, winch control cab and wheelhouse.

CTD/Hydrographic Winch:
Double Drum.

253